A WHEEL-RAIL INTERFACE DESIGN FOR ENHANCED S&C PERFORMANCE

The University of Birmingham

Birmingham Centre for Railway Research and Education

(School of Engineering, Department of Civil Engineering)

UNIVERSITY OF BIRMINGHAM

KWAME ARTHUR

April 2024

Lead Supervisor: Prof Felix Schmid
Second Supervisor: Dr Charles Watson

A Thesis submitted for the Degree of Doctor of Philosophy

Abstract

In railway engineering, the wheel-rail interaction is one of the most important research topics because it affects the safety, performance and economic efficiency of the railway. It is influenced by the vibrations of the track, the suspensions of the rolling stock and the track structure. The wheel-rail impact forces can lead to significant economic loss to railway track owners as a consequence of damage to rails and sleepers. Records at Network Rail show that about 25% of annual renewal and maintenance budgets are spent on switches and crossings (S&C). To achieve a safe, reliable and efficient railway network, it is important to manage the risk caused by the wheel-rail contact complexities of the switch and crossing arrangement.

Therefore, his PhD research project was initiated to enhance S&C design by modelling a novel switch called NR60C MK2, which has an improved wheel-rail contact behaviour to address the various damage modes of the existing RT60/NR60 MK1 switch. This is the first time that modelling work has been carried out on a switch before attempts are made to bring into use on the Network Rail infrastructure. For instance, no modelling work was conducted for RT60/NR60 MK1 switches before they were brought into use. The author explores whether and how the deployment of finite element modelling using simulation tools such as Abaqus and Vampire software will allow the creation of better S&C designs for railway track in a timely manner.

For the present research, the NR60C MK2 switch was created virtually through three-dimensional (3D) finite element (FE) modelling. The wheel-rail contact was assessed using ABAQUS / CAE as the finite element software package that could be validated by an existing simulation. The newly developed switch (NR60C MK2) was then tested in the model space. The results predicted a significant reduction in the stress level from 1050 MPa to 580 MPa at the switch blade. Vertical displacement was similarly reduced from 0.35 mm to 0.12 mm and an improved PEEQ value of 2.1% was obtained. To enhance the switch performance, 3 mm of material (steel) was added to the switch blade. This is the first time a novel switch has been developed in the United Kingdom through the addition of a 3 mm material to the switch blade to enhance the service life of the switch. The simulation results gave a design log life of 4.95, which implied that the revised switch is predicted to have a service life that is longer than that of the existing switch.

Previous research work in this area has been focused either on modelling material strength or on carrying out vehicle dynamics simulations. The candidate is not aware of any research combining these approaches. The author of this thesis has therefore capitalised on this knowledge gap to conduct a research that will combine FEA with MB Dynamic simulation to enhance S&C performance which is the first time that material strength analysis has been

carried out vis-a-vis vehicle dynamic simulation. Therefore, to assess the efficacy of the newly developed switch, vehicle dynamic simulations using VAMPIRE® were carried out to evaluate the wear, RCF performance and derailment analysis of the new NR60C MK2 switch. The wheel-rail interface was assessed for two passenger vehicle types (Desiro and MK3) and a laden freight vehicle. The results from facing direction travel revealed no contact at the switch tip, thus eliminating any fear of switch tip damage. For all the vehicles, the NR60C MK2 switch is predicted to suffer less wear and for a shorter length along the switch planing section than the existing NR60C MK1 switch. In both the facing and trailing moves, the freight vehicle produced the worst performance, due to its high axle load and greater Primary Yaw Stiffness (PYS). However, there was a significant improvement with the application of rail lubrication. The T-Gamma value for the freight vehicle was reduced from 3018 J/m to 900 J/m. Similarly, the gauge corner wear indices at the switch planing section for all the vehicles were shown to be reduced by 30% with the application of rail gauge lubrication. The results also showed that all three vehicles used for the modelling fell below the derailment risk threshold of 1.2.

To conclude, the outcome of the simulation has enabled the author to provide recommendations to Network Rail with respect to how to enhance the performance of future S&C assets through modelling and simulation. The author has combined FEA with Multi-Body dynamic simulation to enhance S&C performance. This is the first time that material strength analysis has been carried out with respect to vehicle dynamic simulation.

Acknowledgements

I would like to thank my supervisors at the University of Birmingham for their support and guidance throughout the duration of my PhD research. Special thanks go to Professor Felix Schmid for granting me the opportunity to undertake the PhD research and allowing me the freedom to excel as an independent researcher. His constant enthusiasm, support and technical guidance have paved the way for the successful completion of this thesis. I would also like to thank Dr Charles Watson for his insightful support on the layout and guidance on the simulation tools. Reflecting on his previous work gave me a clear understanding of what is expected technically from the research.

I am very grateful to Network Rail for providing me with all the technical materials required to undertake this research. Most importantly, a special thanks goes to Dr Sin Sin Hsu who, as an industry supervisor and expert in this subject matter, played a monumental role by providing me with the technical guidance to complete this research. I thank her for taking the time to read through the thesis and providing excellent feedback to further improve the content and structure of my work. I would also thank Dr Patrik Mak of Network Rail for his meticulous review and contribution.

Finally, I would like to give special thanks to my wife, Anita for her continued support and patience and also to my children Caroline, Sarah, Joseph and Moses for keeping me smiling during the years of this research.

Table of Contents

Contents

List of Figures

List of Tables

Nomenclature

Symbol	Units	Meaning
(. , .)		Notation for the inner Product in the Hilbert space
A	-	Stiffness Matrix
a(. , .)		The bilinear Form in the weak Formulation
B	-	Load Vector
E	MPa	Young's Modulus of Elasticity
F		Facing Direction
f		Load vector
I	-	Identity Matrix
i_1, i_2, i_3		Base Vectors of the Cartesian Coordinate System
NR60C MK1		Existing S&C Design
NR60C MK2		Revised S&C Design
P(x,y)	MPa	Hertzian Normal Pressure Distribution
Rij	mm	Contact Radius
T	tonnes	Unit of Mass of hauled Train
T		Trailing Direction
Tγ	J/m	T-Gamma
U		Displacement of the interior line of the rail beam
$\underline{U}_h$		FEM Approximation to u from a space corresponding to a mesh indicated by h
U_N		Galerkin Approximation to u from an N-dimensional subspace
V	m/s	Velocity
V		The Hilbert space used in the weak formulation
V_N		N-dimensional Subspace of V
x		The Variable in one-dimensional problems
x_1		Axis of undeform Rail Beam. This is often abbreviated to x
x_1, x_2, x_3		Positions such that x_1, x_2, x_3 in a Cartesian coordinate system

$\varepsilon_{i,j}$		The infinitesimal Strain Components, 1 <*i, j* < 3
Θ		The Angle of Twist of the Rail. This is always 0 in our Example
M	-	Coefficient of Friction
ν	-	Poisson's Ratio
$\sigma_{i,j}$		The Cauchy Stress Components, 1 < *i, j* < 3
σy	MPa	Yield Stress
v		Test Function in a scalar Problem
$\underline{v}$		Test Vector in the weak Formulation of the Beam Problem
φ_j		Basis function

Glossary

Abbreviation	Meaning
BRR	British Rail Research
BEM	Boundary Element Method
CAD	Computer Aided Design
CAE	Computer Aided Engineering
CWR	Continuous Welded Rail
EMGTPA	Equivalent Million Gross Tonnes Per Annum
FEA	Finite Element Analysis
GB	Great Britain (England, Scotland and Wales)
IBCL	In Bearer Clamp Lock
kN	Kilo Newton
MBS	Multi-Body Simulation
Mm	Millimetre
MPa	Mega Pascal
NR	Network Rail
ORR	Office of Rail and Road
PEEQ	Accumulated Equivalent Plastic Strain Distribution
PYS	Primary Yaw Stiffness
RA	Route Availability
RAIB	Rail Accident & Investigation Branch
RCF	Rolling Contact Fatigue
RRD	Rolling Radius Difference
RSSB	Rail Safety and Standards Board
S&C	Switch(es) and Crossing(s)
SD	Standard Deviation
TSI	Technical Specification for Interoperability
Tγ	T-Gamma

UIC	International Union of Railways
UK	United Kingdom of Great Britain and Northern Ireland
WLRM	Whole Life Rail Model

1. INTRODUCTION

Switch and crossing wear are a major issue for all railway networks, whether in Great Britain (GB) or elsewhere, and the problem is a significant cost and risk factor on Network Rail's[1] assets. In particular, the existing short-length RT60 and NR60 switches (turnouts) are prone to Rolling Contact Fatigue (RCF) and wear failure modes from trailing moves of passenger and freight vehicles (Hsu, S.S., 2014). In an attempt to address this problem, an NR56 switch was developed, to replace the RT60 and NR60 switches, but this switch became non-compliant following the introduction of the Technical Specifications for Interoperability (TSI). The author of this thesis is therefore proposing an NR60 MK2 switch as a replacement for NR60 MK1 switches. This new switch has been designed to fit into the same footprint as the NR56 and NR60 MK1 suite of S&C, to cause minimal disruption to other railway assets, such as overhead lines, platforms and signalling equipment, during installation. The proposed design has a slight change to the geometry to accommodate the standard track gauge of 1435 mm and a more substantial rail section. A track gauge of 1432 mm for the NR56 and some NR60 versions had been introduced in the belief that this would improve guidance performance but, instead, it resulted in more damage to wheels and rails. A similar approach was tried by German railways (DB) for plain line track in about 2015.

1.1 Background

The railway network plays an important role in the UK transport system and in many other countries of the world. To allow a safe, efficient and reliable rail network and to provide a good ride quality, the railway infrastructure, consisting of structures, the track, overhead power, signals and other systems, must be maintained regularly. Due to increased axle loads[2], greater traffic density and higher speeds of modern railway systems, the contact forces between the rail and wheel have increased, leading to higher rates of wear and rolling contact fatigue, despite considerable improvements in designs and materials over time.

According to Cornish (2014), Britain's railway infrastructure includes 20,327 sets of S&C with more than 200 design variations. Machined longitudinal rail profiles and the complexity of wheel-rail interactions have led to increases in Network Rail's renewal and maintenance budget in recent years. For example, although representing only 5% of track miles, switch and crossing equipment alone has consumed 23% of the renewals budget and 24% of the

[1] Network Rail (NR) is the railway infrastructure owner and manager in Great Britain, that is, England, Scotland and Wales. It is deemed to be a state-owned enterprise. It is not responsible for the railway infrastructure in Northern Ireland.

[2] The current maximum axle load on Network Rail infrastructure in Great Britain is 25.4 t for a Route Availability of 10 (RA10).

maintenance budget. Moreover, switch and crossing defects, such as missing bolts, damaged switch blades, damaged stretcher bars and many other issues, have led to derailments causing injuries and, very occasionally, deaths. Problems have resulted in heavy fines for Network Rail by the Office of Rail and Road (ORR).

An example of such an incident occurred on 28 January 2020: a freight train derailed for about 35 m at a switch and crossing layout at Eastleigh West Junction. Inspection and maintenance implementation within the area were blamed for the event. Some of the fastenings that hold the rails to the concrete bearers that support them had fractured, prior to the passage of the train. This allowed one of the rails to move outwards under the train, breaking further fastenings and causing the locomotive's wheels to drop inside the rail, as it moved further outwards. The design of these fastenings made them more prone to this type of failure when subjected to high lateral forces, which were present at these points due to the track geometry at the site and the curving characteristics of the locomotive (Rail Accident Investigation Branch, 2021). Significant damaged was caused to the railway infrastructure when the 52-tonne wagons derailed. The findings from the Rail Accident and Investigation Branch (2021) was that:

"Network Rail should develop a strategy to assess and control the risk of failure of track fastening systems incorporating elevated shoulders in RT60 switch and crossing layouts. It should also confirm that the failure mode identified in these shoulders does not apply to other elevated designs of track fastening system. In addition, they should review its arrangements for the dynamic measurement of track geometry on the parts of its infrastructure not covered by its track measurement trains. The review should include the identification of high risk locations where additional safeguards are required (such as those subject to high lateral forces, or where there is an increased risk of track geometry faults). Consideration should be given to the number and routing of track measurement trains and alternative ways of measuring track geometry under dynamic conditions" (Rail Accident Investigation Branch, 2021).

The purpose of this recommendation is to minimise the risk of failure of elevated cast iron shoulders like those in RT60 S&C layouts and to consider how dynamic track gauge measurement is undertaken in the areas of its network that are not traversed regularly by its track measurement trains.

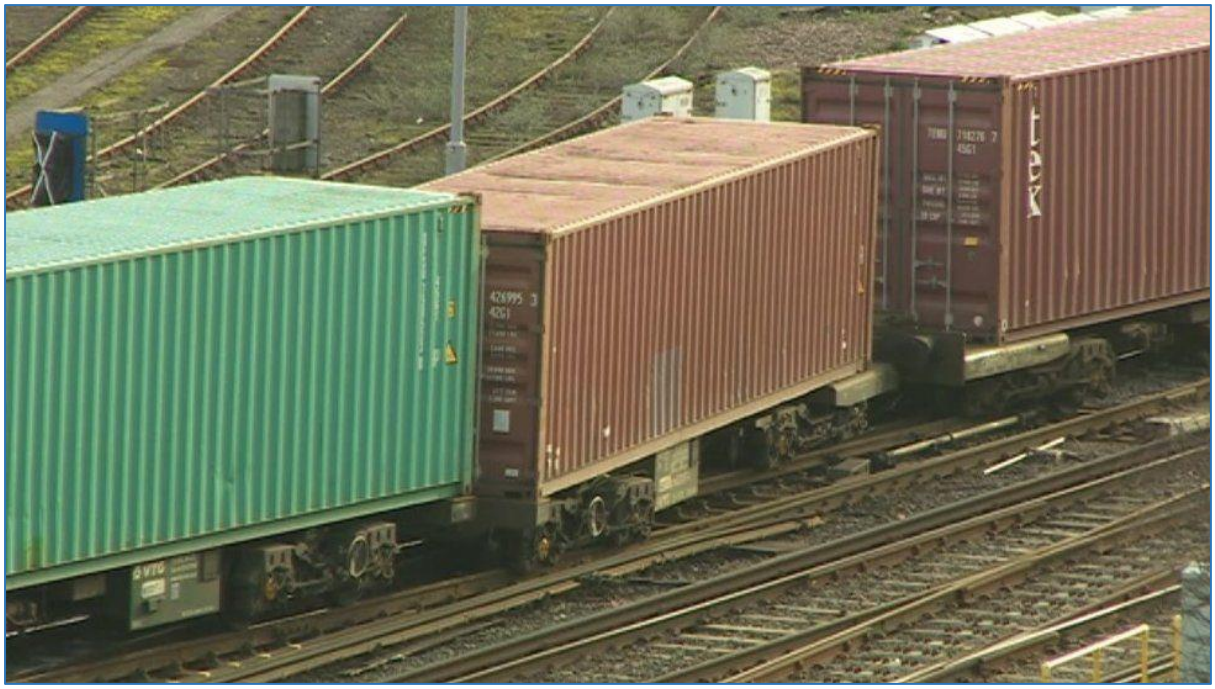

Figure 1: Eastleigh Freight Train Derailment (RAIB, 2021)

S&C systems allow trains to run smoothly while connecting different destinations on a railway network and, in the case of disruptions, they permit diversion from one track to another, to maintain continuity of service. They are therefore key to the railway track infrastructure and cannot be ignored. As mentioned, in recent years, there have been increasing volumes of trains running on the UK railway networks. Most of these modern trains are characterised by higher speeds, greater axle loads and increased primary yaw stiffness (PYS), thus placing greater demands on the track infrastructure.

To meet safety standards and to have acceptable ride quality, railway tracks require a specific level of track alignment. However, the impact of static and dynamic loads to which S&C components are subjected can lead to rapid deterioration and alignment problems because switches and crossings include special components such as slide plates, rollers, switch tips, planed sections, crossing noses. These are all exposed to high dynamic and static forces, hence having a high probability of exhibiting excess deterioration and wear rates at the wheel-rail contact. In view of this, a high percentage of track failures occur at switches and crossings, leading to cancellations and delays, which consequently have a negative impact on the quality of service. A better and fuller understanding of S&C modes of failure can help predict and prevent such disruptions.

To address this problem, to reduce maintenance and renewal cost, increase durability and safety, the simulation of wheel-rail contact, involving the evaluation of stresses, strains and forces and their impacts, has received a lot of attention in recent years. Put simply, in this thesis the author defines wheel-rail interface modelling as bringing together two separate

bodies, the wheel and the rail, into simulated contact to assess their impact on each other. Interactions at the wheel-rail interface create vertical and horizontal forces that put pressure on the railway infrastructure. The horizontal forces are subdivided into longitudinal and lateral forces. These forces have dynamic and static features which are transmitted between the rail and wheel via the contact patch. For a typical wheel load of 12 t, Schmid (2010) describes the contact patch as an elliptical area of about 1 cm^2, where both the rail and wheel are compressed, with transient (elastic) flattening of about 0.08 mm. It is a combination of factors such as wheel tread, cone angle, cross-sectional curvature of the rail head, elasticity modulus of the rail and wheel material and the total per wheel mass of the vehicle that determine the exact shape of the contact patch of the contacting bodies.

To understand this behaviour better, it is necessary to introduce the two different types of contact i.e. conformal and non-conformal. In conformal contact there is uniform contact over the surface boundary, leading to a large contact area with a stress field propagating throughout the bodies. As the wheels travel over the rails, the running surfaces of both the rail and the wheel change due to wear and this can result in a conformal shape turning into a two-point contact or, more accurately, two-patch contact. The second type, non-conformal contact, commences as a line or point contact at zero load and then develops, with increasing load, into an elliptically shaped patch with a small contact area in relation to the contacting bodies' sizes. It is the orthogonal radius of curvature on which the contact patch depends that gives rise to a stress field that is greater than the general stresses in the bulk of the bodies.

Therefore, this research will be based on the mathematical modelling of static and dynamic three-dimensional elastic-plastic stress analysis of wheel-rail contact using the Finite Element Method, a type of wheel-rail study that is not prominent in literature. The outcome of this research will allow other geometric problems to be analysed and solved, such as crack initiation, plastic deformation and wear.

Rail vehicle derailments are caused by many factors, among the most prominent being broken rails, excessive wear, wheel climb and S&C failures, all leading to safety, economic and environmental problems. A major cause of broken rails is the development of cracks due to RCF. Initially, this manifests itself as micro-cracks which initiate a transverse defect in their early stages of growth that may be very difficult to detect, even with ultrasonic testing, because horizontal cracks can cover or obscure transverse cracks. If left untreated, these cracks cause spalling or flaking, growing to a potential depth of 5 mm and this becomes a safety issue. Although a systematic grinding regime has been used over time to control RCF defects (especially dark spots and squats), the removal of metal between the rail and wheel become a major source of concern as frequent rail replacement is not economically prudent.

With high axle load traffic increasing, it looks as if rail wear, wheel wear and RCF defects will continue to pose a major problem within the railway industry. RCF is not only a track issue but also relevant for train operators as deep RCF cracks occur on the wheels of trains. According to Fletcher (2013), high friction coefficient and contact angle between the gauge side of worn rail and worn wheel-flange can also lead to wheel climb and derailment. Apart from the economic and safety issues raised, there are also environmental factors that need addressing. Stick-slip induced squeal, rough rail and wheel surfaces, as well as corrugation induced vibrations, result in noise that is not environmentally friendly and makes for uncomfortable travel.

Through optimisation of the wheel-rail interface, the outlined safety, economic and environmental issues can be brought under control. A full optimisation process should involve friction management, wheel-rail dynamics, metallurgy and contact mechanics but this is difficult to achieve as solving one problem can lead to another problem. For instance, although management of wheel-rail friction through lubrication, as noted in Fletcher (2013), is a good approach for train rolling resistance and wear reduction, without careful management excessive lubrication can lead to increased RCF and wheel slide during braking.

The advent of faster trains, coupled with the Eastleigh derailment findings (Department of Transport, 2021), has created the challenge for Network Rail to provide enhanced switch and crossing systems that are reliable and safe. Extensive research work has already been carried out on metallurgy by Iwnicki et al. (2006) so this thesis will focus on friction management, contact mechanics and wheel-rail interface optimisation.

1.2 Hypothesis

The author had the following hypothesis before starting the modelling-based research:

Accurate Finite Element Modelling via the use of ABAQUS and VAMPIRE software tools has the potential to create better and more efficient S&C designs for railway track. The reason behind this hypothesis is that the author believes technology can be leveraged to develop prototypes of S&C that can be tested before full rollout implementation. For instance, it is possible to predict and test the following assertions via the use of VAMPIRE and ABAQUS before commencing physical development:

- The design of S&C can be improved by applying the dynamic behaviour of rolling stock running through the track;
- Switch blade stress levels can be reduced by adding material to increase the thickness of the switch blade;
- The contact force at the crossing can be managed with efficient track properties;

Derailment risk can be reduced by establishing an effective lubrication regime.

The author will seek to address the hypothesis stated above and demonstrate its validity or otherwise with this research study.

1.3 Rationale

The interaction between rail and wheel poses a significant concern for track maintenance staff, as well as for freight and passenger operating companies for a number of reasons including, but not limited to:

Frequent failure of S&C components;

New train types running on old tracks and vice versa;

Limited land use resulting in complex designs (e.g., significant vertical curves and tight radius horizontal curves);

Running of freight trains on mixed traffic lines, especially in Great Britain;

As such, the rationale behind this thesis is to explore how the design of track geometry can be improved to provide a better wheel-rail interaction through S&C to alleviate the outlined problems and, hence, promote smooth ride quality and lower cost.

1.4 Research Outline

This thesis is organised as follows: it commences with an introduction in chapter 1 after which the author uses chapter 2 to review the work of previous researchers through which gaps in the existing literature can be explored and opportunities developed to bridge some of the gaps. A comprehensive review of switch and crossing design, performance and maintenance is presented in Chapter 3. Chapter 4 showcases the research methodology, which is broken down into three parts, namely, the mathematical implementations of FEM, ABAQUS and VAMPIRE simulations. Results and analysis are presented in Chapter 5 and Chapter 6 concludes with remarks on future work.

2. LITERATURE REVIEW AND BACKGROUND

2.1 Structure of the Literature Review

With the primary aim of developing a novel switch design that has a better wheel-rail contact behaviour, to overcome some of the S&C damage categories mentioned earlier, the author reviews the existing literature in his field of study under three major headings as follows:

- **Wheel-Rail Contact Mechanics**

  This section is used to review the classical theory of contact mechanics with a primary focus on Hertzian and Non-Hertzian models.

- **Finite Element Analysis**

  A comprehensive review of finite element modelling for wheel-rail contact is presented in this section.

- **S&C Damage Categories**

  A review of different types of damage categories associated with the S&C is presented here as well as a critical review of existing computational models adopted to capture the various damage categories.

2.2 Wheel-Rail Contact Mechanics

There has been a great deal of research effort invested in the wheel-rail interface in recent years and this has inevitably resulted in the adoption of a variety of modelling techniques. The application of contact point routines in railways generally will involve much more computational effort in S&C than for plain line due to the complexity of the S&C profiles, as well as their corresponding geometries. By contrast, most rolling contact problems (e.g., bearings) fall under a closed system where operating and modelling assumptions can be predefined with good confidence. This implies that the internal parameters for the model inputs can be reasonably fixed and will not depend on external influences. Damage simulation in this system context can be simplified in the sense that loading conditions, contact geometry and lubrication conditions can be predefined. By contrast, the wheel-rail contact interaction is a non-linear and highly complex open system, where the model inputs depend heavily on external factors to arrive at the final solution. For instance, due to the varying rail and wheel profiles, the dynamics of the vehicle, the system of lubrication to be employed (e.g., water,

dry-lube or grease) and the complexity of the geometry, it is important to monitor and evaluate the simulation continuously to obtain the correct contact forces and the associated modes of degradation of the system components.

This section will seek to address some of the techniques and to discuss their respective merits and demerits that can be used to overcome the wheel-rail contact problems and their applicability to S&C, with reference to contact point detection and material degradation.

2.2.1 Contact Stress

This section is used to review the two types of solutions which exist to solve normal and tangential stress in the wheel-rail contact system.

2.2.1.1 Hertzian Model

The classical theory of contact was first developed by Hertz (1882) where he suggested that for two non-conformal bodies of revolution, the contact area would be elliptical.

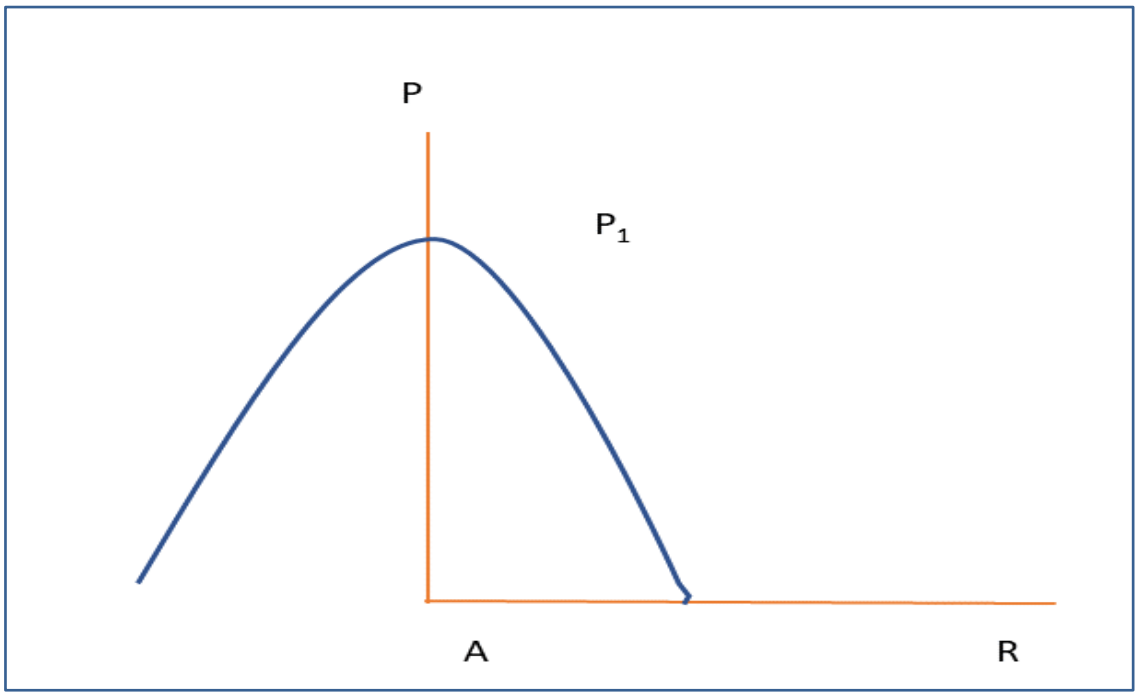

Figure 2: Profile of Pressure (Hertz, 1882)

Figure 2 shows the pressure profile of an elastic body. According to Hertz's (1882) model, for every elastic body, the distribution of pressure will produce on the surface of the elastic body a parabolic depression given by equation (1):

$$P = \frac{\mathrm{P1}\sqrt{1-(R/A)^2}}{1} \qquad (1)$$

According to Figure 2, the compressive normal force P induces contact pressure P_1. Thus, only compressive stress will occur within the contact region. Hertz's (1882) original contact theory was underpinned by the following assumptions:

Continuity and Non-conformity of Contacting Surface.

The assumption disallowed surface irregularities, to have a smooth contact surface that can be described by quadratic functions.

Elastic Half-Space Bodies;

This assumption resulted in limiting the application of Hertz's (1882) model to non-conformal contact bodies because localised contact stress was treated independently from global body stress, thus permitting a small surface contact area in relation to the overall dimensions of the contacting bodies;

Linear Elasticity (Small Strain);

The contacting bodies are to be modelled as linear elastic solids. This will result in only small levels of strain to ensure the solution is within the elastic region of the material response;

Absence of Friction at Contacting Surface.

To ensure there is no coupling between tangential and normal tractions, as well as to allow the transmission of normal pressure only between the contacting surfaces, friction was excluded from the modelling.

The Hertzian theory would have provided an efficient solution perfectly suited for modelling the railway track infrastructure. However, because of the presence of these rigid assumptions it cannot be used to address the modelling requirements of the operation of the modern railway, which is a very complex system. For example, due to the varying nature of rail and wheel profiles with associated complex geometry changes when traversing S&C, the true shape of the contact patch will be non-elliptical, creating irregular distributions of tangential and normal forces. In certain vehicle dynamics situations, it is likely that conformal contact will occur. Moreover, the inclusion of friction analysis in S&C modelling is essential. Thus, unfortunately, it is clear that Hertz' (1882) contact theory cannot be applied fully to the railway in practice, hence paving the way for more robust non-Hertzian models which can overcome some of these constraints and increase computational accuracy.

2.2.1.2 Non-Hertzian Model

Due to Hertz's (1882) assumptions outlined above, the model can only predict non-conformal wheel-rail interaction that is typically associated with contact of the wheel tread and rail head

on plain line sections. In order to assess the validity of Hertz (1882) theory, researchers have recently investigated the differences in contact results between Hertzian and non-Hertzian modelling approaches.

Kalker's (1990) variational model, also referred to as CONTACT, is probably the best-known non-Hertzian model and adopts the boundary element method. CONTACT is a model built on an elastic half-space representation of the wheel-rail contact. The model is based on the complementary virtual work principle that maximises the complementary energy or minimises the elastic energy potential in the contact area. The advent of CONTACT has helped in identifying key output elements such as contact patch size, contact shape, tangential and normal traction, slip and elastic displacements. Although a powerful tool, CONTACT is restricted to the half-space assumption and is also based on the theory of linear elasticity. As such, the model is limited to surface defect modelling, such as RCF and wear, with the exclusion of the impact of material yield on the overall performance of the contact domain. Moreover, the CONTACT model does not consider features, such as inertia effects, which are important during wheel-rail interactions at the crossing nose. Coupled with high computational times, it is very difficult to achieve the full benefits of the variational CONTACT model.

Yan & Fisher (2000) produced a model for conformal gauge corner contact between UIC 60 rail and UIC S1002 wheel profiles and this provided a surprisingly good match to FE analysis.

Wu (2011) categorised wheel-rail contact problems into two main types, namely conformal contact and non-conformal contact. Within these types, there exist different subdivisions. For instance, the conformal contact will model either roller-bearing problems or Non-Hertzian problems whilst the non-conformal contact is designed for Hertzian and non-Hertzian problems. Wu (2011) demonstrated a similar case to Yan & Fisher (2000), however, they showed that the violation of smooth-quadratic surfaces lead to about 72% errors between the normal contact pressure and contact patch area. The errors occur when there are variations in the radii within the area of the contact patch.

During a simulation for conformal contact at the crossing nose of a cast manganese crossing, Wiest (2008) demonstrated a good correlation between the CONTACT theory, elastic finite model and the Hertz model. It must be noted that some of the Hertzian assumptions were violated during the wheel-rail modelling. When non-linear material properties were modelled, the results changed significantly, leading to a reduced normal contact pressure (-42% maximum pressure) and a larger contact area (+25% longitudinal and +75% lateral semi-axes). Non-Hertzian normal contact models must be studied when considering material degradation at S&C.

2.2.3 Contact Detection Point

In wheel-rail modelling, the first thing to consider is the point of contact between the two contacting bodies. Contact detection is defined as the minimum distance between the profile curves of the rail and wheel and this detection is the commencing point of all contact problems. There can be single point contact on either the switch or stock rail and also two-point contact where one is located on either rail. As per Figure 4, the double contact point is observed at both the switch and stock rails whilst the single contact point is observed only on the stock rail.

Figure 3 shows example of single and double contact-point behaviour in S&C using sampled rail profiles arranged 50 mm apart. Two example contact behaviours from Figure 3, when simulated using Vampire Pro software, are shown in Figure 4.

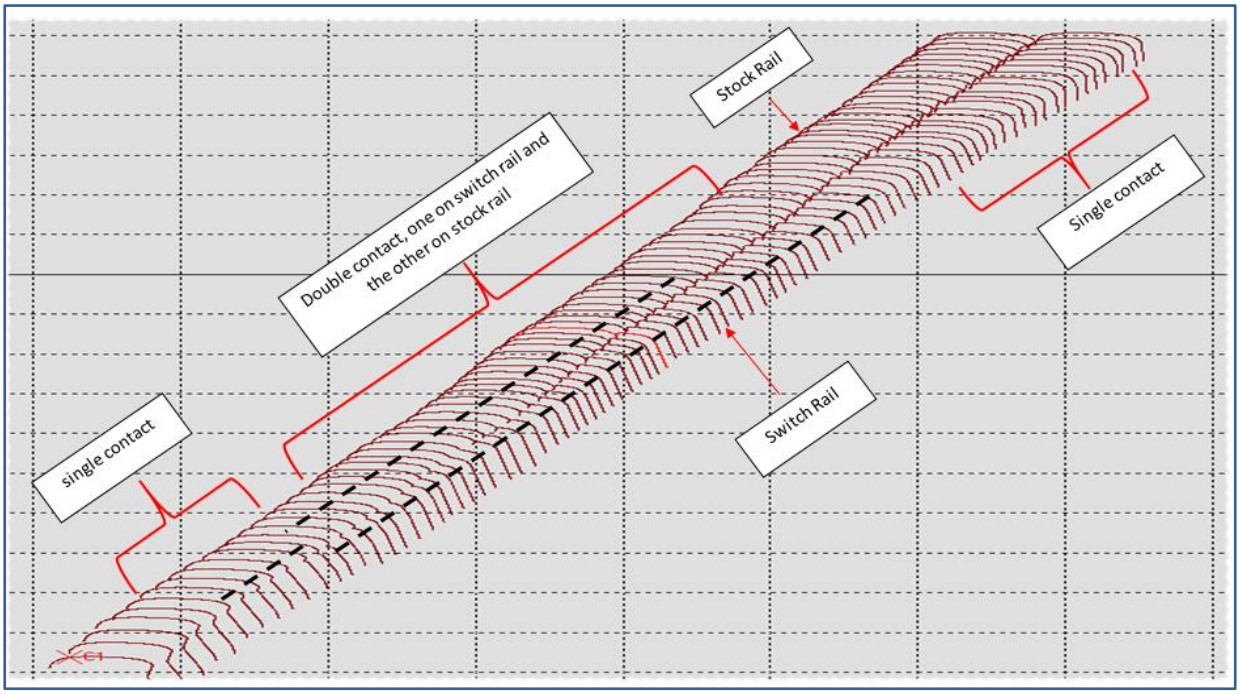

Figure 3: Single and double contact point detection using rail profiles (Arthur, 2017)

As per Figure 4, the double contact point is observed at both the switch and stock rails whilst the single contact point is observed only on the stock rail.

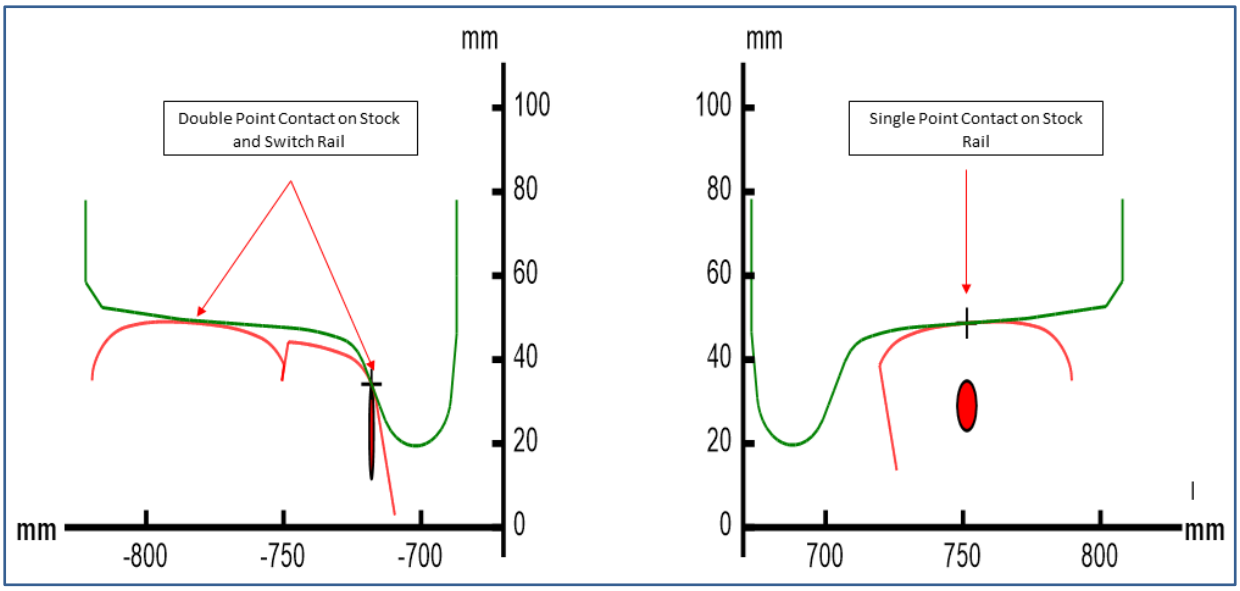

Figure 4: Single and double contact point detection in Vampire Pro (Arthur, 2017)

In assessing the detection of the contact point, Schmid et al (1994) analysed the behaviour of a bogie passing through a railway switch and evaluated the configuration of four contact behaviours, namely:

- single contact point;
- two-point contact;
- transitional contact from stock rail to switch rail;
- multiple contact points.

The results showed that some of the modelled wheel-rail contact points were outliers, that is, they occur in isolated locations along the switch and, hence, it is prudent to exclude these points, given that there is no detriment to the final results for short term analysis. However, during a long-term prediction of S&C damage, all contact points are of utmost interest, especially during conformal contact predictions. One of the processes for determining a contact point was discussed in Ayasse (2006). They suggested that a contact point is defined when the lateral shift of the wheelset is introduced only if the same parameters have been used to locate the rail and wheel profiles at their nominal position. Also, there have been attempts to find an efficient technique that can analyse any spatial wheel-rail configuration. Due to the existence of multiple contact points, the work of Pombo (2007), for example, has illustrated how highly conformal contact points invalidate the procedure.

Accurate prediction of contact point locations and associated contact stresses in any wheel-rail configuration is very important in determining material degradation within the S&C. As

such, a method capable of assessing multiple contact points in the long term will be vital in ensuring there is an accurate representation of material degradation.

2.3 Finite Element Analysis for Wheel-Rail Contact

In this section, the author will review literature on the finite element method using the ABAQUS software, with the actual mathematical implementation referred to in Chapter 4.

Finite element methods (FEM) are numerical procedures for analysing continuum and structures with complicated boundary conditions. FEM is used to obtain approximate solutions for heat transfer, solid and fluid mechanics problems. Although there had been early work under notable researchers, as reported by Larsson (2012), who modelled torsional problems with piecewise polynomial interpolation over triangular elements, it was Clough (1960) who first coined the term Finite Element. The deployment of FEM to solve complex problems is very extensive. It can be relied upon to conduct highly effective deformation and stress analysis of aircraft, bridge structures and automobile bodies. It can also be used to analyse seepage, heat and fluid flow. Closed form techniques can be used to perform simple analysis of geometric structures but, as structures and behaviours of materials become more complex, numerical methods like FEM, which are capable of discretising the structural system into nodes for a better mesh refinement, become inevitable. If the physical problem can be formulated as the minimization of a function, then variational formulation is usually adopted to perform the analysis. Otherwise, if the formulation of the problem is known as a differential equation, then the best approach is the Galerkin method, as suggested in Johnson (2009).

Performance differences between the explicit and implicit methods in ABAQUS have been compared and reported in several papers that include Rebelo et al.'s (Rebelo N., 2004). ABACUS explicit, which employs direct integration methods, is more appropriate for highly nonlinear contact problems. Although the implicit method benefits from the fact that it is unconditionally stable and can capture static and quasi-static events easily (2D), it is not efficient in performing complex analysis which requires more refined meshes (3D). Even though the explicit method has the demerit of being only conditionally stable, it is more efficient in complex non-linear analysis that involves many contact points. For instance, Telliskivi (2000) applied an implicit FE model to understand the complex behaviour of wheel-rail interaction. Similarly, Wiest (2008) used implicit FE analyses for the prediction of the normal pressure of the wheel-rail impact at the nose of a crossing. Based on the detailed stress and strain responses obtained from the FE simulations, Ringsberg (2000) used the implicit approach to predict the fatigue life of crack initiation on the rail surface. However, due to convergence difficulties, these implicit FE models failed to meet the increasing expectations of better accuracy, thus calling for the use of explicit models which can avoid

difficulties in non-linear programming. Pletz (2012) presented a dynamic Finite Element model for a wheel passing a crossing nose where the influence of operational parameters like train speeds, axle loads, stresses, etc on the rail were critically assessed. Moreover, Zhao (2011) developed a 3-D, explicit model for wheel-rail interaction which was verified against Kalker's (1990) CONTACT model and it was discovered that the variation of axle load had a stronger effect on the impacting event than any other operational parameters. Material stress states and the corresponding material responses under different levels of adhesion were investigated by Vo (2015) and it was predicted that the rail was highly prone to damage due to the ratcheting fatigue of the material.

As the Finite Element Method is undoubtedly one of the most recognised models for assessing the interactions between two contacting bodies and is flexible enough to predict their physical attributes, the author of this thesis will therefore adopt this model for the research. The model will be deployed through Abaqus software to assess the wheel-rail interface so that the modelling outcome can be validated against the work of previous researchers.

2.4 S&C Damage Categories

Sawley (2010) categorised the different switch and crossing deterioration modes in two main groups as follows:

Category 1 - Deterioration Mechanisms

- Rolling contact fatigue
- Rail and wheel wear
- Deterioration of profile
- Thermal damage

Category 2 - Deterioration Mechanisms

- Metal fatigue
- Brittle fracture

Rail damage is described as either a change in the profile section along the rail which reduces the life of the rail, or a change in the structure of the rail. Whilst rail wear occurs very slowly, mechanical deformations on the contrary act more quickly. Rail damage categories are not exclusive in the sense that they can overlap to result in more than one damage mechanism affecting a particular section of rail. This thesis will focus on the two main common forms of damage which are rail wear and mechanical deformation.

Key Performance Metrics

T-Gamma is a measure for the frictional energy dissipation at the wheel-rail contact patch. It serves as an input energy for the prediction of the RCF damage index;

The Y/Q quotient is the ratio of the vertical and horizontal force that, when exceeded for a sustained distance, can cause a derailment;

Rail Wear – Measured by T-Gamma. It represent the separation or cutting of rail steel due to friction or abnormal heavy load. T-Gamma is therefore converted to the amount of material removed from the rail per wheel / axle pass.

2.4.1 Rail Wear

The most common form of material degradation in respect of the wheel-rail interface is wear on both rail and wheel. As a result, the prediction of wear has attracted significant academic research effort over the decades. Meng and Ludema (1995) had obtained three wear models from over 5400 research studies on wear patterns that they had conducted. The models use equations based on material failure mechanisms, empirical equations and contact-mechanics-based equations.

When the wheels of rail vehicles travel on the rails, tangential forces are transmitted that cause wear. However, until sliding between the rail and wheel is high, the rate of rail wear is normally relatively low. In practice, where slip is greatest, especially in the track sections where there is contact between gauge face and wheel flange, the rate of wear will become high. A high rate of wear changes the shape of the wheel and rail quickly. In curved track, due to flange contact, the high rail normally wears until it conforms to the corresponding flange root area on the wheels. In tangent track, the crown of the rail wears to become slightly flat hence conforming to the shape of the wheels that run over them.

Predicting the wear damage will inevitably require many simulations to create a load history, thus adding to the computational complexity of an existing complex problem of S&C wheel-rail interface modelling. The work of Coleman (2004) has given insight into how Peace (1991) first implemented a simplified wear accumulation model based on the energy dissipated within the contact patch. The calculation is related to the wear index ($T\gamma$) with the loss of material volume from the corresponding profile radius. Coleman (2004) noted how good predictions were achieved during a simulation of wheel wear on a high mileage P11 profile. Li (2002) and Fries (1988) similarly discussed how the geometry of contact point, load history

(considering variations in the tangential and normal contact forces), material properties and other environmental conditions (friction) affect wear prediction and hence advised their inclusion in any chosen model during rail and wheel wear prediction. More recently, Braghin (2006) in his approach to wear prediction obtained a discrete distribution of wear in a process involving Hertzian normal contact solution. Based on experimental twin disc tests, he developed a wear law, and this was implemented within an overall routine for wheel profile evolution. At each time step, the depth of wear was then summed up before updating the wheel profile at a frequency related to a maximum accumulated wear depth threshold.

2.4.2 Rolling Contact Fatigue (RCF)

According to Burstow (2003) RCF describes the phenomenon where cracks grow over time due to contact stresses between the rail and rolling wheel. For RCF to occur, both tangential and normal stresses are required. Along the gauge corner of the high rail, head cracking (gauge corner cracking) occurs, which is referred to as quasi-continuous RCF. Quasi-continuous RCF is usually associated with poor transverse profile, high traction forces or tight gauge that forces the wheels to travel along the gauge corner of the rail, thus resulting in high contact stresses. The force applied to the high rail is directed towards the inside of the curve and the angle of crack mouths on the rail reflects the angle of the force which initiated the crack. Gauge corner cracks commence at the surface of the rail and then penetrate into the head of the rail at an angle of about 20° to the running surface. Hydraulic entrapment then occurs where water and lubricant penetrate into the crack. Cracks can turn downward, and this can cause the rail to break due to compressive residual stress. The trouble is that there are usually many cracks, hence the consequence of potentially more than one rail break along a section of the track, as experienced at Hadfield on 7 October 2000. On the other hand, spalling occurs when the cracks continue along the rail to join other cracks with the metal falling out. In the absence of liquids, gauge corner cracking remains superficial in the sense that it will not continue to develop after the first few millimetres into the rails.

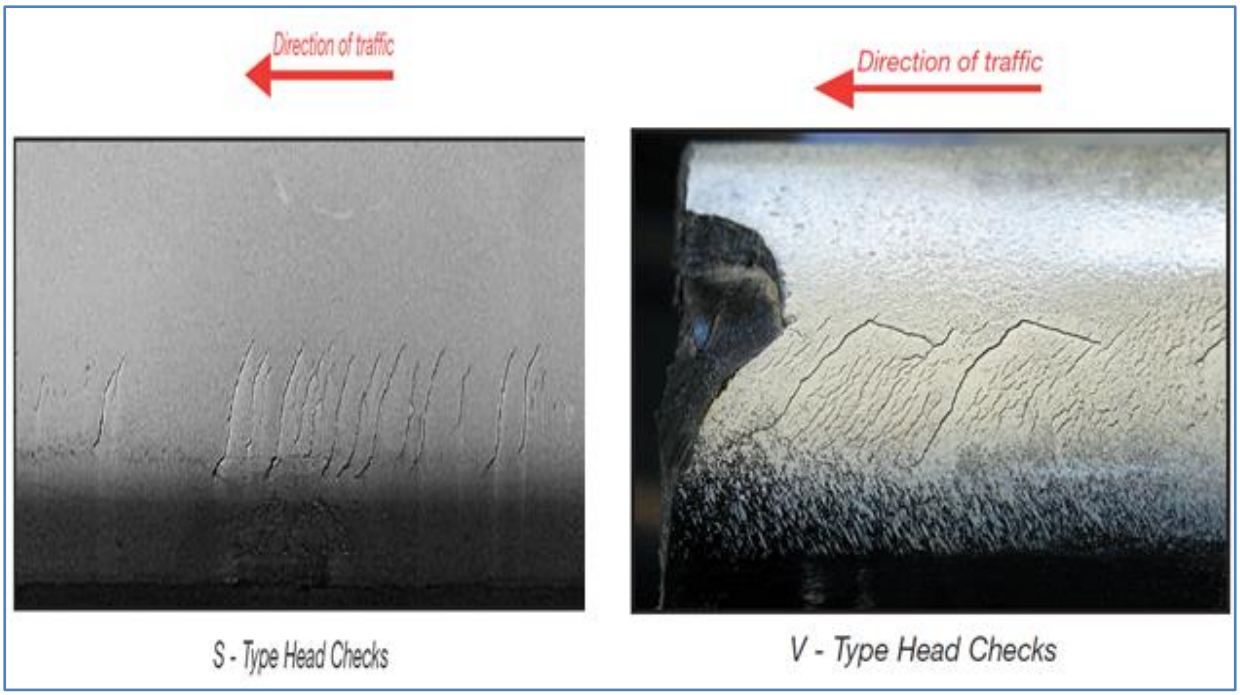

Figure 5: Different Types of RCF Cracks (Network Rail, 2014)

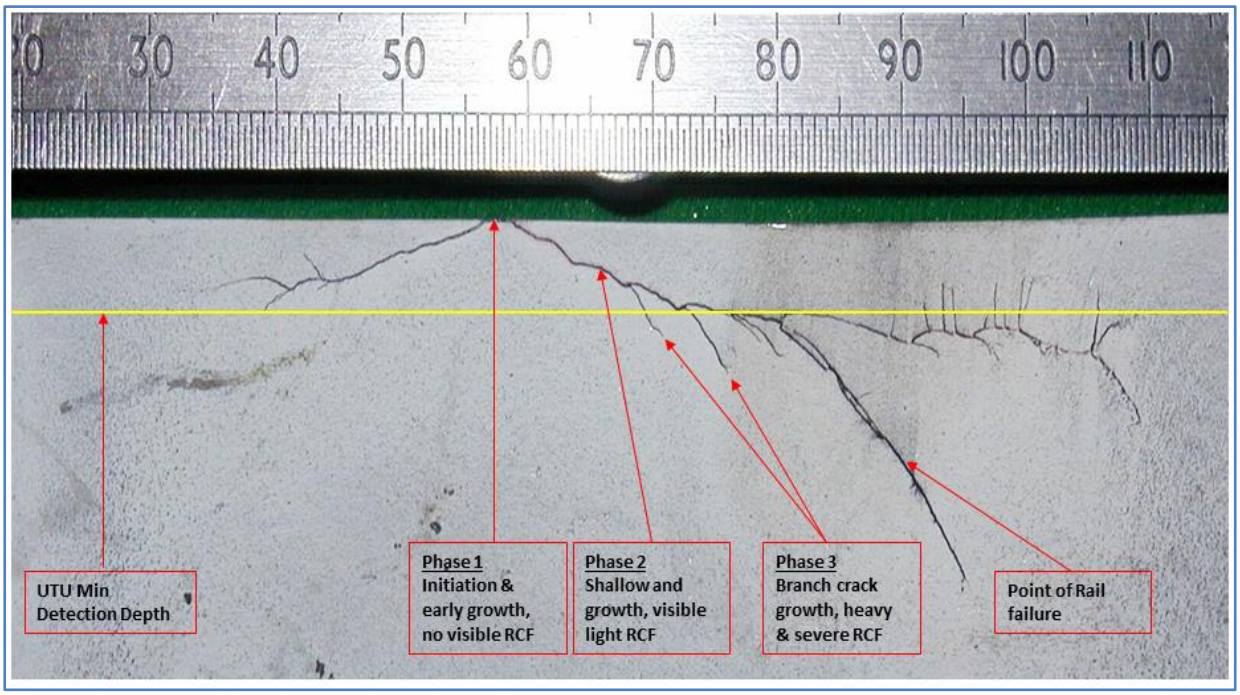

Figure 6: Phases of RCF Leading to Rail Failure (Network Rail, 2014)

The available literature has grouped the RCF prediction models into two categories, namely, models based on empirical studies and models based on theoretical studies. Whilst empirical models relate to modelling outputs of events using experimental measurements in order to predict the likelihood of the event occurring, theory based models attempt to predict the likelihood of an event. Depending on the type of problem they are applied to, both models

have their own merits and demerits. With sample test results, examined with back-scatter-electron microscopy, optical and electron scanning, good quantitative agreements were achieved by Frolish (2002) who discussed a new model for predicting RCF growth, as well as branching of RCF cracks. Fletcher and Beynon (1999) published a method for predicting stress intensity factors that lead to fluid-pressurized inclined surface cracks which are similar to rolling contact bodies. They subsequently presented developments of an advanced twin-disc test rig for investigating the physical processes taking place during rolling contact fatigue in Fletcher and Beynon (2000), against which much of the development of numerical methods has been validated. Burstow (2003) presented empirically based studies as part of the Whole Life Rail Model (WLRM) which has become an industry benchmark model for predicting RCF. The study compared a variety of parameters obtained from rail vehicle dynamics simulations of two sites with known RCF problems, Ruscombe and Acton. Results from the study revealed that the wear number Tγ (contact energy), gave the best correlation between crack location and RCF damage simulation.

Schmid et al (2010) summarised the factors controlling the development of cracks within the rail both in terms of the shape and the rate of growth as:

- contact stress between the wheel and the rail;
- vertical and bending stresses induced as vehicles roll over the rail, which are a function of the vehicle characteristics, rail section and support conditions;
- metallurgy of the rail material;
- entry into surface cracks of flange lubricants, friction modifiers or water;
- state of residual stresses in the rail head, which are a function of the manufacturing process, methods of rail installation and rail temperature.

The most widely accepted treatment of quasi-continuous RCF is routine reprofiling of the transverse profile of the rail to remove short cracks and also to unload critical areas of the rail, such as the gauge shoulder.

Sawley (2010) characterised RCF defects as squats and shells. Squats are sometimes referred to as ‘black spots’ because there is a depression of the rail which is dark in colour above the crack. Black spots initiate when pieces of hard material get trapped at the wheel-rail interface and then cause the growth of cracks. Black spots tend to occur along the running band of the rail crown. They can be detected by running a finger along the sheared surface area. Shells, by contrast, are RCF defects that initiate a few millimetres below the gauge corner of the high rail. A fatigue crack initially will propagate just parallel to the rail below the gauge corner and

then penetrate downwards into the rail to create a transverse defect which is similar to those seen in squats.

2.4.3 S&C Simulation Benchmark Studies

In August 2019, it was announced during the IAVSD conference held in Sweden that, since S&C can be considered as 'hungry assets', then the need for benchmark studies based on the power of simulation tools will help alleviate most of the problems before bringing them into use. According to Björn et al (2023), the focus of the benchmark has been on establishing the general interaction forces while comparing the methods used to represent the varying rail shapes. It was a pure simulation exercise where simulation results were compared to one-another and the kinematic motion of the wheels relative to the rails was one of the main ways to verify and compare modelling approaches. Participants were given the task of modelling separately the switch panel and the crossing panel for two different S&C designs of different length and to simulate dynamic vehicle-track interaction in those panels. Input data was provided in the form of track layout, rail discrete cross-sections at specific positions, while the track properties were represented using co-running track models with specified properties for each panel (Björn et al, 2023).

Dixon et al (2023), in their effort to study the dynamic behaviour of railway turnouts during the passage of trains, proposed a three-layer co-running track model which is a multi-body dynamic model with space-dependent track parameters for analysing the dynamic behaviour of railway turnouts. They applied it to a UIC60-760-1:15 turnout with curve radius 760 m and turnout angle 1:15. Equivalent track properties were then introduced, based on the turnout track flexibility, and the rail receptance and impact force results were compared with the results from a finite element (FE) model. The validation results showed a good agreement with those of the FE model, but with far less computational expense in terms of power and time. The new model is found to capture the dominant dynamic behaviour of the turnout across all frequencies up to 2000 Hz. The results have shown that consideration of higher frequencies is important due to the nature of dynamic forces affecting the crossing region and high-speed cases (Dixon et al, 2023).

Vehicle-track interaction in a switch panel diverging route was studied under Sebès et al (2023) with a focus on the way its components may interact in the lateral direction. Taking one of the cases of the S&C benchmark as the base model, several variants of the co-running

track model were considered. In the first series of simulation, the effect of the lateral separation of the switch rail and stock rail was investigated, with only small differences being found in terms of wheel-rail forces between a track model where both rails are coupled, and one where they are free to move with respect to one another. Only transient effects are visible at the beginning and at the end of the two-point contact on both rails. While small, these differences can have some influence in terms of rolling contact fatigue and wear prediction. The results showed that there was a sharper increase in flange contact due to the rigid connection in the lateral direction. It was also shown that locally these higher transient effects can lead to increase in the wear prediction as well as slightly different contact energy prediction on the stock rail (Sebès et al, 2023).

Björn et al (2023) compared track model formulations for the simulation of dynamic vehicle-track interactions in switches and crossings (S&C, turnouts) in a multi-body simulation (MBS) environment. Their investigation was an extension of the S&C simulation benchmark with the addition of a finite element model of a 60E1-760-1:15 turnout. The simulation constitutes a common reference from which four different track formulations were derived: co-running, modal superposition and finite element incorporated into the MBS model and finite element coupled to MBS using a co-simulation approach. The results showed that the switch rail carries the largest lateral force, when it is in hard flange contact with the wheel. Convergence was achieved at higher frequencies beyond 750 Hz. The results for the diverging route demonstrate a more complex behaviour than for the switch panel. Due to the curve in the diverging route the outer wheel has an extended simultaneous contact with the switch and stock rail.

The author of this thesis has found the research work in the S&C Benchmark Studies of 2023 to be useful confirmation to his work for this thesis. Through the S&C Benchmark Studies, the author has been exposed to simulation tools in addition to those used in his thesis as well as the correct methodology and approach to use in order to capture the dominant dynamic behaviour of the turnout across all frequencies, as discussed in Dixon (2023), or how to achieve convergence of the FE model in Björn et al (2023). Through the S&C Benchmark Studies, the author has gained insight into how important it is to choose the correct simulation tool for S&C modelling as the outcome of enhancing S&C performance is also largely dependent on the software used to do the analysis.

With regards to simulation tools for the research, careful thought was given to the advantages and disadvantages of the various software packages available. Table 1 presents some of the most commonly used simulation tools for similar research work. The author's choice of Abaqus and Vampire simulation software was based on the fact that Abaqus Explicit shows a true representation of FE modelling and that Vampire, apart from the fact that it is industry best practise, Vampire Pro was used as the standard simulation software package at Network Rail Ltd. Although the author would have wished to follow the path of Dixon (2023) who used a method that required less computational time, the licensing requirements for the simulation tools available limited him to Abaqus and Vampire.

Tools	Merits	Demerits
Finite Element in Abaqus	• True representation of FE modelling • Allows for full FE detail modelling capability • Allows for the utilisation of an existing FE model without further modification	• Computationally demanding for complex problems
Finite element in Co-simulation	• True representation of FE modelling • Allows for full FE detail modelling capability • Allows for the utilisation of an existing FE model without further modification	• Computationally demanding
Vampire Pro	• Industry best practice in the UK • Low computational effort • User friendly	• Does not support complex FEA analysis
Co-running	• Low computational effort	• No physical interpretation of track response below the rail level • Requires tuning to target global track behaviour.
Finite element in MBS	• Low computational effort	• Computationally demanding
Network Rail Track-Ex	• Low computational effort	• Cannot handle complex numerical problems • Static application

Table 1: Merits and Demerits of Different Simulation Software

2.5 Discussion Points on Literature Review

To the author's knowledge, there exist many models for wheel-rail contact but none on its own is sufficient do address the current damage mechanism that occurs at the contact point within the S&C. For instance, the prediction of contact patch size and shape via the Hertz (1882) model would be misleading due to the violation of the model assumptions because of the varying nature of S&C switches. Conversely, although the Non-Hertzian models similarly face the challenge of satisfying the requirements for accurate long-term prediction of rail damage at S&C, these model tend to overcome the challenges and or assumptions faced by the Hertzian model.

In summary, there has been significant progress in the field of Finite Element simulation of wheel-rail interface behaviours, from which valuable insights have been gained. However, there is still much work to be done in this research field. For instance, when using implicit analyses, there are gaps in the wheel-rail interface representation which create divergence problems. Similarly, unexpected failures can occur when using the explicit Finite Element model. Moreover, visualisation-based discretisation of the potential contact area could also lead to a mismatched, insufficient or redundant Finite Element meshing, due to a-priori unknown contact locations. Some of these problems have been resolved more recently. Coleman (2004) used a novel coupling strategy that combines the two-dimensional geometrical (2D-Geo) contact analysis and the three-dimensional explicit finite element analysis to improve the performance of Finite Element simulations.

The author of this thesis seeks to address some of the challenges identified here and to model a novel switch that will improve wheel-rail contact specifically for Network Rail, as the company embarks on the revolution of standardising S&C with a new NR60 MK2 series.

2.6 Gaps in the existing Literature

From his comprehensive review of the existing literature, the author identified the following knowledge gaps:

- Existing S&C studies rely heavily on Multi-Body Simulation (MBS) tools to predict S&C damage mechanisms. However, there is a gap in the literature available for this study since S&C damage appears to increase every year in Great Britain, resulting in high maintenance cost. The current process of S&C studies either focuses on vehicle dynamic simulations or evaluation of S&C material strength. It is therefore clear that none of these studies has fully explored the benefits of simulation tools or that the representation of wheel-rail contact models is sufficiently accurate for S&C analysis. There is therefore an opportunity to embark on a different process of S&C studies, which combines both vehicle dynamic simulation and material strength analysis to develop a novel switch that will provide a better wheel-rail contact model, able to offer new approaches to reducing the severity of the impact of the current S&C damage mechanisms.
- S&C degradation is of paramount interest within the railway infrastructure. However, there is a lack of literature assessing the effect of adding or removing part of the S&C steel material on the contact performance with respect to impact forces,

material performance and degradation. Therefore, this presents an opportunity for the author to develop a novel switch that will provide a better wheel-rail interface capable of minimising some of the existing S&C damage mechanisms highlighted in section 2.4 of this thesis. The author seeks to achieve this by adding additional steel material to the switch and crossing nose.

2.7 Opportunities Identified

Many opportunities for improvements have been identified within the literature review but it will not be possible to address all of these in the present research. The focus of this thesis is to bridge the following knowledge gaps:

1. Remove some of the limitations by developing a novel switch that provides a better wheel-rail contact interface.
2. Embark on a different simulation trajectory to develop a novel switch. This will be achieved by a combination of simulation tools such as Vampire Pro and Abaqus. The Vampire work will focus on vehicle dynamic simulation whilst the S&C material strength evaluation will be carried out through the Abaqus software.

These two opportunities will help provide a parallel study that will focus on detailed wheel-rail interaction through the S&C where the author seeks to acquire new knowledge on contact trajectory, material performance and degradation.

3. SWITCH AND CROSSING DESIGNS & PERFORMANCE

3.1 Switch and Crossing Mechanics and Maintenance

S&C allow railway network operational flexibility by enabling vehicles to be directed from one track to another. There are many different S&C layouts and a comprehensive guide can be found in (Cope & al., 2002). To fulfil different traffic demands, the railway uses many types of turnouts which feature straight and diverging routes. A typical turnout commences with a switch panel and a closure panel that joins the switch panel to the crossing panel, then another closure panel that links the crossing panel to the plain line tracks. The switch panel accommodates the switch blades and is the start of the deviating curve. This panel includes actuators that position the switch rails for the required route. The crossing panel permits the wheels to travel along the intersecting rails, hence there is wheel transfer at the crossing nose. This is the location where the highest impact loads occur. To avoid interference contact between the crossing nose and the wheel, check rails are positioned adjacent to the so-called stock rails to constrain the lateral position of the passing wheels. The rail profiles for turnouts feature discontinuities which increase the dynamic loading during wheel passage when compared to the rail profiles of plain line track. As a result, higher levels of track degradation are associated with railway turnouts. Figure 7 shows illustrates an example of a railway turnout.

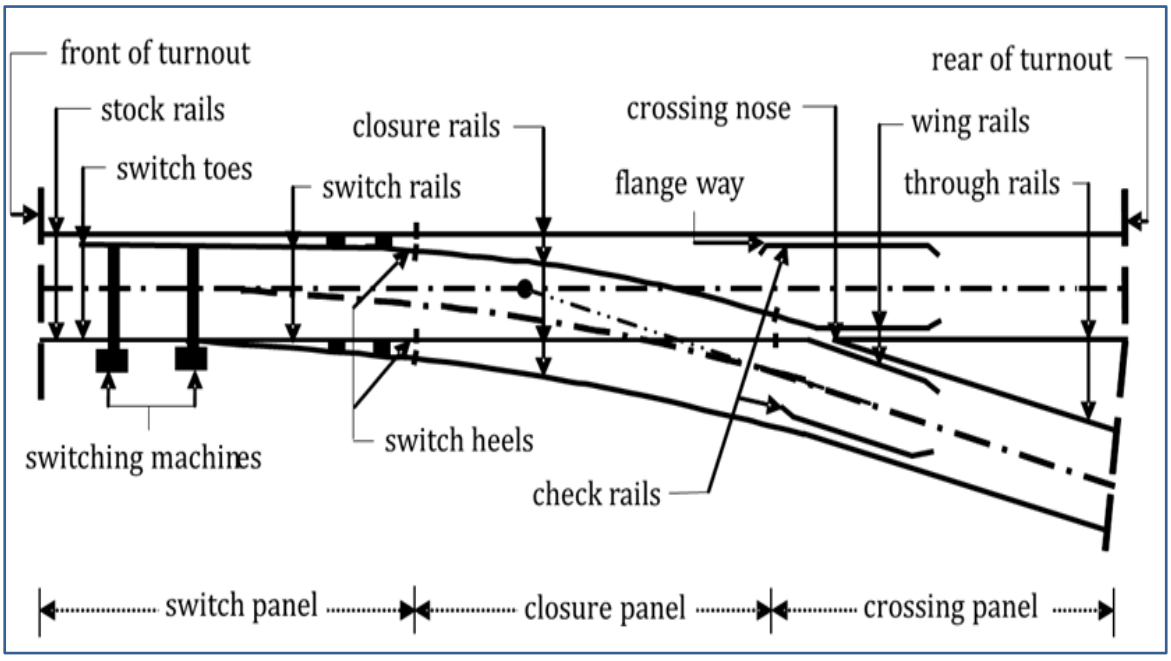

Figure 7: Common Railway Turnout (Network Rail, 2014)

S&C elements play an essential role in connecting the rail network. They are used to guide the train from one line to another hence, they are the junctions that allow the creation of multi-line or multi-routed rail networks. Figure 7 shows the three parts to every S&C which

are the switch panel, closure panel and the crossing panel. The switch panel starts from the switch toes (Figure 7) to the last weld abutting the closure panel. The switch is the moveable part of the S&C layout and consists of long blades that guide the train one way or the other. The non-moveable part is the stock rail. The two switch blades are held together by a stretcher bar to ensure when one side of the switch blade is against the stock rail, the other side is fully clear, so as to provide room for the wheel flange to pass through freely. There are many types of S&C such as turnouts, diamond crossovers and slip-diamonds currently being used in the railway network but the type to use depends on many factors, such as line speed, frequency of use, and the number of tracks. For instance, a high speed track will require a longer switch than a low speed track.

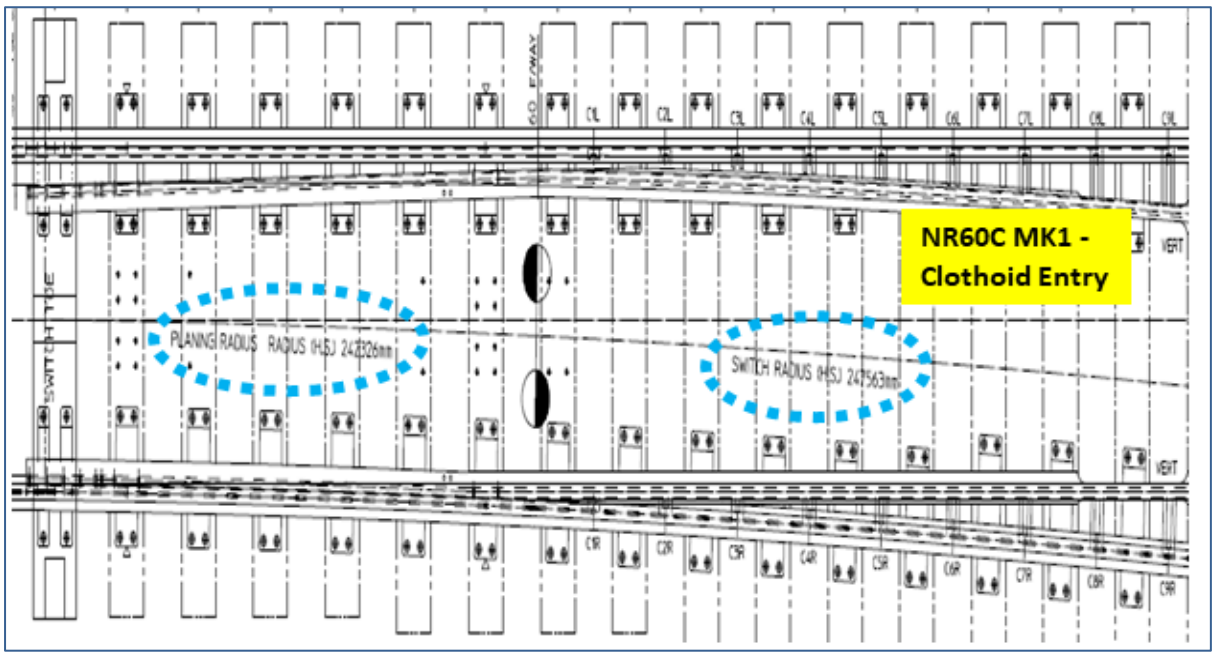

Figure 8: NR60C MK1 Switch Showing Clothoid Entry (Network Rail, 2017)

Figure 8 shows the switch panel of the existing NR60 MK1 design. This switch panel has a jerk inducing effect on the vehicle due to the clothoid entry into the switch which causes problems. With this switch panel, the switch toes sit on a transition followed by a radius and another radius thus causing a reduced lateral ride quality.

Railway maintenance activity is based around track categories and inspection frequencies. The track category was originally fixed as a means of assessing problems on the track with the associated maintenance intervention level required to address degradation. Figure 9 illustrates the track category matrix currently used by UK infrastructure maintainers, and this has been extracted from (Network Rail, 2002).

Track categorisation is a very complex subject which is governed by Network Rail standards and requires detailed design calculations. Factors used to assess the category of a section of track are the annual tonnage, equivalent tonnage and line speed. Long distance routes are characterised by highs speed and fewer stops whilst short distance routes are governed by low speed and frequent stops. Annual tonnage is therefore dependent on the traffic type taking into consideration the type of train that moves over the line. Equivalent Million Gross Tonnes per Annum (EMGTPA) is derived from the annual tonnage and measures the overall load and resulting degradation of the track for both passenger and freight vehicles. Freight vehicles are assigned a larger EGMPTA because of their greater impact on track degradation, largely due to greater axle loads and less effective suspension systems. Figure 9 illustrates the track category matrix currently used in Great Britain.

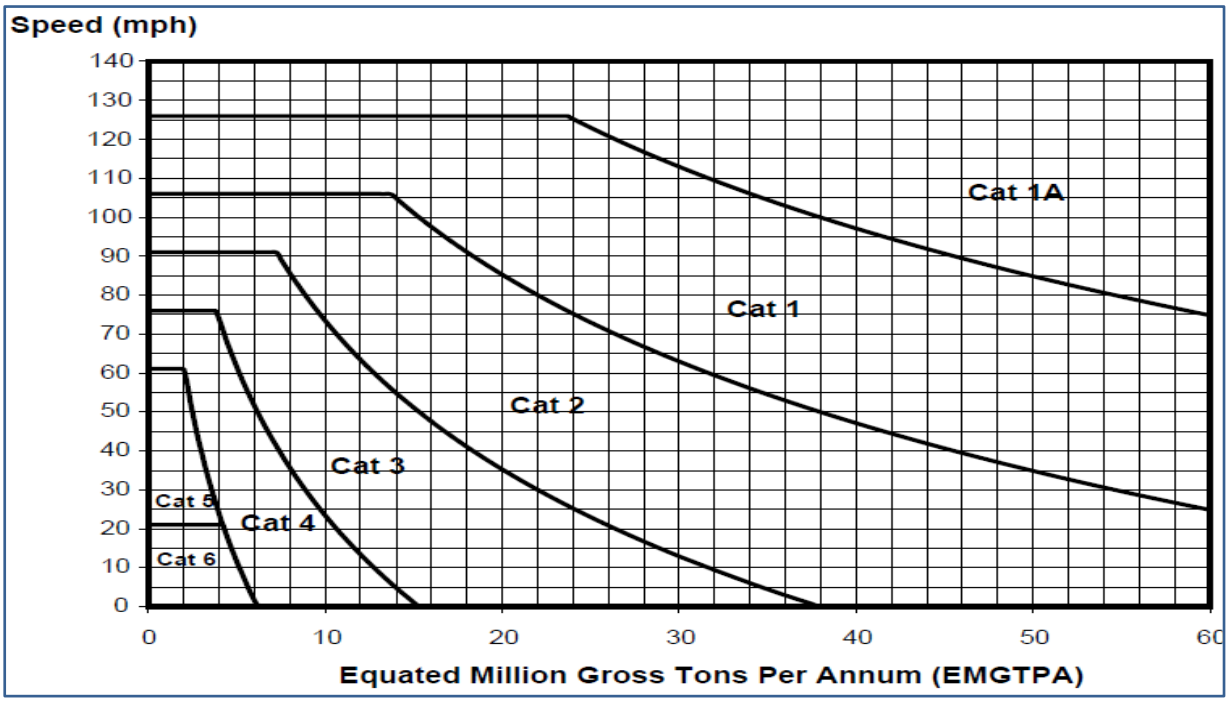

Figure 9: Track Category Matrix Railtrack Company Standard, (Network, 2009)

There are three sections to the track category matrix in Figure 9. The vertical axis of the matrix denotes the speed of the types of traffic and the horizontal axis plots the EMGPTA. The curved sections are used to assign a track category. This category specifies the likely damage to the track caused by EMGPTA for a particular route. EMGTPA measures the tonnage effects of both freight and passenger vehicles on the overall degradation of the track. Track category 1A is for the route with the highest speed (e.g., routes used by Eurostar and High Speed 1 trains) and category 6 is for low speed routes like sidings. Track categories are reviewed annually and updated to take into account revised traffic flows and new train timetable services. After assessing the track category in which the switch and crossing resides, the minimum inspection frequencies are obtained.

Table 1 shows inspection regimes tabled for switch and crossing assets in Network Rail. The striking common feature in the table is that whether the S&C asset is strengthened or not strengthened, S&C inspection engineers must carry out more frequent inspections on high speed routes than on low speed routes.

Track Category	Visual Inspection for Strengthened S&C	Visual Inspection for Non-strengthened S&C	Supervisory Visual Inspection
1A	Once A Week	N/A	5 Weekly
1	Once A Week	Twice A Week	8 Weekly
2	Once A Week	Twice A Week	8 Weekly
3	Once A Week	Once A Week	13 Weekly
4	Once A Week	Once A Week	13 Weekly
5	Once A Week	Once A Week	13 Weekly
6	Once Every 2 Weeks	Once Every 2 Weeks	13 Weekly

Table 2: S&C Inspection Frequencies (Network Rail, 2014)

S&C units are complex infrastructure assets, both in terms of their operation and design. Different rail inclinations, high impact loads, rail cross section variation and sudden changes in track curvature are among the factors that present significant challenges to the already complex S&C units. The rate of track degradation tends to be higher in S&C than in plain line. With the combination of additional complicating attributes of rolling stock, such as axle-load, speed etc, the situation has become a non-linear process which presents an important risk to the industry. Thus, there is the need for a robust maintenance regime to sustain its efficiency and effectiveness.

Unfortunately, the current industry practice is to embark on a ‘search and fix’ infrastructure maintenance philosophy, thus resolving failures as they occur, instead of monitoring progressive degradation and/or predicting where and when asset maintenance should take place. Attention given to each unique S&C unit is ignored when S&C inspection and maintenance are carried out in this manner. To improve the efficiency of S&C deliverables, there is therefore a need to move away from the current ‘search and fix’ approach to a more proactive ‘predict and prevent’ strategy. To achieve this objective, each type of S&C unit must be modelled as a complex non-linear system, an example of which the author aims to achieve in this research.

3.2 Curving Behaviour of Railway Vehicles

3.2.1 Rolling Radius Difference (RRD)

The RRD is one of the main features of wheel-rail contact that defines the behaviour of a wheelset on a track. An appropriate RRD between the wheels of a wheelset is required to pass over a curved track without slippage between wheels and rails. As noted in Schmid (2010), when the wheelset is centrally positioned with respect to the track, then the rolling radius of the right and left wheelset are the same. A lateral displacement of the wheelset from its midpoint relative to the rails causes an instantaneous rolling radius difference between the right and left wheelset. The rolling radius at the wheel-rail contact point decreases as the wheelset moves away from flange contact and will conversely increase as it moves towards the flange. During this movement, the leading wheelset will roll towards the outside curve whilst the trailing wheelset rolls forward towards the inside of the curve. This behaviour results in a difference in the rolling radii of the two wheels. The development of a RRD generates creep forces that attempt to steer the wheelset into radial alignment with the rails.

If wheelsets were to be free, then anytime they negotiate a curve, an equilibrium rolling line can be achieved at the point where the ratio of the lengths of both rails are equal to the rolling radii of inner and outer wheels. Unfortunately, conventional wheelsets are attached to a bogie frame by the primary suspension and hence do not move freely. As such, the suspension will ensure the wheelsets are aligned with the bogie frame.

3.2.2 Primary Yaw Stiffness (PYS)

In railways, the curving behaviour is influenced by a number of factors, including RRD, the wheelbase and bogie centre distances of the rolling stock, the limiting friction force, curve radius and flangeway clearance. Obviously, primary yaw stiffness also has an effect on the curving behaviour in the sense that the steering forces needed to rotate the wheelset into the radial position are directly proportional to this stiffness. The amount of creep forces required to rotate a wheelset into its radial alignment depends on the yaw stiffness of the primary suspension and the angle to be overcome. Where wheelsets are to curve free of any flange contact, the 'normal' situation, then a RRD is required to generate the steering forces between the wheel and rail to rotate the wheelsets against the primary yaw stiffness and into radial alignment with the curve. Since steering is resisted by the primary yaw suspension, then any attempt to reduce the PYS will have a positive impact on curving behaviour and, hence, improve the wheel-rail contact. As the curve radius tightens, the steering forces needed to maintain the radial alignment increase. This can be achieved by the wheelset moving further from the equilibrium rolling line, thus increasing the rolling radius difference and consequently the longitudinal creep forces. However, there is a practical limit to the minimum

stiffness of bogies which imply no bogie can steer effectively around the tightest curve, without flange contact. An appropriate level of yaw stiffness is also required at high speed to maintain stable operation. An insight from Schmid (2010) explains that an improved bogie, where the trailing wheelset moves closer to the outside, will reduce the angle of attack to be overcome by the steering at the leading wheelset and consequently reduce the total force at the leading wheelset where most of the wear and RCF damage occur.

Remarkably, although it is important to use bogies with soft PYS, the presence of a soft PYS alone will not guarantee a perfect curving behaviour as the wheelbase also has to be taken into consideration. The curving behaviour demonstrated in Schmid (2010) illustrates how a balance must be achieved between the wheelbase and PYS. The work mentioned showed poor curving behaviour under the conditions of soft primary yaw suspension and long wheel-base. Conversely, the shorter wheelbase with a stiffer primary yaw suspension produced a good curving behaviour. This is because bogie vehicles have a more flexible secondary suspension than primary suspension and thus, when the same curving principles are applied, the vehicle with a short wheelbase will be able to steer successfully round the radius of a curve irrespective of the fact that the leading axle has moved close to flange contact. The fact remains that, there will still be significant lateral forces towards the outside of the leading wheelset and the inside of the trailing wheelset, although the net lateral force at balancing speed is zero. As a result, the direction of steering forces will be reversed because the trailing axle has been pushed outwards and beyond the equilibrium rolling line. Paradoxically, the pattern of wear can vary significantly with the type of vehicle and route. As such a straight route will lead to tread wear whilst a route with tight curves or bogies with a stiff yaw suspension can cause high flange wear to predominate.

3.2.3 Conicity

Evans et al. (2010) define conicity as the change in wheel radius as a function of the lateral shift of the wheelset relative to the track. Conicity is an important factor which determines the running stability of vehicles. In the UK, conicity measurement assumes that the lateral position of a wheelset will vary in accordance with a normal distribution about the zero-shift position. A weighted best-fit line is then calculated to the slope of the RRD graph where a standard deviation of 2.5 mm is quoted out of three values of standard deviation of the distribution. The conicity of a pure coned wheelset is equivalent to the cone angle hence a 1:20 coned wheelset will have a conicity of 0.05. For worn wheelsets with hollow treads, a linear approximation to the nonlinear slope is defined, which is the equivalent conicity. The critical speed of railway vehicles above which they will suffer hunting instability is determined by the (1) primary yaw stiffness in the yaw and lateral directions and (2) conicity. The higher the conicity the lower the critical speed. High secondary yaw damping, primary yaw and

lateral stiffness are required in order to maintain stability levels with high conicity but, unfortunately, high PYS generates high RCF and wear damage in curves. Similarly, under low conicity when the car body yaw frequency coincides with the kinematic frequency of the wheelset, body hunting sets in, which is a form of instability. Some of the conditions that will tend to increase conicity include increased hollowness of wheel tread, tight track gauge (rolling radius close to flange), flat rail crown and reduced rail inclination (wheel rolling on gauge corner).

Serial No.	Parameter Range	Type of Conicity
1	< 0.15	Low
2	> 0.15 < 0.30	Medium
3	> 0.30	High

Table 3: Levels of Conicity (Network Rail Company Standard NR/L2/TRK/001)

Table 2 illustrates the range of conicity levels permitted on the GB railway network. It is worth noting that:

- A high conicity value is required to counteract the curving forces on curved track, however, it produces periodic movement on straight sections which is capable of reducing ride comfort;
- A low conicity improves ride quality, but it can create contact between the rail gauge face and the wheel flange on curved tracks thus producing excessive wear for both wheel and rail.

3.3 Problems associated with the existing RT60/NR60 MK1

During its inception, Network Rail Ltd employed four S&C manufacturers, namely, Balfour Beatty, Corus Cogifer, VAE and Edgar Allen to design the RT60/NR60 MK1 S&C, thus giving rise to four different designs as each designer took a different approach within the common design principles. The intention was to select one design after a series of trials. The common design philosophy was based on inclined rail, CEN 60 rail section, 30 tonnes axle load capacity, 140 mph speed capacity, common crossing footprint and the use of ball and claw[3]. For instance, whilst Balfour Beatty used concrete bearers with direct fastenings and dummy cast baseplate to provide rail inclination, Corus Cogifer focused on the use of plastic wedges for rail inclination and Pandrol e+ direct fastenings. The VAE design was later modified to the

[3] Ball and Claw refers to a mechanism that limits the movement of the switch rail with respect to the stock rail, see **Error! Reference source not found.**.

Edgar Allen design and selected as the preferred NR60 MK1 design. Under this design, the switch was base-plated throughout with spacer blocks between the base plates and fastening being via the use of Vossloh type screws only. The type of point operating equipment adopted for the NR60 switch was HyDrive. Installation of the Edgar Allen NR60 MK1 switch and crossing designs commenced in 2000.

A typical example of an Edgar Allen NR60 MK1 switch layout is shown in Figure 9. The switch is characterised by ball and claw for creep monitoring, spacer blocks between the rails, in-bearer clamp, tubular stretcher bar and many more features.

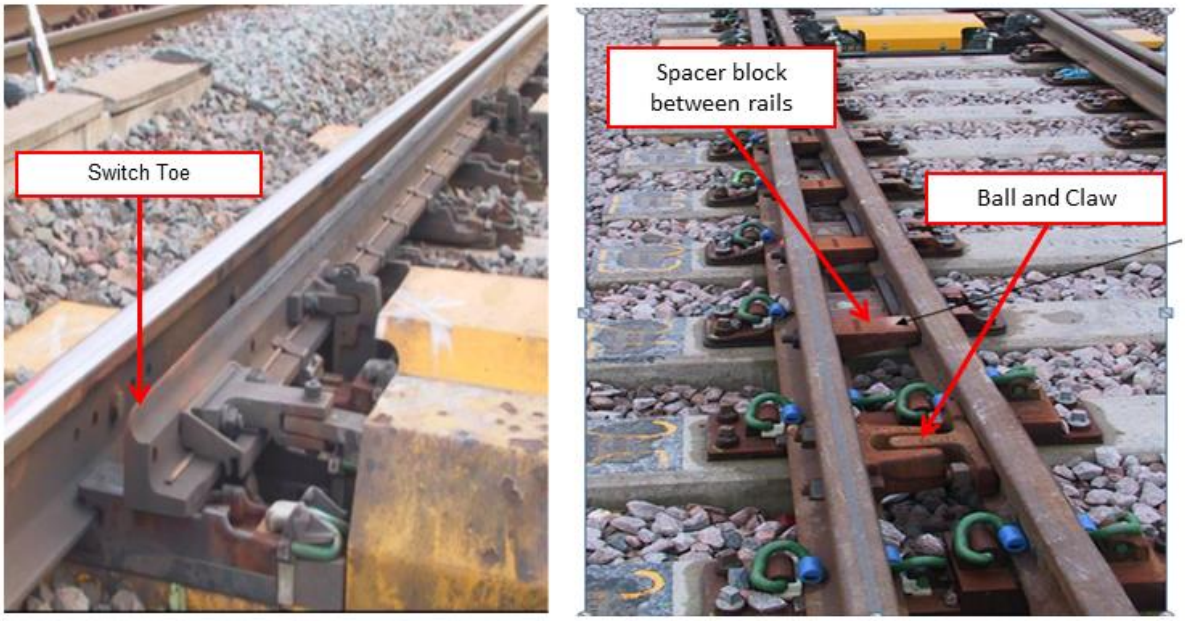

Figure 10: Edgar Allen adapted NR60 MK1 Switch Design (Hsu, S.S., 2014)

After a few years in operation, the switch and crossing started to experience problems. To begin with, switch wear appeared frequently and is more pronounced at the switch toe due to the fact that wheel-rail contact occurs very close to the switch tip. A groove normally commences at the back of the switch and is often followed by a crack. Most of the NR60 MK1 switches have lost their shape due to these problems and require frequent maintenance interventions. Investigations have similarly revealed that the use of Schwihag slide baseplates loses its effectiveness as the plain phosphor bronze inserts securing pins are driven out through the application of high impact loads over time. Hsu (2014) illustrated that the problem of switch wear has been exacerbated by the geometry of the trailing move and, despite changes being made to the sequencing of machining, this problem still exists, especially with similar flexure curves. The situation with respect to the cast crossings is no different from that of the switch as the crossings on RT60/NR60 MK1 concrete layouts are failing every 5 to 10 years. Data taken from Hsu (2014) shows 823 crossing defects cases were opened between November 2012 and November 2013 for the Wessex route alone. Out of

this, only 207 crossing defects cases were closed in that year leaving, 616 cases open to be cleared the following year, on top of any new cases. This clearly demonstrated the importance of a new, more robust design.

Although NR56 S&C was initially designed as an alternative to the RT60/NR60 S&C suite, unfortunately, this type of S&C is not TSI compliant[4]. Moreover, it has its own inherent problems not dissimilar to those of the NR60 MK1 switches. Under these circumstances, it is clear that NR has to keep a high but unsustainable maintenance budget in order to service/replace the failing RT60/NR60 switches and crossings. Thus, the quest for a more robust S&C design which is capable of overcoming these issues was essential. **Error! Reference source not found.** shows examples of the extent of rail damage associated with NR60 MK1.

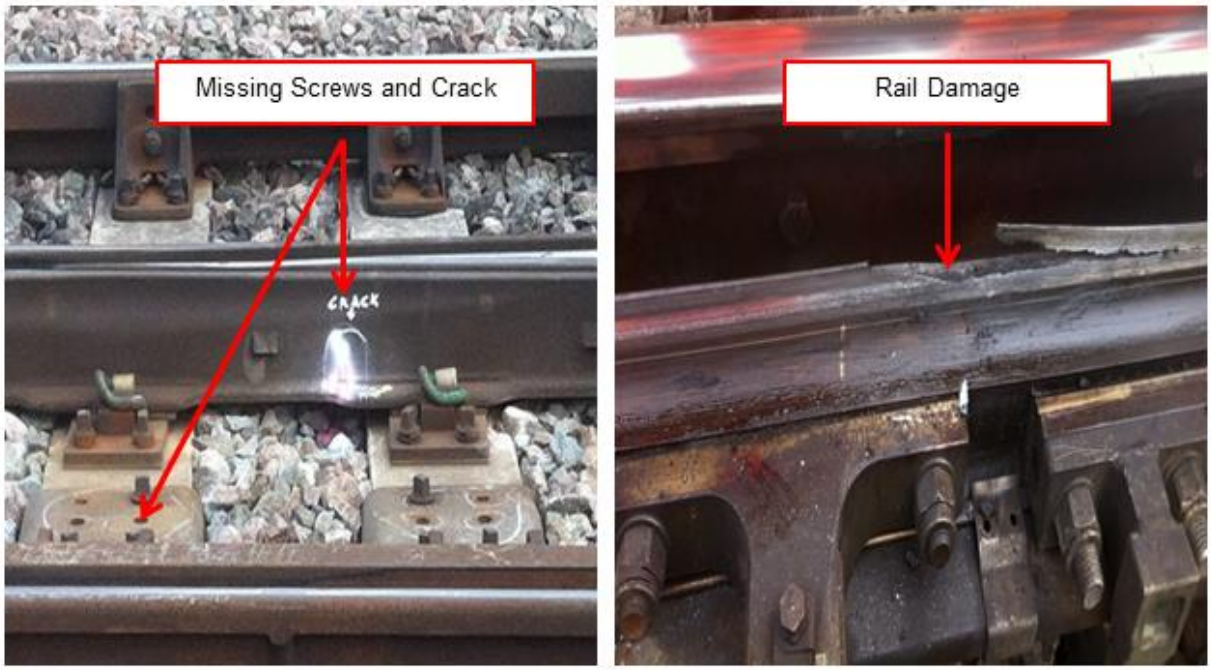

Figure 11: Rail Damage associated with NR60 MK1 (Hsu, 2012)

[4] Although the UK is no longer bound by the Technical Specifications for Interoperability (TSIs), most of the requirements of the TSIs have been kept within the National Technical Specification Notices (NTSNs), which came into force on 1 January 2021.

4. METHODOLOGY AND TECHNIQUES

4.1 Problem Statement for the Wheel-Rail Contact

In non-mathematical terms, let us consider two rigid elastic bodies (rail and wheel) pressed together to create a contact between them. As the wheels roll over the rail about the wheel axle, friction and slip occur which consequently lead to tangential forces arising. The tangential and normal forces will be accompanied by an elastic field of displacements (U1 and U2), stresses and strains. The aim is therefore to find this elastic field at the surface of the bodies where contact will occur.

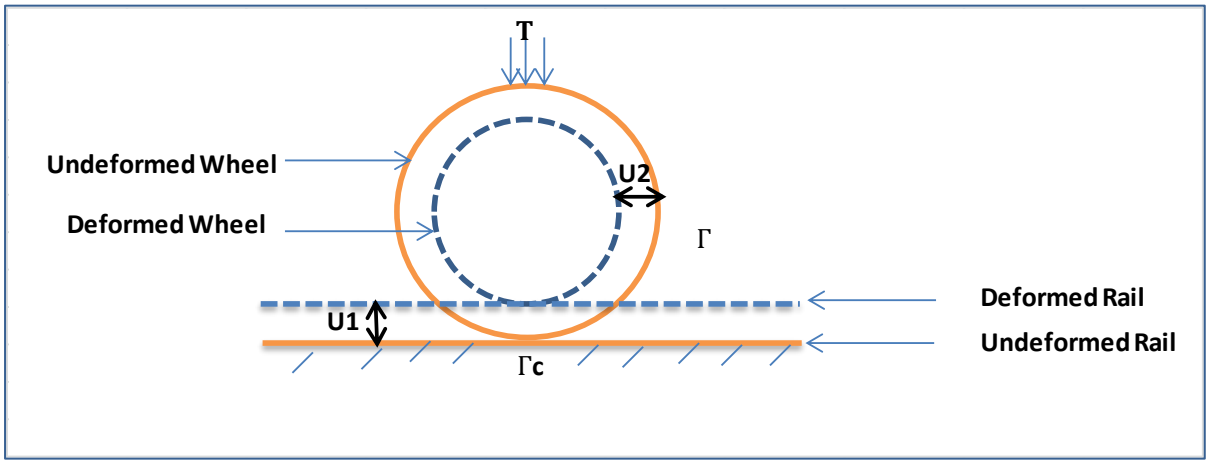

Figure 12: Deform and undeform Rail under Pressure (Arthur, 2016)

The following section is used to discuss the workflow involved in achieving the author's objective of creating a new design of S&C, namely, the NR60C MK2

4.2 NR60C MK2 Switch Design Workflow and Simulation Tools

The research was divided into two parts. The first part comprised the finite element modelling of the wheel-rail contact using ABAQUS, through which stresses, strain and forces are discussed. The second part will cover vehicle dynamic simulation with the VAMPIRE software through which the various rail damage mechanisms are thoroughly reviewed.

The workflows are shown in 3 (Abaqus) and 4 (Vampire). The combination of the two workflows is novel and provides useful results.

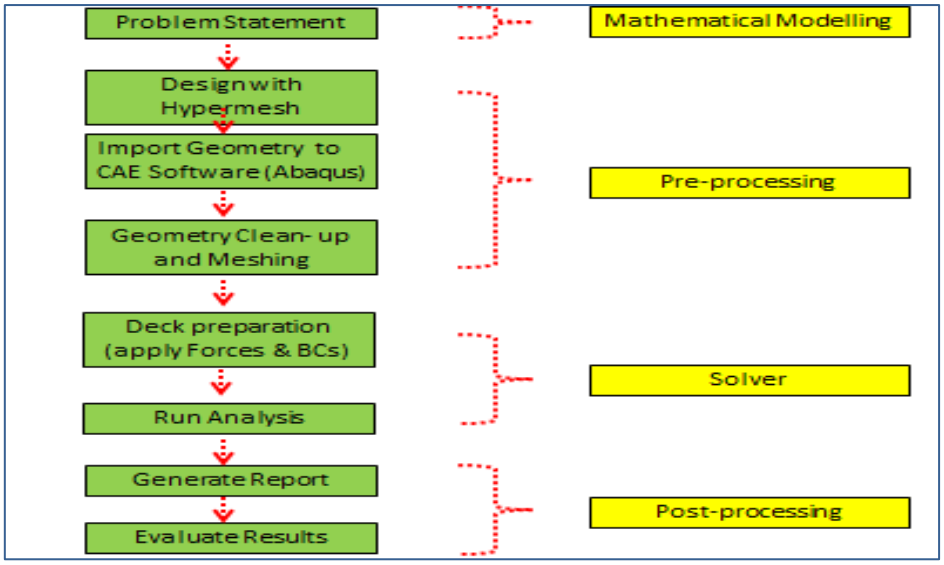

Figure 13: ABAQUS Workflow (Arthur, 2015)

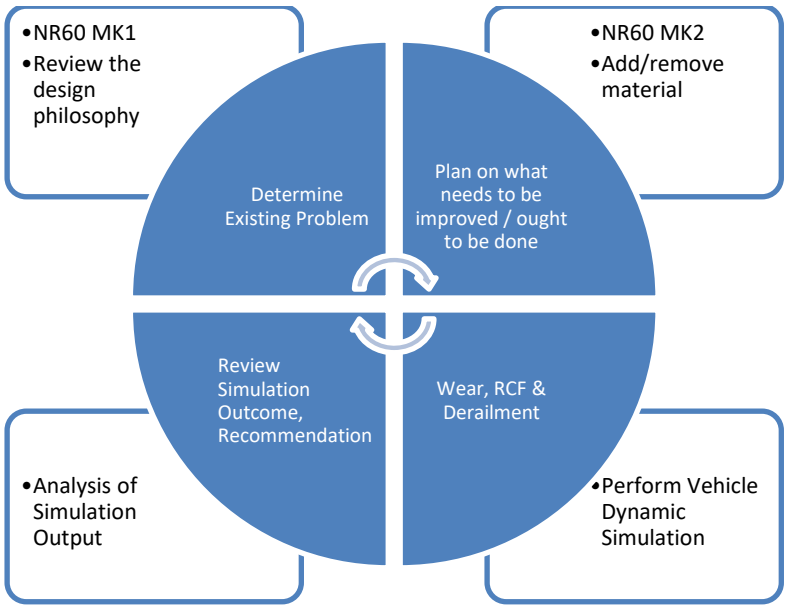

Figure 14: VAMPIRE Workflow (Arthur, 2015)

4.3 Finite Element Modelling for the Scalar Model Problem

4.3.1 Weak Formulation

Consider two elastic body systems with friction in the contact area: it could be that there will be slip in part of the contact area and adhesion elsewhere. As a result, creepage could occur because the bodies will slide slowly within the contact region. Taking the rail and wheel combination as an example, tangential and normal forces will be transmitted within the contact region causing friction and slip which consequently lead to wear. The evolution of the change

in shape of the contact region because of the contact has a major role to play when it comes to component replacement policy.

The research is based on finite element modelling which is a process of dividing complex problems into simple elementary parts by creating a mesh of elements and nodes and observing the response of the network, such as deformation. When deformation occurs, parts of the model may come into contact or lose contact, hence the aim of the present research is to investigate this contact behaviour and analyse its effect in the wheel-rail setting.

Let us begin with a simple scalar model problem of a beam as described in the author's Masters dissertation (Arthur K. , 2011). There are several models using beam theory, such as the Timoshenko beam model and the Euler- Bernoulli beam models and this thesis draws inferences from the Euler-Bernoulli beam theory. To be able to approximate the displacement u at any given point, the theory assumes that normal to the middle line of a beam remains straight and normal, to the interior line during the deformation.

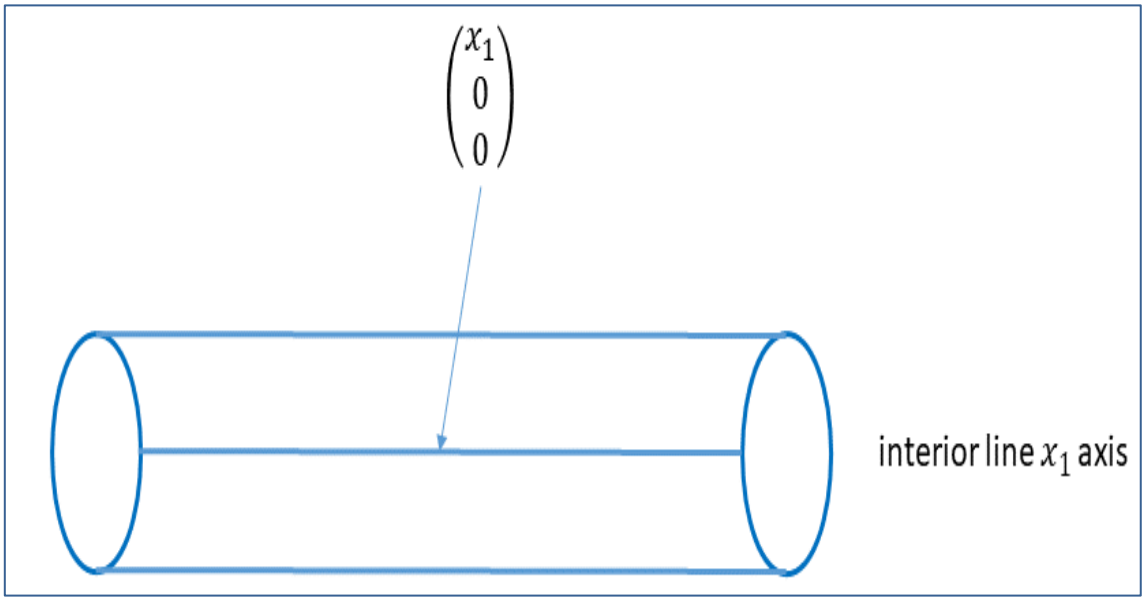

Figure 15: Undeform Beam

Now, if we let

$$\begin{pmatrix} u_1 \\ u_2 \\ u_3 \end{pmatrix}$$

be the displacement of the interior line, the deformed beam will, therefore, be

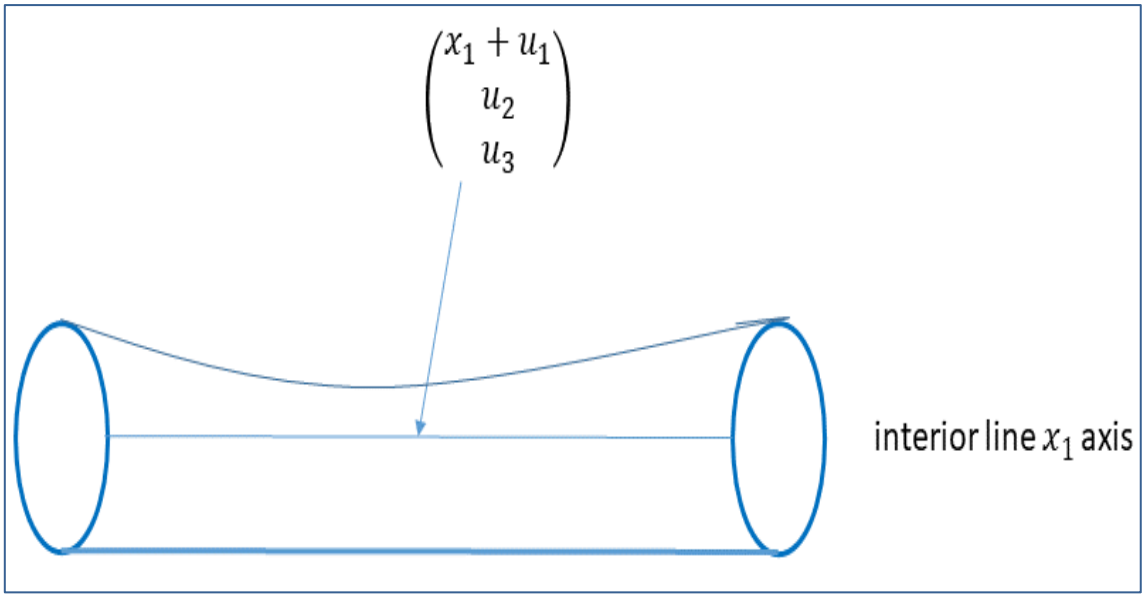

Figure 16: Deformed Beam

Let Ω be an open, bounded, connected subset of Euclidean space R^n, $n = 1, \ldots.3$, with the Lipschitz boundary Γ = ∂Ω. Consider the model problem: given $f \varepsilon C(\Omega)$ and $g \varepsilon C(\Gamma)$, find $u \varepsilon C^2(\Omega) \cap C(\underline{\Omega})$ such that

$$-\nabla^2 u = f \text{ in } \Omega$$

$$u = g \text{ on } \Gamma \qquad (1)$$

A solution $u \varepsilon C^2(\Omega) \cap C(\Omega)$ satisfying (1) is said to be a classical solution of this equation. This is Poisson's equation with Dirichlet boundary conditions. If g= 0, it describes the deformation of a stretched elastic membrane clamped to the wireframe boundary of shape Γ subject to a load f(x). It also relates the gravitational potential and mass density in Newtonian mechanics, and the electric potential and charge distribution in electrostatics. It describes incompressible inviscid irrotational flow, and many other phenomena besides.

$$-u'' = f \text{ on } (0,1) \qquad (2)$$

with

$$u(0) = u(1) = 0 \qquad (3)$$

The objective here is to weaken the condition that suggests that u is twice differentiable and continuous to enable us to approximate it with smooth functions. In applying the Galerkin method, the initial step is to prescribe a space for the weak problem as

$$\{v \varepsilon H^2(0,1), v(0) = v(1) = 0\} \qquad (3)$$

This implies the variational problem we hope to achieve is to ind $u \varepsilon V$ such that:

$$a(u,v) = f(v)\ \forall v\ \varepsilon\ V \tag{4}$$

After prescribing the finite element space, the next step is to formulate the weak form of the model problem. The purpose here is to find an approximation of the function u which will satisfy the differential equation in the model problem and, to achieve this, we look for a test function $(v\ \varepsilon\ V)$, multiply it with the model problem and integrate it over the interval (0, 1).

$$\int_0^1 -u''vdx = \int_0^1 fvdx \tag{5}$$

$$-u''(1)v(1) + -u'(0)v(0) + (u', v') = (f, v) \tag{6}$$

But, since

$$v(0) = v(1) = 0 \tag{7}$$

the weak form of the model becomes

$$(u', v') = (f, v)\ \forall v\ \varepsilon\ V \tag{8}$$

If we allow the bilinear form to be $a(u,v) = (u', v')$ and $f(v) = (f, v)$ to represent a bounded linear function defined on *V,* the weak problem becomes:

Find $(u\ \varepsilon\ V)$ such that

$$a(u,v) = f(v)\ \forall v\ \varepsilon\ V \tag{9}$$

4.3.2 Discretisation

The next stage in the finite element analysis is to solve the variational formulation problem in the FE dimensional subspace, such as $V_h\ of\ V$ usually consist of piecewise polynomial functions. If we let:

$$0 = x_0 < x_1 <. \ldots < x_N < x_{N+1} = 1 \tag{10}$$

be a set of nodes on $(0,1)$, then the partition on $(0,1)$ will be prescribed as

$$\{I_j = (x_{j-1}, x_1): j = 1; \ldots \ldots; N+1\} \tag{11}$$

where I_j are the elements. Let $I_j = h_j = (x_{j-1}, x_1)$. This implies that the max h_j will be the size of the mesh. As a result, the aim now is to analyse the mesh sequence as $h \rightarrow 0$.

First, we define the linear space as

$$V_h \begin{cases} v: v \text{ is continuous on } (0,1) \\ V|I_j \text{ is linear } j = 1, \ldots \ldots .. N+1 \\ v(0) = v(1) = 0 \end{cases} \tag{12}$$

so that the finite element problem becomes to find

$$u_h\ \varepsilon\ V_h$$

such that

$$(u_h\,, v_h\,) = (f, v)\ \forall v\ \varepsilon\ V_h \tag{13}$$

In order to ascertain the value of u_h the basis function for V_h must first be determined after which the coefficient of u_h is calculated by setting up a set of linear equations. In FE analysis, a piecewise linear basis function for V_h will incorporate a function φ_j that will satisfy:

$$\varphi_j \begin{cases} 1 \text{ if } i = j \\ 0 \text{ otherwise} \end{cases} \tag{14}$$

where I_j and I_{j+1} become the support for the basis function φ_j . As such $U_h\ \varepsilon\ V_h$ shall have the following representation

$$U_h\,(x)\ =\ \sum_{t=1}^{N}\ \tau_i\,\varphi_i\ \ x\ \varepsilon\ (0,1) \tag{15}$$

with $\tau_i\ =\ U_h$ as the unique real numbers. To arrive at an unknown solution, we have to establish a one-to-one relationship between the vector space γ^N and V_h and this can be achieved by choosing the basis function $\varphi_j : j = 1 \ldots\ldots . N$. The standard interval is then mapped to the actual interval in the following sequence:

Lets consider $(x_{i-1}\,, x_1)$ and $h_i\ =\ (x_1\ -\ x_{i-1}\,)$:

$$(x_{i-1}\,, x_1)\ \rightarrow (0,1) \tag{16}$$

$$x(s)\ =\ (\,x_{i-1}\ +\ (\,x_1\ -\ x_{i-1}\,)s \tag{17}$$

$$= h_i s\ +\ x_{i-1} \tag{18}$$

$$= x_i s\ +\ x_{i-1}\,(1 - s) \tag{19}$$

$$\text{If } \varphi_1(s)\ =\ 1 - s \text{ and } \varphi_2(s) = s \tag{20}$$

for element $(x_{i-1}\,, x_1)$:

$$\varphi_i(x(s))\ =\ \varphi_2(s) \tag{21}$$

for element $(x_{i\,,} x_{i+1}\,)$

$$\varphi_i(x(s))\ =\ \varphi_1(s) \tag{22}$$

$$\mathrm{U}_h'\,\varphi'_i\ = (b, \varphi_i) \text{ for } i = 1,2\ \ldots\ldots N \tag{23}$$

$$\mathrm{U}_h'\,\varphi'_i\ =\ \sum_1^N \int_{x_{i-1}}^{x_i} \mathrm{U}_h'\,\varphi'_i\ \ dx \tag{24}$$

$$u_h\,(x)\ =\ \sum_1^N \tau_i\,\varphi_i\,(x) \tag{25}$$

hence

$$\tau_i\ = u_{\,h}\,(x) \tag{26}$$

We now have to evaluate $\tau = (\tau_{1\ldots\ldots}\tau_N)\ \varepsilon\ \gamma^N$ from the linear system

$$b = A\tau \tag{27}$$

where

$$b = \begin{pmatrix} f,\varphi_1 \\ f,\varphi_2 \\ f,\varphi_N \end{pmatrix}, A = \begin{pmatrix} a_{11} & a_{12} & a_{1N} \\ a_{21} & a_{22} & a_{2N} \\ a_{N1} & a_{N2} & a_{NN} \end{pmatrix} \varepsilon \cap^{N\,x\,N}, \tau = \begin{pmatrix} \tau_1 \\ \tau_2 \\ \tau_3 \end{pmatrix} \varepsilon \cap^N \tag{28}$$

such that: $a_{ij} = (\varphi_i' , \varphi_j')$ (29)

$$b_i = (f, \varphi_i\ ) \tag{30}$$

$$i\ , j\ = 1 \ldots\ldots N \tag{31}$$

In finite element analysis, column vector b represents the load vector whilst matrix A reflects the stiffness matrix which is positive definite and symmetrical. The resistance of the elastic material under deformation is determined with this. Hence, to ascertain the true value of *A,* it should be recalled that

$a_{ij} = (\varphi_i' , \varphi_j')$ = 0 whenever $a_{ij} = \left(\varphi_i , \varphi_j\right) = 0$ on the boundary $(0,1)$.

Since the stiffness matrix is symmetrical, it follows that $(a_{j-1\,,j}\ = \ a_{j\,,j-1}\,)$ thus for a diagonal entry, we have

$$(\varphi_i' , \varphi_j') = \int_{x_{j-1}}^{x_j} \frac{1}{h_j^2} dx + \int_{x_j}^{x_{j+1}} \frac{1}{h_{j+1}^2} dx \tag{32}$$

Similarly, the non-zero non-diagonal entries shall be

$$(\varphi_i' , \varphi_{j-1}') = -\int_{x_{j-1}}^{x_j} \frac{1}{h_j^2} dx \tag{33}$$

4.3.3 Error Estimate and Convergence

This is the final point in the model problem where we interpolate to get and a priori error estimate by comparing the exact solution with the approximate solution using Cea's Lemma.

Let us commence by taking $k(.)_G$ as a linear form and $a(.,.)_G$ as the bilinear form of the vector *G* containing the inner product $(.,.)_G$.

We first apply the assumption of ellipticity on the bilinear form:

$$a(v,v) \geq a||v||_G^2\ \forall v\ \varepsilon\ G \tag{34}$$

After this, we use the continuity assumption, namely, there exists $M\ > 0$ so that:

$$a(v,u)\ \leq M||v||_G\ ||u||_G\ \forall v\ \varepsilon\ G \tag{35}$$

Similarly, by applying the assumption of continuity on the linear form, there exists $M > 0$ so that:

$$a(v) \leq M_l ||v||_G \; \forall v \; \varepsilon \; G \tag{36}$$

Defining the finite element space as $V_h \subset G$, the finite element formulation will be:

Find $(u \; \varepsilon \; V)$ such that

$$a(u_h, v_h) = l(v_h) \; \forall v_h \; \varepsilon \; V_h \tag{37}$$

Approximation:

At this juncture, we search for the approximation. This can be achieved by setting $v = v_h$ in the variational formulation:

Find $u \; \varepsilon \; V$ such that

$$a(v, u) = l(v) \; \forall v \; \varepsilon \; V \tag{38}$$

applying Galerkin orthogonality

$$a(u - u_h, v_h) = 0 \; \forall v_h \; \varepsilon \; V_h \tag{39}$$

thus $\forall v_h \; \varepsilon \; V_h$ will be approximated as

$$a(u - u_h, u - v_h) = a(u - u_h, u - v_h + v_h - u_h) \tag{40}$$

$$= a(u - u_h, u - u_h) \tag{41}$$

applying Cauchy Schwartz inequality on this bilinear form, we obtain:

$$a(u - u_h, u - u_h) \leq a(u - u_h, u - v_h)^{\frac{1}{2}} \, a(u - v_h, u - v_h)^{1/2} \tag{42}$$

$$a(u - u_h, u - u_h)^{\frac{1}{2}} \leq a(u - u_h, u - u_h)^{\frac{1}{2}} \; \forall v_h \; \varepsilon \; V_h \tag{43}$$

The mathematical implementation illustrated above shows how a typical Finite Element methodology is defined in Abaqus Explicit which the author used to model the wheel-rail interface. For every Finite Element analysis, the main thrust is to achieve convergence of the approximate solution to the model problem. Following this mathematical implementation, a reasonable convergence for this thesis research was achieved at the point where increasing the number of elements to 9000 only resulted in a corresponding increase of 1.2% in vertical displacement, as shown in Figure 25. With this result, the author can conclude with reasonable confidence that the level of element size is good enough to estimate load transfer.

4.4 NR60C MK2 Novel Switch Development Process

As part of Network Rail industry's pursuit of improved network performance and capacity, the search for new S&C components capable of revolutionising the current ageing assets has

become inevitable. The quest was to investigate and develop radically new concepts of S&C that have the potential to lead to increases in reliability, to be safer, to increase passenger capacity whilst reducing operational and investment costs. The author's contribution to the proposed NR60C MK2 switch is set to improve the mechanisms used for moving trains from one track to the other. The NR60 MK2 is a standardised S&C system that has been designed to take over from the NR60 MK1 S&C suite. The research focuses primarily on the NR60C[5] switch (i.e., NR60C MK2) but the design philosophy can be extended to other switch lengths, such as NR60D MK2, NR60E MK2 and NR60F MK2 switches. The NR60C MK2 switch was chosen for the research, rather than any other types of switches in the suite, because it has very a high wear rate since it is the most frequently used switch. Of necessity, for interchangeability, the NR60C MK2 system is built around the footprints of NR60 S&C and NR56 S&C. This implies that the new design must incorporate some features and enhancements from the existing NR60 MK1 since the NR56 S&C was also designed along the footprint of NR60 MK1. Some key features of the switch that the author had to change during the development of the new switch design are as follows:

- Track Kink: Unlike the existing switch, a track kink was added to the new design. The author considered the design using two different scenarios, i.e., a design with no kink and a design with a kink. In the case for no kink, the wheelset appeared to be oscillating to the right and then left from the switch toe during testing, indicating potential wheelset hunting whilst the addition of a kink had no significant effect on the position of the onset of wheel and switch blade contact.
- Switch Head Profile: The NR60C MK2 switch head profile has been designed to be conformal so that it will eliminate any sharp contact with the wheel, thereby avoiding heavy switch wear. As opposed to NR60C MK1, which uses a toe relief cut that has a linear offset skewed relative to the running edge of the switch rail, the new design will have a lateral toe relief defined by radius and offsets. To reduce the stress at the switch rail, hence reducing the incidence of switch tip breakout, the stock rail machining has been shifted 3 mm into the stock rail to increase the thickness of the switch at the expense of the stock rail. In order to reduce switch replacement cost without the need for any major remodelling such as OLE structure movement, signal asset relocation and platform extensions or cutbacks, the NR60C MK2 has been designed as a like for like replacement for existing layouts such that the footprints are

[5] The letter 'C' in NR60C provides the curvature of the diverging track. A is the smallest radius type of S&C.

compatible with that of vertical shallow depth designs. Geometry has been optimised to reduce switch wear, particularly on trailing moves.

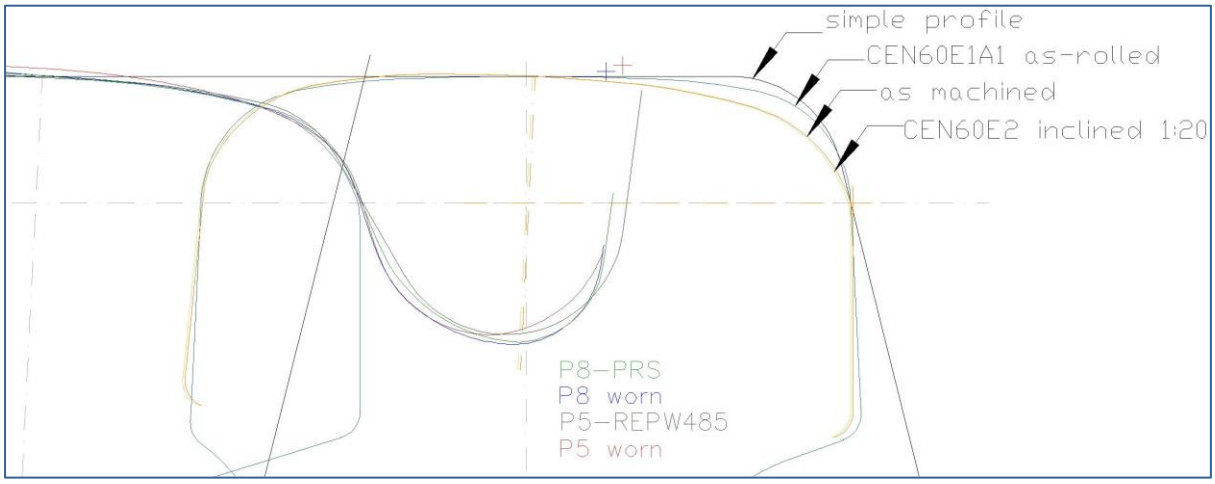

Figure 17: Wheel and Switch profiles (Network Rail, 2017)

- Figure 17 compares the different types of switch rail head profiles to illustrate the difference between the RT60/NR60 MK1 switch and the NR60 MK2 switch. In relation to the existing NR60 MK1, the new NR60 MK2 switch head profile has been machined to eliminate any sharp contact.

a) Switch Radius

- The switch radius has been increased from the existing 194,930 mm to 247,563 mm. The philosophy here was to avoid a sharp curve when entering the S&C.

b) Intersecting Geometry

- In a typical switch and crossing configuration, there are many ways to shape the divergence of the two tracks. The three most commonly used are tangential, intersecting and non-intersecting switch geometries. In a tangential switch geometry, the switch curve is set to be tangential to the straight track at the switch curve origin, i.e., the switch curve aligns perfectly with the straight gauge line of the track. If, on the other hand, the switch curve origin is set outside the gauge line such that the intersection occurs with a finite switch entry angle, then we have an intersecting switch geometry also referred to as the outside shift. For a non-intersecting geometry, the origin of the switch curve is set inside the gauge line, hence the switch curve will not intersect itself. This arrangement, also called inside shift, features a clothoid curve to give it a smooth transition. The author applied a double intersecting geometry, as shown in Figure 18 for the new switch design. According to Schmid et al (2010), intersecting switch designs tend to be more robust. With excessive wear characterising the existing

NR60C MK1 switch, the idea is to use a double intersecting geometry that will reduce the abruptness at the switch toe hence making it a better option to use.

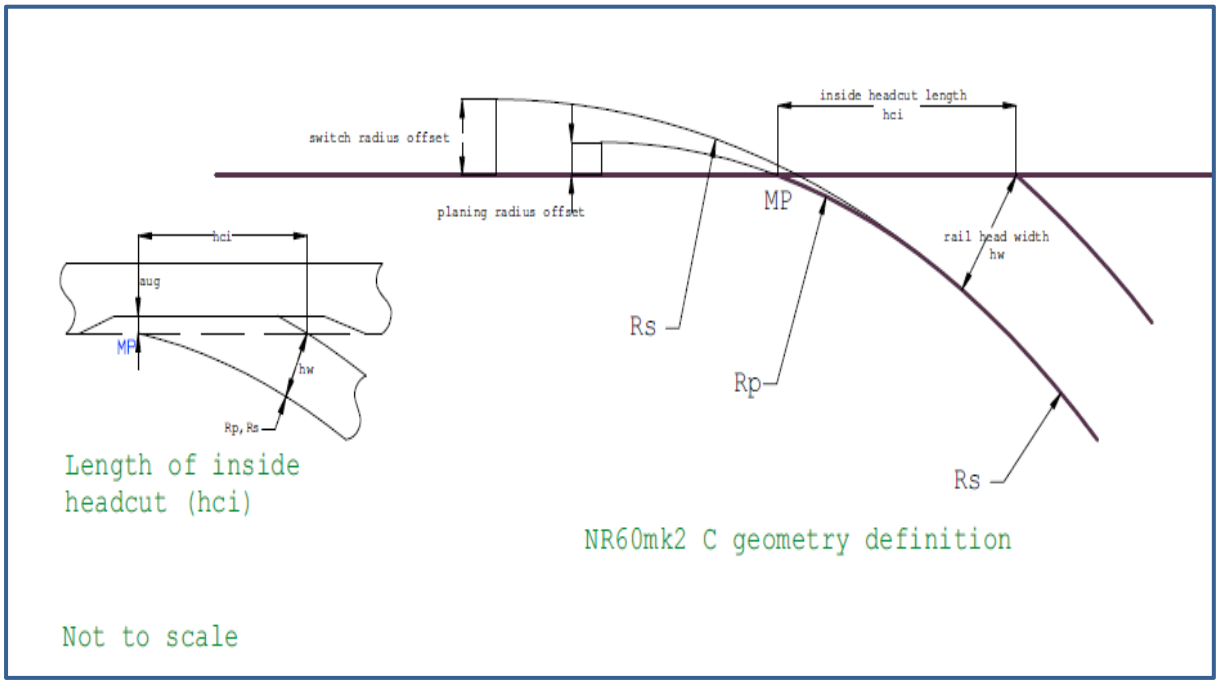

Figure 18: Double Intersecting Geometry Design for NR60C MK2 (Network Rail, 2017)

c) Type of Entry

- The existing NR60C MK1 has a clothoid entry which produces a jerk effect at the switch toe upon entry. With respect to the new NR60C MK2 design, a straight entry has been adopted, hence allowing for a smooth transition into the switch and beyond.

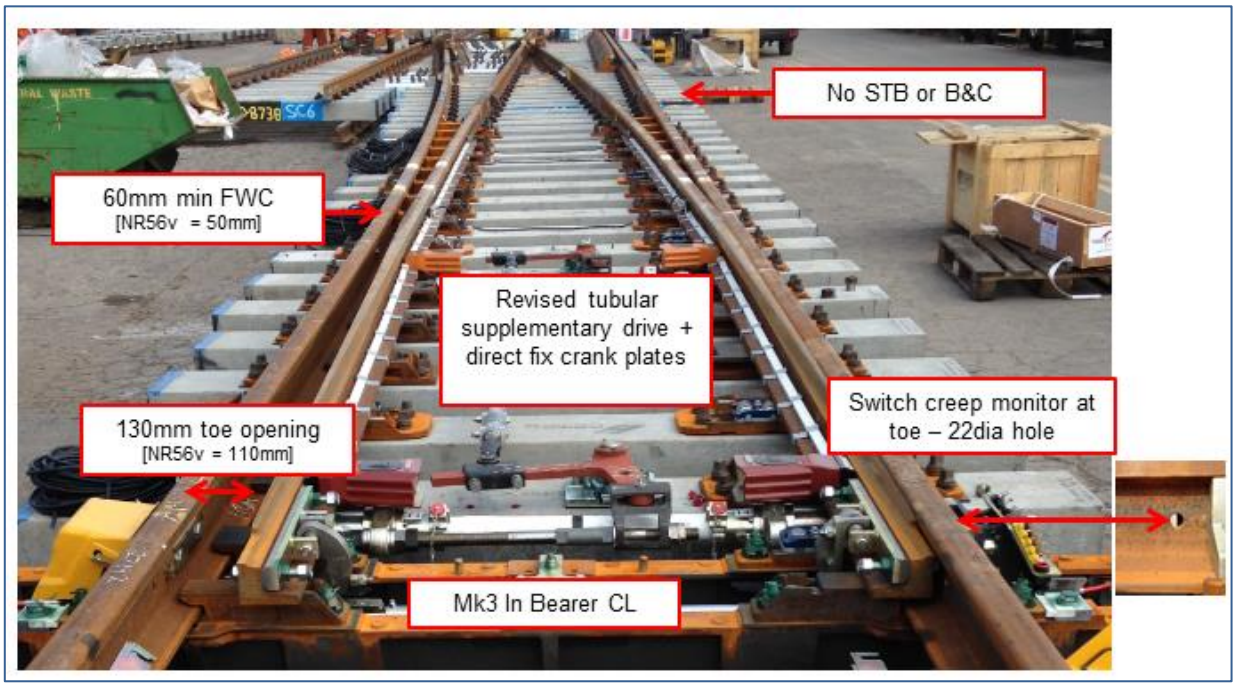

Figure 19: NR60C MK2 Switch Arrangement (Network Rail, 2017)

As well as exploring the different design concepts, the author also explored the development of materials and components that could be applied to enhance the performance of the design. These developments can be applied individually or in combination to contribute to the objectives of next generation S&C. The NR60C MK2 switch comprises inclined stock rails with shallow depth switches on concrete bearers. It has been designed with rails base-plated through the moveable length of the switch, with differential heel baseplates immediately behind the moveable length. The crossing and check rail area is also base-plated. Rails are directly fixed to the bearer at all other locations. A typical NR60C MK2 switch layout configuration is illustrated in

Figure 19, with new design features such as a creep monitor, MK3 in-bearer clamp, direct fixings etc, (Network Rail, 2017)

The author carried out a material strength analysis for the components using Abaqus and recommends the following:

- Bearer positions, lengths and quantity have been adjusted to improve bed widths and support conditions. Bearer spacing has been reduced to 600 mm to provide support against high impact loads.
- Stress Transfer Blocks are not required because the new design is to be installed under CWR track conditions. However, there will be exceptions to this where the layouts are not located in CWR track (e.g., traps and bay platforms). Instead of using a Ball & Claw creep monitoring device, the design will include a feature that allows the switch toe to align itself centrally to a hole in the stock rail (Track Design Handbook, 2017).
- In Bearer Clamp Locks (IBCL) Mk 3 will be used as the primary drive with an enhanced mechanical supplementary drive and Hy-Drive as further available options to reduce operational delays (Track Design Handbook, 2017).
- Clipping arrangement – Vossloh SKL fastenings to be used throughout the layout. Like Pandrol fastenings, the clip is a spring tension clamp. It is recommended that narrower Skl 14 Clip (toe load of 9 Kn/clip) should replace Skl 21 (toe load of 10 Kn/clip). Screw installation torque of 250 Nm / 184 lb-ft to be applied and no 'bancing' is permitted (Track Design Handbook, 2017).

Figure 20: Direct Fixing based on Vossloh W21T System (Network Rail, 2017)

- Crossing

- NR60 MK 2 is expected to use a cast monoblock crossing design with welded-on leg ends. Wing and nose profile will be optimised to improve wheel transfer and reduce the risk of crack development. Crossings will be explosively hardened (EDH) as standard and with no fishplate ends. The crossing will be mounted on baseplates to the bearers using bespoke plates and SKL24 clips. Where applicable, cast crossing blocks is to be provided in the vees of the crossing and at the wing fronts. The interior feature of the cast crossing is to be modified to provide improved service life and reduced risk of premature fatigue failure. Figure 21 illustrates an example of the crossing nose of an NR60 MK2 cast crossing. Just like the switch, the crossing nose has been designed with 1.2 mm of additional material to enable it withstand high impact loads.

Figure 21: NR60 MK2 Cast Crossing at S&C Manufacturer's Yard (Network Rail, 2016)

The above changes/recommendations have been proposed in order to improve wheel-rail interface contact and also to make the switch TSI compliant. For S&C design, it is important to consider the system performance. An S&C unit can have a perfectly designed geometry but without good components to support the geometry, failure mode and limitation of the design may not be fully understood. The components must be fully tested to determine their material strength using finite element analysis or similarly effective modelling tool.

4.5 FE Simulation of Wheel-Rail Interface Using Abaqus

The railway turnout components are subjected to static, dynamic and often impact loading conditions due to wheel-rail interactions associated with the abnormalities in the life cycles

of the rail and wheel. Thus, a full explicit FEM simulation of wheelset passing through switch and crossing is required to effectively assess the impact of wheel-rail interface problems. To address this, ABAQUS has been employed to carry out the modelling and post-processing of the complete 3D railway turnout structures. ABAQUS is an advanced explicit FEM analysis program with multi-physics analysis capability. It can solve the complex dynamic interaction problems including interaction of wear, fatigue and impact, which can be well described by explicit ABAQUS program.

The two main parts of wheel-rail contact classification are elastic (elasto-plastic) which solves problems in contact mechanics from a solid mechanics point of view and geometric (kinematics) which aims to establish the contact detection point. Under the kinematic part, geometrical data for wheel and rail is required to evaluate the tangential force. Figure 22 shows how rail and wheel were coupled together in the dynamic system to create a contact between them on a simple fixed bedding. The material and operational properties in Table 4 for the Abaqus modelling was partly sourced from the Abaqus/CAE user manual version 6.11 and partly tuned in manually.

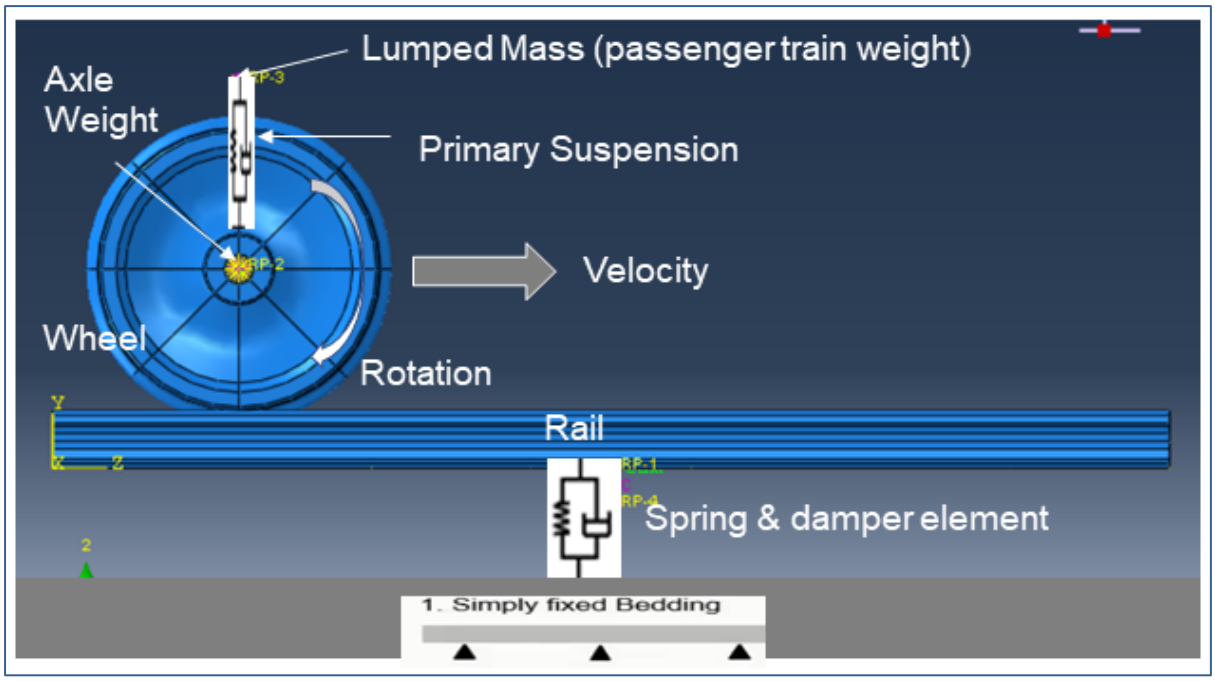

Figure 22 : Coupling of Rail and Wheel to Create Contact (Arthur 2017)

The numerical approach of the wheel-rail contact was based on Wiest (2008) where FE analysis was deployed at the contact zone to analyse the effect of variation of wheel-rail profile parameters on the contact stress, contact dimension and contact pressure.

In this study, a three-dimensional (3D) FE model for a wheel passing through a turnout was developed to find the dynamic response at the wheel-rail contact location for the switch and

crossing. The implementation was based on a plastic nonlinear solid material from which contact detection points could be analysed.

The rails were supported by simple fixed bedding that comprised damper and spring elements. The spring stiffness for the bedding was set to 90 kN/m whilst the damping constant was set to 250 kNs/m. The concrete bearers were spaced at 600 mm with a 10 mm nylon pad placed on top of the bearers to prevent deformation of the bearers and also to avert any rail-bearer abrasion. The wheel was damped in the vertical direction with a damping coefficient of 53 kNs/m and modelled as having the elastic behaviour of steel.

The wheel-rail contact investigation covered the area from the switch toe to just beyond the planing section of the switch. Similarly, a section along the 3 m of the crossing was also investigated with particular attention given to the movement between the wing rail and crossing nose (Figure 20) since this transition section is where high impact loads tend to occur.

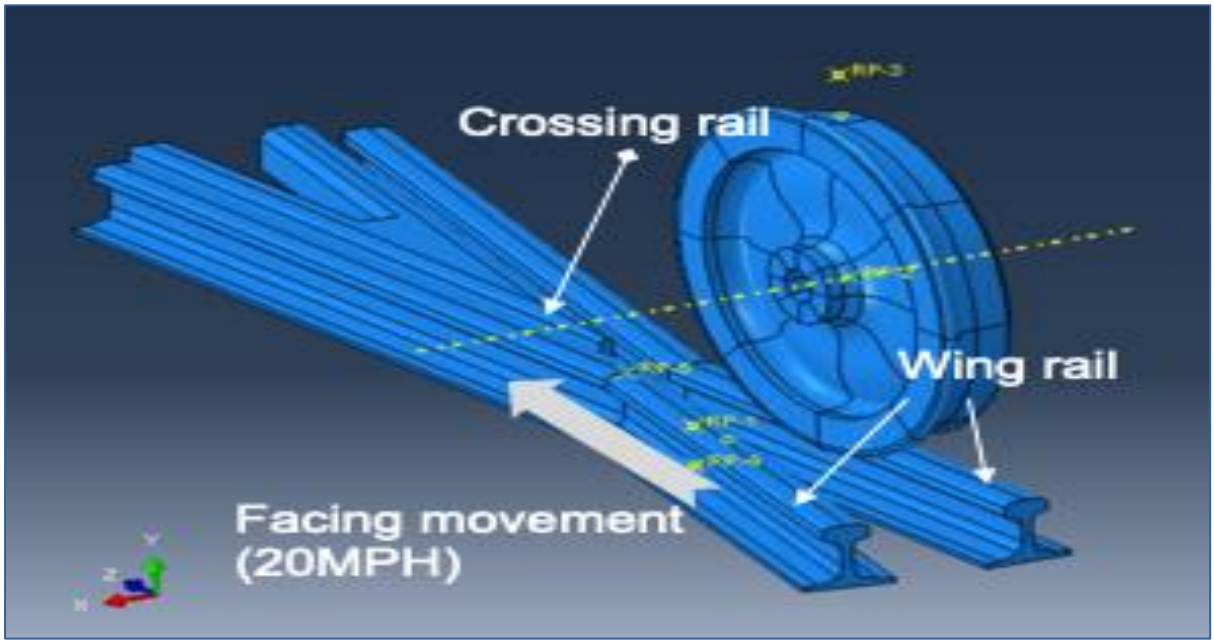

Figure 23: Crossing Model in the Facing Direction (Arthur 2017)

Material and Operational Properties			
Speed	8.94m/s(25MPH)	Wheel (elastic) Modulus	210 GPa
Vehicle Sprung Mass	66250 kg	Wheel Poisson's ratio	0.3
Wheelset Unsprung Mass	1025 kg	Wheel density	7850 kg/m^3

Friction coefficient	0.3 (wheel & rail)	Rail Modulus	190 GPa
Primary suspension	53 kN/m	Rail Poisson's ratio	0.3
Spring stiffness(bedding)	90 kN/m	Rail density	7800 kg/m^3
Damping constant (bedding)	250 kNs/m	Rail Yield stress	360 MPa

Table 4: Input Parameters

The input material parameters for the Abaqus simulation are shown in Table 4. At the commencement of the simulation, the wheelset was placed on the stock rail about 400 mm before the switch toe in the facing direction and at the same distance before the crossing nose. 80 kN axle load and a velocity of 25 mph were applied to the tread of the wheel with the coefficient of friction set to 0.3 for both rail and wheel.

As the wheelset runs along the rail, geometrical discontinuities are observed due to the presence of the angle of attack and lateral displacement of the wheelset. According to Courant's (1967) stability condition, the time step must be small enough to be proportional to the smallest mesh size in any numerical simulation. However, for wheel-rail contact problems, dissipation of energy will be sufficient to avoid any tangential and normal contact fluctuation so long as the time increment size is small. In respect of high modelling nonlinearities, ABAQUS explicit solver is efficient, but the stability of the solution depends on the time step. As a result, the computational cost for the explicit integration scheme increases linearly with the reduction of the time increment size for nonlinear problems.

During the contact modelling, an investigation was carried out for penetrations between the master and slave elements. The penalty-based method was employed to ascertain any potential penetrations at every time step between the two contacting bodies. Any time penetration was identified, a force which is the product of contact stiffness and the depth of penetration was applied to eliminate the penetration.

The expectation here is to predict whether the input materials will deform plastically based on von Mises calculation of elastic stress levels.

Figure 24 highlights the switch mesh designs for the existing and proposed NR60C designs. Case 1 shows the existing NR60C MK1 switch mesh with a thin switch toe. Case 2 illustrates how the stock rail machining has been shifted 3 mm into the stock rail for NR60C MK2, so as to increase the thickness of the switch rail at the expense of the stock rail and Case 3 depicts the crossing nose which has been strengthened with 1.2 mm of additional material. The author of this thesis is of the view that this proposed strategy will help reduce stress at the

switch rail because the revised switch will now be strengthened to withstand high impact forces.

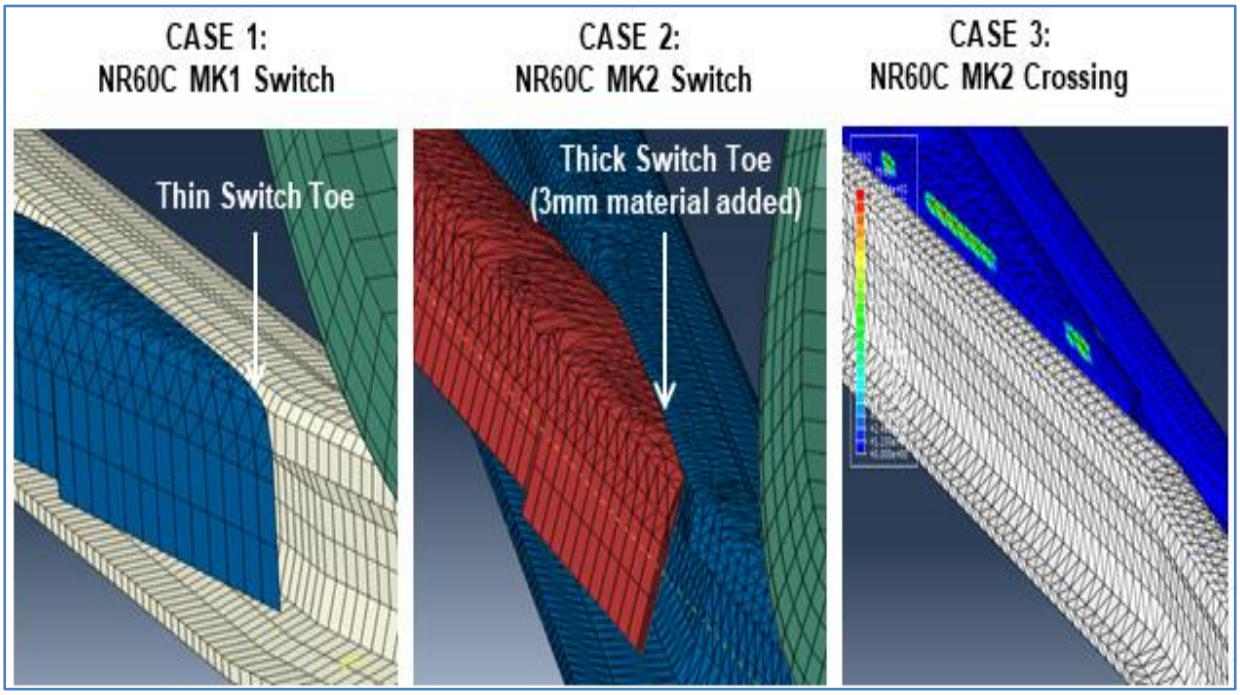

Figure 24: Simulation Cases (Arthur, 2016)

4.5.1 Mesh Model

In the case of a 3D mesh analysis model, tetrahedral, hexahedral, triangular prismatic and pyramidal elements can be used. In this model, the author created and used hexahedral elements that, according to Zienkiewcz (2014), are known as the most accurate element type. Based on the provided standard drawings, the wheel solid model was created by revolving the profile through 360 degrees. The ABAQUS/CAE sketch tracing function was utilized to trace the outline of the wheel drawing. To create a mesh using hexahedral elements, partitions were generated by dividing them into eight in the radial direction. In total 8928 linear hexahedral C3D8R elements were used for this wheel part in Figure 26.

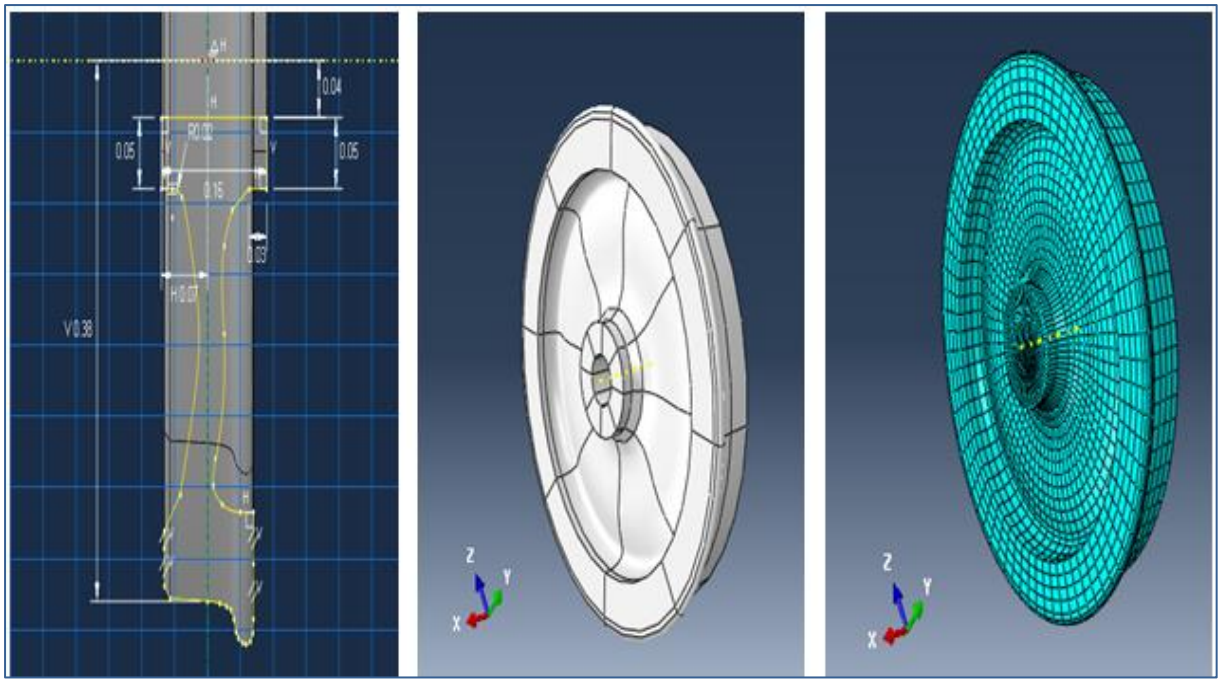

Figure 25: P8 Wheel Mesh Generation (Arthur, 2016)

Likewise, the rail section was created using the same method. Hexahedral elements were used to generate the mesh illustrated in Figure 23. A total of 4800 hexahedral elements (C3D8R) were used for this part. In order to create compatibility between the contact surfaces of wheel and rail, similar size elements were generated with a length ranging from 2 mm to 2.5 mm for both contact surfaces. The size of the mesh is relatively large and is considered appropriate when considering computational efficiency of the explicit analysis time. Linear static analysis could be easily carried out quickly with a large number of nodes and elements, but this type of analysis will take a long time to process. Keeping control of the number of nodes and elements is very important for a reasonable result to be achieved. The overall length of contact patch size obtained was between 2 mm to 2.5 mm. Thus, similar scales of the elements were adopted for efficient analysis. The author tried to determine the most suitable combination of element length and mesh size to capture a reasonable approximation of the load transfer behaviour.

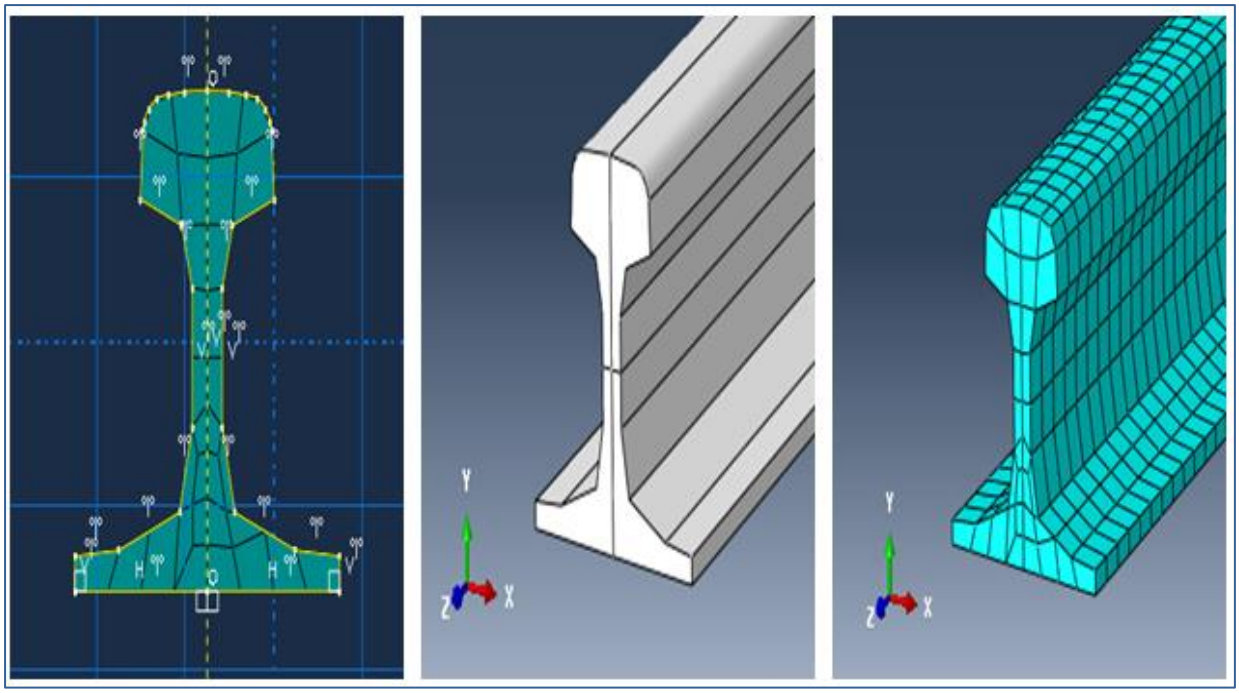

Figure 26: Rail Mesh Generation for CEN 60 E2 (Arthur, 2016)

In order to capture a more detailed contact response, a sub-model of the wheel was generated with a refined mesh. In total, 63246 linear hexahedral elements were used for this sub-model to estimate a more accurate contact behaviour between the rail and wheel contact surfaces.

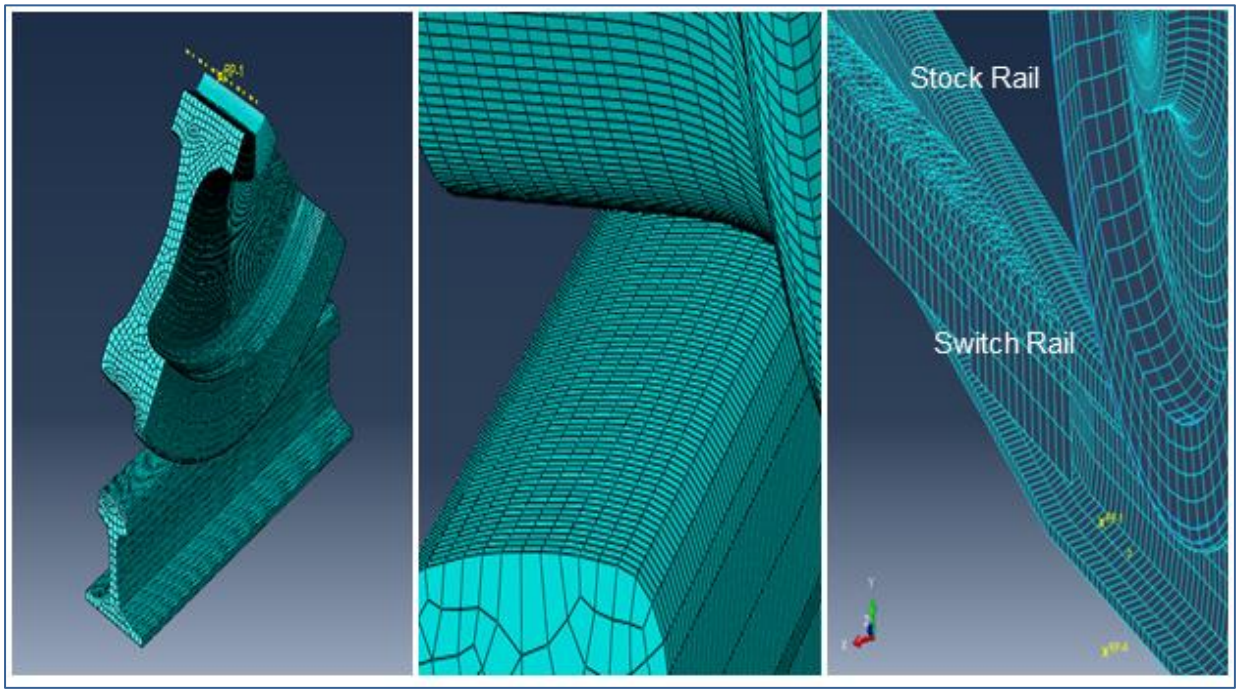

Figure 27: 3D Sub-Model Mesh Generation for Contact Analysis (Arthur, 2016)

In this sub-model (Figure 27), the more refined mesh was manually created on the contact surfaces themselves. Due to the nature of this type of dynamic contact analysis, finer elements are needed to estimate accurate contact behaviour.

4.5.2 Convergence

Convergence was achieved for vertical displacement of the wheel under a static wheel load. Five trials were conducted with a number of wheel elements (approximately 5,000 / 6,000 / 7,000 / 8,000 / 9,000). It was found that increasing the number of elements by 160% from 5,000 to 8,000, led to an 18.1% increase in the vertical displacement of the rail. Increasing the quantity of element further to 9,000 only resulted in a 1.2% increase in the vertical displacement of the rail. The results were plotted as per Figure 28 which indicates a reasonable convergence of the last case because there is a smaller maximum percentage difference in the stress value. It is determined that 9,000 elements results in an element size that is good enough to estimate load transfer with reasonable accuracy.

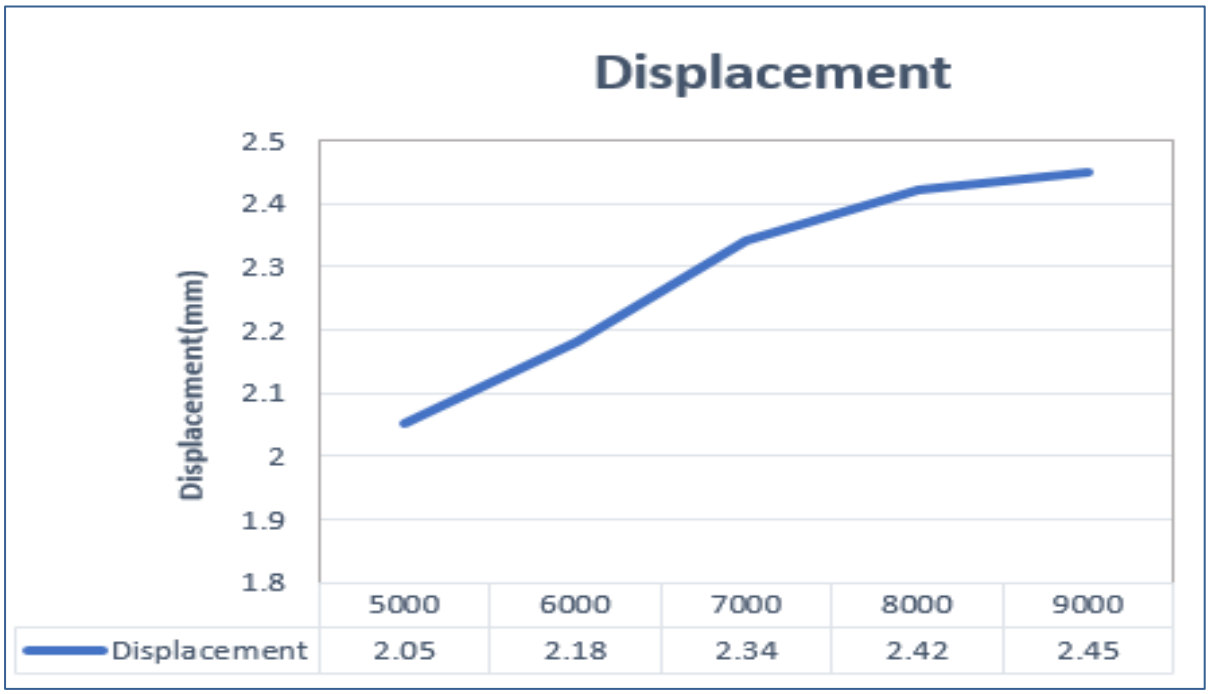

Figure 28: Mesh Sensitivity Analysis for Rail-Wheel Contact Interface (Arthur, 2017)

4.6 Vehicle Dynamic Simulation Using VAMPIRE Pro

VAMPIRE Pro is an industry standard software package which is used to simulate rail vehicles on railway tracks. It is often used for modelling derailment, design of vehicles and evaluation, and also for ride quality simulation. The software has an Interactive Vehicle builder which allows the user to create different railway vehicles via a graphical interface.

The author's choice of VAMPIRE to undertake the wheel-rail interface investigations was based on the fact that the software is able to provide in-depth performance-based

assessments of both vehicle and track conditions. It is the industry standard at Network Rail, thus presenting the author with the opportunity to collaborate with other industry experts to undertake a project which can be tested in the future under real life conditions. With respect to track conditions, VAMPIRE can be used to evaluate new and existing tracks. New tracks can be evaluated and optimized before construction in order to assess derailment, RCF and wear performance. Using a track recording vehicle, existing tracks can be simulated to identify derailment risk locations or prioritize track geometry defects. During derailment investigations, VAMPIRE is able to perform "what if" analysis to determine which track, vehicle or operational conditions are the primary contributors to derailment. The user is able to discern the contributors to derailment and ascertain whether it is wide-gauge, wheel climb, rail rolling etc that caused the derailment. All these benefits are not associated with ABAQUS hence the author's adoption of VAMPIRE as an additional simulation tool for this research. The aim of the author in this section is to assess the performance of the new switch in relation to S&C damage categories in terms of wear, RCF and also, derailment risk.

The overall track length in the simulation is 100 m, taking into consideration appropriate transition lengths as defined in Network Rail (2014) suitable for the new design. The applied track model consists of rigid massless sleepers attached to two rails by spring damper elements. Over 150 rail profiles have been used to build the complete turnout system under investigation. No super elevation was applied in the track design.

Starting from the switch toe which is set at 0 mm, both the stock and switch rail profiles are generated every 50 mm for a distance up to 4400 mm (i.e., up to the transition point between planing and switch radius). When compared to the existing NR60C MK1 design, the new NR60C MK2 design has a secant arrangement, i.e., double intersecting geometry whose layout is shown in Figure 27. Unlike the NR60C MK1 which has a clothoid entry where ride quality is compromised as a result of the jerking effect, the NR60C MK2 has a straight entry with a smaller entry angle and a bigger switch radius so as to improve the track geometry, hence providing a better ride quality. The Vampire software will perform an interpolation between the wheel-rail contact data so as to simulate the changes in rail profile along the turnout. As discussed already, Figure 3 shows how a single and two-point wheel-rail contact will occur on the rail profiles arranged from 0 mm to 4400 mm. Table 5 summarises the main differences between the switch geometries for the NR60C MK2 switch and the existing NR60C MK1 switch.

Switch Type	Type of Entry	Turnout Speed (mph)	Entry Angle (1 in X)	Switch radius (mm)	Track Gauge (mm)	Crossing Foot Flange	Rail Profile	Rail Stengthening
Existing NR60C MK1	Clothoid	25	263	194930	1435	Continuous & Discontinuous	No data	-
Proposed NR60C MK2	Straight	25	145	247563	1435	Continuous	Measured at every 50 mm	3 mm

Table 5: NR60C MK1 and NR60C MK2 Switch Geometry (Arthur, 2017)

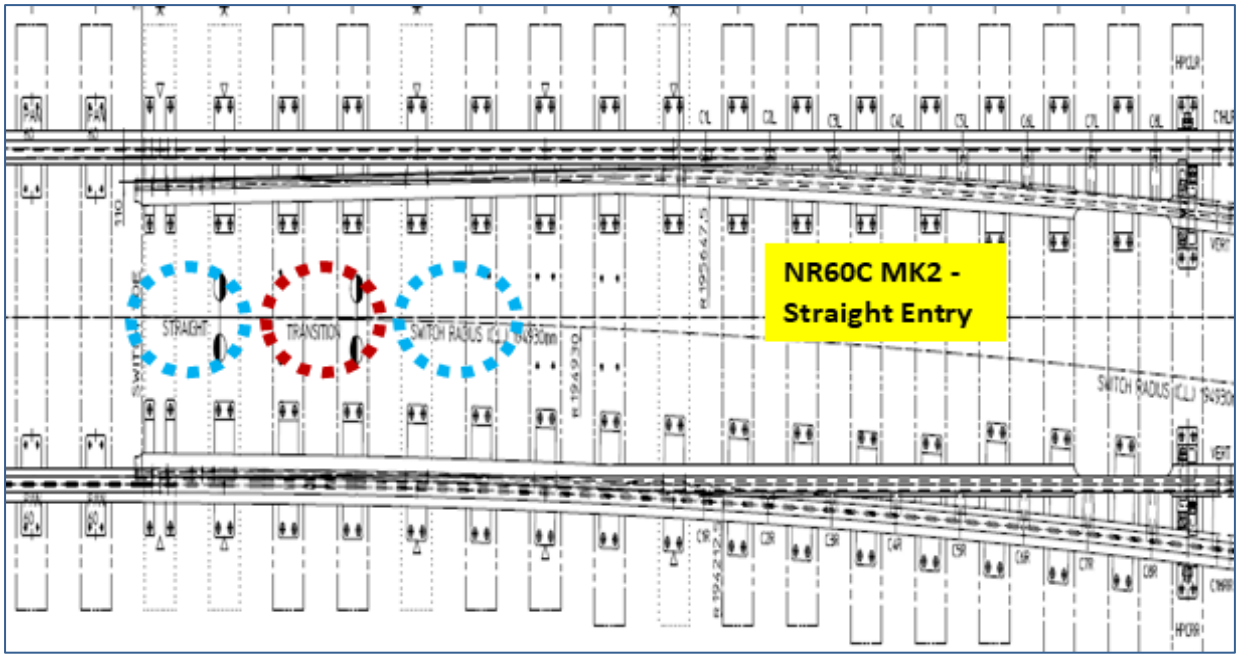

Figure 29: NR60C MK2 Switch Showing Straight Entry (Network Rail, 2017)

Figure 30 describes the switch toe arrangement and the type of rails to be used. The switch configuration is bound by entry and exit extension curves which requires full rail installation. Within this boundary is the switch toe transition where chamfered stock rails are used. The lengths of the head-cut and the head-cut transitions will also both require switch and stock rails.

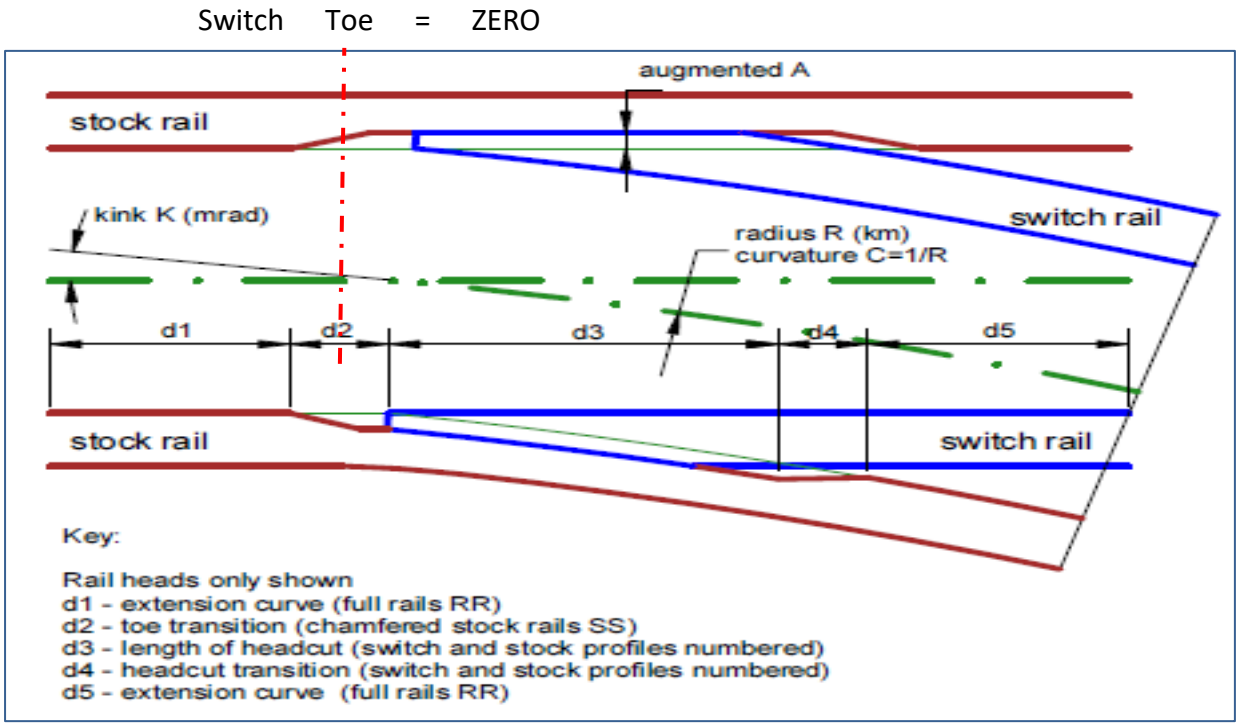

Figure 30: NR60C MK2 Showing Rail Types and Datum Point (Network Rail Track, 2016)

With respect to the vehicle dynamics analysis, twelve simulation runs were undertaken as per Table 6 with 3 vehicle models MK3, Desiro and Freight Wagon (i.e., 2 passenger trains and 1 freight train) under facing and trailing conditions. The author's choice for the vehicle selection was based on their laden weight so as to understand the full impact of all vehicle types (heavy, medium and light weight vehicles) in the simulation.

As mentioned already, the switch toe was set at 0 m for both facing and trailing moves. A track kink of 6.9 milli-rad was applied at this distance to replicate the entry angle as the vehicle negotiates the turnout. The simulation outcome is presented in the results section for both trailing and facing direction of travel at two different speeds; first at maximum speed of 11.3 m/s (25 mph) and then at 5.6 m/s (12.5 mph) which is 50% of the maximum allowable speed.

Vampire Run	Vehicle Type	Rail Gauge Corner Lubrication	Train Speed mph	Wheel Profile (Passenger)	Wheel Profile (Freight)	Direction of Travel
1	MK3 (PYS=16)	No	25	P8 New		Facing
2	MK3 (PYS=16)	No	25	P8 Worn		Trailing
3	MK3 (PYS=16)	No	12.5	P8 New		Facing
4	MK3 (PYS=16)	No	12.5	P8 Worn		Trailing
5	Desiro (PYS=24)	No	25	P8 New		Facing
6	Desiro (PYS=24)	No	25	P8 Worn		Trailing
7	Desiro (PYS=24)	No	12.5	P8 New		Facing
8	Desiro (PYS=24)	No	12.5	P8 Worn		Trailing
9	Wagon (90t)	No	12.5		P5 Worn	Facing
10	Wagon (90t)	No	25		P5 Worn	Facing
11	Wagon (90t)	No	12.5		P5 Worn	Trailing
12	Wagon (90t)	No	25		P5 Worn	Trailing

Table 6: List of Vampire Simulation Runs without Track Lube (Arthur, 2017)

Table 6 lists the parameters used for each of the 12 simulation runs. Attention was paid to the weight of the vehicles since the amount of vertical force exerted on the switch was of particular interest; thus the use of a lighter train vehicle (MK3), medium train vehicle (Desiro) and heavy train vehicle (freight wagon) to run over the switch. The vehicles were run in both the facing and trailing directions with worn and new P8 wheels for the passenger vehicles and worn P5 wheels for the freight wagon. As new wheels wear out quickly, the author's primary focus was on the worn wheels.

In addition to the above, four additional simulation runs (Table 7) were also conducted for all the vehicles traveling in the trailing direction only, at full turnout speed with the application of track lubrication. This choice was because most of the S&C suffer a lot of damage in the trailing direction, a case presented by Network Rail, the author of this thesis wanted to examine the impact of an effective track lubrication on the S&C.

Vampire Run	Vehicle Type	Rail Gauge Corner Lubrication	Train Speed mph	Wheel Profile (Passenger)	Wheel Profile (Freight)	Direction of Travel
13	MK3 (PYS=16)	Yes	25	P8 New		Trailing
14	Desiro (PYS=24)	Yes	25	P8 New		Trailing
15	Desiro (PYS=24)	Yes	25	P8 Worn		Trailing
16	Wagon (90t)	Yes	25		P5 Worn	Trailing

Table 7: List of Vampire Simulation Runs with Track Lube (Arthur, 2017)

5. RESULTS AND ANALYSIS OF SIMULATION

5.1 FEM Results from ABAQUS

5.1.1 Von Mises Stress

The evolution of von Mises stress levels at the wheel-rail contact point between the existing and proposed designs were compared and the results plotted. Maintaining the same axle load of 80 kN and longitudinal velocity of 25 mph in the facing direction, it can be observed that the maximum recorded von Mises stress, 1050 MPa, occurred in the existing design NR60C MK1 switch. This is because, as the wheel traverse this section, a small contact radius was formed along the rail and this led to a corresponding small contact patch which produced the high stress level of 1050 MPa (Figure 29).

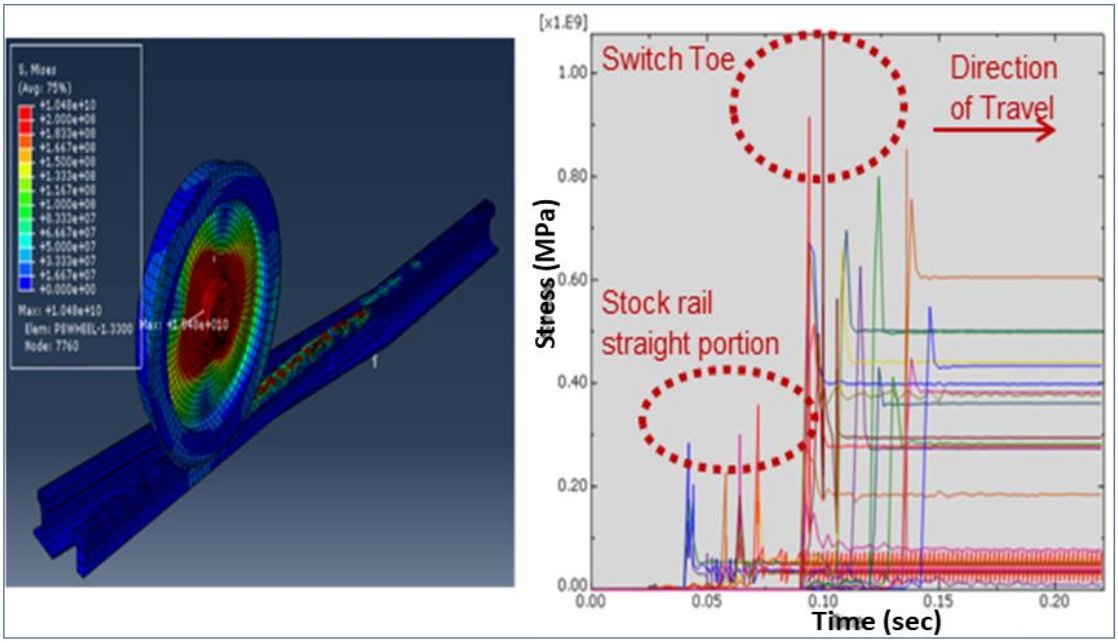

Figure 31: NR60C MK1 Von Mises Stress Distribution (Arthur, 2017)

On the other hand, the addition of 3 mm material created a large contact radius for the proposed NR60C MK2 design and, hence, predicted a low stress level of 580 MPa (Figure 32). This suggests that in the presence of high axle load, the MK1 design will undergo high plastic deformation when compared to the MK2 design. As GB track is used by mixed traffic where both passenger and freight trains use the same track, it is evident from the results that the revised design is better suited for this mixed traffic system due to the low stress level at the switch rail.

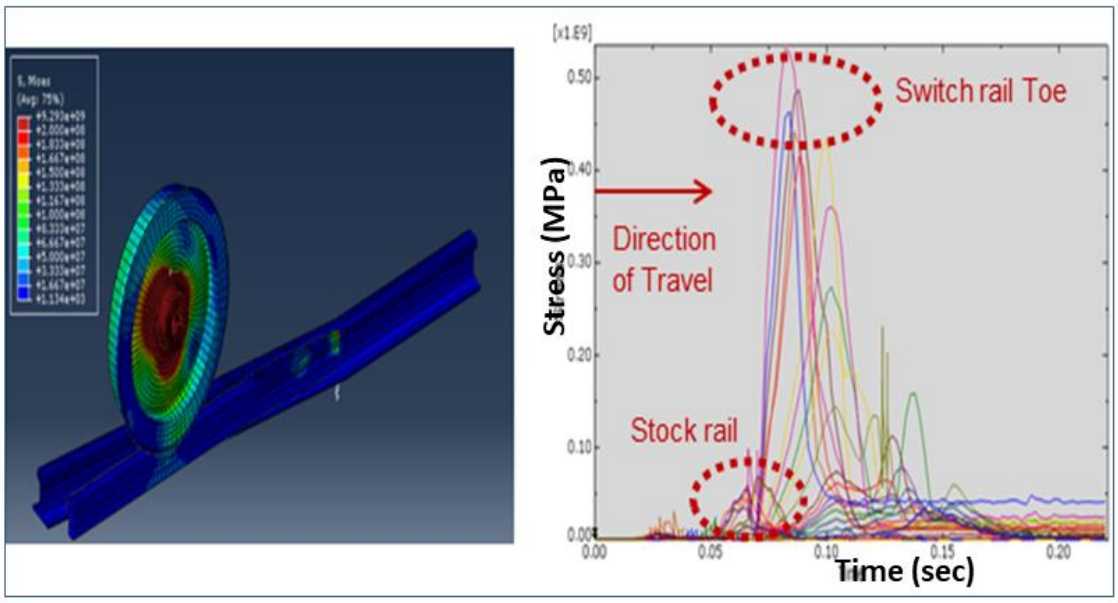

Figure 32: NR60C MK2 Von Mises Stress Distribution (Arthur, 2017)

5.1.2 Equivalent Plastic Stain (PEEQ) Distribution

A measure of the extent of plastic deformation was captured by the PEEQ which is used to describe the history of deformation. It is caused by forces acting on the contact surface due to wheel movement. To arrive at this, nodal values along the rail were extrapolated to generate a PEEQ plot. As a plastic strain, once PEEQ exceeds its elastic limit, it keeps its value throughout the analysis. At each cross section along the switch rail in the facing direction, the maximum PEEQ was evaluated and the results shows that PEEQ was more localized at long time duration (along the switch rail) than short time duration (along the stock rail) implying more plastic deformation along this region (switch rail).

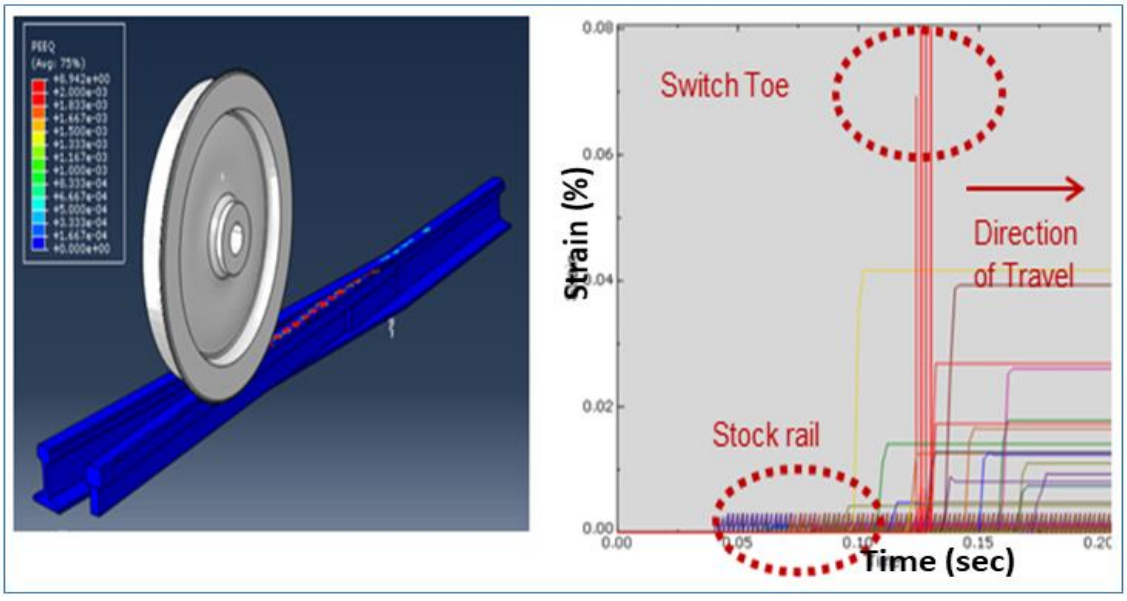

Figure 33: NR60C MK1 PEEQ Distribution (Arthur, 2017)

The modelling predicted PEEQ levels of 8% plastic strain for NR60C MK1 (Figure 33) and 2.1% plastic strain for NR60C MK2 (Figure 34) implying the existing design was subjected to high inelastic deformation as the train passed over it when compared to the revised design.

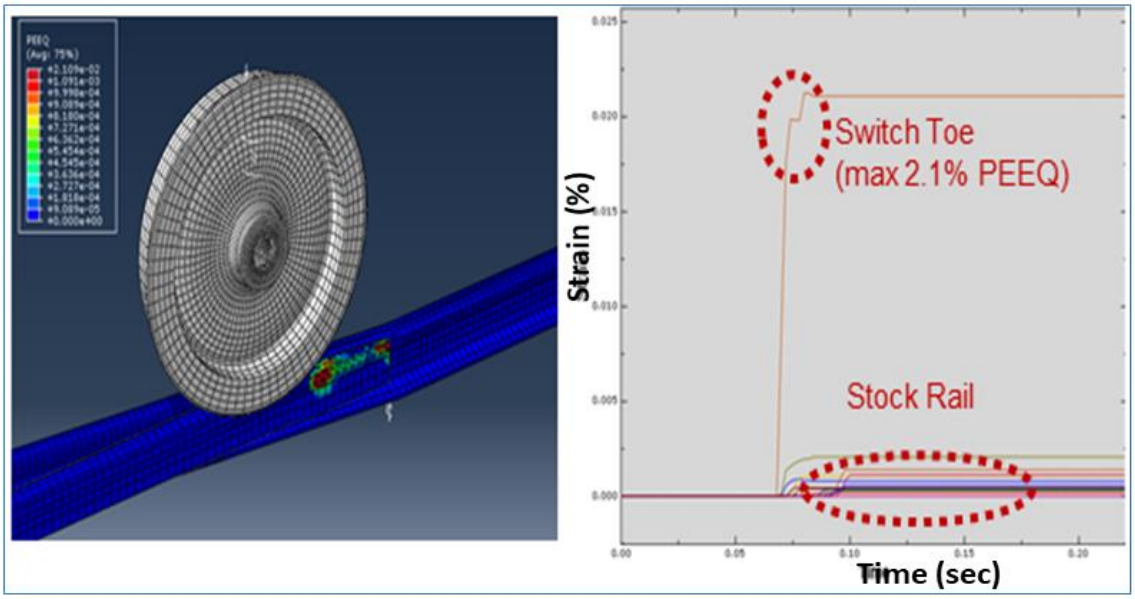

Figure 34: NR60C MK2 PEEQ Distribution (Arthur, 2017)

5.1.3 Displacement

As the train negotiated the turnout, there was minimal displacement along the stock rail for both designs as a result of the material strength of the stock rail. In comparison to the switch, displacements occurred between the switch toe and the planing section in both designs.

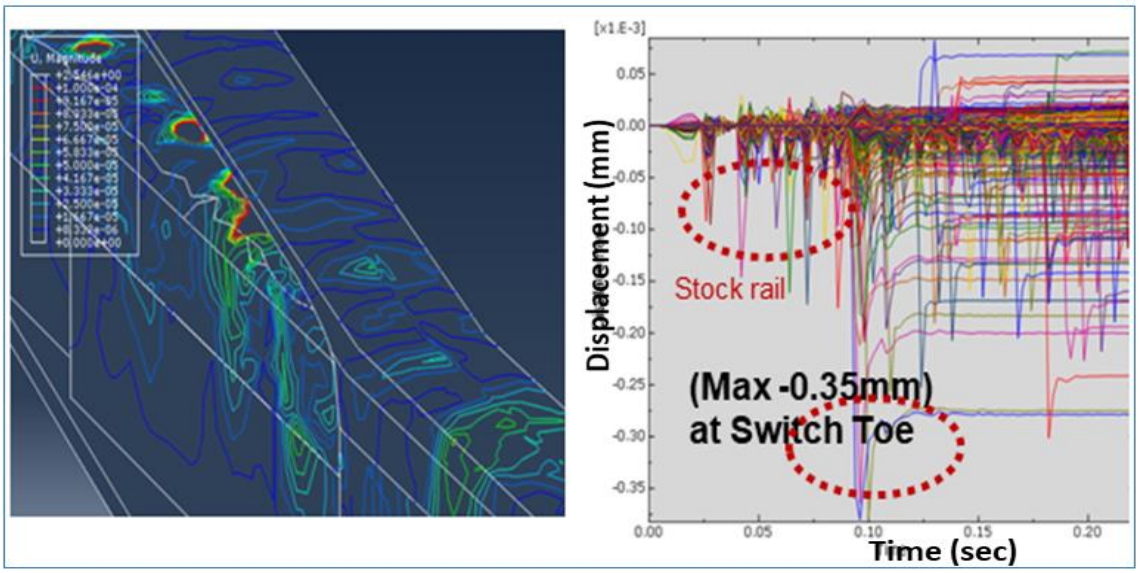

Figure 35: NR60C MK1 Displacement Plot (Arthur, 2017)

When the magnitude of displacements for both designs are compared, Figure 35 recorded large displacements (max of -0.35 mm) on the switch rail of the existing NR60C MK1 switch

and smaller displacements (max of -0.12 mm) for the revised NR60C MK 2, as evident from Figure 36.

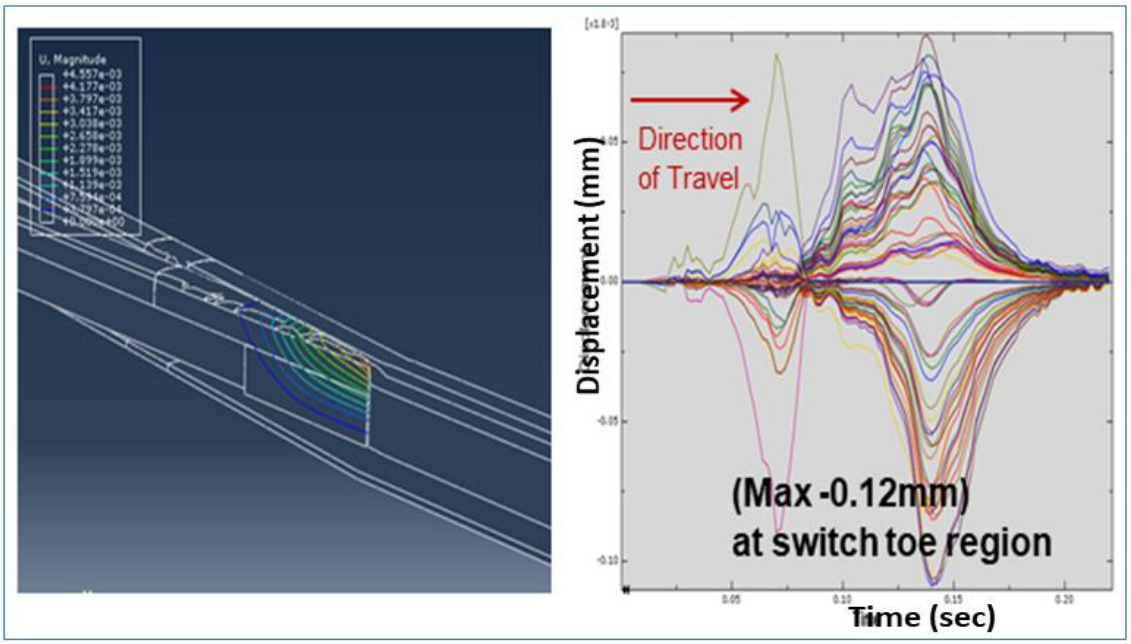

Figure 36: NR60C MK2 Displacement (Arthur, 2017)

5.1.4 Contact Force

The plot in Figure 37 illustrates a maximum vertical contact force of 71 kN for the existing NR60C MK1 switch at the switch toe which is higher than that of the new design NR60C MK2 switch which clocked a maximum of 22 kN as per Figure 38. The vertical contact force will increase under high running velocities and high axle loads.

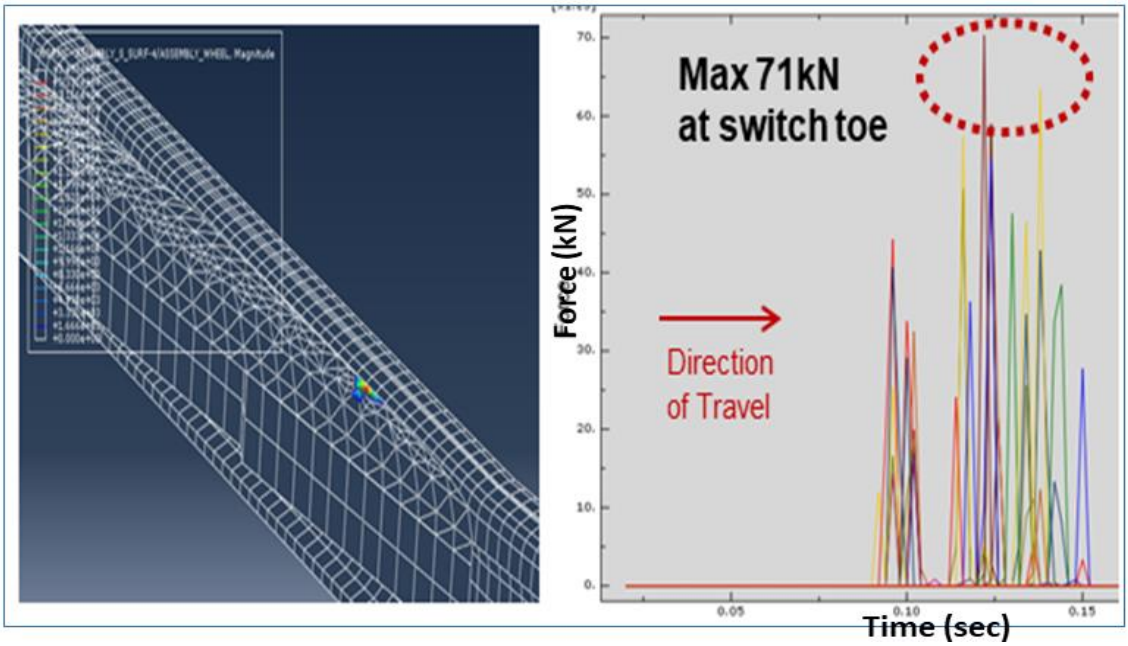

Figure 37: NR60C MK1 Contact Force (Arthur, 2017)

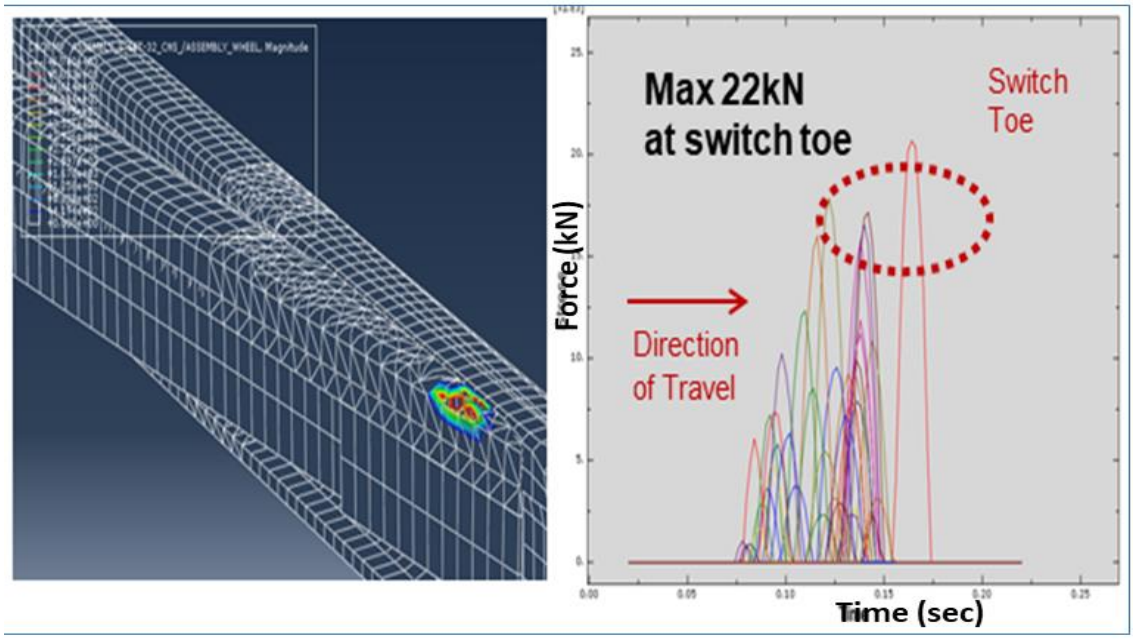

Figure 38: NR60C MK2 Contact Force (Arthur, 2017)

5.1.5 Crossing Nose

The author reviewed the challenges facing the crossings on the GB network and made some changes to the crossing configuration in relation to its dependencies. In particular, bearer spacing was reduced to 600 mm in the simulation and an additional bearer placed under the crossing knuckle to absorb the effects of high impact forces at the crossing nose. The model considered a crossing with a continuous foot flange and an additional material thickness of 1.2 mm at the tip of the crossing nose for the proposed NR60C MK2 crossing. During the FE modelling, the dynamic responses for von Mises stress, contact force, PEEQ and vertical displacement were obtained for the NR60C MK2 crossing and validated against Pletz (2012).

Figure 37 illustrates the results of stress distribution for the proposed design.

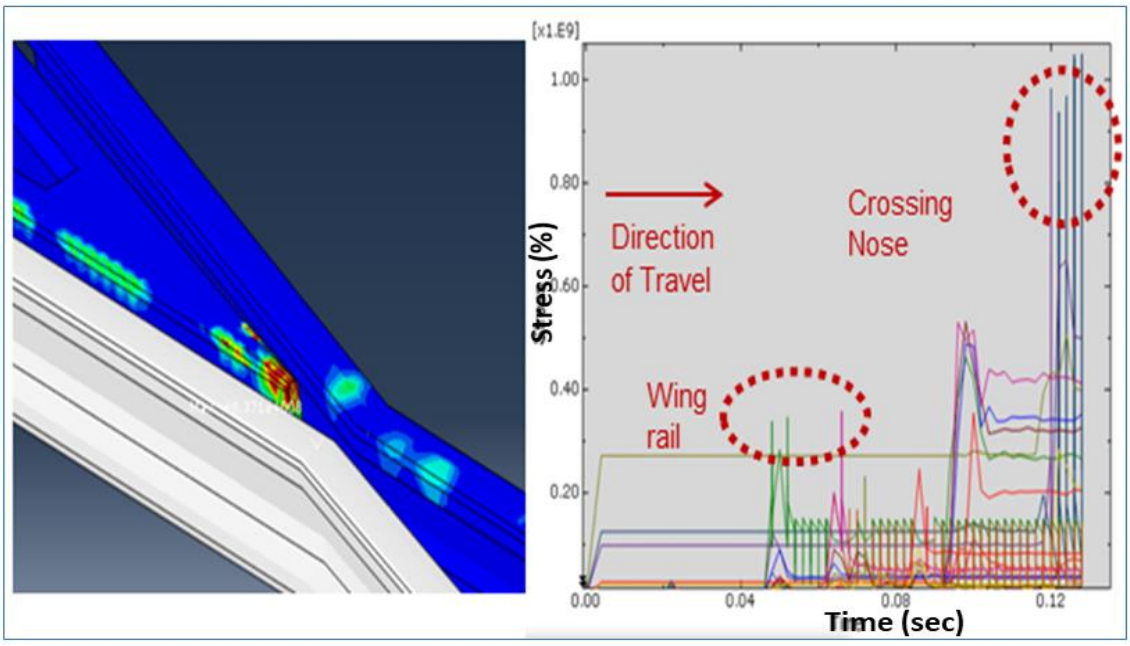

Figure 39: NR60 MK2 Crossing Nose Stress Distribution (Arthur, 2017)

Initially, the stress levels at the wing rail were compared with that of the crossing nose under high impact forces and Figure 39 shows a Von Mises stress of 1060 MPa at the crossing nose and 400 MPa at the wing rail of the existing design. This is due to the small radii at the tip of the crossing nose which is a constraint of the crossing geometry, hence this is the section where the maximum von Mises stress occurs.

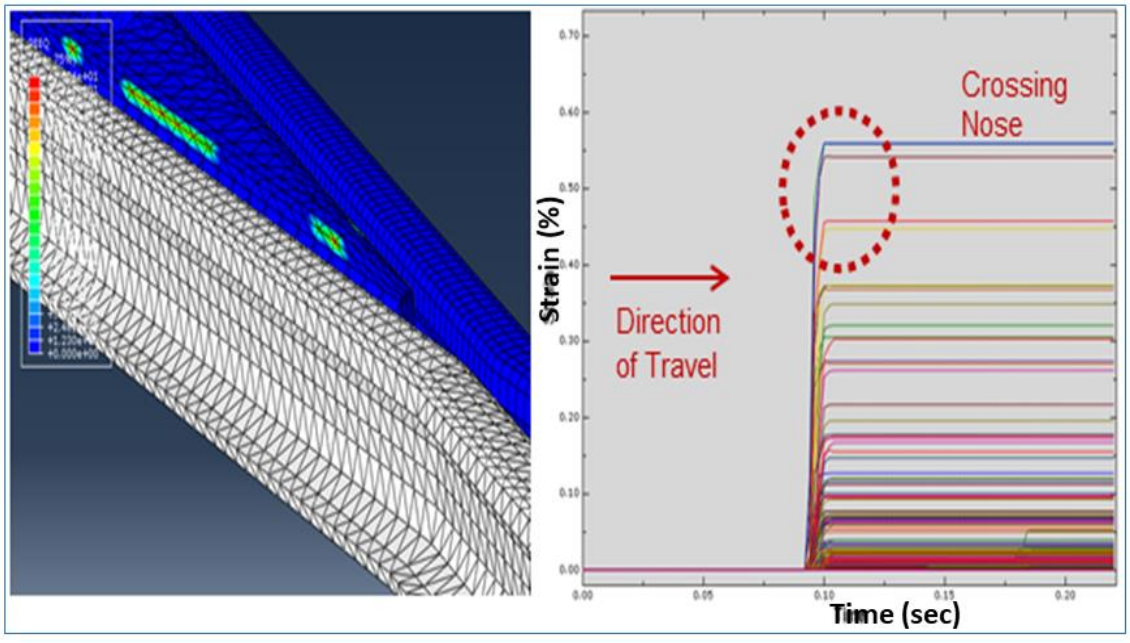

Figure 40: Crossing Nose NR60C MK2 PEEQ Distribution (Arthur, 2017)

Figure 40 shows the PEEQ distribution of the proposed crossing. The simulation predicted the maximum accumulated equivalent strain calculated for the crossing nose to be 5.6%. There is a geometrical adaptation of the wing rail and crossing nose which is caused by the plastic strain. During manufacturing, the manganese steel becomes very soft at first loading and hardens quickly after successive cycles. As such, based on further additional loading, elastic shakedown can be reached due to the crossing geometry changes and also material hardening. The calculated plastic strains shown in Figure 38 indicate a positive effect on the performance of the crossing.

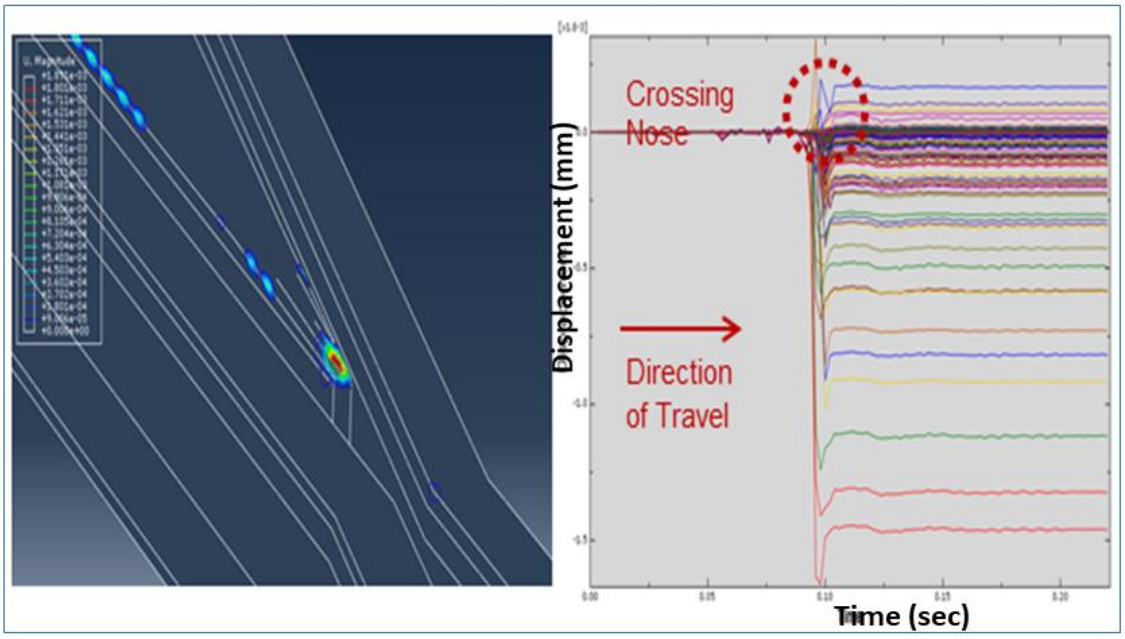

Figure 41: NR60C MK2 Crossing Nose Vertical Displacement (Arthur, 2017)

Figure 41 illustrates a vertical displacement of -1.67 mm at the crossing nose. During wheel transfer between the wing rail and crossing nose, a high impact load tends to arise and as a result of this, the maximum contact force predicted by the simulation was 82 kN as recorded in Figure 42.

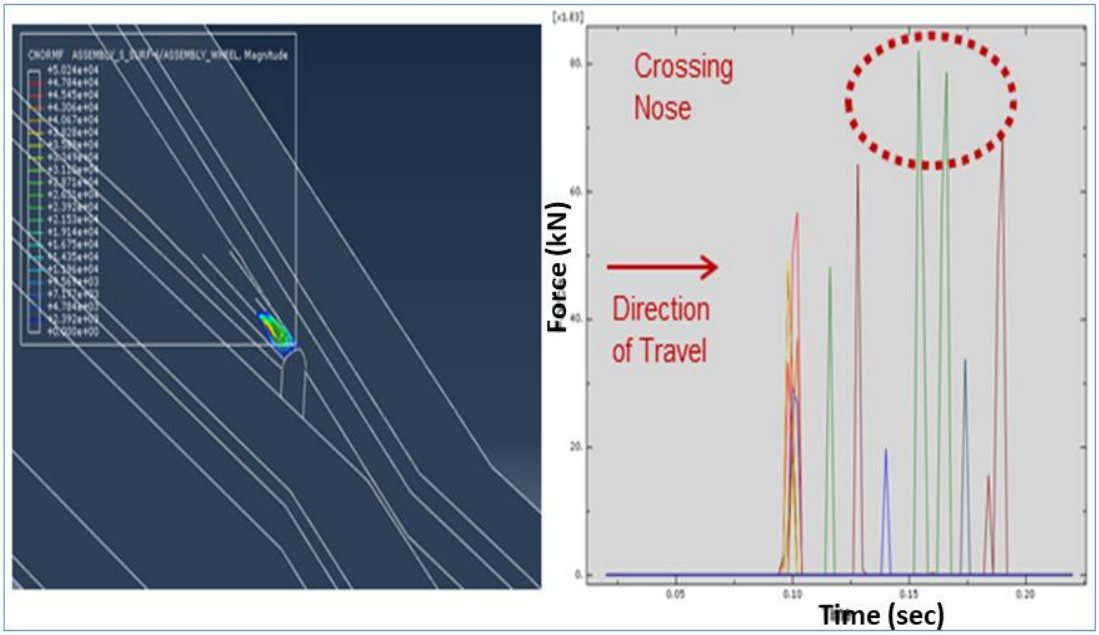

Figure 42: NR60C MK2 Crossing Contact Force Distribution (Arthur, 2017)

5.1.6 Contact Analysis

A contact analysis study was undertaken to investigate the behaviour of the two designs when in contact and to assess the impact of the contact size when using normal or worn wheel profiles. As the rolling wheelset comes into contact with either the switch or the crossing at different positions, a two-point contact is formed (shown in 43). The simplified 2D contact analysis seems to be the best approach to investigate contact location and contact stress distribution with various wheel profiles and rail geometries.

The level of stress in the switch and crossing is largely dependent on the contact radii. As the wheel negotiates the turnout, contact radii are formed and these are usually small at the tip of the switch and crossing nose. A small contact radius will result in a small contact patch which will produce a higher contact stress levels. During the investigation, the normal P8 wheel produced a maximum force of 22 kN (43) as a result of small contact radii whilst the worn P8 wheel produced a maximum force of 19 kN due to the greater contact radii.

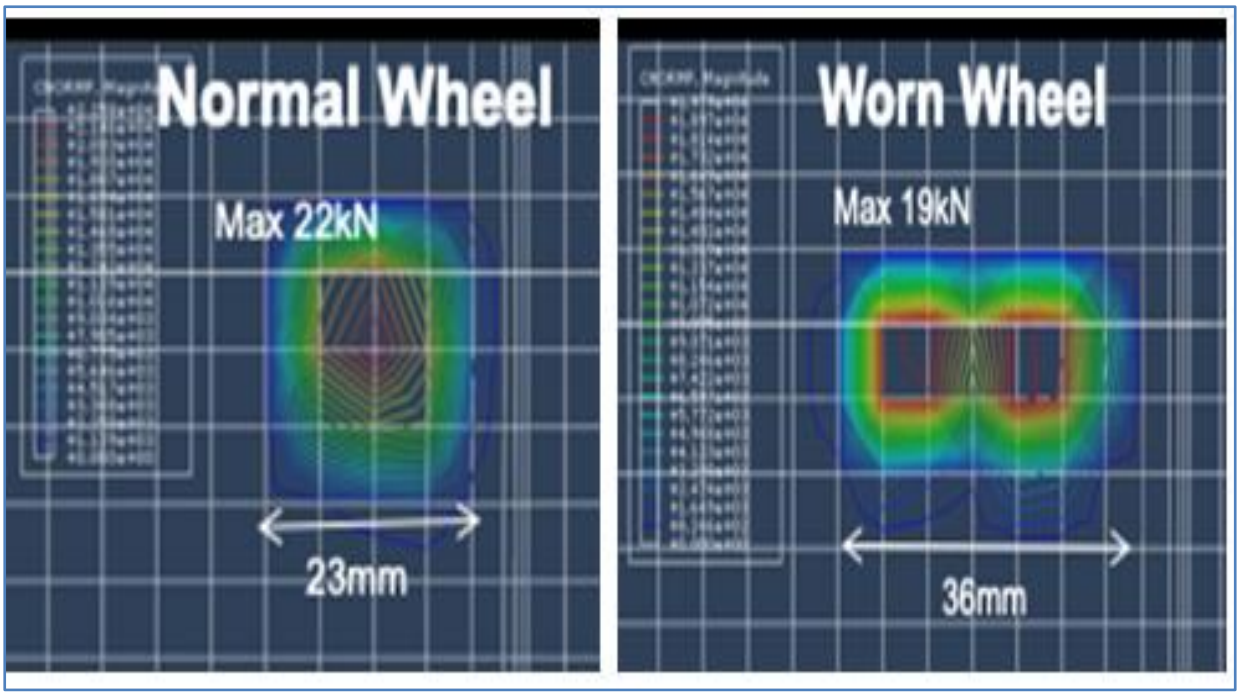

Figure 43: Contact Patch for Normal & Worn P8 Wheel (Arthur, 2018)

A worn wheel profile would inevitably result in more conformal contact conditions and hence increase the likelihood of multiple points of contact occurring. As shown in the contact patch shapes (Figure 43), worn wheel showed a bigger contact size than the as new wheel and, hence, exhibits two-point contact. The outcome from this 2D study concludes that a worn wheel has a greater conformal contact region with a smaller contact stress.

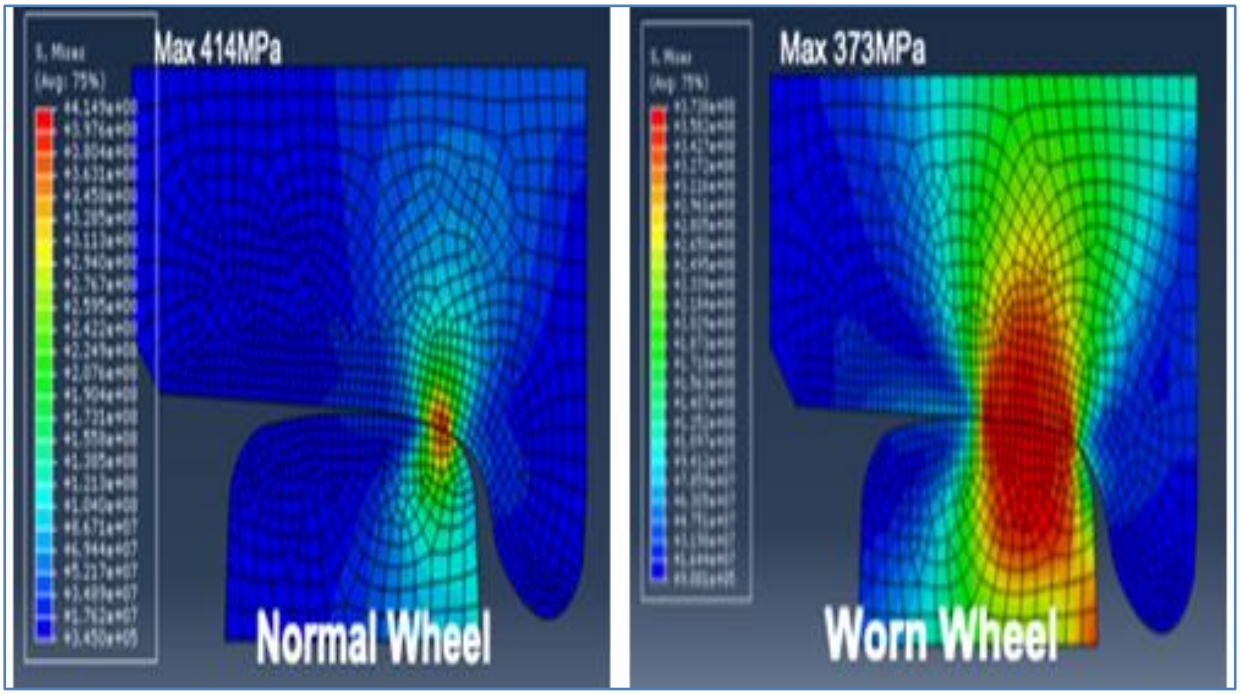

Figure 44: Stress Distribution for Normal & Worn P8 Wheel (Arthur, 2018)

From the 2D contact analysis, the worn wheel shows much a smaller stress distribution (373 MPa) than the normal wheel (414 MPa) as noted in Figure 44. Also, the extended rail top surface of the revised design resulted in a more conformal wide contact zone with lower stress levels.

5.1.7 Fatigue Life Analysis (FE – SAFE using S-N Approach)

Bai (2016) defined fatigue as the failure induced on a material, upon cyclic load action. Unlike fatigue, failure therefore relates to dynamic loads that are repeated. Due to the mode of occurrence (abrupt and sudden), it is very difficult to predict fatigue as it is not visible from the onset. Fatigue consists of three stages labelled as crack initiation stage, crack propagation and fracture stage.

To present a complete analysis of the simulation, an integrated Finite Element analysis based on fatigue stress-life was conducted where the switch rail was subjected to variable amplitude loads under different loading conditions. The approach was employed to investigate the life of the existing and proposed designs. Material, geometry and load history information obtained from the Finite Element analysis were used as input data. The stress-life approach which evaluates elastic stresses and their corresponding impact on material life was employed to evaluate the fatigue life of both the NR60C MK1 and NR60C MK2 designs. The stress versus number of cycles (S-N) relationship within the finite region can be expressed as a log-log linear relationship and this was used to determine the fatigue life using a failure criterion such as von Mises. A typical S-N curve can be defined by

$$S^t N = C \qquad (44)$$

Where N is the number of cycles, at a given stress to failure, S is stress, t and C represent material parameters. In a high cycle fatigue region, the slope of the S-N curve is represented by t. Some materials may show a lower fatigue limit beyond which fracture may not occur under conditions of low amplitudes. Equation 44 illustrates that there is a positive correlation between the applied stress and the fatigue damage of a component.

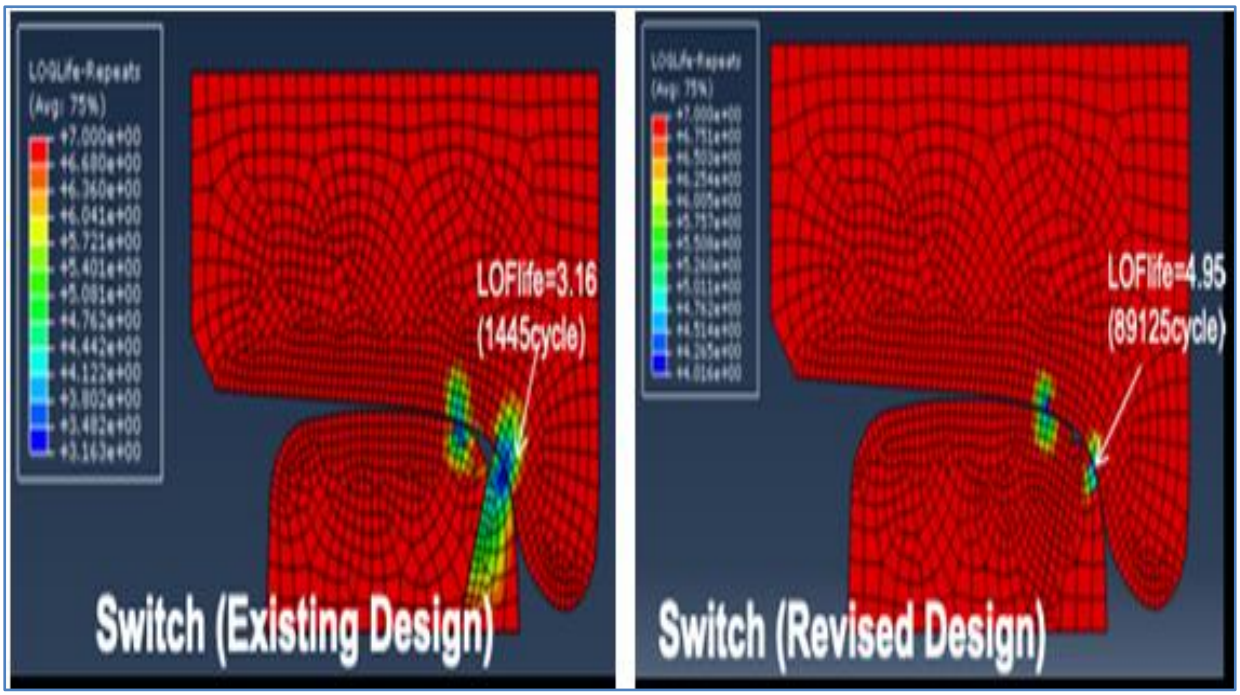

Figure 45: Fatigue life NR60C MK1 and NR60C MK2 Switches (Arthur, 2018)

The results of the simulation show the existing NR60C MK1 switch design recorded a log life of 3.16 and the augmented NR60C MK2 switch design predicted a log life of 4.95. This implies that the revised NR60 MK2 switch design has a longer service life, by about 60%, than the existing design based on the FE-SAFE analysis.

5.1.8 Validation of Results

Table 8 below illustrates that the summary results obtained are consistent with the predictions outlined in section 1.2 of this thesis. According to the results, the addition of 3 mm of material to the switch rail has reduced the stress level for the NR60C MK2 switch rail by about 47% to 580 MPa. Similarly, equivalent strain levels have fallen to 2.1% and there were minimal displacement levels when compared to the existing design.

	Existing Switch NR60C MK1	Proposed Switch NR60C MK2	Proposed Crossing
Von Mises Stress	1050 MPa	580 MPa	1050 MPa
PEEQ	8%	2.1%	5.6%
Vertical Displacement	0.35 mm	0.12 mm	1.67 mm
Contact Force	71 kN	22 kN	82 kN

Table 8: Summary of Results (Arthur, 2018)

To validate the model, the maximum values of contact pressure were compared with (Hertz, 1882) who recorded 2566 MPa and (Wiest, 2008) who recorded 1085 MPa in their work using Elastic-Plastic FE Method. A more recent analysis by (Pletz, 2012), who investigated a wheel

passing through a switch and crossing under a high axle load, noted the maximum contact pressure as 1550 MPa. It is evident that the results from the revised NR60C MK2 switch is consistent with the work of these researchers as highlighted in Table 9 below. However, this is to serve as a guide only because the geometry, material properties, operational conditions and modelling methodology for all this thesis and previous research work are different.

	Contact Area [mm2]	Max Contact Pressure [MPa]
Hertz	65	2566
Elastic-Plastic FEM (Wiest et al)	70	1085
Pletz	128	1550
Proposed NR60C MK2	36	1050

Table 9: Validation of Results (Arthur, 2018)

5.2 Vehicle Dynamic Simulation Results

In order to undertake a Vampire Analysis, a set of input files are required: RUN file (the control file), Track Design file, Track Contact file and wheel-rail contact data file (see Appendix B: Simulation Input). Three wheel-rail contact data files were generated for each selected wheel profile for both directions of travel.

5.2.1 Contact Position and Effect of T-Gamma on RCF Predictions

T-Gamma is a measure for the frictional energy dissipation at the wheel-rail contact patch and this will increase when the contact between the wheel and rail shifts from the top of rail to the gauge corner. It serves as an input energy for the prediction of the RCF damage index. The two models widely used in the railway industry for RCF prediction are theoretical (desktop calculations) and empirical models (evidence based). Theoretical models attempt to predict the likelihood of an event to happen like RCF crack growth models through calculations and the empirical studies focus on the likelihood of an RCF crack growth based on experimental output. (Burstow M. , 2003) applied the empirical model of RCF prediction in his Whole Life Rail Model (WLRM). In this, a parameter derived from T-Gamma which gave the best correlation between RCF simulation and location of crack has become the industrial benchmark in the UK. Due to a lack of resources, the author of this thesis had to adopt the theoretical model approach for RCF prediction since there was no field experimental output.

In this section, damage models based on the calculated energy dissipation were used to evaluate the rate of rail wear and RCF predictions. In reviewing the results, the main focus

will be on the impact on the freight wagon in the trailing direction as it has the train with highest axle load and so is the most likely to cause significant damage to the switch rail.

5.2.1.1 90t Freight Wagon (P5)

Freight Wagon Facing Move

The simulation results show that for all the different types of trains, T-Gamma values for flange contact were greater than those of tread contact. In particular, the freight train recorded a T-Gamma value of 1079 J/m for flange contact in Figure 44 whilst the same train recorded T-Gamma value of 400 J/m for tread contact. The first flange contact occurs at rail profile number '1800' (1.8 m from the switch toe) and is continuous throughout the turnout. The dominant form of damage to the surface of the switch rail is wear and this occurs at high T-Gamma levels. Using the rail wear index charts in Figures 60 and 61, attention is drawn to the vehicle with the highest T-Gamma value which happens to be the freight wagon. With a T-Gamma of 1079 J/m at the gauge corner, it is expected that rail profiles from '1800' to '3500' (Appendix D) are likely to be worn down quickly along the planing section, as highlighted in red in Figure 48 below.

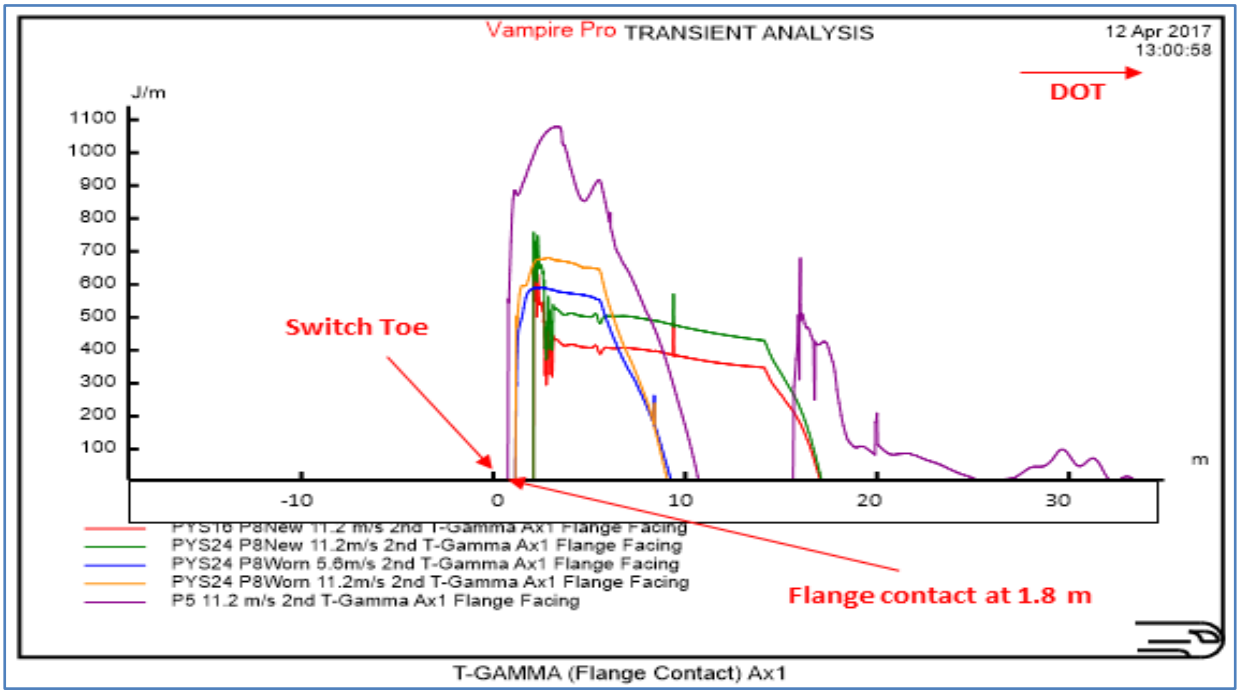

Figure 46: T-Gamma for Flange Contact Facing Direction for Freight Wagon (Arthur, 2017)

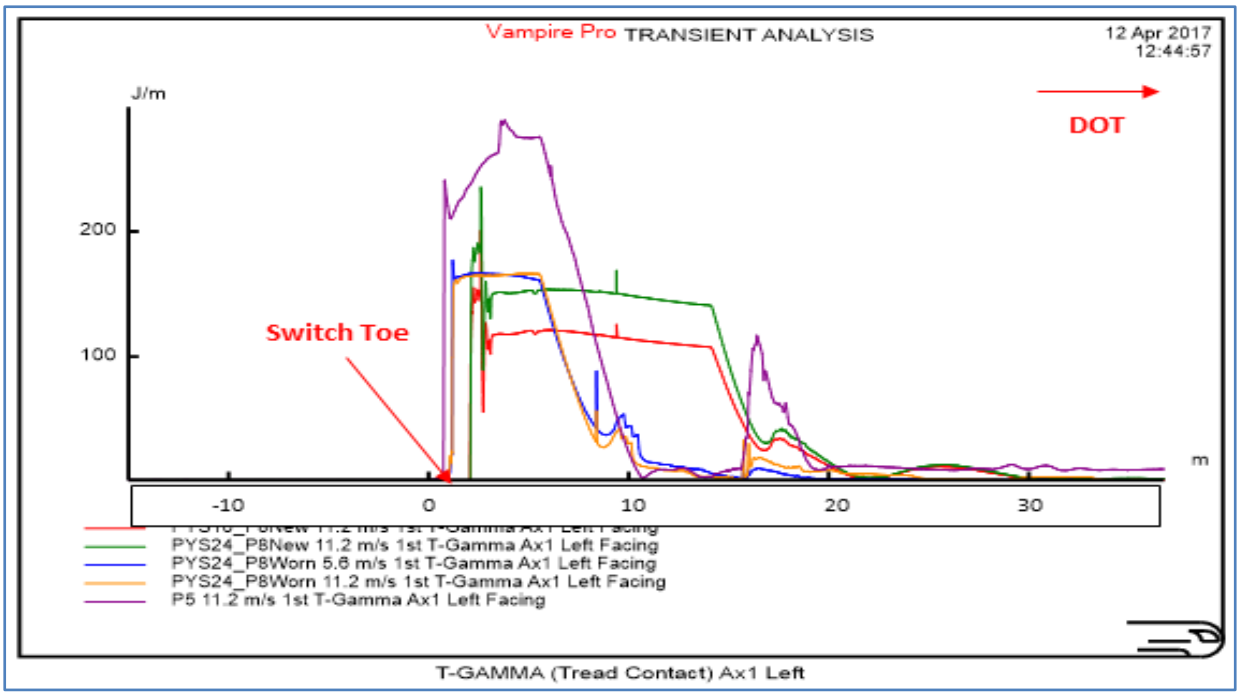

Figure 47: T-Gamma for Tread Contact for Freight Wagon (Arthur, 2017)

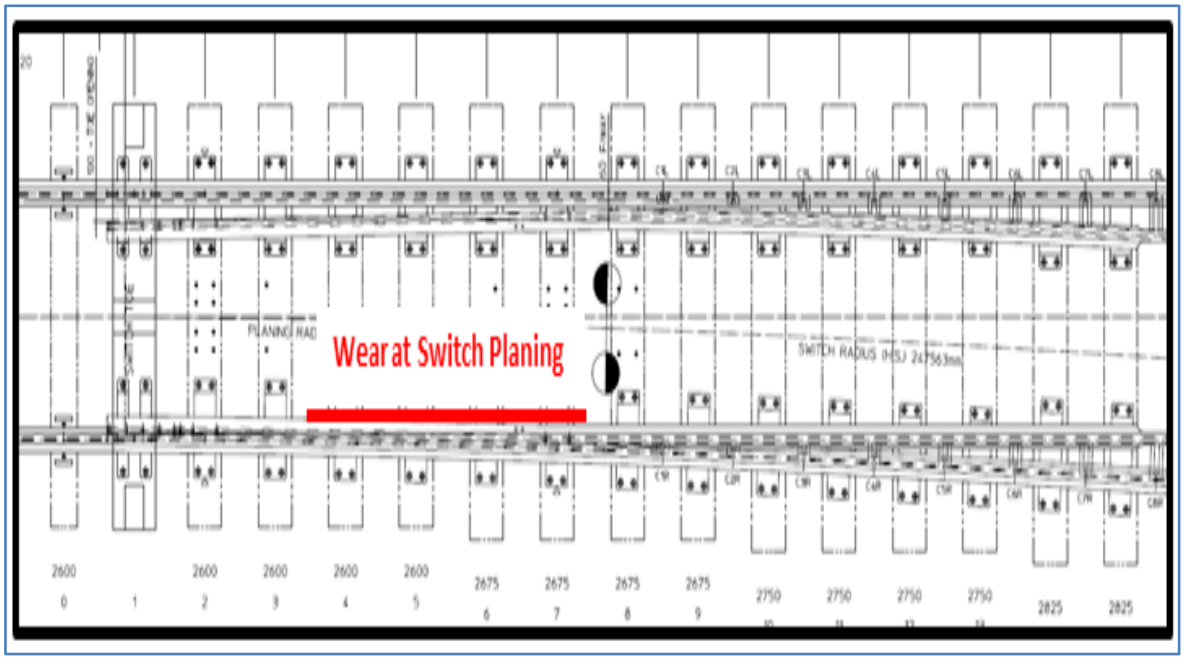

Figure 48: RE/PW 4001 NR60C MK2 showing Location of Rail Wear (Arthur, 2018)

Freight Wagon Trailing Move

During the trailing move, flange contact was observed from the '3800' rail profile (Appendix D) causing the freight wagon (P5) to generate a higher T-Gamma value of 3018 J/m (Figure 48) than the facing move. It predicted the gauge corner wear pattern to be more localised around the toes and higher than the facing move. However, the wear rate reduces further along when the flange contact is lost between '4000' and '4400' rail profiles (Appendix D)

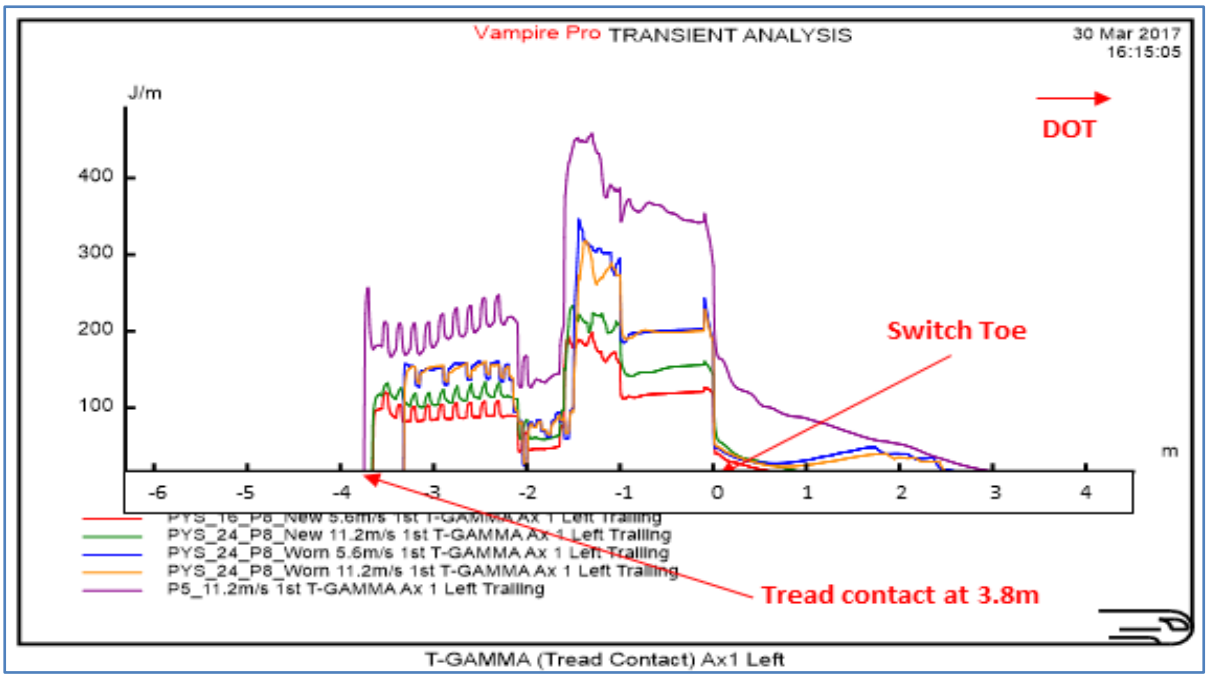

Figure 49: T-Gamma for Tread Contact Trailing Direction for Freight Wagon (Arthur, 2017)

As expected, the tread contact (Figure 49) recorded lower T-Gamma values than the flange contact (Figure 50). The high T-Gamma generated was dissipated into severe gauge corner wear as a result of the flange contact rather than RCF damage.

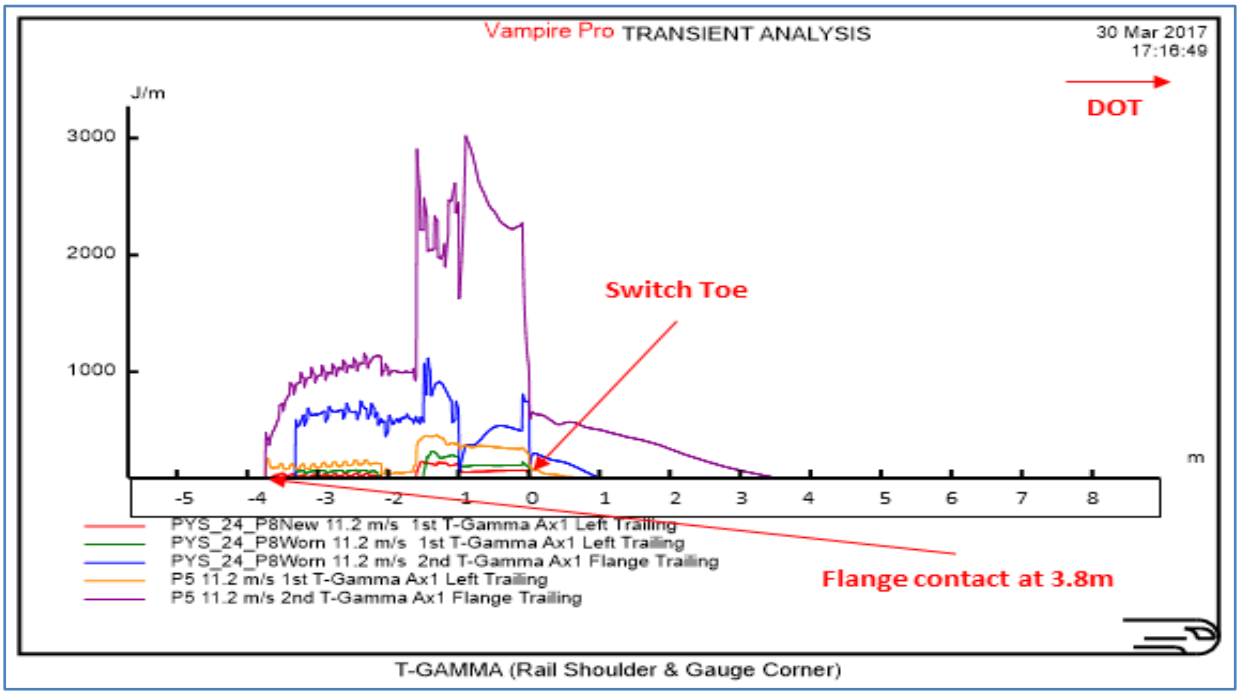

Figure 50: T-Gamma for Flange Contact for Freight Wagon (Arthur, 2017)

5.2.1.2 Desiro Passenger Coach (PYS_24)

Desiro Passenger Coach Facing Move

Flange contact occurred at 2m from the switch toe '2000' rail profile (Appendix D) and throughout the turnout. However, this contact is more subdued with a lower T-Gamma of 680 J/m (Figure 51) when compared with the freight wagon (Figure 44) using the worn wheel at full turnout speed who recorded 1079 J/m. In terms of gauge corner wear, it was localised around the switch toes at the planing section. At full turnout speed, the predicted T-Gamma difference between worn wheel (680 J/m) and new wheel (730 J/m) was not that pronounced.

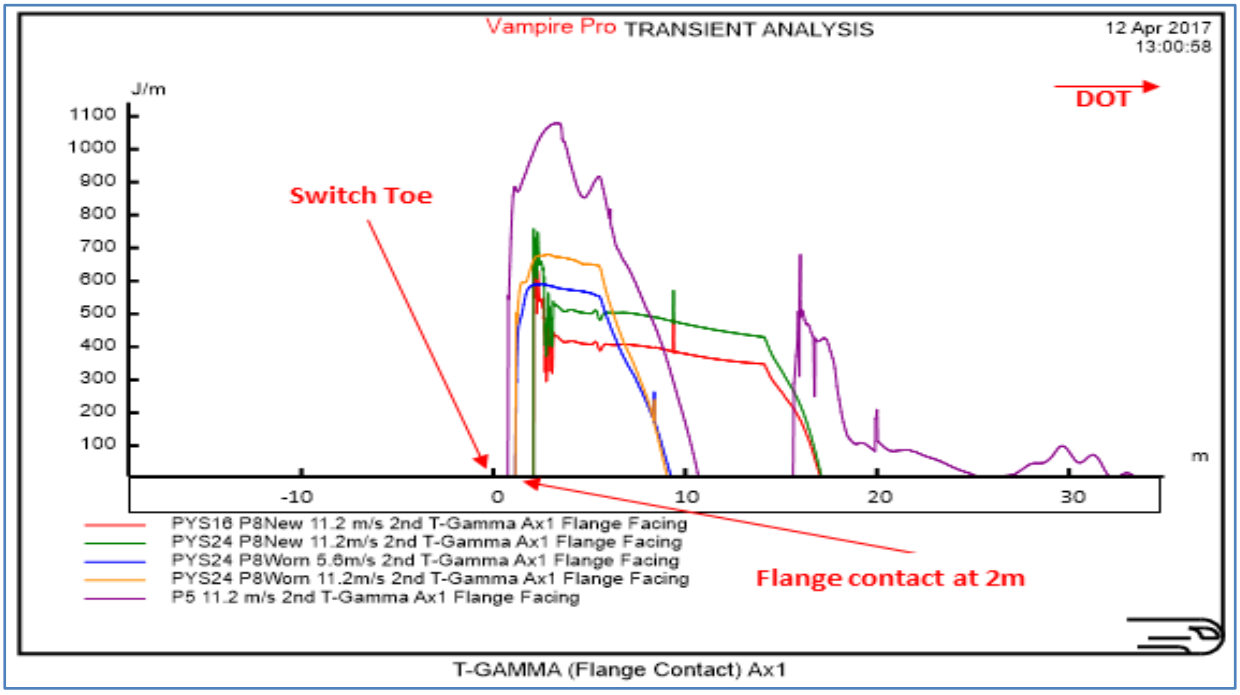

Figure 51: T-Gamma for Flange Contact for PYS_24 (Arthur, 2017)

Desiro Passenger Coach Trailing Move

During the trailing move, two distinct peaks were observed for T-Gamma. The first peak is as a result of flange contact which later translates into a second peak when the train negotiates the multiple contact point (i.e., switch and stock rails). The T-Gamma value of 1117 J/m presented in Figure 52 was generated because of flange contact between rail profiles '1900' and '3400' for the worn P8 wheel, whilst within the same region, 2778 J/m T-Gamma was recorded for the new P8 wheel making it more pronounced when compared with the facing direction. When the T-Gamma values are translated into wear rate, the analysis predicted the new P8 wheel generated high wear than the worn P8 wheel. Just like the facing move, most of the side wear was localised along the planing section.

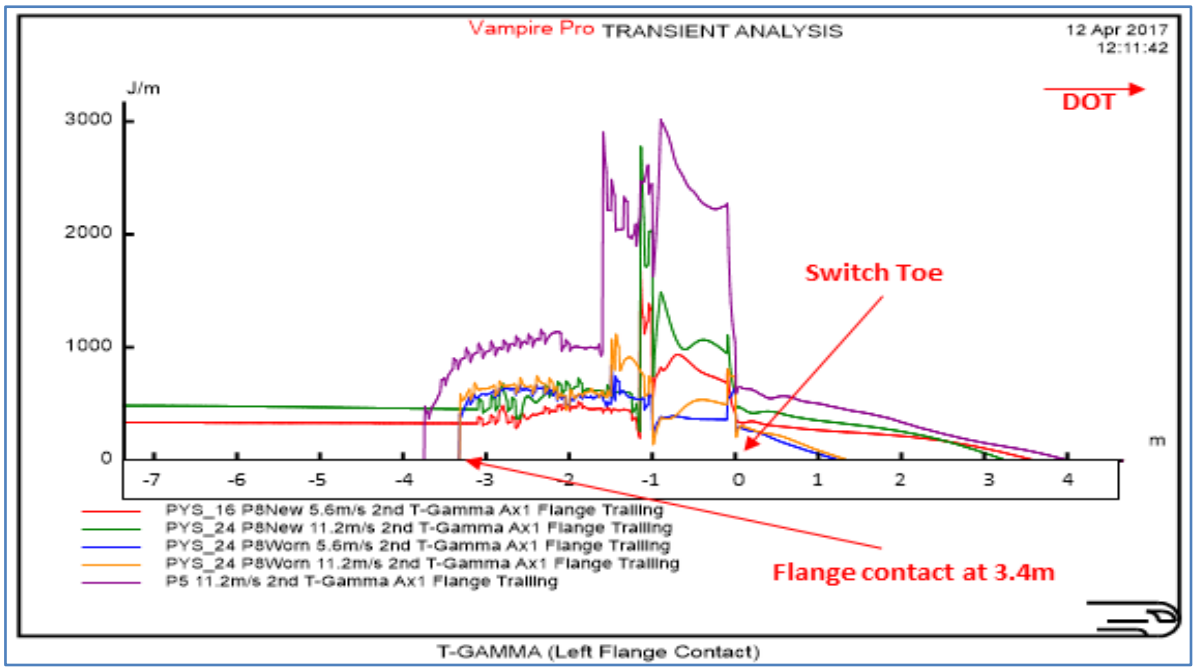

Figure 52: T-Gamma for Flange Contact for PSY_24 (Arthur, 2017)

5.2.1.3 MK3 Passenger Coach (PYS_16)

MK3 Passenger Coach Facing Move

Flange contact for the MK3 passenger coach occurred further along the switch 2.5 m from the switch toe profile and throughout the turnout giving rise to T-Gamma of 665 J/m (Figure 53). Consequently, gauge corner wear was delayed further until '2500' (Appendix D) profile along the planing section of the switch and the wear rate is less severe when compared to Desiro passenger coach which recorded T-Gamma of 680 J/m for the facing move (Figure 49).

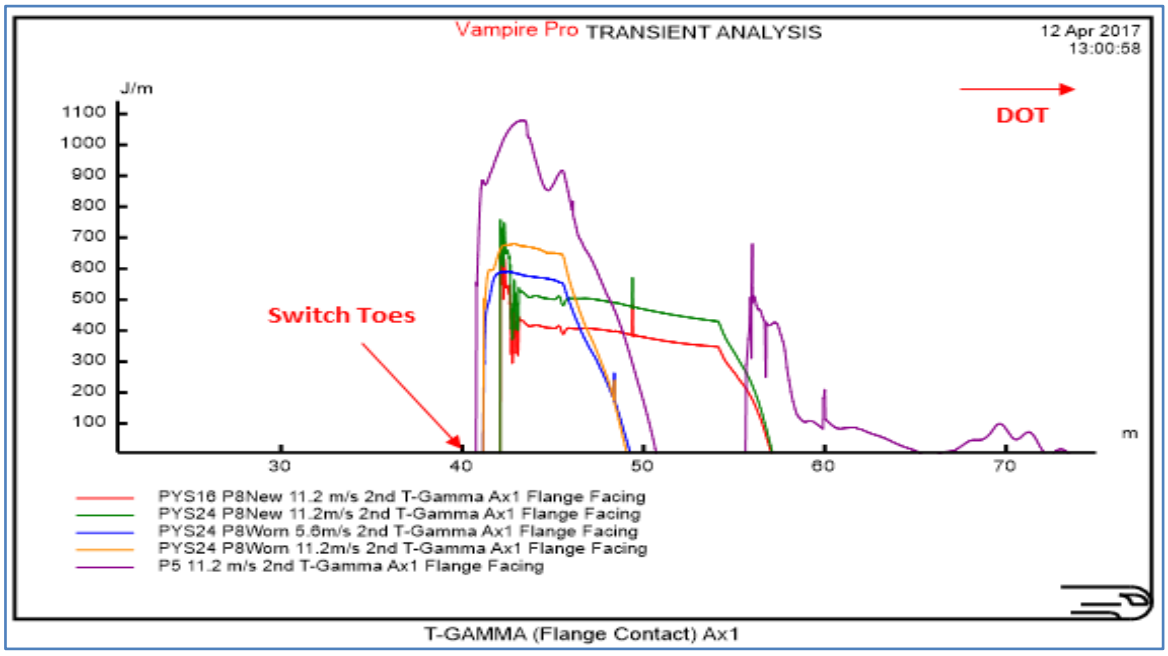

Figure 53: T-Gamma for Flange Contact for PYS_16 (Arthur, 2017)

MK3 Passenger Coach Trailing Move

Figure 54 presents how the MK3 passenger coach trails the switch as it negotiates the turnout. Flange contact occurred 3.5m from the switch toes resulting in a T-Gamma of 1400 J/m. Gauge corner wear commences from '3500'profile (Appendix D) along the planing section of the switch rail but this is higher than that of the facing move.

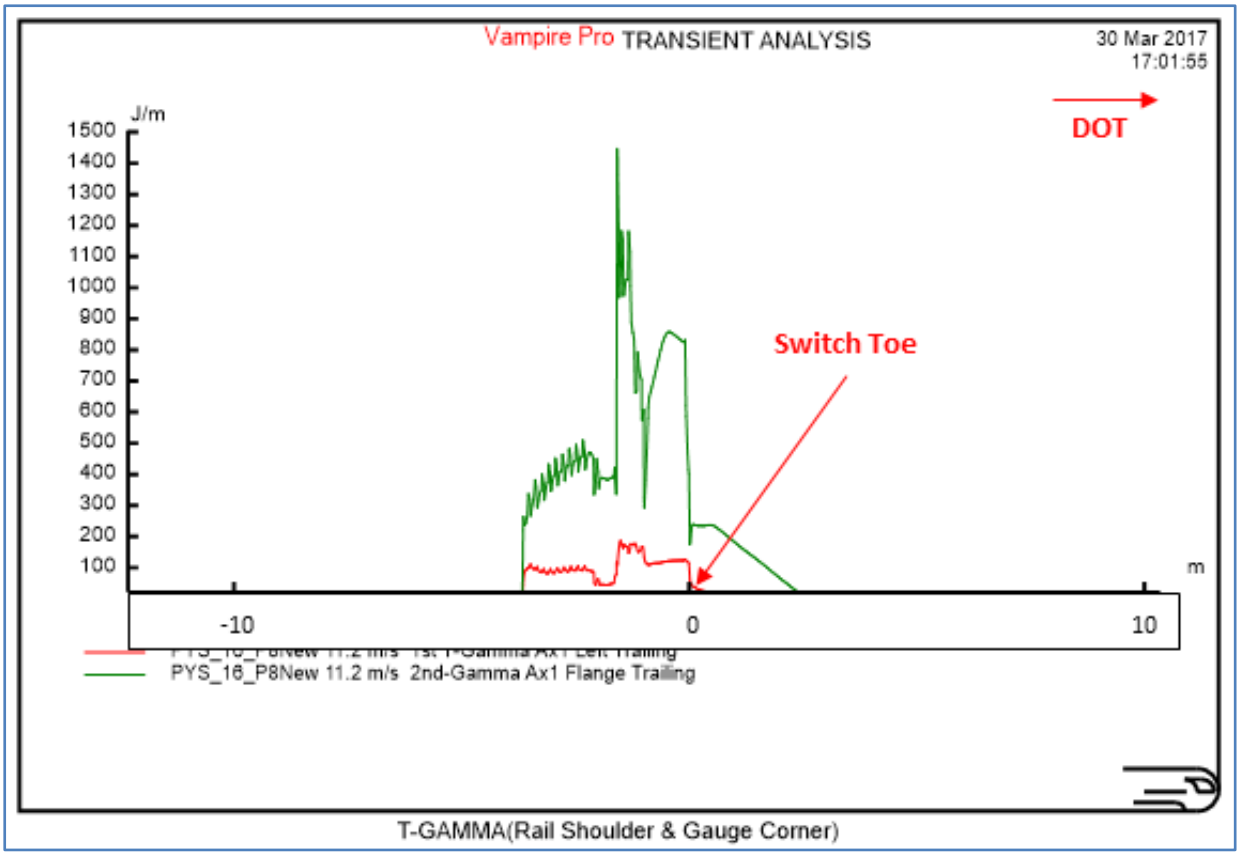

Figure 54: T-Gamma for Flange Contact for PYS_16 (Arthur, 2017)

5.3 Derailment

A derailment risk assessment was carried out using Nadal's criteria prescribed in (Iwnicki S. , 2006) where, at the wheel flange, comparison is made between the horizontal force (Y) and vertical force (Q). The criterion states that there is a critical ratio Y/Q, of the vertical and horizontal force that, when exceeded for a sustained distance, can cause a derailment. (Network Rail, 2002) specifies that on a sliding mean of 2 m length, the Y/Q ratio measured should not exceed a value of 1.2 for any rail and wheel under consideration. This implies that a high value of Y/Q will demonstrate a risk of flange climb as a result of high lateral forces over vertical force as shown in Figure 55.

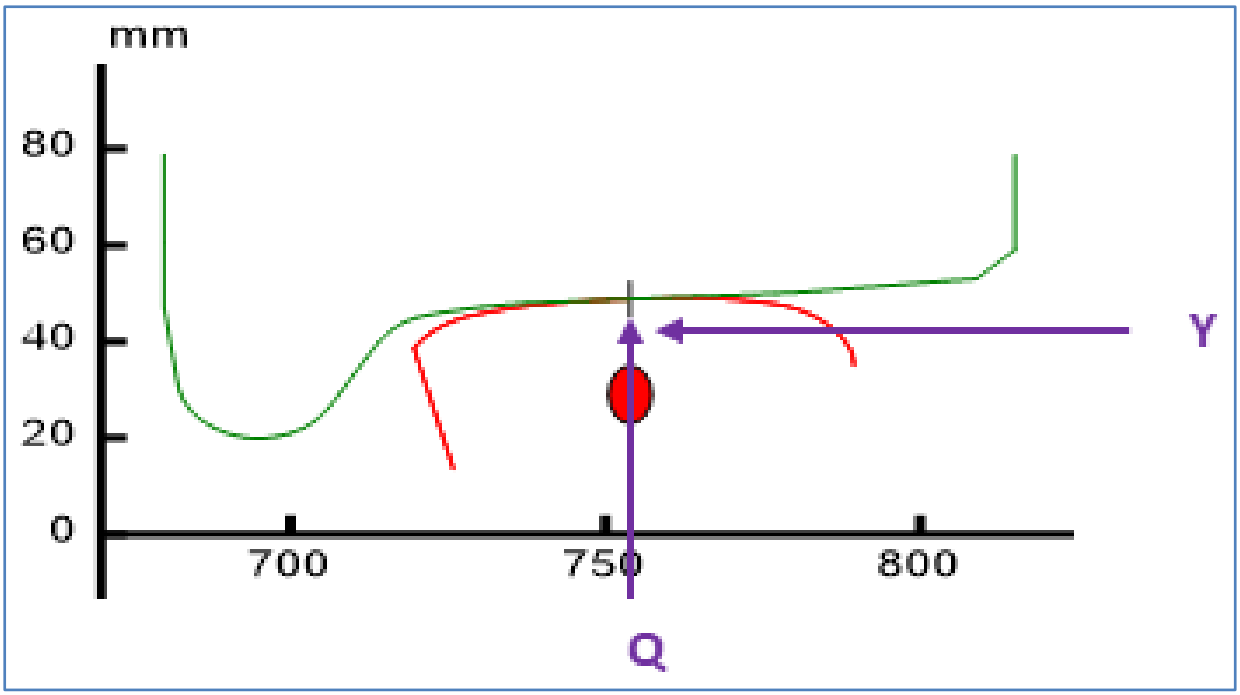

Figure 55: Y/Q Relationship (Arthur, 2020)

Figures 56 and 57 illustrates that all the three vehicles were below the derailment risk threshold of 1.2 in both facing and trailing direction of travel. However, when negotiating the first curve during the trailing move (Figure 57), the lighter vehicle MK3 (PYS16) experienced a higher derailment quotient at full speed than the other two vehicles Desiro and Freight Wagon (PYS24 and P5) and this pattern continued almost throughout the entire distance. The high Y/Q quotient value for MK3 passenger coach is due to the fact that it is the vehicle with the smallest laden weight thus likely to experience the high value in the presence of high lateral forces. It is important to note that Y/Q quotient value for all the three vehicles is lower than the standard critical value of 1.2 and, hence, the revised NR60C MK2 switch does not pose a significant derailment risk for light, medium and heavy vehicles. Furthermore, effective lubrication at wheel/rail flange contact will reduce derailment risk for the MK3 passenger vehicle.

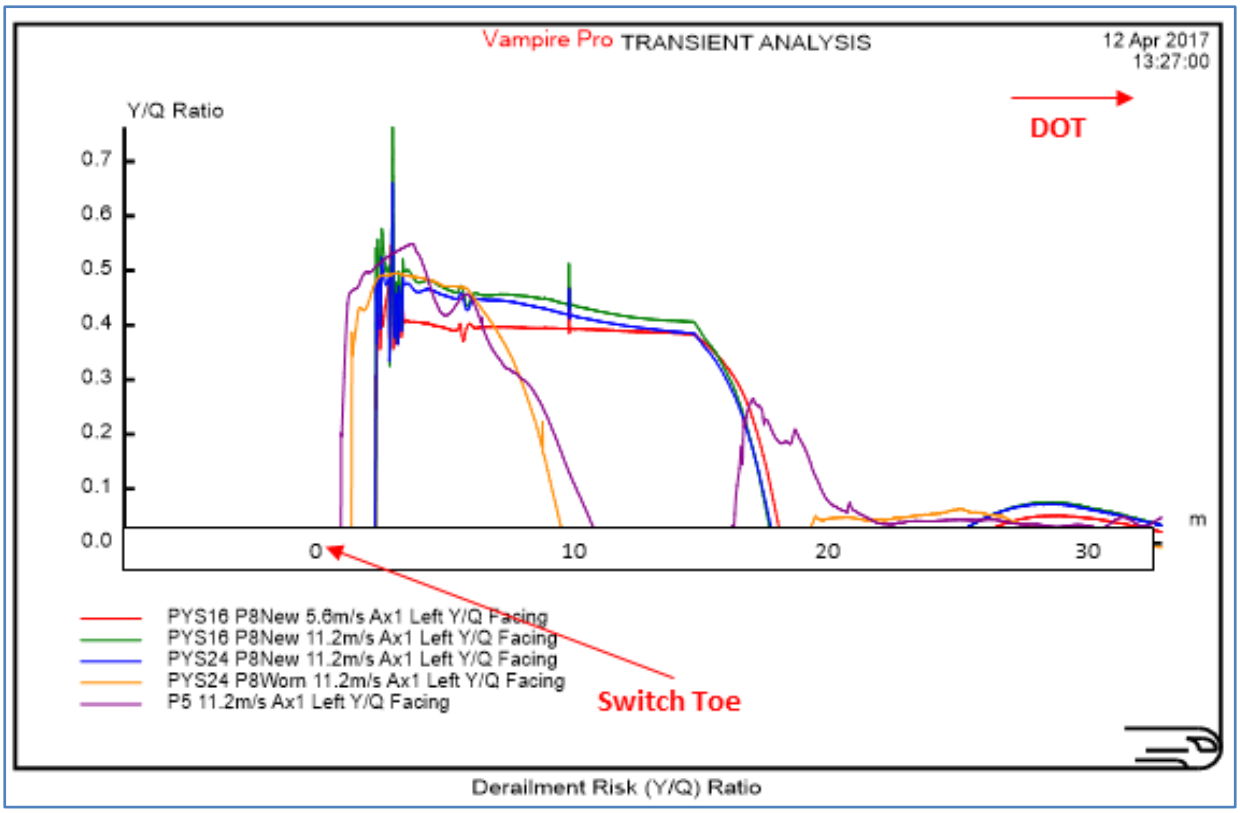

Figure 56: Low Derailment Risk – Facing Direction (Arthur, 2017)

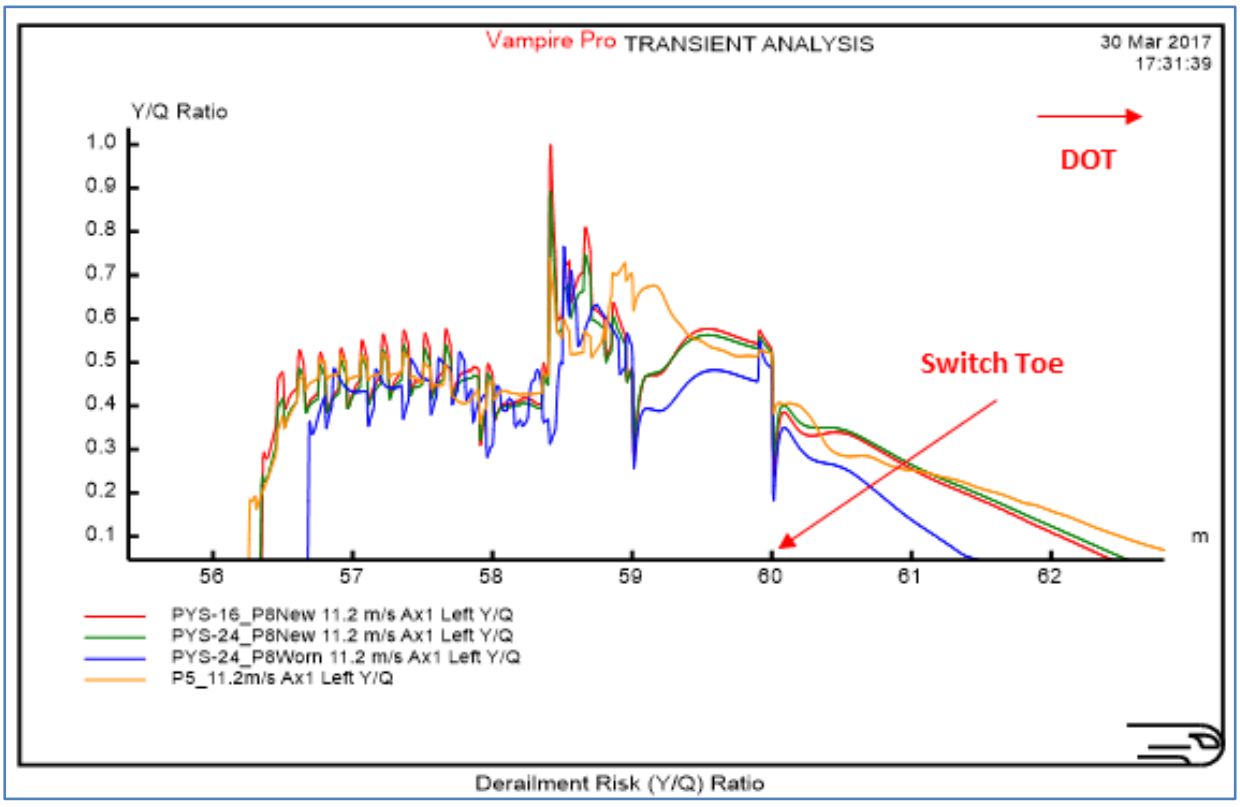

Figure 57: Low Risk of Derailment – Trailing Direction (Arthur, 2017)

5.4. Effect of T-Gamma on RCF Predictions

T-Gamma is a function of many variables that include the weight of a vehicle, level of track cant, rail and wheel profiles and Primary Yaw Stiffness. A change in any of these variables can increase or decrease the level of T-Gamma and therefore the corresponding impact on RCF and wear. For instance, T-Gamma grows with tight curvature tracks. Vehicles with low Primary Yaw Stiffness, i.e., soft bogies will cause RCF in narrow bands of tight curves whilst vehicles with high Primary Yaw Stiffness, i.e., stiff bogies will cause RCF in broad bands of mid to shallow curves. Table 8 shows the results of the simulation run for the NR60C MK2 switch where vehicles with three different Primary Yaw Stiffness were selected to run in both the facing and trailing directions. T-Gamma levels and the corresponding RCF damage index predictions have been highlighted as well as the locations where they occurred.

VAMPIRE Run	Type of Vehicle	Direction of Travel	Vehicle Speed (mph)	T-Gamma (J/m)	RCF Damage Index	Distance from Switch Toe (m)
1	MK3 PYS16 F25	Facing	25.0	665	3.40	2.5
2	MK3 PYS16 T25	Trailing	25.0	1400	4.99	3.5
3	MK3 PYS16 F12.5	Facing	12.5	507	3.08	2.0
4	MK3 PYS T12.5	Trailing	12.5	1309	4.93	3.2
9	Desiro PYS24 F25	Facing	25.0	680	3.83	2.0
10	Desiro PYS24 T25	Trailing	25.0	1117	4.79	3.4
11	Desiro PYS24 F12.5	Facing	12.5	590	3.15	2.0
12	Desiro PYS24 T12.5	Trailing	12.5	1020	4.19	3.4
13	Wagon 90t F25	Facing	25.0	1079	4.29	1.8
14	Wagon 90t T25	Trailing	25.0	3018	9.88	3.8
15	Wagon 90t F12.5	Facing	12.5	1009	4.10	1.8
12	Wagon 90t T12.5	Trailing	12.5	2882	8.01	3.8

Table 10: Results of Vampire Simulation Run (Arthur, 2018)

The trains were tested at different speeds i.e., at full turnout speed of 25 mph and then at half turnout speed of 12.5 mph. The outcome presented in Table 8 clearly shows train speed had little influence on T-Gamma therefore there was no significant impact on the RCF predictions, an observation consistent with Johansson (2006) who concluded that the influence of train speed on contact pressure is small, given a particular combination of axle load and rail profile.

According to Table 10, the lowest T-Gamma level was recorded by the MK3 passenger train running on worn wheels in the facing direction. The fact remains that MK3 has soft Primary

Yaw Stiffness hence this train was able to negotiate the curve well. In contrast, vehicles with high Primary Yaw Stiffness like the freight wagon, had the greatest magnitude of T-Gamma predicted by the simulation. The high levels of T-Gamma prediction for Rail Shoulder and Gauge Corner for the freight wagon were due to a combination of factors including high axle loads, stiff bogies and direction of travel.

In order to ascertain the material effect of the RCF predictions in Table 10, attention will be drawn to Network Rail (2014) which illustrates the RCF Damage Index and the corresponding surface crack length categorisation. This has been summarised in Table 11. Table 10 illustrate the maximum RCF damage index at the gauge corner to be 9.8. Relating this to the RCF categorisation in Table 11 shows that the simulation has predicted the proposed NR60C MK2 switch will undergo a heavy RCF damage index regime for the freight wagon in the trailing direction. This outcome shows an improvement in design when compared with the NR60C MK1 which predicted severe RCF damage in Hsu (2011). Conversely, the simulation predicted moderate RCF damage index for both MK3 and Desiro passenger train vehicles.

High Rail RCF Severity	Damage Index	Length of Longest Crack Measured [mm]
Light	0 - 1	< 10
Moderate	≥ 1 < 5	≥ 10 < 20
Heavy	≥ 5 ≤ 10	≥ 20 < 30
Severe	> 10	≥ 30

Table 11: RCF Damage Index and Surface Crack Length Categorisation (Arthur, 2018)

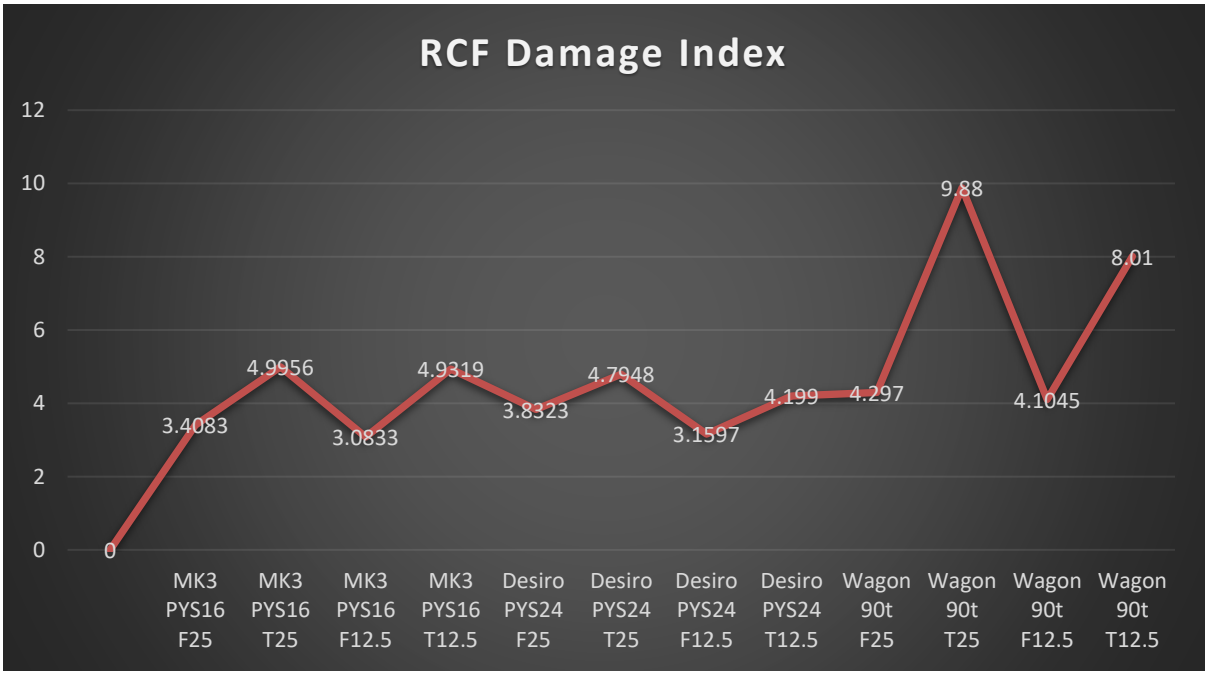

Figure 58: Predicted RCF Damage Index for All Vehicles (Arthur, 2021)

In general, due to the impact of angle of attack and lateral shift, bogies negotiating a curve will generate lower lateral forces and higher longitudinal forces on the leading axle than on the trailing axle. It is, therefore, due to the dominance of longitudinal forces that there is so much RCF in railway turnouts. The longitudinal forces will cause RCF cracks to grow on the high rail and, usually, at right angles to the resultant contact patch force thus, the material immediately underneath the point of wheel-rail contact will undergo plastic deformation. Regardless of any other factors, the trailing axle high rail wheel will not have a T-Gamma sufficient to generate RCF unlike the leading axle on the high rail wheel which will have a T-Gamma sufficient to generate RCF.

Figure 56 is a graphical presentation of the RCF damage index predicted by the vehicles as they negotiate the turnout in both facing and trailing directions. It can be observed that the revised switch NR60C MK2 switch will undergo moderate RCF damage with the passenger vehicles whilst the freight wagon will cause the switch to suffer from heavy RCF. This results is an improvement compared to Hsu (2014), where both the passenger vehicles with soft and medium Primary Yaw Stiffness predicted severe RCF damage index according to the existing NR60C MK1 simulation. Similarly, the freight vehicle under Hsu (2014) also predicted a severe RCF damage index. The main difference between the existing NR60C MK1 switch and the proposed NR60C MK2 switch is the addition of 3 mm extra steel material to the switch toe which the author of this thesis proposes as an enhancement to S&C turnout geometry. The revised NR60C MK2 switch is therefore stronger and has a wider surface area to withstand vertical stress thus making it a better option in minimising rail damage due to RCF in S&C turnouts than the existing NR60C MK1 switch.

5.5 Effect of T-Gamma on Rail Wear Predictions

A similar methodology for predicting rail damage (i.e., RCF and wear) in switch and crossing has been demonstrated in (Nielsen, 2015) where dynamic wheel-rail interaction was simulated to assess the development of RCF and rail wear. Since wear load is a function of tangential force and creepage, the expected behaviour of rail wear can therefore be extrapolated from the T-Gamma.

Wear is likely to occur when two contacting bodies slide against each other and (Lewis, 2004) identified three types of wear patterns, namely, mild, severe and catastrophic. Mild wear is when the rate of wear is low with smooth surfaces and no resulting debris and this occurs when protective oxide layers prevent inter-metallic contact as noted in (Lim, 2002). Over time, as wear loading increases, there is a transition from partial slip to full slip with associated characteristics such as deformation, crack growth and material removal which becomes the severe stage in wheel-rail contacting bodies. The severe stage is mainly driven by adhesion

within the contacting bodies and (Johnson K. , 1995) concluded that severe wear occurs as a result of plastic strain accumulation referred to as ratchetting. The catastrophic wear stage is the final mode which occurs as a result of the temperature effects of the contacting bodies. During this stage, material hardening curves are used to assess the response of cyclic stress and (Ponter, 2006) presented the shakedown map for a 3D rolling sliding contact. They outlined the limits of shakedown above which accumulation of plastic strain normally referred to as ratchetting will occur. The ratchetting mechanism becomes more localised at the surface under high coefficients of friction (greater than 0.4) and cumulative plastic flow occur at sub-surface under low coefficient of friction (less than 0.3). As such, rail head lubrication can be used to control friction and relieve the surface area of ratchetting.

As expected, the simulation predicted a higher rate of wear for the trailing move than the facing move. According to Figure 45, the freight wagon during the facing move recorded the highest T-Gamma value of 1100 J/m at the full track speed of 25 mph and this occurred at the flange contact, implying more wear within this area. Moreover, the track seemed to have worn out more using a new P8 wheel for the passenger vehicles than a P8 worn wheel. The simulation results also predicted that the switch rail will wear out more with T-Gamma values peaking at 1400 J/m during a trailing move, even with lighter vehicles such as the MK3 passenger train than a freight wagon. A British Rail Research report (1986) concluded that in setting maintenance regime, T-Gamma values greater than 200 J/m can be used as a guide to determine the rail wear threshold. However, this figure, applied to both plain line and S&C, has been heavily criticised by maintenance engineers as being too low for S&C track, hence not realistic in practice. The existing NR60C MK1 design has a minimum wear threshold of over 400 J/m rendering the proposed design a better option for wheel-rail interface management.

T-Gamma can be converted to the amount of material removed from the rail per axle pass by a laboratory derived relationship published in British Rail Research report 'TM VDY 004: Interpretation of Wheel/Rail Wear Numbers (1986)'. It is noted that the predictions are likely levels of wear based on several assumptions and the outcome is generally pessimistic, representing the worst possible wear. The predictions should therefore be viewed as comparative values and not be used as absolute levels for setting maintenance regimes. It is predicted that for T-Gamma > 200 J/m:

Rail Wear Rate [mm^2 / 1000 axles] = (2.5 x T-Gamma - 322) x 10^{-3} mm^2 / 1000 axles (44)

According to the BRR report, a plain line side wear limit of 9 mm equates roughly to 190 mm^3 of material being removed for the standard 220 rail grade. The wear rate will be less for a harder grade steel such as 260 and even less for premium grade.

5.5.1 Rail Wear and Lubrication

To better appreciate the simulating outcome in all facets, the author applied lubrication to the NR60C MK2 switch and the results changed significantly, thus illustrating the fact that better RCF results can be achieved than those outlined in Table 9.

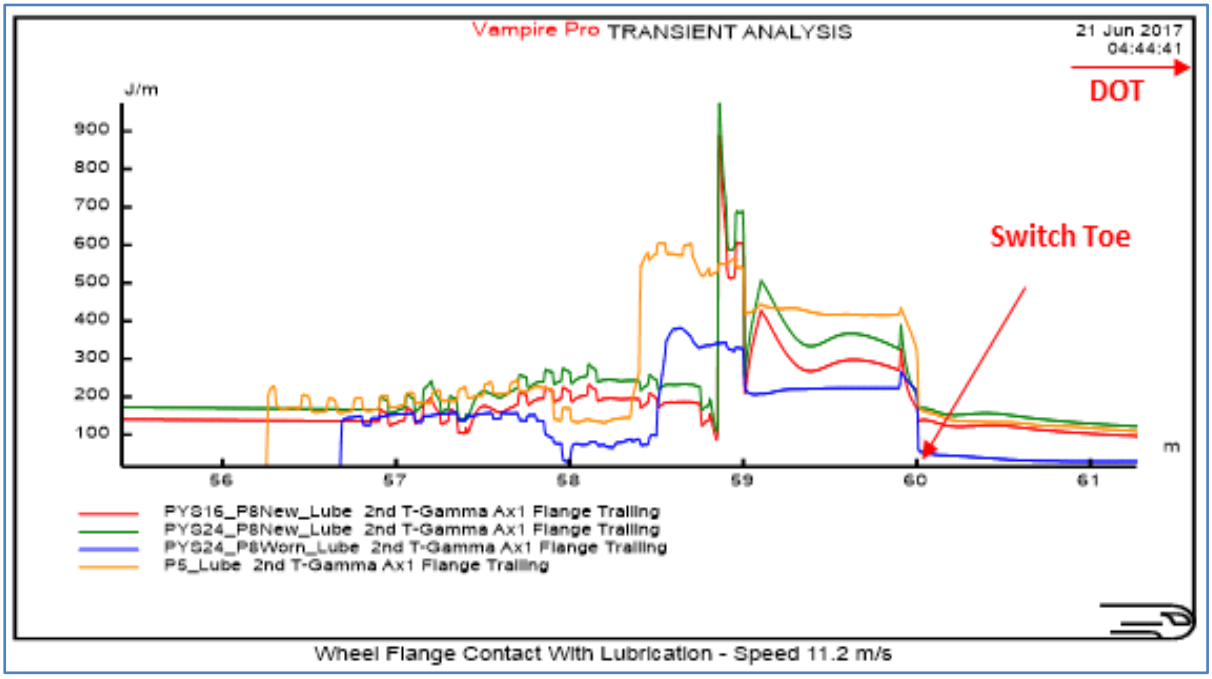

Figure 59: Effect of Lubrication on Wheel Flange Contact (Arthur, 2017)

Figure 59 identifies the effect of directional travel on the wear load. Using the P5 wagon as the worst-case scenario, it can be seen that T-Gamma generated as a result of flange contact was reduced from 3018 J/m (Figure 52) to 900 J/m (Figure 59). This will translate to a rail damage index of 4.01, hence downgrading the RCF categorisation for the freight wagon from heavy RCF damage index to a moderate RCF damage index. In fact, the trigger point for Network Rail in its search for alternatives for the existing NR60C MK1 was the excessive wear in the trailing direction for all three vehicle types, as presented in Hsu (2014).

This result has highlighted the impact of friction coefficients on the level of T-Gamma as well as the corresponding wear loading of S&C turnouts. The T-Gamma values were extracted from the simulation and used in the calculation of the wear index in Figures 60 and 61 so as to ascertain the impact of rail lubrication as a means to reduce the rate of rail wear in S&C tracks. The results predicted that decreasing the friction coefficient through effective rail lubrication regime will halve the lateral wear loading at the flange and rail gauge of the switch.

For the lubricated switch (low friction condition) in Figure 61, the resulting wear index values is half that of the non-lubricated switch (high friction condition) in Figure 60, implying an improvement in the RCF damage index.

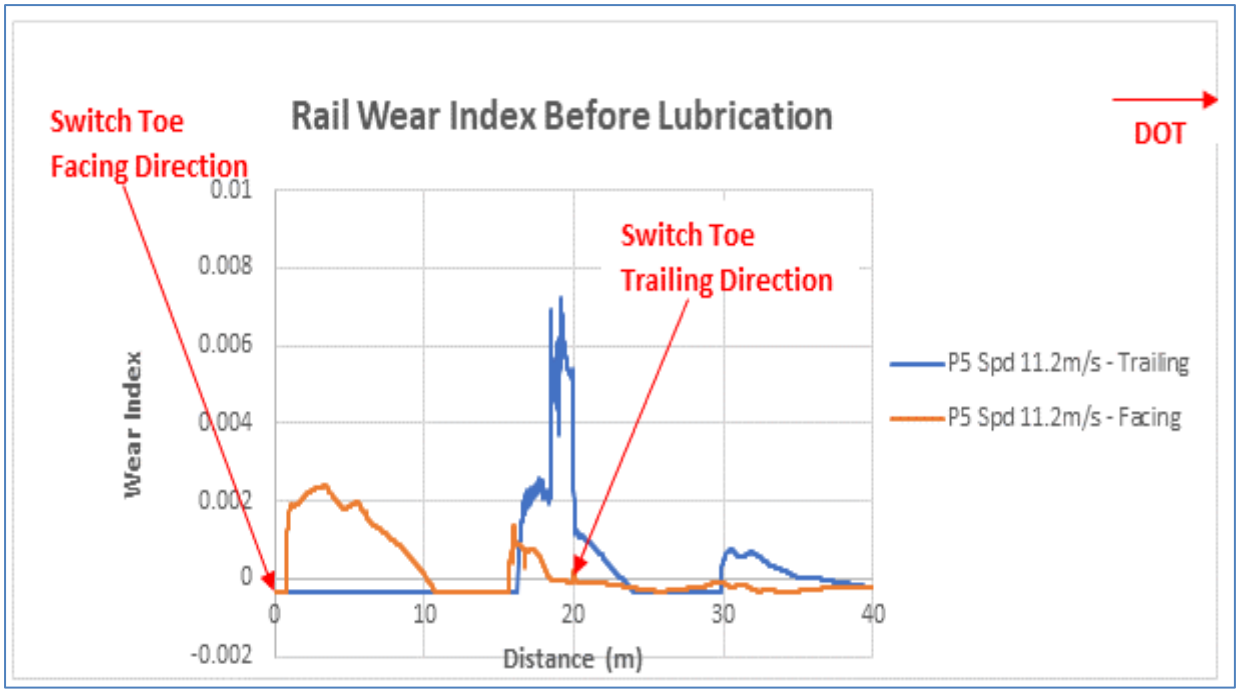

Figure 60: Wear Index without Lubrication (Arthur, 2020)

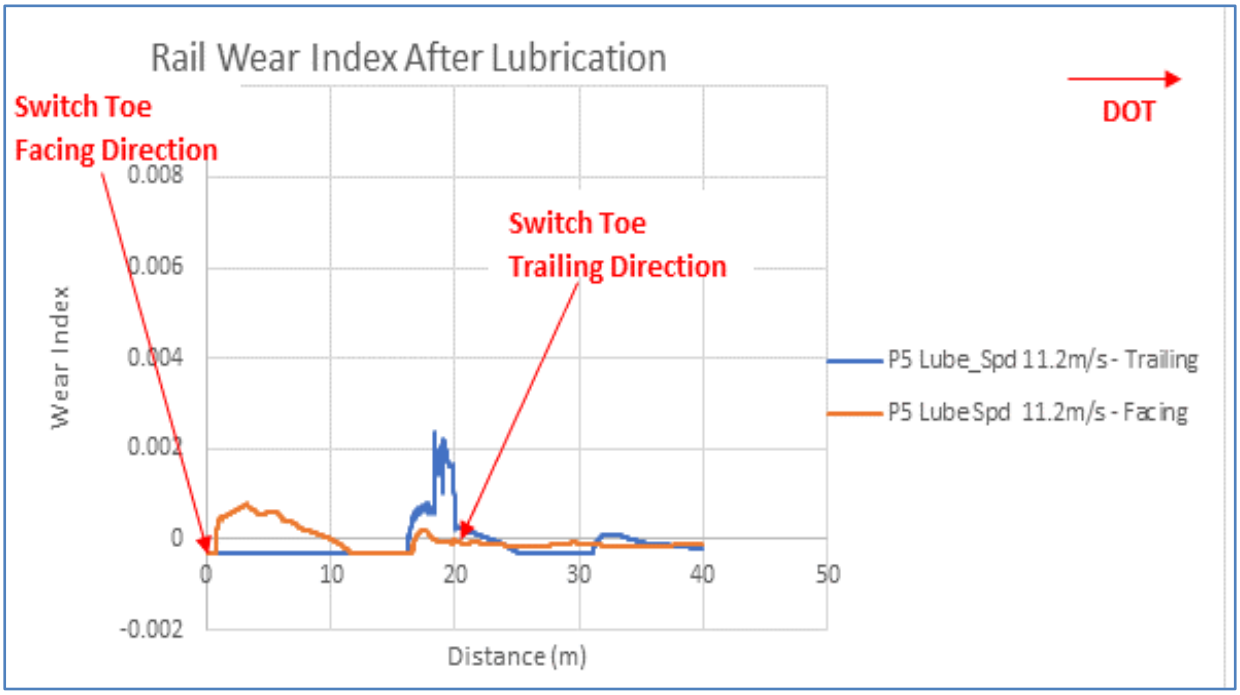

Figure 61: Wear Index with Lubrication (Arthur, 2020)

6. CONCLUSION AND RECOMMENDATIONS

6.1 Summary of Findings

A novel development and application of a dynamic Finite Element analysis was carried out for a wheel passing through a double intersecting geometry switch, based on adding 3 mm of material to the switch and 1.2 mm of material added to the crossing nose. Comparison was then made between the existing NR60C MK 1 switch and the revised NR60C MK2 switch. The dynamic Finite Element model results predicted lower levels of stress, vertical displacement, PEEQ and contact force for the revised switch as opposed to the existing switch, as noted in Table 7. The fatigue life analysis (Figure 45) using the S-N approach also demonstrated that the revised NR60C MK2 design has a service life more than 60 times longer than the existing NR60C MK1 design. Similarly, vehicle dynamics simulations have been carried out to assess RCF, wear and derailment performance of the revised NR60C MK2 switch during the facing and trailing directions for 2 types of passenger coaches and a freight wagon, initially without track lubrication. The two passenger vehicles recorded moderate RCF damage indices whilst heavy RCF damage index (T-Gamma 3018 J/m) was observed for the freight wagon. After the application of track lubrication on the freight wagon (worst case scenario), the T-Gamma value reduced to 900 J/m, thus downgrading the RCF damage index from severe to moderate RCF. The overall performance of the NR60C MK2 S&C was better than that of the existing design and this can be summarised as:

- The material strength analysis has shown that with the addition of a small amount of steel, the components of NR60 MK2 S&C will suffer less von Mises stress, displacement, PEEQ for both the switch and crossing nose (Table 8);
- The NR60C MK2 switch design is expected to have a service life of about 60% longer longer than NR60C MK1 (Figure 45);
- Table 10 shows that during the facing and trailing moves, the revised NR60C MK2 switch has been predicted to suffer less wear and for a shorter length along the switch planing section;
- There was no risk of derailment for all the vehicles with the revised NR60C MK2 switch as predicted in Figures 56 and 57;
- The risk of RCF damage to the revised NR60C MK2 switch has been shown to be marginally lower for both the facing and trailing moves compared to the existing design (Table 11);

- Application of lubrication (Figures 57 and 59) has reduced the RCF level of vehicle with the worst case scenario (Freight Wagon) from 3018 J/m to 900 J/m, thus improving the rail damage index from heavy to moderate RCF with respect to this vehicle.

6.2 RECOMMENDATIONS AND FUTURE WORK

The author of the thesis presents a range of recommendations as follows:

- Model validation through field experiment should be conducted once the revised switch becomes available in the United Kingdom rail infrastructure;
- Alternative methods of reducing rate of wear in the absence of rail lubrication should be explored, e.g. by means of surface coatings. If this cannot be achieved, then an investigation should be conducted into automatic rail lubrication, where the risk of endangering the life of railway workers can be reduced;
- Thorough investigation into the track formation should be carried out, especially at the switch and crossing sections as well as damping and track stiffness properties interfacing the ballast and bearers;

6.3 RESEARCH KNOWLEDGE CONTRIBUTION

The author has developed a novel switch which has the potential to reduce RCF and rail wear at turnout curves significantly. This was achieved by adding 3 mm of material to the switch and 1.2 mm material to the crossing, a design concept which is the first in the United Kingdom railway infrastructure. This new concept will not only enhance rail service life, but will also provide better ride quality and improve safety within the switch and crossing section of the track infrastructure.

In addition to the above, the author has also carried out material strength analysis on the new S&C design to ensure that it would be able to withstand the high impact forces from all directions.

The author has combined a finite element analysis with a dynamic multi-body simulation to enhance S&C performance. This is the first time that a material strength analysis has been carried out for a rail vehicle dynamic simulation.

7. REFERENCES

Aknin, P. C., & Sebes, M. (2005). *Expro, Exploration de profils roue-rail, Version 4.0.* Lille: INRETS.

Anderson W., a. A. (2000). Testing of Two-layer Railway Track Ballast. *Journal of Geotechnical and Geoenvironmental Engineering, American Society of Civil Engineers* , vol. 126, no. 4,.

Andersson, S. (2009). *Friction and Wear Simulation of Wheel-Rail Interface. In: Lewis R., Olofsson U., (eds.).* Wheel-Rail Interface Handbook.

Arthur. (2017). Single and double contact point detection using rail profiles. London.

Arthur, K. (2011). Finite Element Modelling of Beams. *Masters Dissertation, Brunel University*. Uxbridge, Middlesex, UK.

Arthur, S. (2014). *Issues with NR60/RT60 Switches and Crossings.*

Ayasse, J. (2006). Curved Squeal of Urban Rolling Stock Part 3: Theoretical Model. *Journal of sound and vibration,* , Vol.293 (3), p.710-727.

Ayasse, J. C. (1994). Wheel to Rail Contact. In S. Iwnicki, *Handbook of Railway Vehicle Dynamics* (pp. 86-20). London: Taylor & Francis.

Bai, Y. J.-L. (2016). *Fatigue Capacity.* in Marine Structural Design (Second Edition).

Bell, B. R. (2003). Reducing Rail Surface Defect Service Failures on the CSXT Railroad, Proceedings IHHA Specialist Technical Session. *Wear*, 191, 131-140.

Bhaskar A., K. J. (1997). Wheel-rail dynamics with closely conformal contact Part 1: Dynamic modeling and stability analysis. *Institution of Mechanical Engineers,* , Part F.

Boutle, N. (1978). *A Fatigue-Orientated Analysis of Strains Measured from Two Crossings of Different Design Installed at Watford Junction.* British Railways Board, British Railways Research and Development Division - Track Group, Report No: 263-190-16.

Bower, A. J. (1991). Plastic flow and shakedown of the rail surface in repeated wheel-rail contact, . *Wear - An international journal on the science and technology of friction, lubrication*, 144(1-2): 1-18.

Bowness D, L. A. (2007). Monitoring the dynamic displacements of railway track, Proceedings of the Institution of Mechanical Engineers . *Part F - Journal of Rail & Rapid Transit*, vol. 221: 13-22.

Braghin, F. L.-J. (2006). A mathematical model to predict railway wheel profile evolution due to wear. *Wear pp. 1253-1264*, 261.

British Standards Institute. (1992). Railway rolling stock materials: Part 6: Specification for wheelsets for traction and trailing stock. *British Standards Institute, BS5892-6*.

Burstow, M. (2006). Background the to Tgamma RCF damage function. *Railway Systems Engineering* . Network Rail.

Burstow, M. (2003). Whole Life Rail Model application and development: Development of a rolling contact fatigue damage parameter. *RSSB*, T115.

Burstow, M. (2004). *Whole Life Rail Model Application and Development for RSSB - Continued Development of an RCF Damage Parameter.* Rail Safety & Standards Board, AEA Technology Rail, September, Report No: AEATR-es-2004-880.

Busquet M, C. H. (2006). From railway dynamics to wheel/rail contact mechanics, an approach for the modelling of the wheel/rail contact: elasto-plastic response of the railhead. *Proceedings of the Institution of Mechanical Engineers - Part F - Journal of Rail & Rapid Transit*, 220(3): 189-200.

Carter, E. (1963). *The Railway Encyclopedia. Harlod Starke Ltd.* London.

Cheesewright, P. (1977). Wheel/Rail Forces Measured at Crossings of Cast Manganese and. *Built-up Types, British Railways Research and Development Division - Track Group, British Rail*, Report No: 263-191-24.

Claisse, P. C. (2006). Rail ballast: conclusions from a historical perspective . *Institution of Civil Engineers*.

Clarke, R. (1981). *Measurement of wheel-rail contact forces at a selection of switches and.* crossings using the HSFV1 equipped with load measuring wheelsets: British Rail Research (BRR), Report No: TM DA 39.

Clough, R. (1960). The Finite Element Method in Plane Stress Analysis. *Proceedings of Second ASCE Conference on Electronic Computation*. Pittsburg, Pennsylvania.

Clough, R. (2001). Thoughts about the origin of the finite element method. *Computers & Structures*, Vol.79 (22), p.2029-2030.

Coleman, I. (2004). The Development of Modelling Tools for Railway Switches and Crossings. *Imperial College Phd Thesis*.

Cope, D., & al., e. (2002). *Switch & Crossing Maintenance.* United Kingdom: The Permanent Way Institution.

Cope, G. (1993). British Railway Track: Design, Construction and Maintenance. *The Permanent Way Institution*.

Cornish, A. (2011). Development of Predictive Maintenance of Switches and Crossings based on Experiemental Analysis and Numerical Modelling, Future Railway Research. *Centre Department of Mechanical Engineering*.

Cornish, T. (2014). *Life-time monitoring of in-service switches and crossings through field experimentation.* London: Imperial College.

Courant, R. F. (1967). On the partial differential equations of mathematical physics. *Math.Ann.100(1928)*, 32-74.

D.H., C. (1971). British Railway Track – Design, Construction and Maintenance. *Permanent Way Institute*, 4th Ed.

Dassault Systèmes Simula Corp. (2012). Abaqus User Guide, Version 6.12.

Dembosky, M. a. (2004). A Revised RCF Hypothesis, Interim AntiRCF Limits, and a Summary of Previous WRISA Studies.

Department of Transport. (2021). *Derailment at Grayrigg.* Derby, UK: Rail Accident Investigation Branch, Department for Transport, Report No: 02/202021.

Enblom, R. (2009). Deterioration mechanisms in the wheel–rail interface with focus on wear. *A literature review, Vehicle System Dynamics: International Journal of Vehicle Mechanics and Mobility*, 47(6): 661-700.

Esveld C. (1978). Comparison between theoretical and actual transfer functions of track maintenance machines. *PhD Thesis, Warsaw Technical University*.

Evans, J., Urban, C., & Elkins, J. (2010). Steering of Rail Vehicles. In F. Schmid, M. Burstow, S. Clarke, B. Eickhoff, M. Hiensch, S. Hsu, & K. S, *Best Practice in Wheel-Rail Interface Management for Mixed Traffic Railways 1st Edition.* Birmingham: Birmingham University Press and A&N Harris.

Fletcher, D. (2000). The effect of contact load reduction on the fatigue life of pearlitic rail steel in lubricated rolling-sliding contact. *Fatigue & Fracture of Engineering Materials & Structures*, 23, pp. 639-650.

Fletcher, D. (2013). A new two-dimensional model of rolling-sliding contact creep curves for a range of lubrication types. *Journal of Engineering Tribology*, 227, pp. 529-537. .

Fletcher, D. B. (1999). A simple method of stress intensity factor calculation for inclined fluid-filled surface-breaking cracks under contact loading. *Journal of Engineering Tribology*, 213, pp. 299-304.

Fletcher, D. B. (2000). Development of a machine for closely controlled rolling contact fatigue and wear testing. *Journal of Testing and Evaluation*, 28, pp. 267-275. .

Fletcher, D. B. (2000). Equilibrium of crack growth and wear rates during unlubricated rolling-sliding contact of pearlitic rail steel. *Journal of Rail and Rapid Transit*, 214, pp. 93-105.

Fletcher, D. I. (2000). The effect of intermittent lubrication on the fatigue life of pearlitic rail steel in rolling-sliding contact. . *Journal of Rail and Rapid Transit,* , 214, pp. 145-158.

Franklin, F. I. (2001). Computer simulation of wear and rolling contact fatigue. *Wear*, Vol. 251, 949-955.

Franklin, F. W.-J. (2005). Rolling Contact Fatigue and Wear Behaviour of the Infrastar Two-Material Rail. *Wear* , 258(7-8), 1048-1054.

Fries, R. e. (1988). Analytical Methods for Wheel and Rail Wear Prediction. . *International Association of Vehicle System Dynamics, IAVSD*, 10, pp. 112-125. .

Frolish, M. F. (2002). A quantitative model for predicting the morphology of surface initiated rolling contact fatigue cracks in back-up roll steels. *Fatigue and Fracture of Engineering Materials and Structures*, 22, pp.1073.

Garciavadillo E, G. J. (1984). Wheel Rail Contact - Geometrical Study, Vehicle System Dynamics. *International Journal of Vehicle Mechanics and Mobility*, 13(4): 207-214.

Grassie, S. &. (2005). Tractive effort, curving and surface damage of rails: Part 1. Forces exerted on the rails. *Wear - An international journal on the science and technology of friction, lubrication and wear*, 258(7-8): 1235-1244.

Grassie, S. a. (2001). Alleviation of Rolling Contact Fatigue by Grinding the Worn Rail Profile.

Hertz, H. (1882). UÈ ber die BeruÈhrung fester elastischer KoÈrper. J. reine und angewandte . *(see in Authorised English translation by D.E. Jones and G.A. Schott 1896*, Mathematik 92 156±171.

Hibbitt, K. (2002). ABAQUS/CAE User's Manual ABAQUS/CAE User's Manual.

Hiensch E.J.M., e. a. (2003). Prevention of RCF damage in curved track through development of the Infrastar two material Rail. *Fatigue & Fracture of Engineering Materials and Structures*, Vol. 26, No 10, 1007-1017.

Hirakawa, K. K. (2001). On the fatigue design method for high speed railway axles", Proc. *Institution of Mechanical Engineeers*, Vol 215 Part F.

Hsu, S. (2011). *Wear and RCF Performance of Revised Switch Planing Geometry for NR60 .* Network Rail.

Hsu, S. (2012). *Switch Topping Study of a Vertical Turnout .* Network Rail, UK: NR/E/SE/SSH2012-01.

Hsu, S.S. (2014). *Issues with NR60/RT60 Switches and Crossings.* Network Rail.

Inspection and Maintenance of Permanent Way. (n.d.). Network Rail NR/L2/TRK/001.

Iwnicki, S. (1998). Computer Simulation of Rail Vehicle Dynamics. *Vehicle System Dynamics* , Vol. 30.

Iwnicki, S. (2006). *Handbook of Railway Vehicle Dynamics.* CRC Press, Taylor & Francis Group.

Jendel, T. (1986). Interpretation of wheel/rail wear numbers. *British Rail Research*, TM VDY 004.

Jenkins, H. e. (1974). The Effect of Track and Vehicle Parameters on Wheel/Rail Vertical Dynamic Forces. *Railway Engineering Journal, January* .

Johansson, A. (2006). Out-of-round railway wheels—assessment of wheel tread irregularities in train traffic . *Journal of Sound and Vibration 293* , 795-806 .

Johansson, A., & Andersson, C. (2005). Out-of-round railway wheels - a study of wheel polygonalization through simulation of three-dimensional wheel-rail interaction and wear. *Vehicle System Dynamics - International Journal of Vehicle Mechanics and Mobility*, 43(8): 539-559.

Johnson, C. (2009). Numerical Solution of Partial Differential Equations vy the Finite Element Method. *Dover Publications Inc*.

Johnson, K. (1985). Contact Mechanics. *Cambridge University Press, Cambridge, UK* .

Johnson, K. (1995). Contact mechanics and the wear of metals. 190:162–170.

Johnson, K. K. (1971). *Surface Energy and the Contact of Elastic Solids .* Proceedings of the Royal Society of London A324, pp. 301-313.

Kalker, J. (1967). On the rolling of two elastic bodies in the presence of dry friction. *Doctoral Thesis, Delft University of Technology*.

Kalker, J. (1990). Three-dimensional elastic bodies in rolling contact. *Kluwer Academic Publishers, Dordrecht/Boston/London,* .

Kassa E, J. G. (2007). Simulation of train–turnout interaction and plastic deformation of rail profiles. *International Journal of Vehicle Mechanics and Mobility*, 44:349–359 .

Kassa E, W. M. (2008). Assessment of methods for calculating contact pressure in wheel-rail/switch contact, Wear - An international. *Wear - An international on the science and technology of friction, lubrication and wear*, 265(9-10): 1439-1445.

Kikuchi, N. (1988). *Contact Problems in Elasticity: A Study of Variational Inequalities and Finite Element Methods.* Society for Industrial and Applied Mathematics.

Larsson, e. a. (2012). Continuous piecewise linear finite elements for the Kirchhoff–Love plate equation. *Numerische Mathematik,*.

Lewis, R. (2004). Wear mechanisms and transitions in railway wheel steels. *Proc Instit Mech Eng, Part J: J Eng Tribol*, 218(6):467–478.

Li MXD, B. E. (2010). A study of the effect of Global Track Stiffness and its Variation on Track Performance: Simulation and Measurement. *Proceedings of the Institution of Mechanical Engineers Part F - Journal of Rail & Rapid Transit*, vol. 224, 375-382.

Li, H., & Xu, Y. &. (2011). Field Measurement and Performance evaluation of HighSpeed Railway Turnouts on Ballasted Track of Passenger Dedicated line. *Railways Engineering 2011, Forde M. C. (eds.), University of Westminster Engineering Techics Press*, 1-6.

Li, Z. (2002). Wheel-rail rolling contact and its application to wear simulation. *PhD Thesis. T U Delft*.

Li, Z. K. (1998). Proceedings of the 6th International Conference on Computer Aided Design, Manufacture and Operation in the Railway and other Mass Transit systems, 2-4 September, Lisbon. *Portugal, Computational Mechanics Publications,*, pp. 393-402. .

Licciardello, R. B. (2008). Some experience on the dynamincs of turnouts due to passing trains. *In: 8th World Congress on Railway Research, (eds.), Seoul, Korea*, 1-9.

Lim, S. (2002). The relevance of wear-mechanism maps to mild-oxidational wear . *Tribol International* , 35:717–723. .

Magel, E. K. (2002). The application of contact mechanics to rail profile design and rail grinding. *Elsevier, Wear 253, Issue 1-2*, pp 308-316.

Meng, H. L. (1995). Wear Models and Predictive Equations - their Form and Content. *Wear, 181* , pp. 443-457.

Moncef, T. H. (2016). Finite element analysis of the frictional wheel-railrolling contact using explicit and implicit methods.

Network Rail. (2002). Railway Group Standard. *GM/RT 2141*.

Network Rail. (2008). NR/L2/TRK/0053, Inspection and repair to reduce the risk of derailment at switches. Milton Keynes, UK: Network Rail.

Network Rail. (2014). Switch and Crossing Inspection Frequencies . *Network Rail Company Standard NR/L2/TRK/001*. Milton Keynes: Network Rail.

Network Rail. (2014). Track Design Handbook NR/L3/TRK/2049.

Network Rail. (2014). Track Ex Training. *Guidance Document*. Milton Keynes, UK: Network Rail.

Network Rail. (2016). NR60C MK2 Switch Geometry Showing Datum Point. *Guidance Document*. Milton Keynes, UK: Network Rail.

Network Rail. (2016). Wheel and Switch profiles. *Network Rail NR/STE/1533/GN/001*. Milton Keynes, United Kingdom: Network Rail.

Network Rail. (2017). NR/STE/1533/GN/001 – NR60 Mk2 . *Guidance Note*. Milton Keynes: Network Rail.

Network Rail. (2017). RE/PW/4001 NR60 MK2 Inclined S&C C Switch Assembly & Machining. *Guidance Notes*. Milton Keynes: Network Rail Standard.

Network, R. (2009). Inspection and Maintenance of Permanent Way - Specific Requirement for Switches and Crossings. *NR/L2/TRK/001/D02*.

Nicklisch D, N. J. (2009). Simulation of Wheel-Rail Contact Forces and Subsequent Material Degradation in Switches & Crossings. *In: 21st International Symposium on Dynamics of Vehicles on Roads and Tracks, (eds.), Stockholm, Sweden,* , 1-14.

Nielsen, J. P. (2015). *Switch panel design based on simulation of accumulated rail damage in a railway turnout.* USA: CM2015, Colorado Springs.

Ofiice of Rail Regulation. (2013). Periodic Review 2013: Final determination of Network Rail's outputs and funding for 2014 - 2019. *Crown*.

Oswald, J. ,. (2001). Optimization of Turnout Layout and Contact Geometry through Dynamic Simulation of Vehicle-Track Interaction.

Paling, K. (1974). *Investigation into derailments on facing switches by flange climbing.* Derby: Report No: 203-81-29 : British Rail Research and Development Division.

Palsson, B. (2014). *Optimisation of Railway Switches and Crossings, CHALMERS UNIVERSITY OF TECHNOLOGY.*

Patric, M. (2016). *NR60E MK2 Switch Draft Report.*

Peace, T. S. (1991). *Prediction of Wheel Profile Wear.* pp. 343-351: Wear, 144.

Pennycook, J. (1977). *Investigation intoTrack Stiffness, Sleeper Load and settlement using Rolling Load Rig Experimental Results.* British Rail Research (BRR), Report No: TM-SM-45.

Pletz, M. D. (2012). A wheel passing a crossing nose: Dynamic analysis under high axle loads using finite element modelling. . *Journal of Rail and Rapid Transit*, 226, pp. 603.

Polach, O. (2000). A fast wheel-rail forces calculation computer code", Proc. of the 16th IAVSD. *Vehicle System Dynamics Supplement; Royal Swets and Zeitlinger*, 33, pp. 728-739.

Pombo, J. (2007). A new wheel-rail contact model for railway dynamics. *Vehicle system dynamics*, Vol.45 (2), p.165-189.

Ponter, A. (2006). Shakedown analyses for rolling and sliding contact problems. *Int J Solids Struct*, 43:4201–4219.

Quinn, A. M. (2010). A full-scale experimental and modelling study of ballast flight under high-speed trains. *Journal of Rail and Rapid Transit, Proceedings of the Institution of Mechanical Engineers*, Vol. 224, Part F, No. 2, pp. 61-74.

RAIB. (2021). *Rail Accident Report 02/2021: Freight train derailment at Eastleigh, 28 January 2020.* UK Government, Department for Transport. Derby: Rail Accident Investigation Branch. Retrieved March 13, 2022

Rail Accident Investigation, B. (2009). *Rail Accident Report: Derailment at Grayrigg, 23 February 2007.* The Wharf, Stores Road, Derby, UK, DE21 4BA: Rail Accident Investigation Branch, Report No: 20/2008, Department for Transport.

Rail, N. (2016). Track Design Handbook NR/L3/TRK/2049 .

Rail, N. (2017). Track Design Handbook NR/L3/TRK/2049 .

Railtrack PLC. (1999). GC/RT/5023. Categorisation of Track. *House, Euston Square Floor DP01, Railwaytrack*. London, UK: Railtrack PLC.

Rebelo N., G. X.-Y. (2004). *Proceedings of the ABAQUS Users Conference* . Boston, Massachusets.

Reiff, R. (2005). Implementing Top of Rail Friction Control North American Freight Railroad Experience.

Reiff. R., C. D. (1999). Systems Approach to Best Practices for Wheel/Rail Friction Control. *IHHA STS*.

Ringsberg J, e. a. (2000). Prediction of fatigue crack initiation for rolling contact fatigue. . *Int Journal of Fatigue* .

Ringsberg, J. (2000). Cyclic Ratchetting and Failure of a Pearlitic Rail Steel. *Fatigue & Fracture of Engineering Materials & Structures*, Vol.23 (9), p.747-75.

Rochard, B. (2007). Best Practice in the Management of Railway Maintenance. *PhD Thesis, Department of Mechanical Engineering University of Sheffield*.

Sawley, K. (2010). Wheel-rail Deterioration and its Impact and Mitigation. In F. Schmid, M. Burstow, S. Clark, B. Eickhoff, M. Hiensch, S. Hsu, & S. Kent, *Wheel-Rail Best Practice Handbook for Mixed Traffic Railways.* London: University of Birmingham Press and A&N Harris.

Sawley, K. R. (2000). Rail Failure Assessment for the Office of the Rail Regulator, an Assessment of Railtrack's Methods for Managing Broken and Defective Rails. *Transportation Technology Center Inc*.

Schijve, J. (2001). Fatigue of structures and materials. *Kluwer Academic*, ISBN: 0792370139, 2001.

Schmid, F. (2001). Organisational Ergonomics, A Case Study from the Railway Systems Area. *IEEE International Conference on Human Interfaces in Control Rooms, Cockpits and Command Centres*.

Schmid, F. (2010). *Best Practice in Wheel-Rail Interface Management for Mixed Traffic Railways.* London: ISBN-10: 0-9529997-3-0.

Schmid, F. (2010). Best Practice in Wheel-Rail Interface Management for Mixed Traffic Railways 1st Edition. Birmingham: University of Birmingham Press and A&N Harris.

Schmid, R. E. (1994). Computer-Simulation of the Dynamical Behavior of a Railway-Bogie Passing a Switch. *Journal of Veh. Syst. Dyn.,*, 23, pp. 481-499.

Schmid, R., Endlicher, K., & Lugner, P. (1994). Computer-Simulation of the Dynamical Behavior of a Railway-Bogie Passing a Switch, 23, pp. . *Journal of Veh. Syst. Dyn., 23*, 481-499.

Shen, Z. H. (1984). A comparison of alternative creep force models for rail vehicle dynamic analysis. *Proceedings of the 8th IAVSD Symposium, Cambridge, MA*, pp. 591-605.

Smith, R. (2000). Fatigue of Railway Axles: A Classic Problem Revisited. *Fracture Mechanics: Applications & Challenges, Elsevier*.

South, G. (2011). *Principal Switch and Crossing Engineer. Personal communication.*

Standard, R. C. (1995). Basic Track Category Matrix. *Track Standards Manual - Section 1* .

Takahashi S, S. T. (2009). Residual stress evaluation of Railway Rails. *International Centre for Diffraction data*, 240-247.

Telliskivi T & Olofsson U, W.-r. w. (2004). Wear . *An international journal on the science and technology of friction, lubrication and wear,*, 257(11): 1145-1153.

Telliskivi, T. O. (2000). A tool and a method for FE analysis of wheel and rail interaction. Stockholm, Sweden. *Royal Institute of Technology* .

Thompson, D. J. (2000). A review of the modelling of wheel/rail noise generation. *Journal of Sound and Vibration*, 231, 519-536.

Tyfour, W. J. (1995). The Steady State Wear Behaviour of Pearlitic Rail Steel Under Dry Rolling-Sliding Contact Conditions. *Wear*, Vol. 180, pp. 79-89.

Vo, e. a. (2015). FE Method to Predict Damage Formation on Curved Track for various worn status of Wheel/Rail Profiles. *Wear, Vol.322-323*, p61-75.

Wang WJ, G. J. (2009). Study on relationship between oblique fatigue crack and rail wear in curve track and prevention, . *Wear - An international journal on the science and technology of friction, lubrication and wear*, 267(1-4): 540-544.

Wickens A. H. (2003). *Fundamentals of Rail Vehicle Dynamics: Guidance and Stability.* Handbook of Rail Vehicle Dynamics; Swets and Zeitlinger Publisher.

Wickens, A. (1966). *A refined theory of the lateral stability of a four wheeled railway vehicle having a flexible, undamped suspension.* British Rail Research (BRR), Report No: 261-032-023.

Wickens, A. (1968). *Static and Dynamic stability of railway vehicle wheelsets having profiled wheels.* Derby: British Rail Research (BRR), Report No: TN-DYN-90, (BRR) British Rail Research.

Wiest, M. K. (2008). *Assessment of methods for calculating contact pressure in wheel-railcontact wear.*

Williams J, D. I. (1998). Repeated Loading, residual stresses, shakedown and tribology. *Journal of Materials Research*, 14(4): 1548-1559.

Williams, J. G. (2007). *S&C Failure and Delay Analysis, Report No: SA/TSS/17754/S3/R001, .* Warrington, Cheshire, WA3 6GA: Serco Assurance Thornson House, Birchwood Park.

Wilson, A. (2005). Easier Done Than Said - A sociological analysis of tacit knowledge in railway maintenance systems. *PhD Thesis, School of Social and Political Studies", University of Edinburgh*.

Wilson, A. F. (2003). Workers in Complex Environments – A Railway Maintenance Case Study. *IEE Seminar, Human Factors in the Railway Industry*.

Wu, e. a. (2011). Three-dimensional elastic-plastic stress analysis. *Wear*, 271, pp. 426-436.

Yan, W., & Fischer, F. (2000). Applicability of the Hertz contact theory to rail-wheel contact problems. *Archive of Applied Mechanics*, 70, pp. 255-268.

Yastrebov, V. (2013). Numerical Methods in Contact Mechanics .

Yokoyama, H. e. (2000). Effect of the angle of attack on flaking behaviour in pearlitic and bainitic steel rails. *CM 2000*.

Zarembski, A. (2003). Heavy Axle Load Case Study in Planning Freight Railways. pp 52-57.

Zerbst U, L. R. (2009). Introduction to the damage tolerance behaviour of railway rails - a review. *Engineering Fracture Mechanics*, 76(17): 2563-2601.

Zhao, X. L. (2011). The solution offrictional wheel-rail rolling contact with a 3D transient finite elementmodel: validation and error analysis. *Wear271*, 444–452.

Zienkiewicz, O. T. (2014). *The Finite Element Method for Solid and Structural Mechanics.* The Finite Element Method for Solid and Structural Mechanics.

Zwanenburg, W. (2007). The Swiss experience on the wear of railway switches and crossing. *In: 7th Swiss Transport Research Conference - STRC 07, Patterson Z. (eds.); September; Monte Verita / Ascona*.

Zwanenburg, W. (2009). Modelling Degradation Processes of Switches & Crossings for Maintenance & Renewal Planning on the Swiss Railway Network. PhD Thesis: Delft University of Technology. *École Polytechnique Federale De Lausanna*.

Rail Accident Investigation Branch (2021). Eastleigh Derailment Report

Abaqus/CAE Users Manual (2011). Dassault Systemes, Abaqus 6.11

Björn A. Pålsson, Ramakrishnan Ambur, Michel Sebès, Ping Wang, Jou-Yi Shih, Demeng Fan, Jingmang Xu & Jiayin Chen (2023). A comparison of track model formulations for simulation of dynamic vehicle–track interaction in switches and crossings, Vehicle System Dynamics, 61:3, 698-724, DOI: 10.1080/00423114.2021.1983183

Dixon R, Jou-Yi Shih & Ramakrishnan Ambur (2023) Developing a detailed multi-body dynamic model of a turnout based on its finite element model, Vehicle System Dynamics, 61:3, 725-738, DOI: 10.1080/00423114.2021.1981952

Sebès M and Bezin Y (2023) Considering the interaction of switch and stock rails in modelling vehicle-track interaction in a switch panel diverging route, Vehicle System Dynamics, 61:3, 765-781, DOI: 10.1080/00423114.2021.1947510

Network Rail (2017) NR/L3/TRK/2049 – Track Design Handbook

APPENDIX A: OTHER VAMPIRE RESULTS

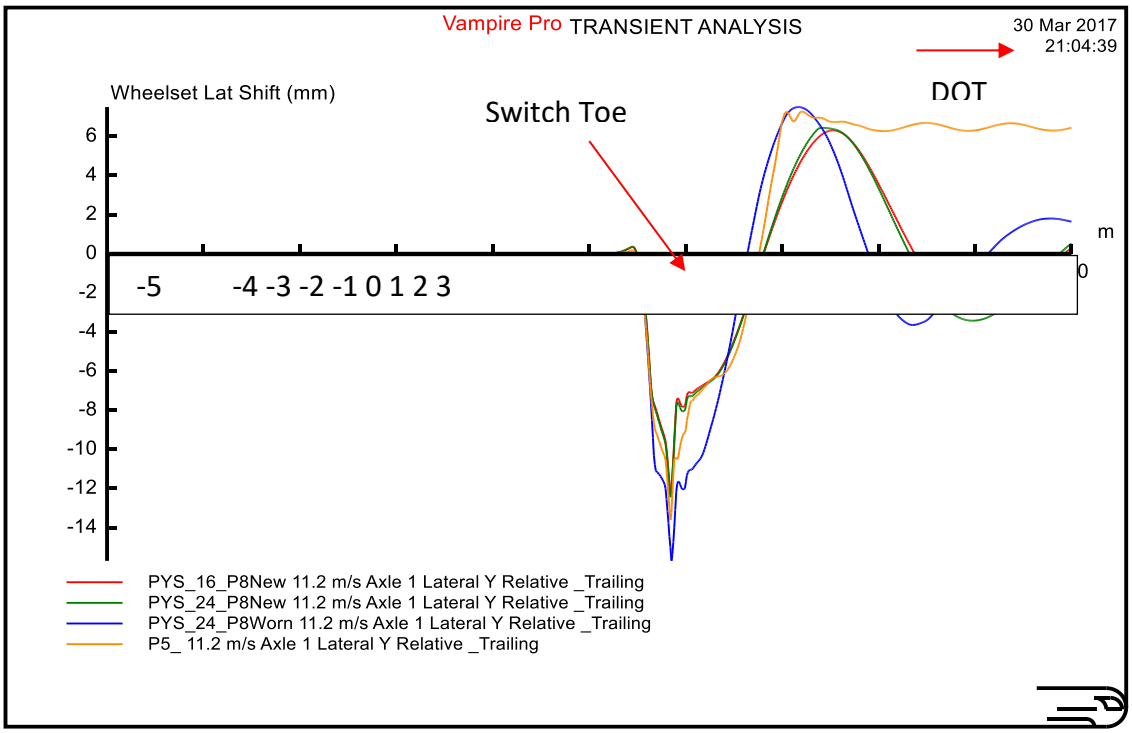

Leading Wheelset Lateral Shift from Track Centre

Figure 62: Wheelset Lateral Shift

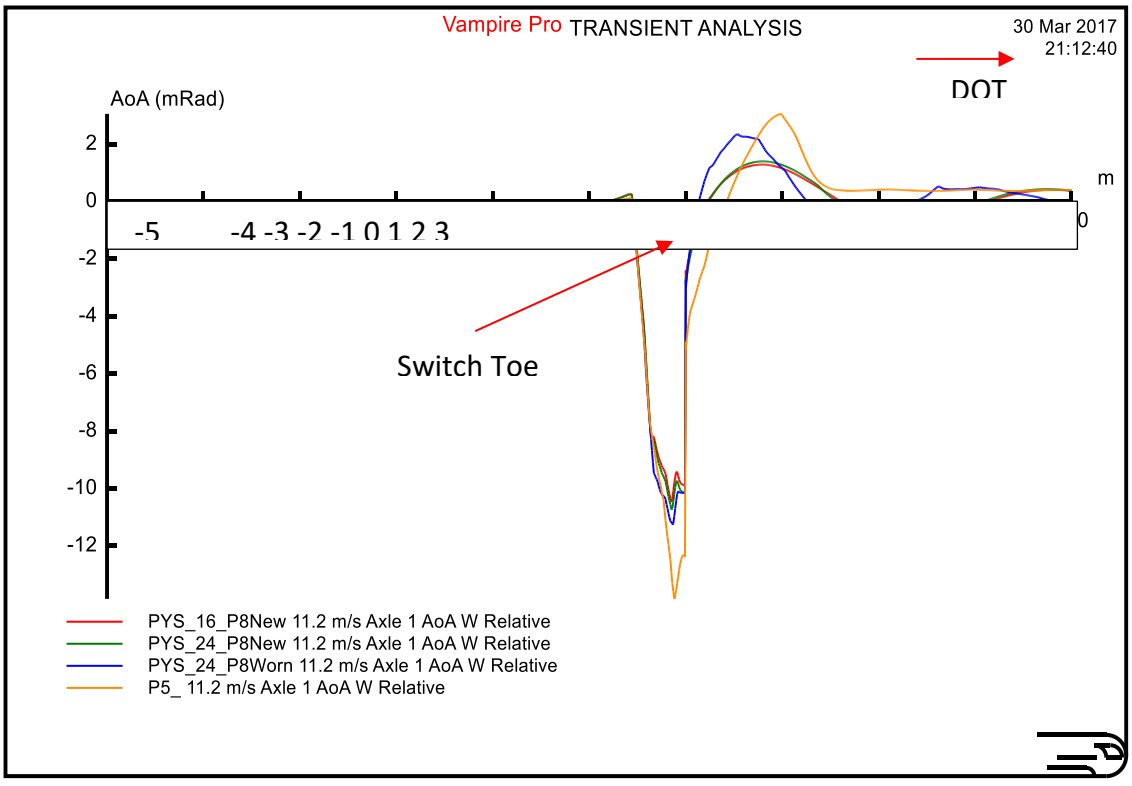

AoA for Leading Wheelset

Figure 63: Wheelset Angle of Attack for Trailing Direction

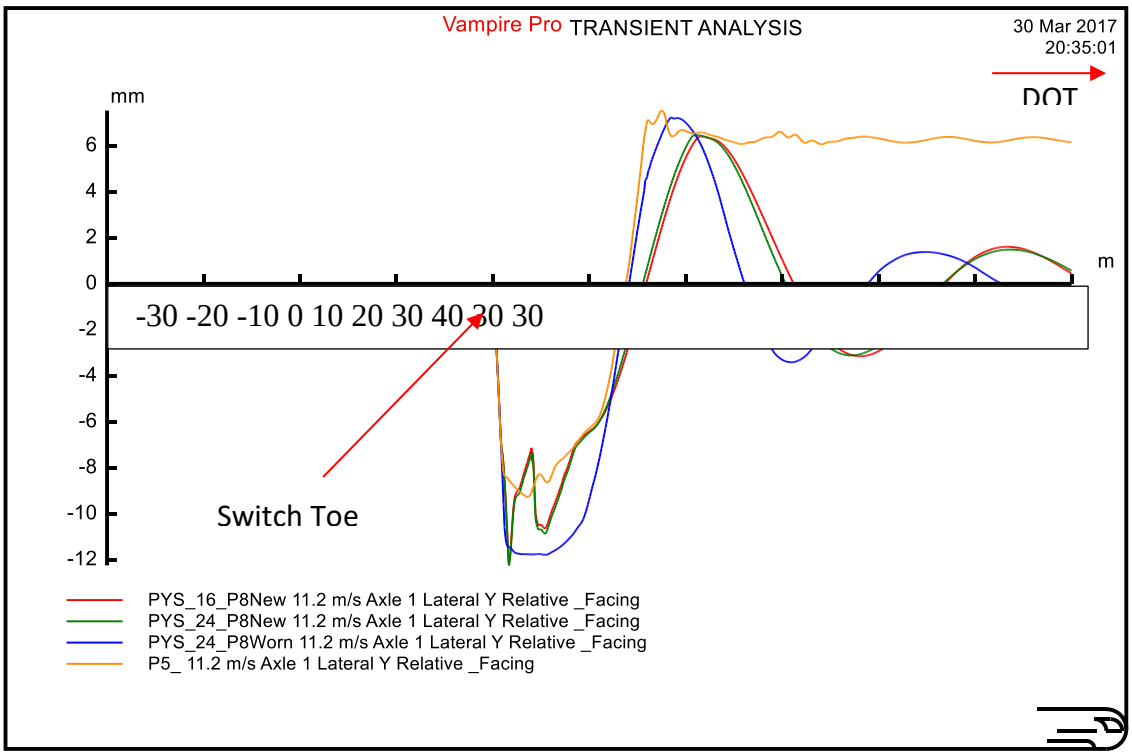

Leading Wheelset Lateral Shift from Track Centre

Figure 64: Wheelset Angle of Attack for Trailing Direction

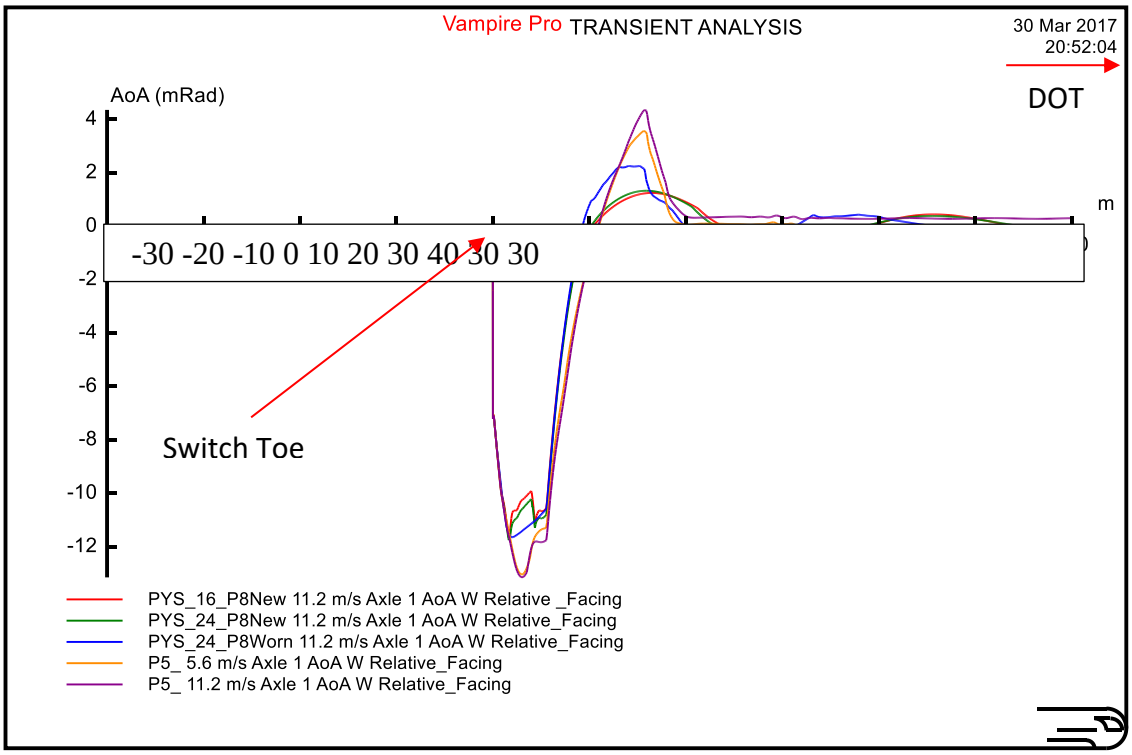

AoA for Leading Wheelset

Figure 65: Angle of Attack (AoA)

APPENDIX B: VAMPIRE Pro SIMULATION INPUT

Track Design Facing

DESIGN

UNITS VAMPIRE

NR60mk2 C switch (Diverging Facing)

DISTANCE	CURV	VERT	XLEVEL	KINK
0	0	0	0	0
40	0	0	0	6.909357
40.1	4.138931	0	0	0
44.55161	4.138931	0	0	0
44.65161	4.051117	0	0	0
45.51326	4.051117	0	0	0
45.61326	0	0	0	0
85.61326	0	0	0	0
100	0	0	0	0

Track Design Trailing

DESIGN

UNITS VAMPIRE

NR60mk2 C switch (Diverging Trailing)

DISTANCE	CURV	VERT	XLEVEL	KINK
0	0	0	0	0
14.38674	0	0	0	0
54.38674	0	0	0	0
54.48674	4.051117	0	0	0

55.34839	4.051117	0	0	0
55.4484	4.138931	0	0	0
59.9	4.138931	0	0	0
60	0	0	0	-6.9093
100	0	0	0	0

CONTACT file - NR60mk2 C Switch

UNITS
VAMPIRE

Contact file - NR60mk2 C Switch

DISTANCE	CONTACTDATA
0	C:\\NR60C MK2 Modelling Report\CONTACT DATA\NR60mk2C-RR_br-p8
40	C:\\NR60C MK2 Modelling Report\CONTACT DATA\NR60mk2C-RR_br-p8
40.1	C:\\NR60C MK2 Modelling Report\CONTACT DATA\NR60mk2C-SS_br-p8
40.9	C:\\NR60C MK2 Modelling Report\CONTACT DATA\NR60mk2C-SS_br-p8
41	C:\\NR60C MK2 Modelling Report\CONTACT DATA\NR60mk2C-0_br-p8
41.05	C:\\NR60C MK2 Modelling Report\CONTACT DATA\NR60mk2C-50_br-p8
41.1	C:\\NR60C MK2 Modelling Report\CONTACT DATA\NR60mk2C-100_br-p8
41.15	C:\\NR60C MK2 Modelling Report\CONTACT DATA\NR60mk2C-150_br-p8
41.2	C:\\NR60C MK2 Modelling Report\CONTACT DATA\NR60mk2C-200_br-p8
41.25	C:\\NR60C MK2 Modelling Report\CONTACT DATA\NR60mk2C-250_br-p8
41.3	C:\\NR60C MK2 Modelling Report\CONTACT DATA\NR60mk2C-300_br-p8
41.35	C:\\NR60C MK2 Modelling Report\CONTACT DATA\NR60mk2C-350_br-p8
41.4	C:\\NR60C MK2 Modelling Report\CONTACT DATA\NR60mk2C-400_br-p8

41.45 C:\\NR60C MK2 Modelling Report\CONTACT DATA\NR60mk2C-450_br-p8

41.5 C:\\NR60C MK2 Modelling Report\CONTACT DATA\NR60mk2C-500_br-p8

41.55 C:\\NR60C MK2 Modelling Report\CONTACT DATA\NR60mk2C-550_br-p8

41.6 C:\\NR60C MK2 Modelling Report\CONTACT DATA\NR60mk2C-600_br-p8

41.65 C:\\NR60C MK2 Modelling Report\CONTACT DATA\NR60mk2C-650_br-p8

41.7 C:\\NR60C MK2 Modelling Report\CONTACT DATA\NR60mk2C-700_br-p8

41.75 C:\\NR60C MK2 Modelling Report\CONTACT DATA\NR60mk2C-750_br-p8

41.8 C:\\NR60C MK2 Modelling Report\CONTACT DATA\NR60mk2C-800_br-p8

41.85 C:\\NR60C MK2 Modelling Report\CONTACT DATA\NR60mk2C-850_br-p8

41.9 C:\\NR60C MK2 Modelling Report\CONTACT DATA\NR60mk2C-900_br-p8

41.95 C:\\NR60C MK2 Modelling Report\CONTACT DATA\NR60mk2C-950_br-p8

42 C:\\NR60C MK2 Modelling Report\CONTACT DATA\NR60mk2C-1000_br-p8

42.05 C:\\NR60C MK2 Modelling Report\CONTACT DATA\NR60mk2C-1050_br-p8

42.1 C:\\NR60C MK2 Modelling Report\CONTACT DATA\NR60mk2C-1100_br-p8

42.15 C:\\NR60C MK2 Modelling Report\CONTACT DATA\NR60mk2C-1150_br-p8

42.2 C:\\NR60C MK2 Modelling Report\CONTACT DATA\NR60mk2C-1200_br-p8

42.25 C:\\NR60C MK2 Modelling Report\CONTACT DATA\NR60mk2C-1250_br-p8

42.3 C:\\NR60C MK2 Modelling Report\CONTACT DATA\NR60mk2C-1300_br-p8

42.35 C:\\NR60C MK2 Modelling Report\CONTACT DATA\NR60mk2C-1350_br-p8

42.4 C:\\NR60C MK2 Modelling Report\CONTACT DATA\NR60mk2C-1400_br-p8

42.45 C:\\NR60C MK2 Modelling Report\CONTACT DATA\NR60mk2C-1450_br-p8

42.5 C:\\NR60C MK2 Modelling Report\CONTACT DATA\NR60mk2C-1500_br-p8

42.55 C:\\NR60C MK2 Modelling Report\CONTACT DATA\NR60mk2C-1550_br-p8

42.6 C:\\NR60C MK2 Modelling Report\CONTACT DATA\NR60mk2C-1600_br-p8

42.65 C:\\NR60C MK2 Modelling Report\CONTACT DATA\NR60mk2C-1650_br-p8

42.7 C:\\NR60C MK2 Modelling Report\CONTACT DATA\NR60mk2C-1700_br-p8

42.75 C:\\NR60C MK2 Modelling Report\CONTACT DATA\NR60mk2C-1750_br-p8

42.8 C:\\NR60C MK2 Modelling Report\CONTACT DATA\NR60mk2C-1800_br-p8

42.85 C:\\NR60C MK2 Modelling Report\CONTACT DATA\NR60mk2C-1850_br-p8

42.9 C:\\NR60C MK2 Modelling Report\CONTACT DATA\NR60mk2C-1900_br-p8

42.95 C:\\NR60C MK2 Modelling Report\CONTACT DATA\NR60mk2C-1950_br-p8

43 C:\\NR60C MK2 Modelling Report\CONTACT DATA\NR60mk2C-2000_br-p8

43.05 C:\\NR60C MK2 Modelling Report\CONTACT DATA\NR60mk2C-2050_br-p8

43.1 C:\\NR60C MK2 Modelling Report\CONTACT DATA\NR60mk2C-2100_br-p8

43.15 C:\\NR60C MK2 Modelling Report\CONTACT DATA\NR60mk2C-2150_br-p8

43.2 C:\\NR60C MK2 Modelling Report\CONTACT DATA\NR60mk2C-2200_br-p8

43.25 C:\\NR60C MK2 Modelling Report\CONTACT DATA\NR60mk2C-2250_br-p8

43.3 C:\\NR60C MK2 Modelling Report\CONTACT DATA\NR60mk2C-2300_br-p8

43.35 C:\\NR60C MK2 Modelling Report\CONTACT DATA\NR60mk2C-2350_br-p8

43.4 C:\\NR60C MK2 Modelling Report\CONTACT DATA\NR60mk2C-2400_br-p8

43.45 C:\\NR60C MK2 Modelling Report\CONTACT DATA\NR60mk2C-2450_br-p8

43.5 C:\\NR60C MK2 Modelling Report\CONTACT DATA\NR60mk2C-2500_br-p8

43.55 C:\\NR60C MK2 Modelling Report\CONTACT DATA\NR60mk2C-2550_br-p8

43.6 C:\\NR60C MK2 Modelling Report\CONTACT DATA\NR60mk2C-2600_br-p8

43.65 C:\\NR60C MK2 Modelling Report\CONTACT DATA\NR60mk2C-2650_br-p8

43.7 C:\\NR60C MK2 Modelling Report\CONTACT DATA\NR60mk2C-2700_br-p8

43.75 C:\\NR60C MK2 Modelling Report\CONTACT DATA\NR60mk2C-2750_br-p8

43.8 C:\\NR60C MK2 Modelling Report\CONTACT DATA\NR60mk2C-2800_br-p8

43.85 C:\\NR60C MK2 Modelling Report\CONTACT DATA\NR60mk2C-2850_br-p8

43.9 C:\\NR60C MK2 Modelling Report\CONTACT DATA\NR60mk2C-2900_br-p8

43.95 C:\\NR60C MK2 Modelling Report\CONTACT DATA\NR60mk2C-2950_br-p8

44 C:\\NR60C MK2 Modelling Report\CONTACT DATA\NR60mk2C-3000_br-p8

44.05 C:\\NR60C MK2 Modelling Report\CONTACT DATA\NR60mk2C-2050_br-p8

44.1 C:\\NR60C MK2 Modelling Report\CONTACT DATA\NR60mk2C-3100_br-p8

44.15	C:\\NR60C MK2 Modelling Report\CONTACT DATA\NR60mk2C-3150_br-p8
44.2	C:\\NR60C MK2 Modelling Report\CONTACT DATA\NR60mk2C-3200_br-p8
44.25	C:\\NR60C MK2 Modelling Report\CONTACT DATA\NR60mk2C-3250_br-p8
44.3	C:\\NR60C MK2 Modelling Report\CONTACT DATA\NR60mk2C-3300_br-p8
44.35	C:\\NR60C MK2 Modelling Report\CONTACT DATA\NR60mk2C-3350_br-p8
44.4	C:\\NR60C MK2 Modelling Report\CONTACT DATA\NR60mk2C-3400_br-p8
44.45	C:\\NR60C MK2 Modelling Report\CONTACT DATA\NR60mk2C-3450_br-p8
44.5	C:\\NR60C MK2 Modelling Report\CONTACT DATA\NR60mk2C-3500_br-p8
44.55	C:\\NR60C MK2 Modelling Report\CONTACT DATA\NR60mk2C-3550_br-p8
44.6	C:\\NR60C MK2 Modelling Report\CONTACT DATA\NR60mk2C-3600_br-p8
44.65	C:\\NR60C MK2 Modelling Report\CONTACT DATA\NR60mk2C-3650_br-p8
44.7	C:\\NR60C MK2 Modelling Report\CONTACT DATA\NR60mk2C-3700_br-p8
44.75	C:\\NR60C MK2 Modelling Report\CONTACT DATA\NR60mk2C-3750_br-p8
44.8	C:\\NR60C MK2 Modelling Report\CONTACT DATA\NR60mk2C-3800_br-p8
44.85	C:\\NR60C MK2 Modelling Report\CONTACT DATA\NR60mk2C-3850_br-p8
44.9	C:\\NR60C MK2 Modelling Report\CONTACT DATA\NR60mk2C-3900_br-p8
44.95	C:\\NR60C MK2 Modelling Report\CONTACT DATA\NR60mk2C-3950_br-p8
45	C:\\NR60C MK2 Modelling Report\CONTACT DATA\NR60mk2C-4000_br-p8
45.05	C:\\NR60C MK2 Modelling Report\CONTACT DATA\NR60mk2C-4050_br-p8
45.1	C:\\NR60C MK2 Modelling Report\CONTACT DATA\NR60mk2C-4100_br-p8
45.15	C:\\NR60C MK2 Modelling Report\CONTACT DATA\NR60mk2C-4150_br-p8
45.2	C:\\NR60C MK2 Modelling Report\CONTACT DATA\NR60mk2C-4200_br-p8
45.25	C:\\NR60C MK2 Modelling Report\CONTACT DATA\NR60mk2C-4250_br-p8
45.3	C:\\NR60C MK2 Modelling Report\CONTACT DATA\NR60mk2C-4300_br-p8
45.35	C:\\NR60C MK2 Modelling Report\CONTACT DATA\NR60mk2C-4350_br-p8
45.4	C:\\NR60C MK2 Modelling Report\CONTACT DATA\NR60mk2C-4400_br-p8
48.45	C:\\NR60C MK2 Modelling Report\CONTACT DATA\NR60mk2C-RR_br-p8

54.085 C:\\NR60C MK2 Modelling Report\CONTACT DATA\NR60mk2C-RR_br-p8

54.185 C:\\NR60C MK2 Modelling Report\CONTACT DATA\NR60mk2C-RR_br-p8

94.185 C:\\NR60C MK2 Modelling Report\CONTACT DATA\NR60mk2C-RR_br-p8

100 C:\\NR60C MK2 Modelling Report\CONTACT DATA\NR60mk2C-RR_br-p8

APPENDIX C: BBR Wear Model

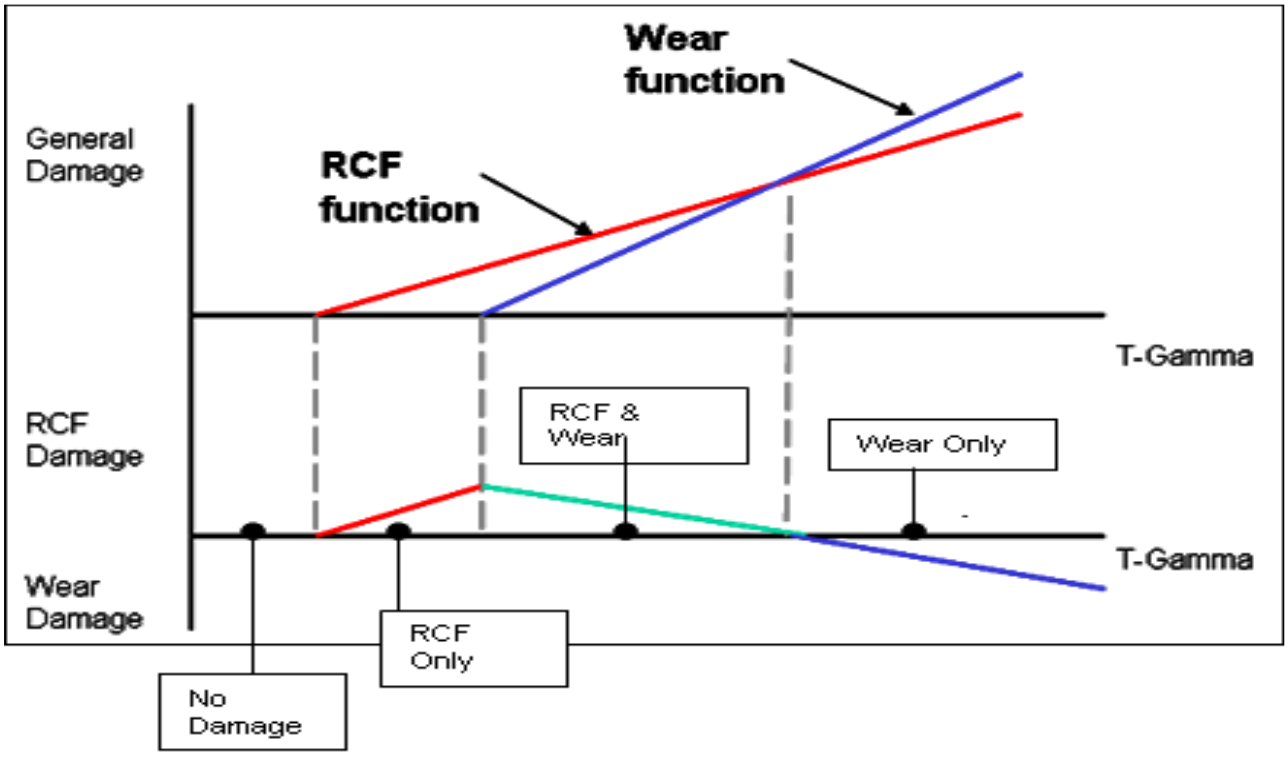

Figure 66: Whole Life Rail Model As A Function of T-Gamma (Adapted from Track-Ex)

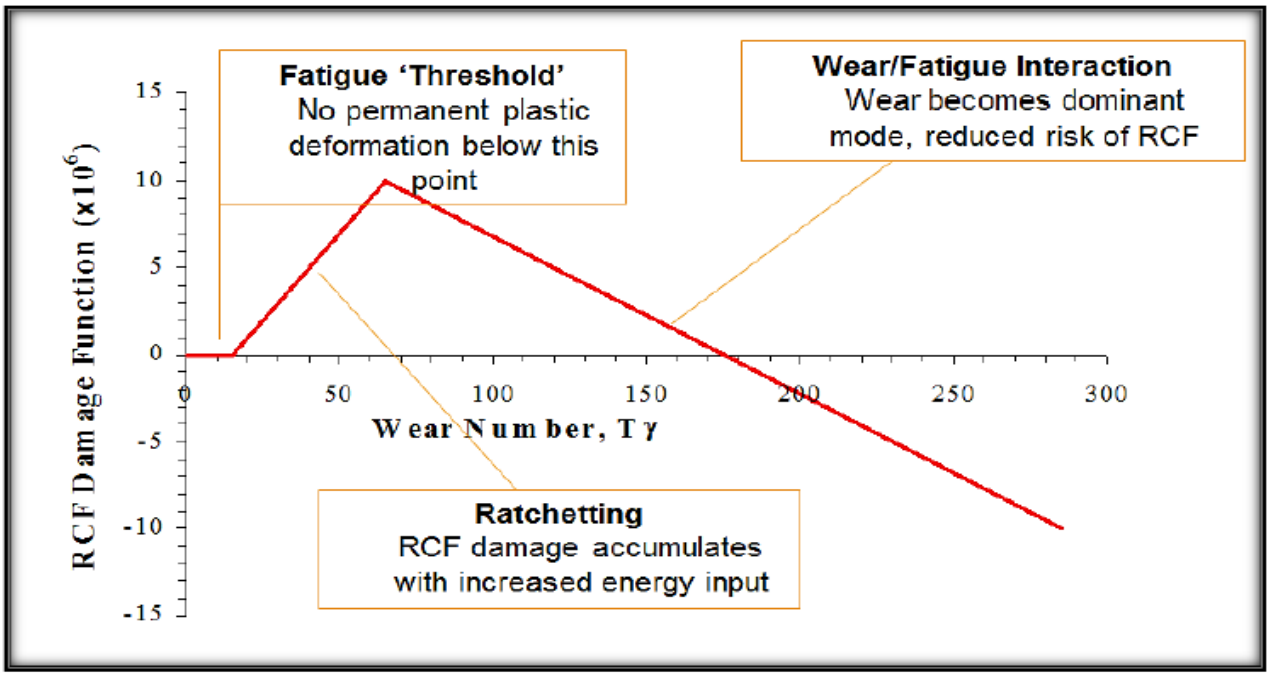

Figure 66: Whole Life Rail Model (Adapted from Track-Ex)

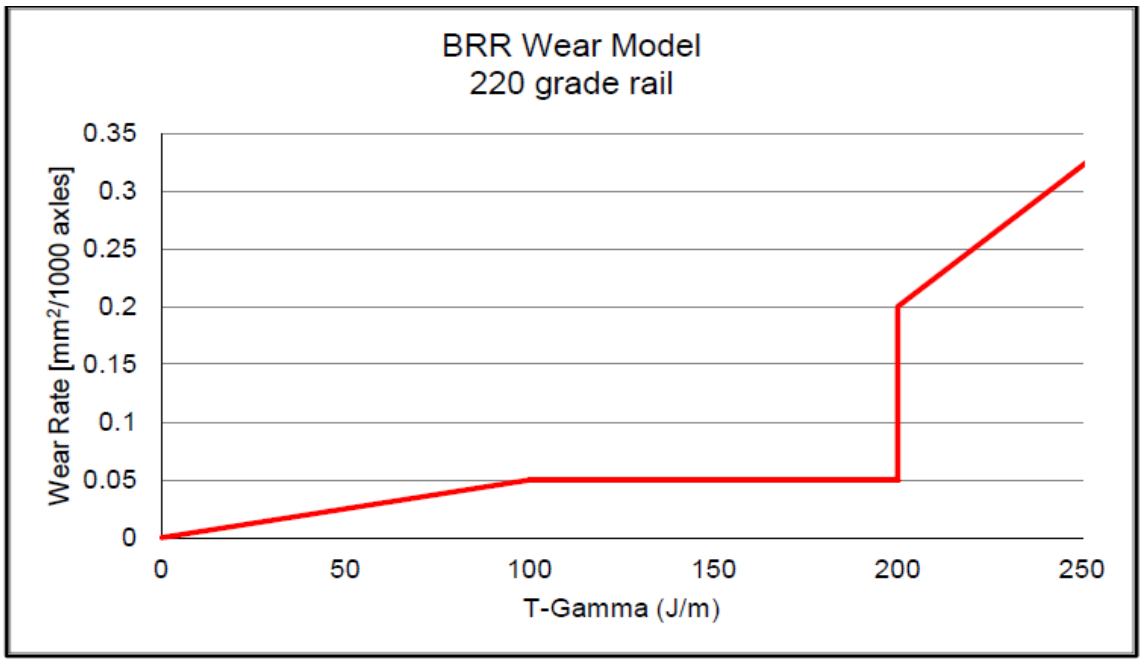

Figure 67: BRR Wear Model - Wear due to Contact Patch Energy

T-Gamma can be converted to the amount of material removed from the rail per axle pass by a laboratory derived relationship published in British Rail Research report 'TM VDY 004: Interpretation of Wheel/Rail Wear Numbers (1986)'. It is noted that the predictions are likely levels of wear based on several assumptions and the outcome is generally pessimistic, representing the worst possible wear. The predictions should therefore be viewed as comparative values and not be used as absolute levels for setting maintenance regimes. For T-Gamma > 200 J/m:

Rail Wear Rate [mm^2 / 1000 axles] = (2.5 x T-Gamma - 322) x 10^{-3} mm^2 / 1000 axles

According to the BRR report, a plain line side wear limit of 9mm equates roughly to 190 mm^2 of material being removed for 220 grade rail. The wear rate will be less for a harder grade steel such as 260 and even lesser for premium grade.

APPENDIX D: RAIL PPROFILES AND CONTACT PATCH PLOT

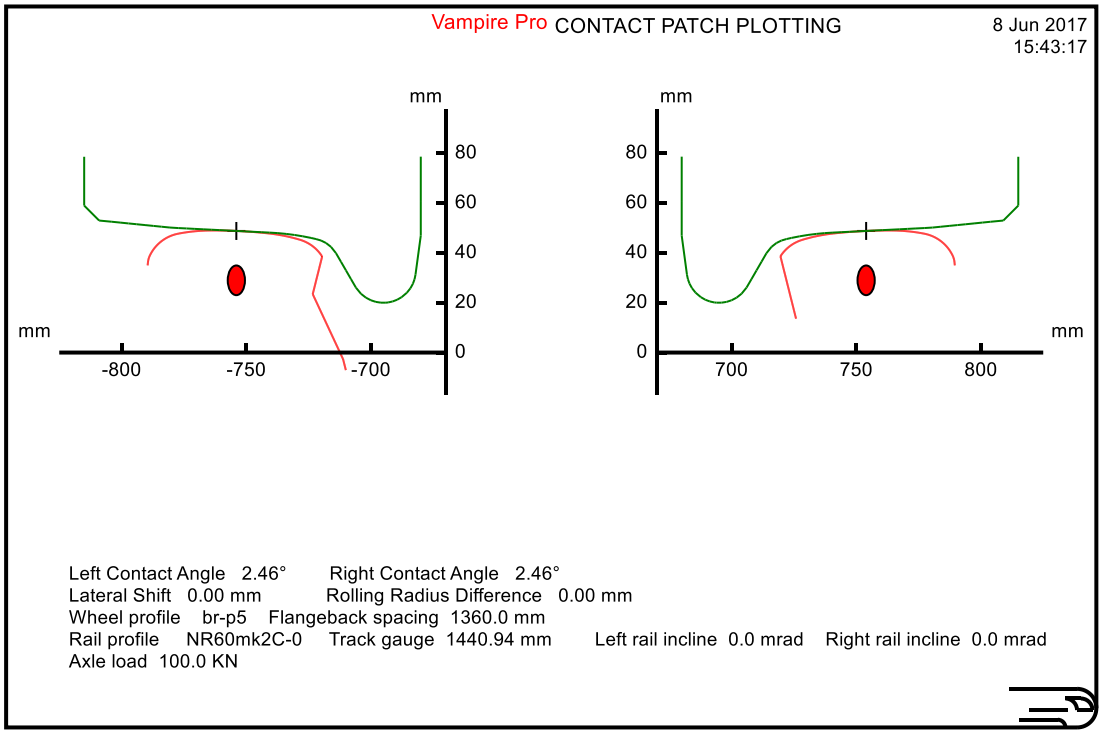

VAMPIRE Plot

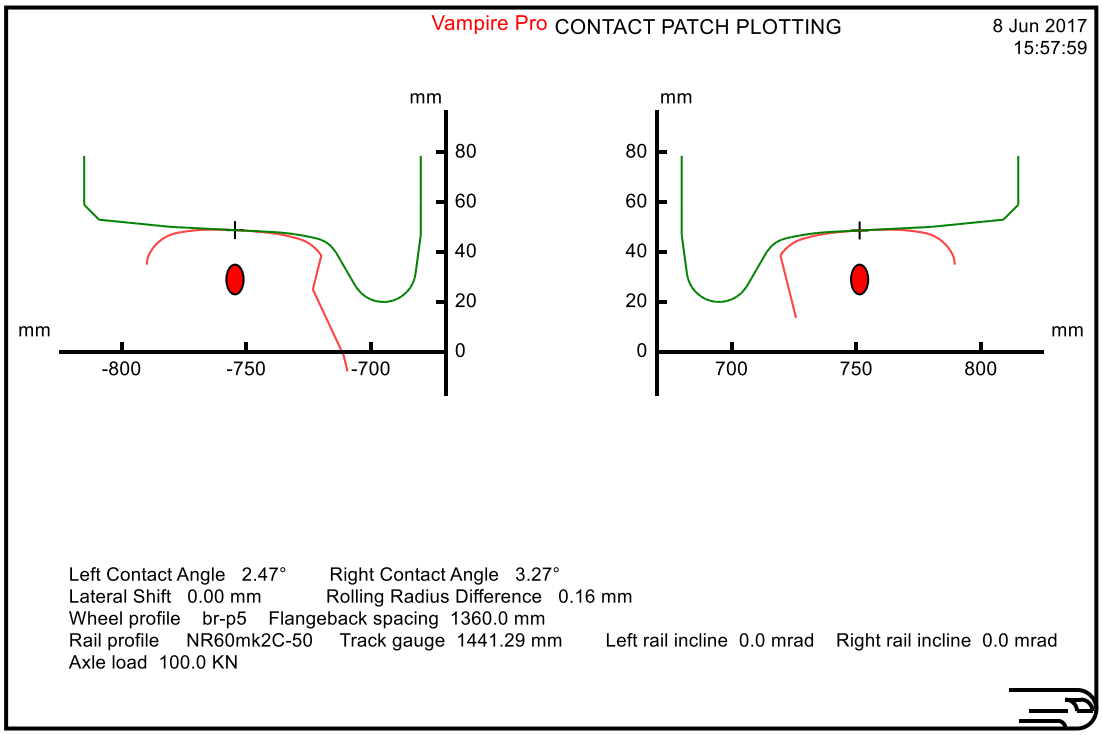

VAMPIRE Plot

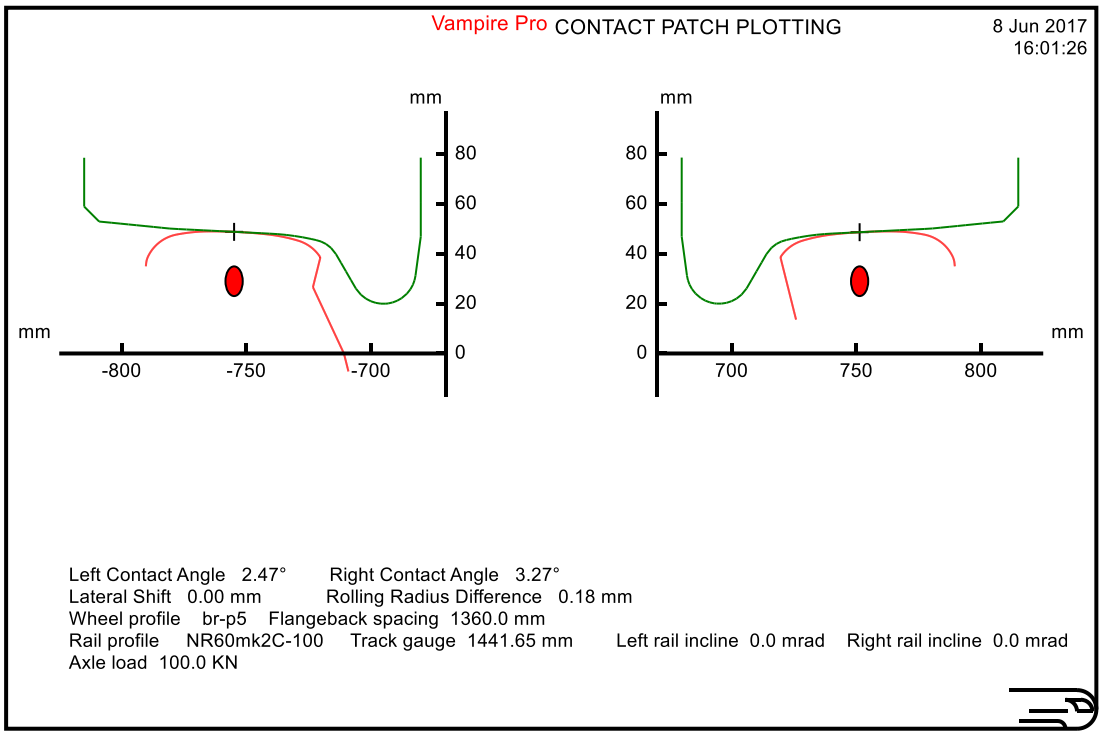

VAMPIRE Plot

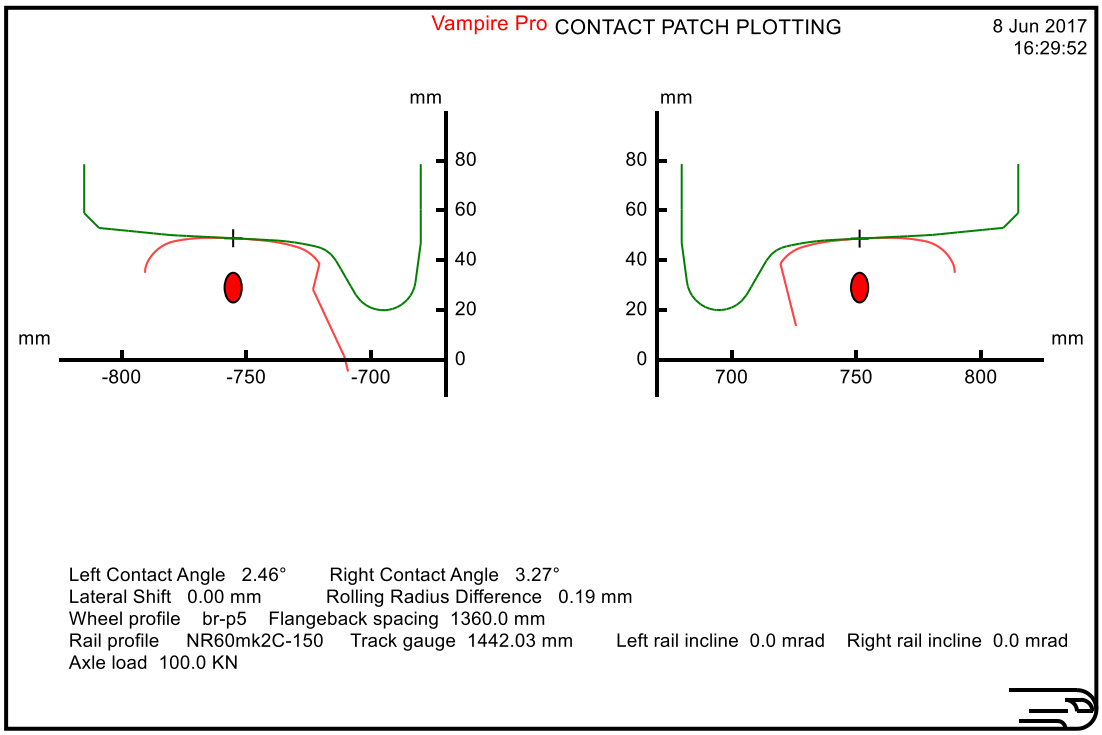

VAMPIRE Plot

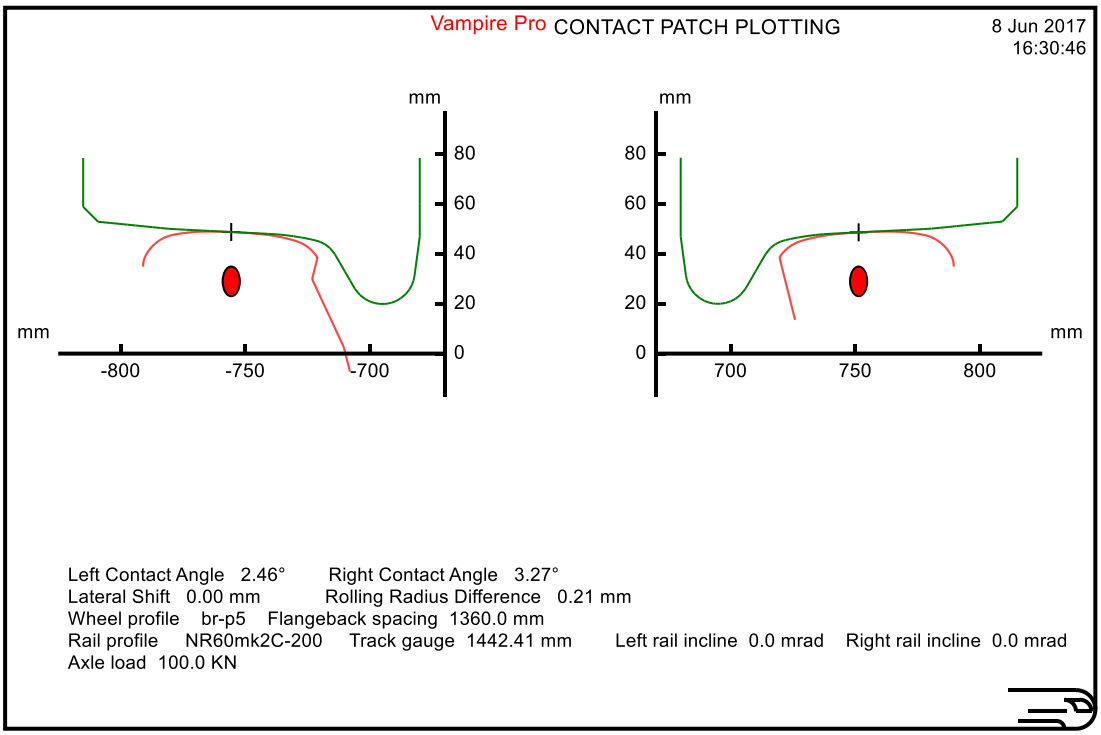

VAMPIRE Plot

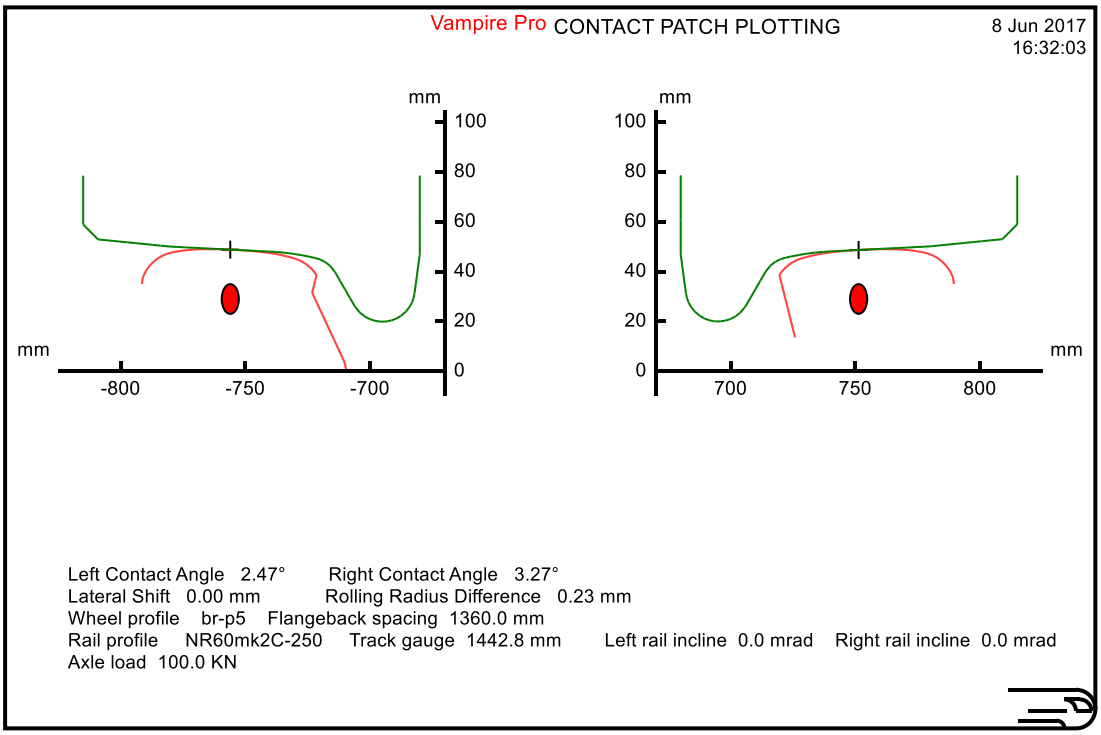

VAMPIRE Plot

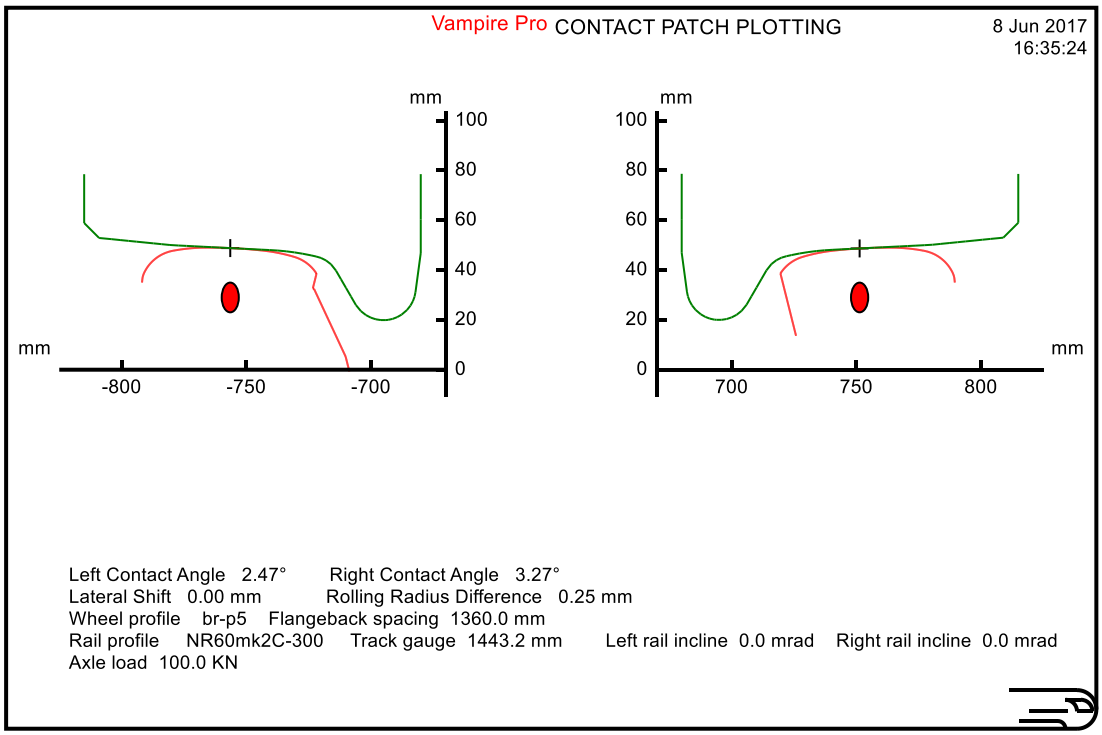

VAMPIRE Plot

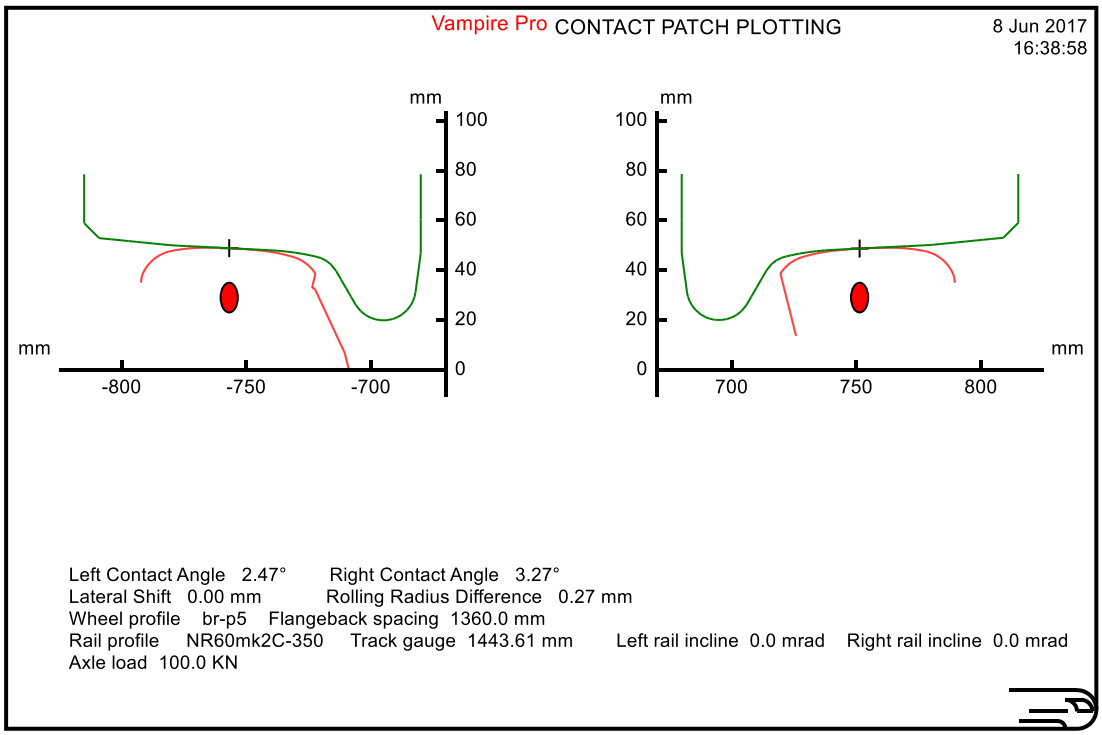

VAMPIRE Plot

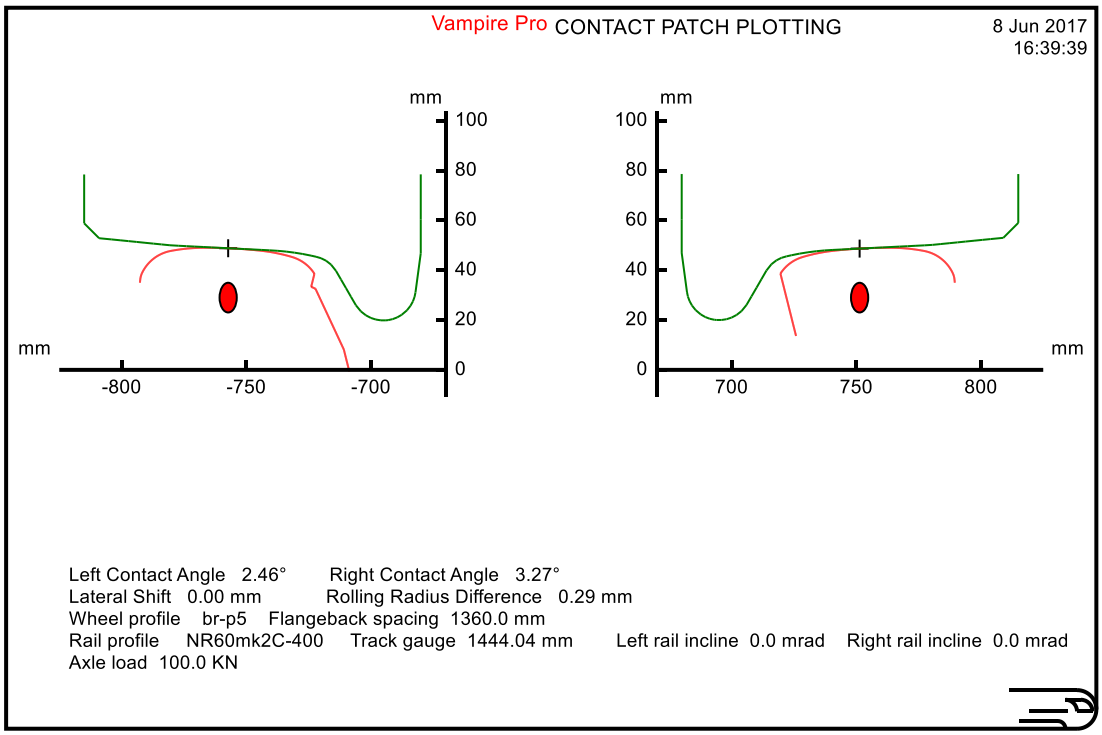

VAMPIRE Plot

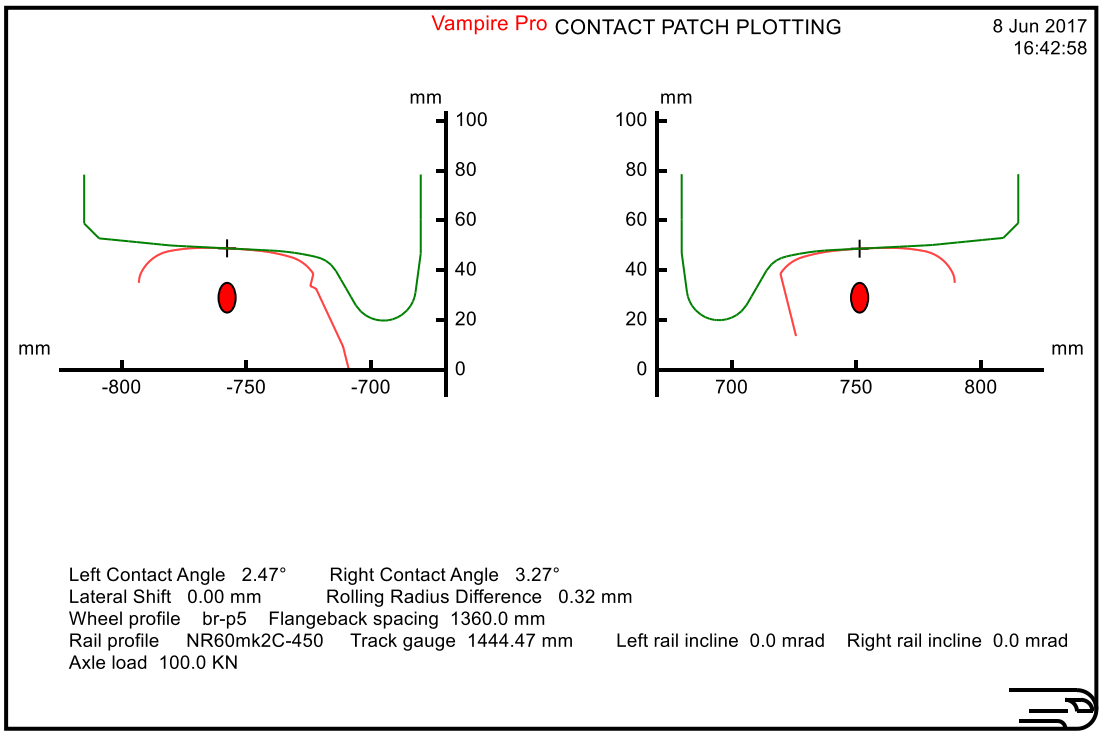

VAMPIRE Plot

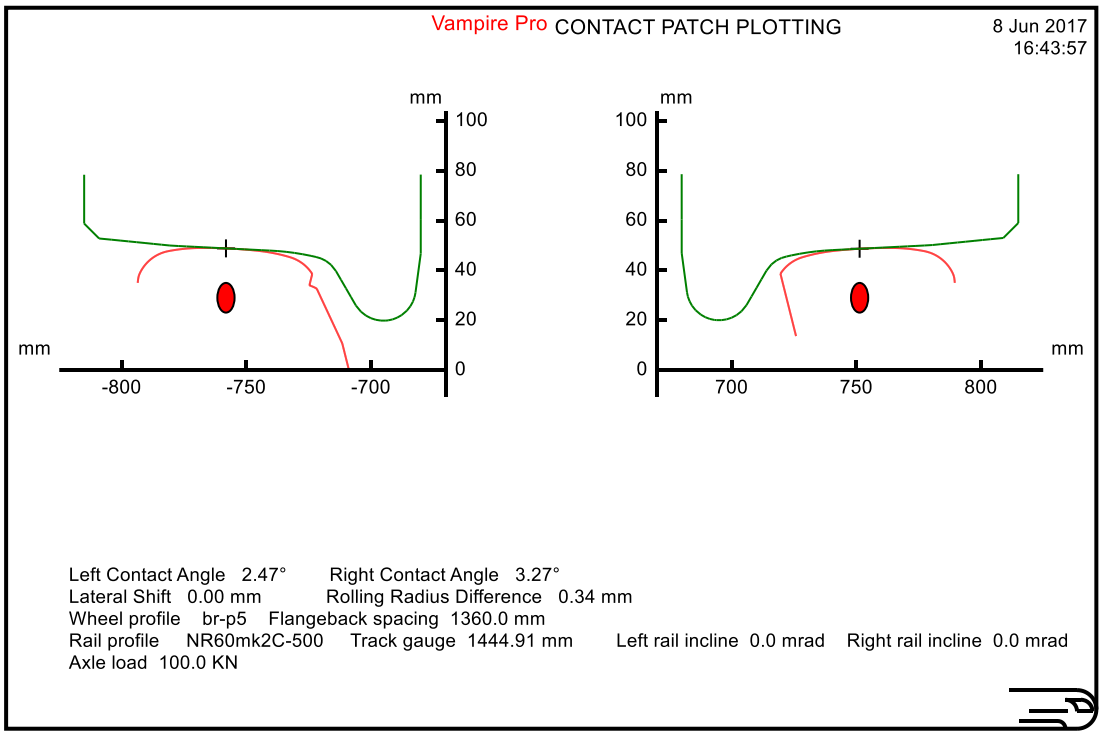

VAMPIRE Plot

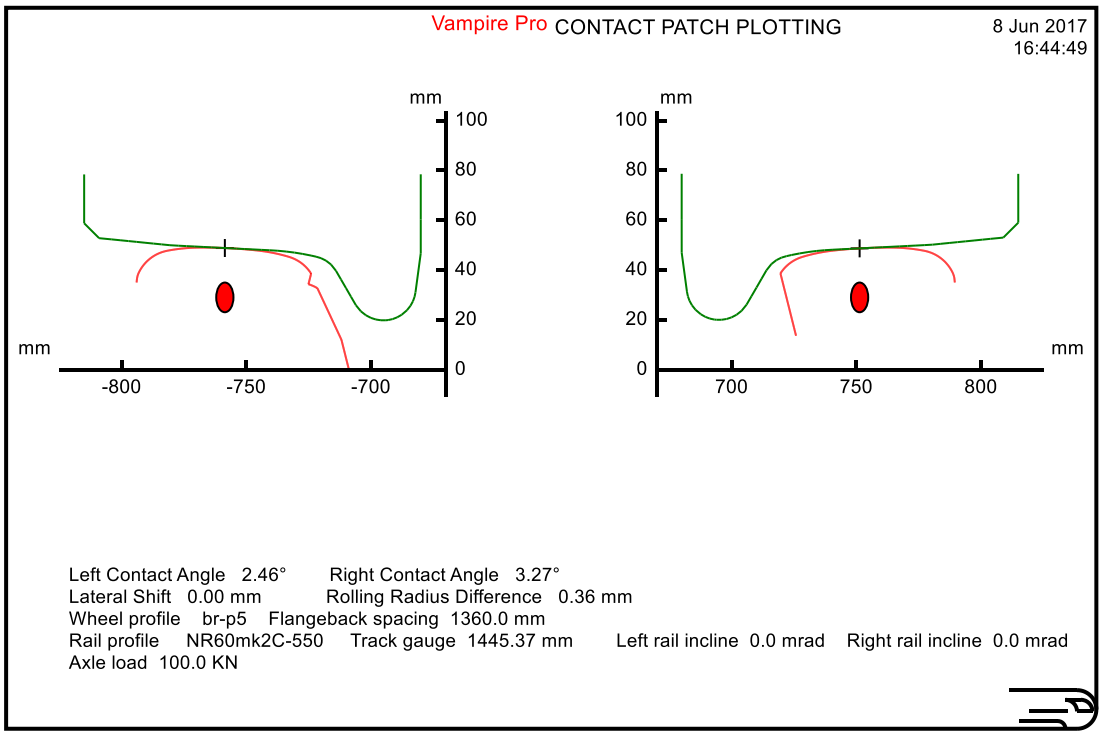

VAMPIRE Plot

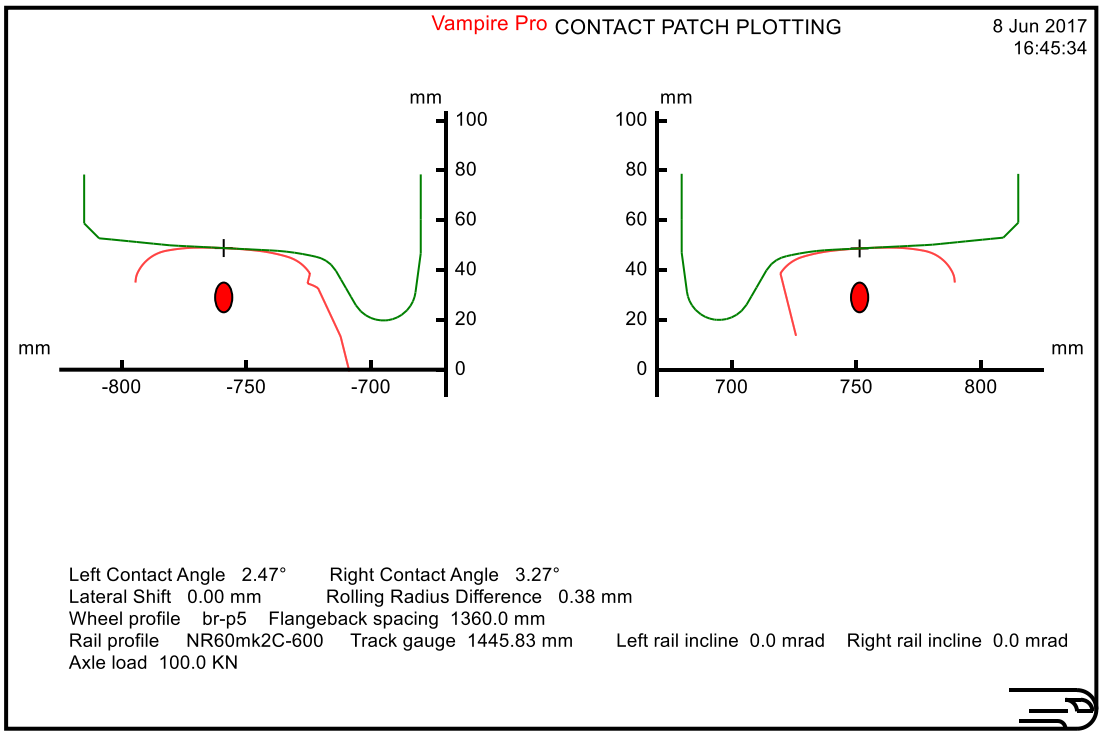

VAMPIRE Plot

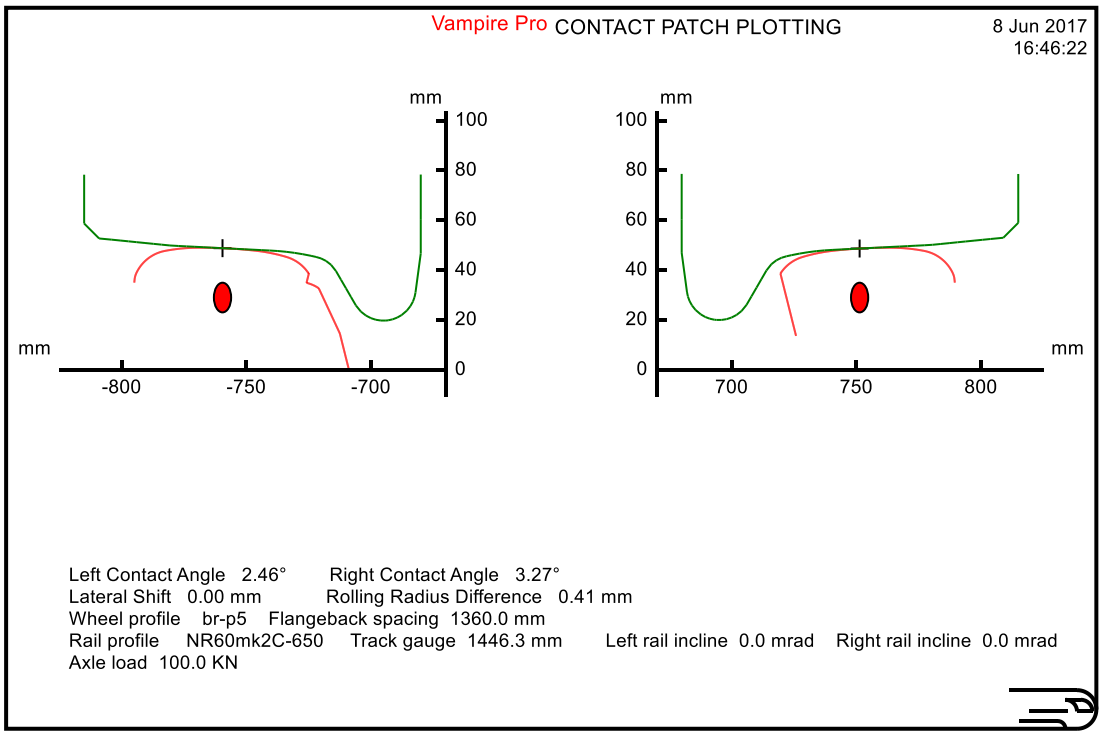

VAMPIRE Plot

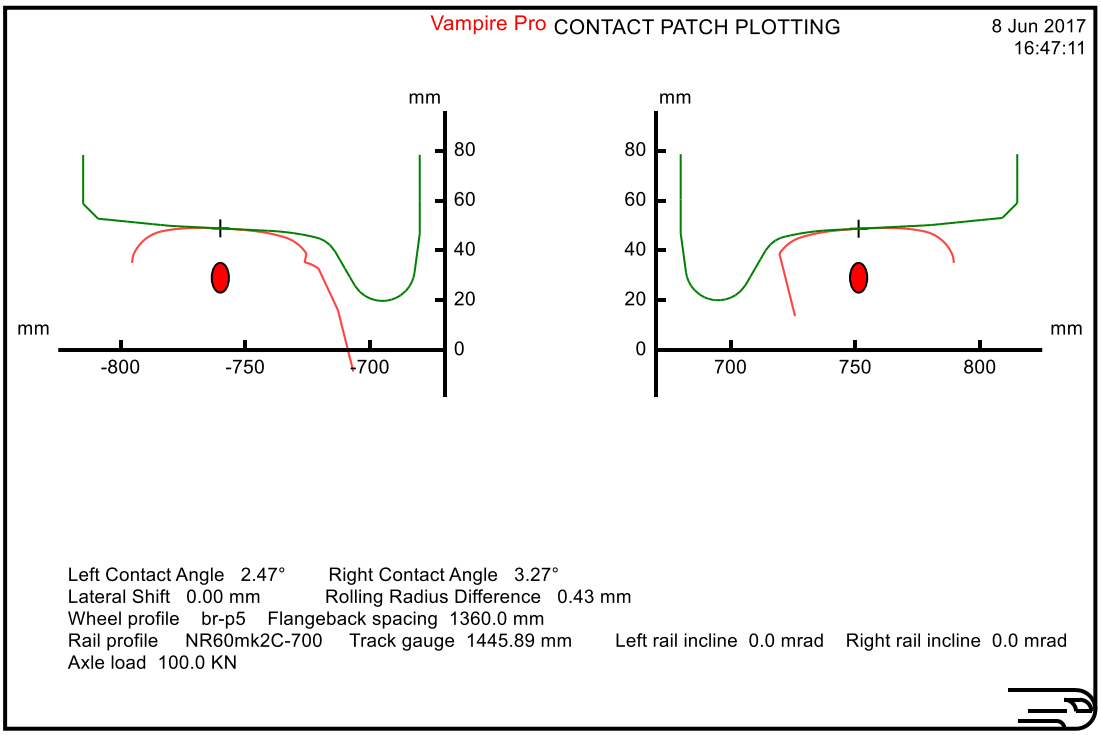

VAMPIRE Plot

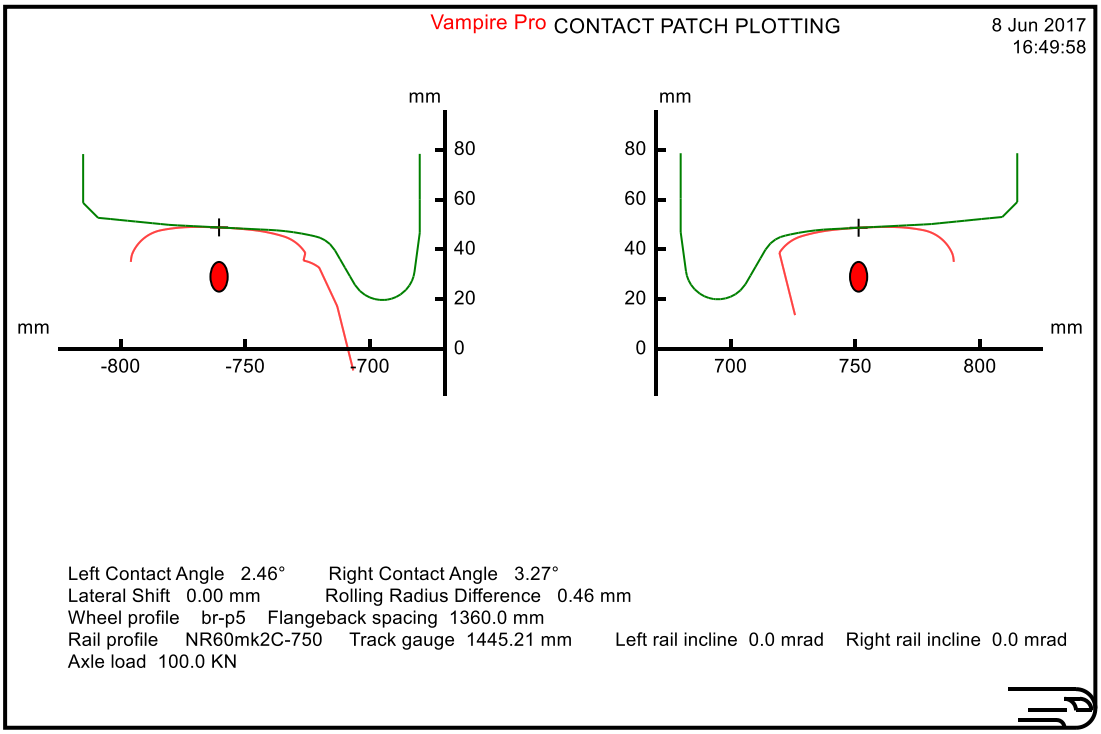

VAMPIRE Plot

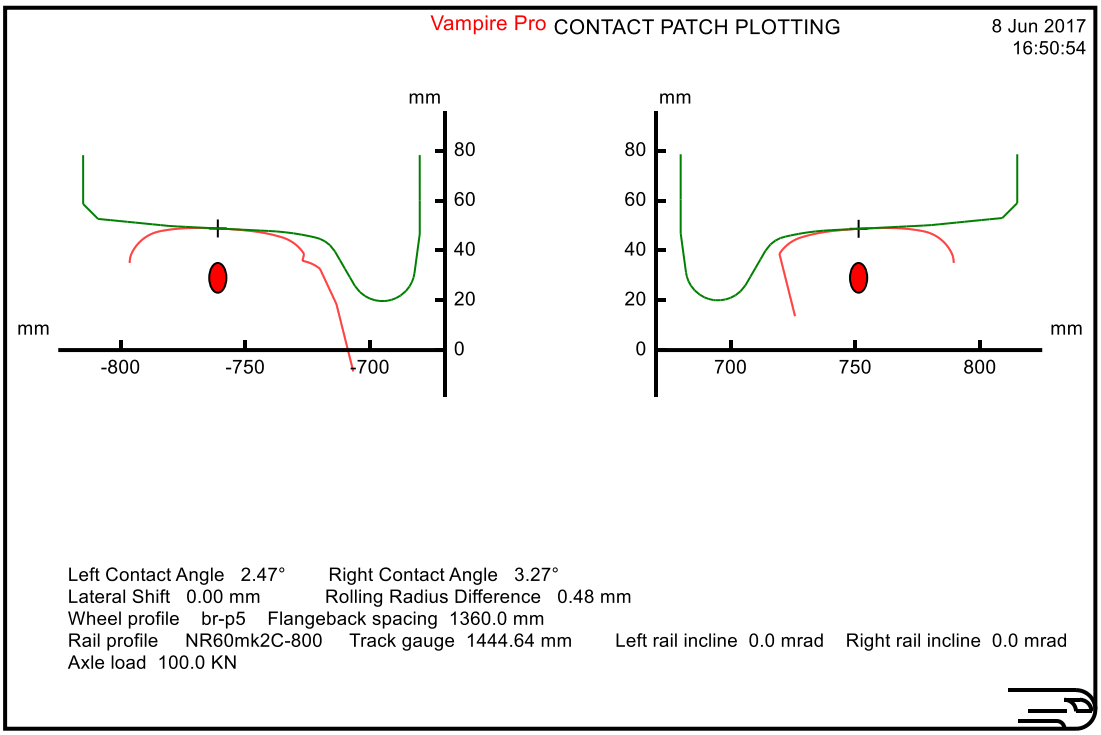

VAMPIRE Plot

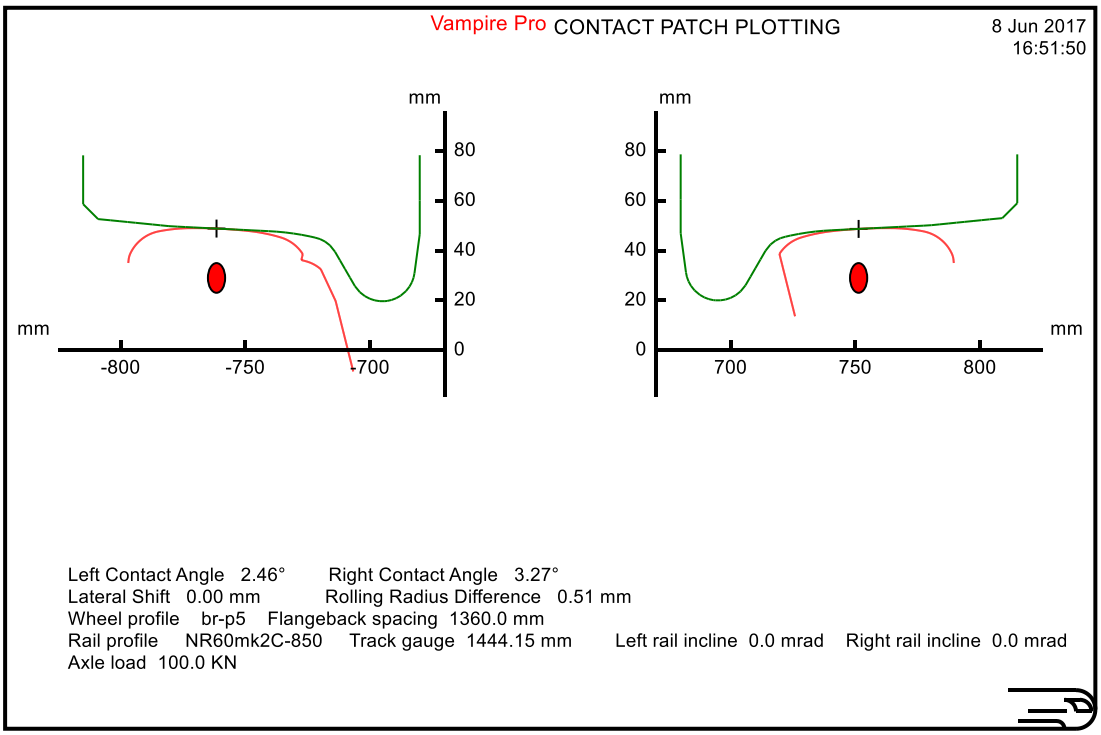

VAMPIRE Plot

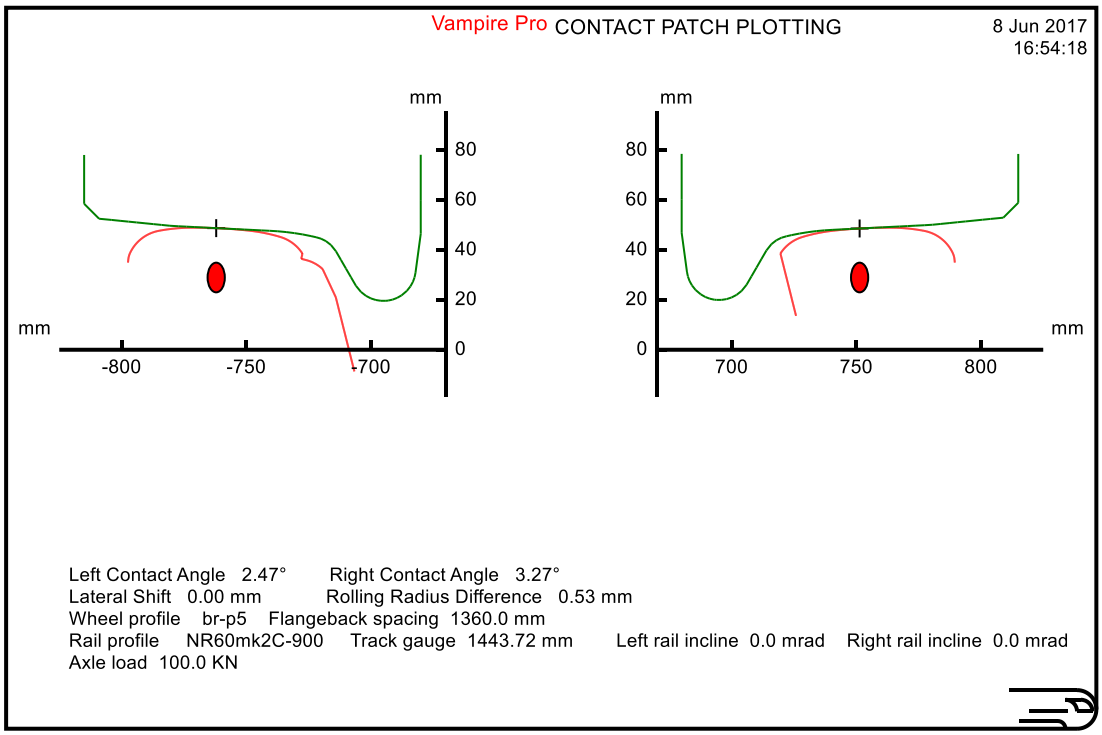

VAMPIRE Plot

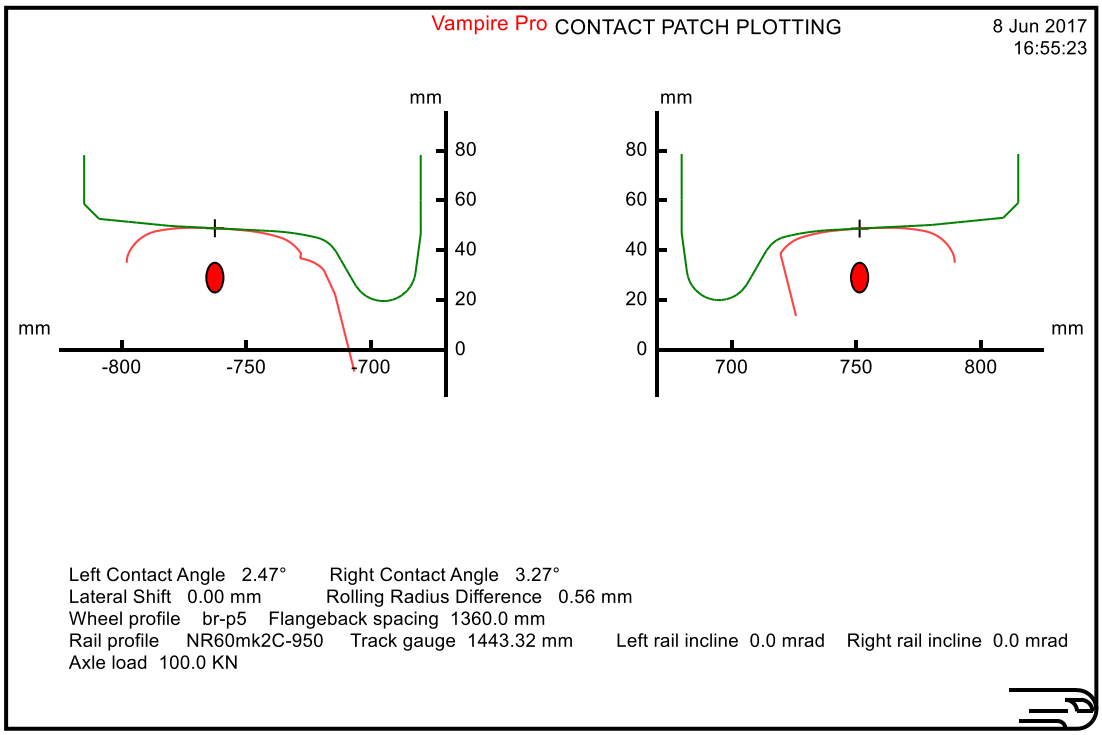

VAMPIRE Plot

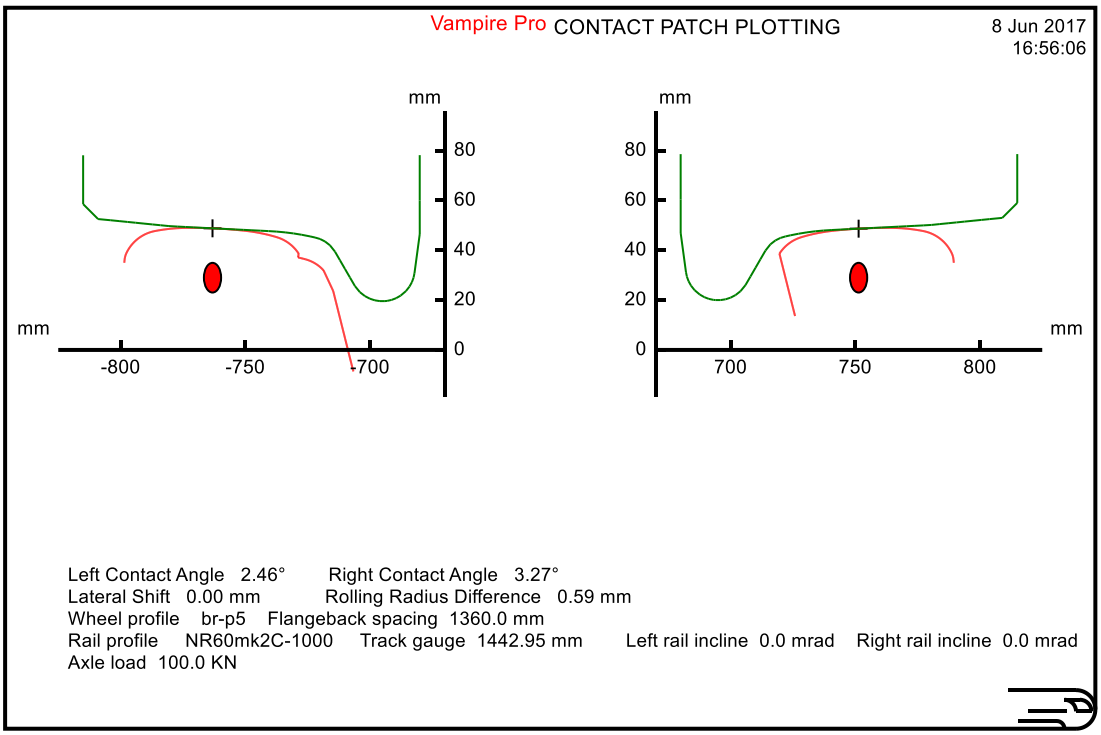

VAMPIRE Plot

P5

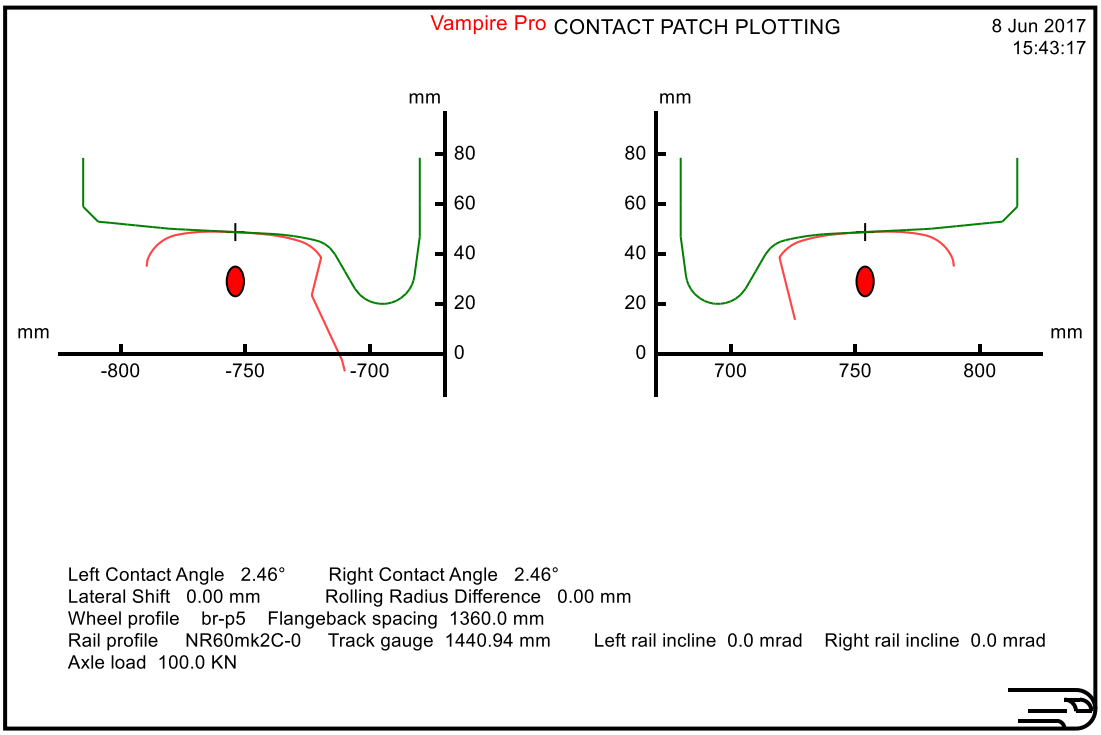

VAMPIRE Plot

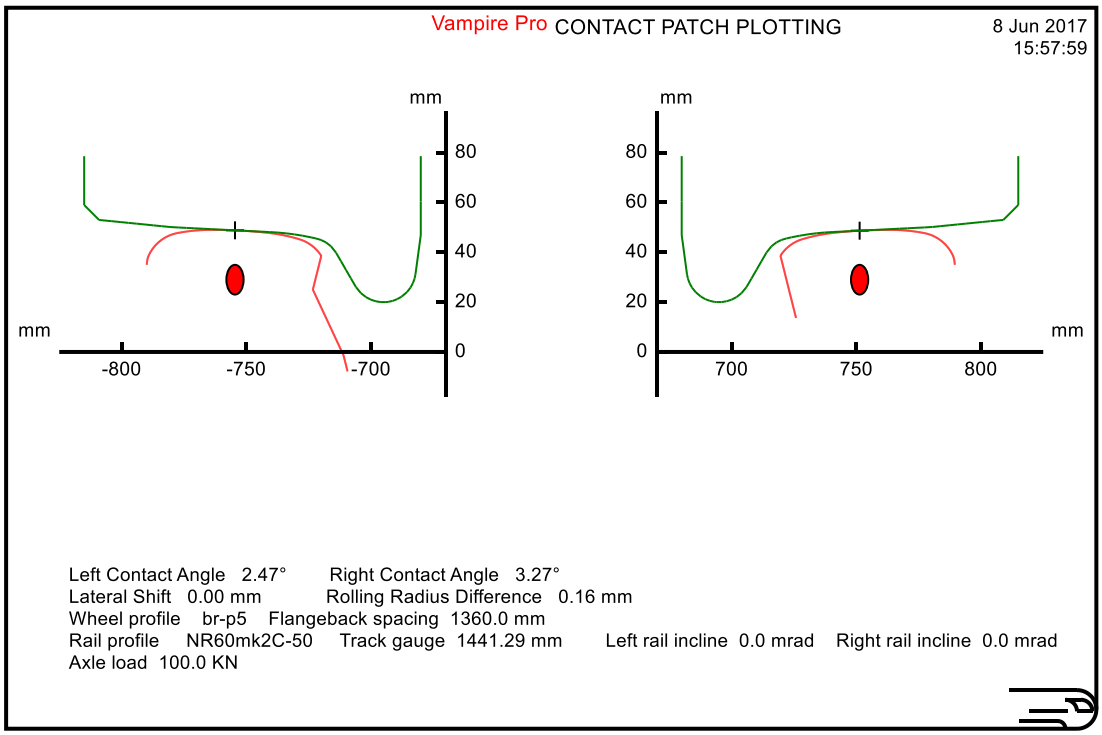

VAMPIRE Plot

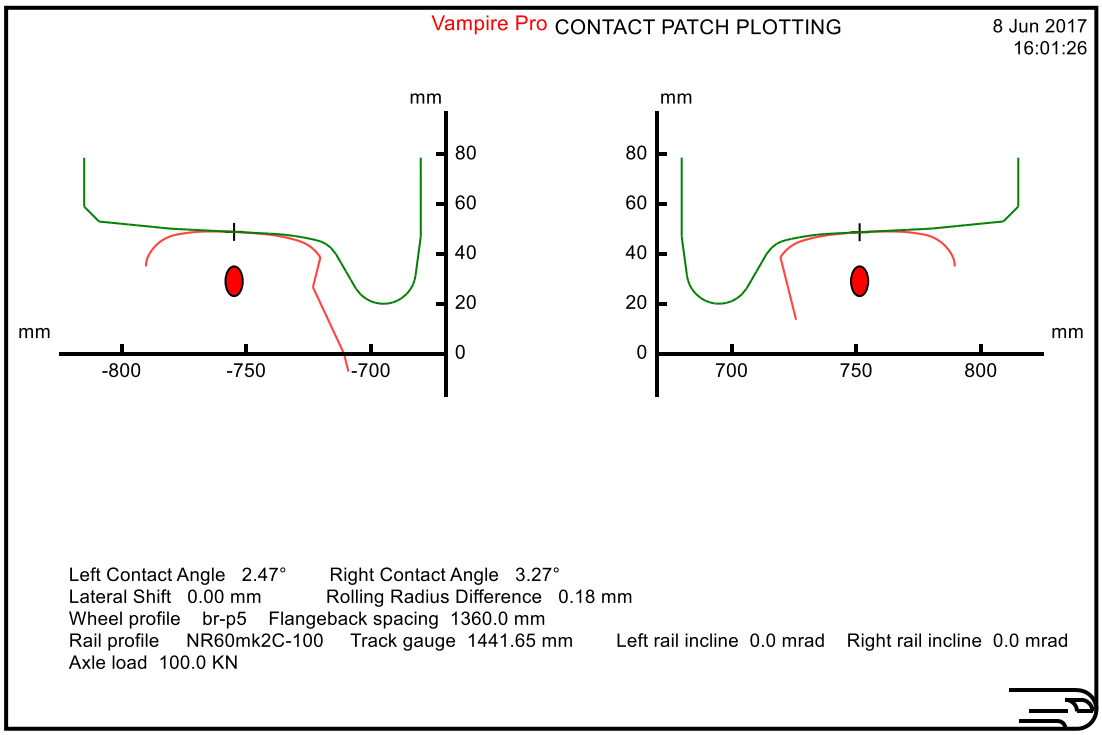

VAMPIRE Plot

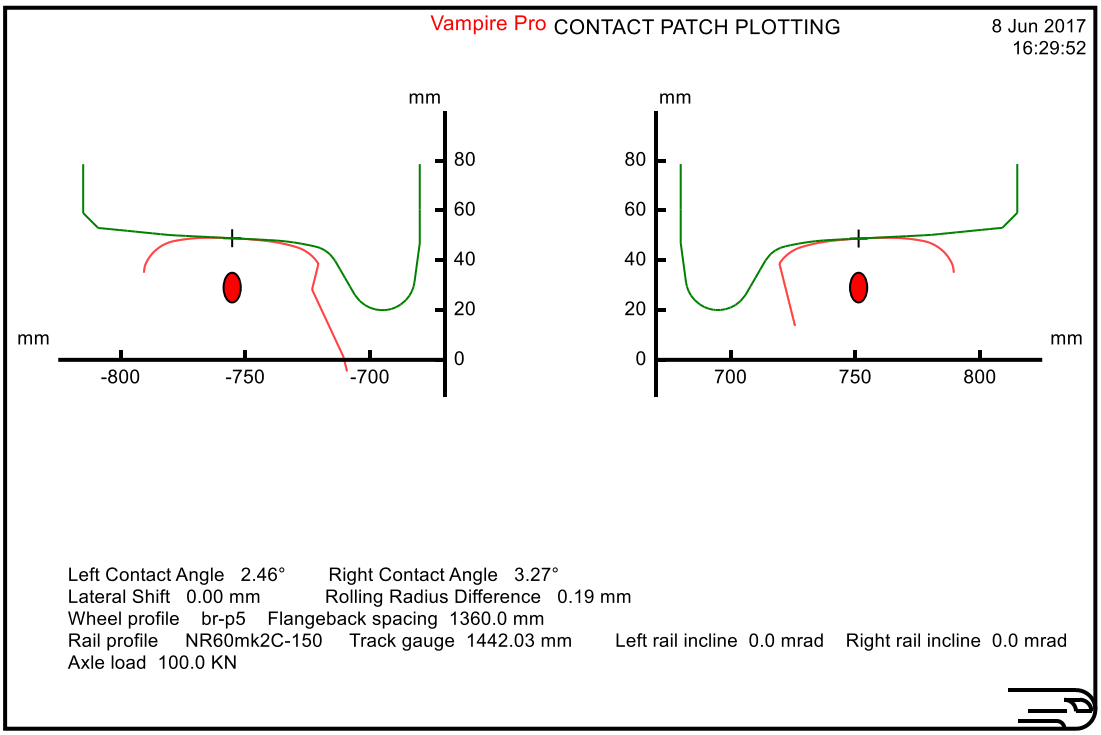

VAMPIRE Plot

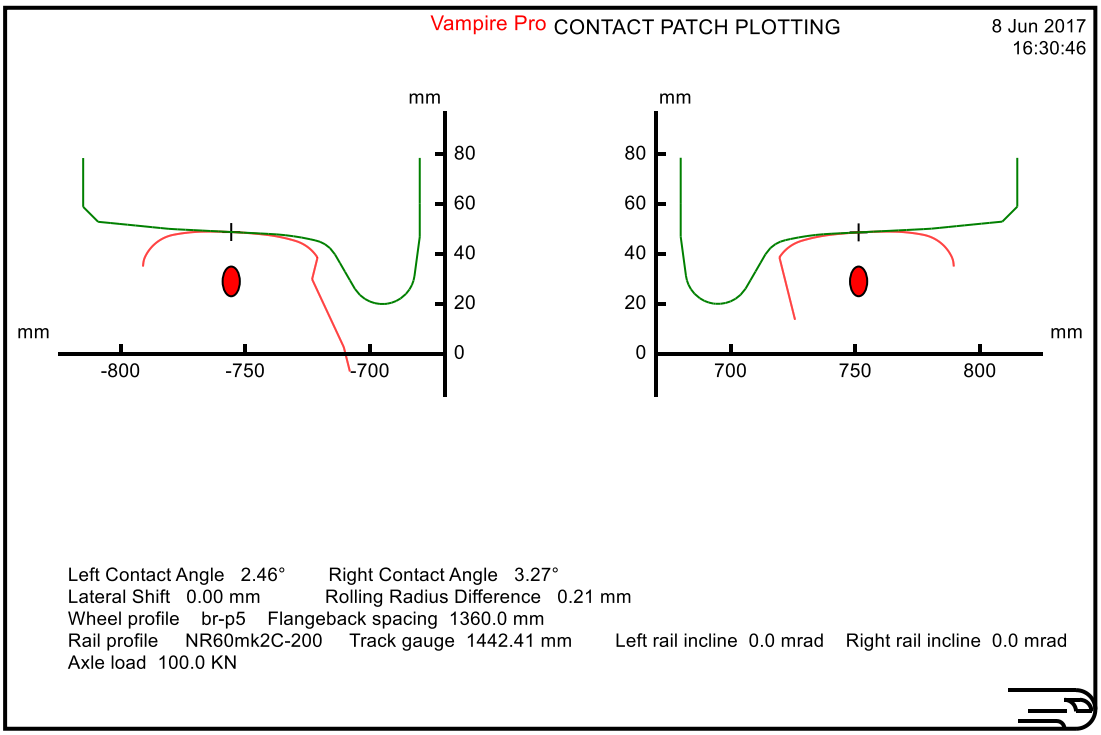

VAMPIRE Plot

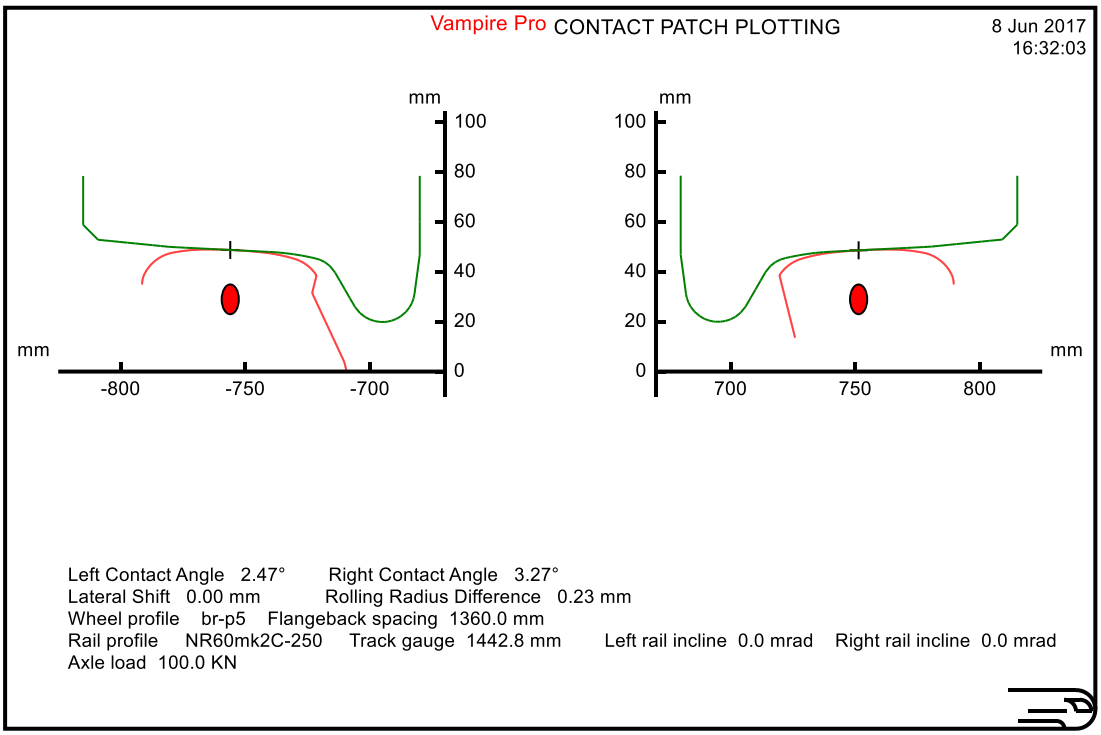

VAMPIRE Plot

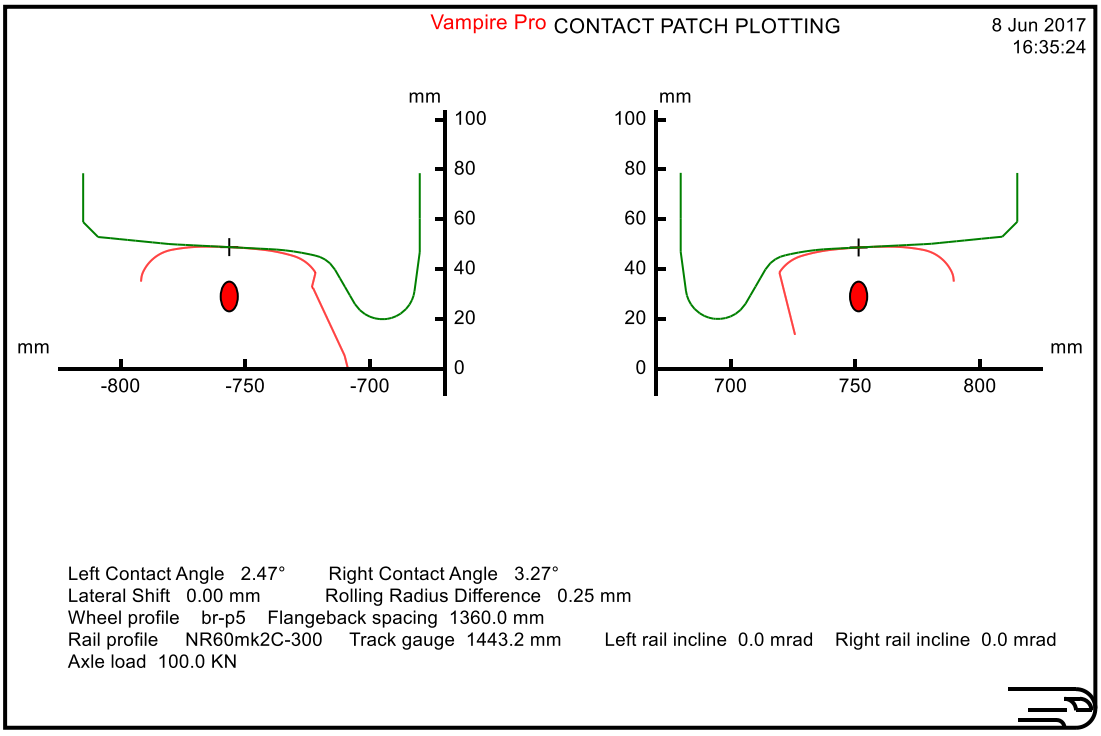

VAMPIRE Plot

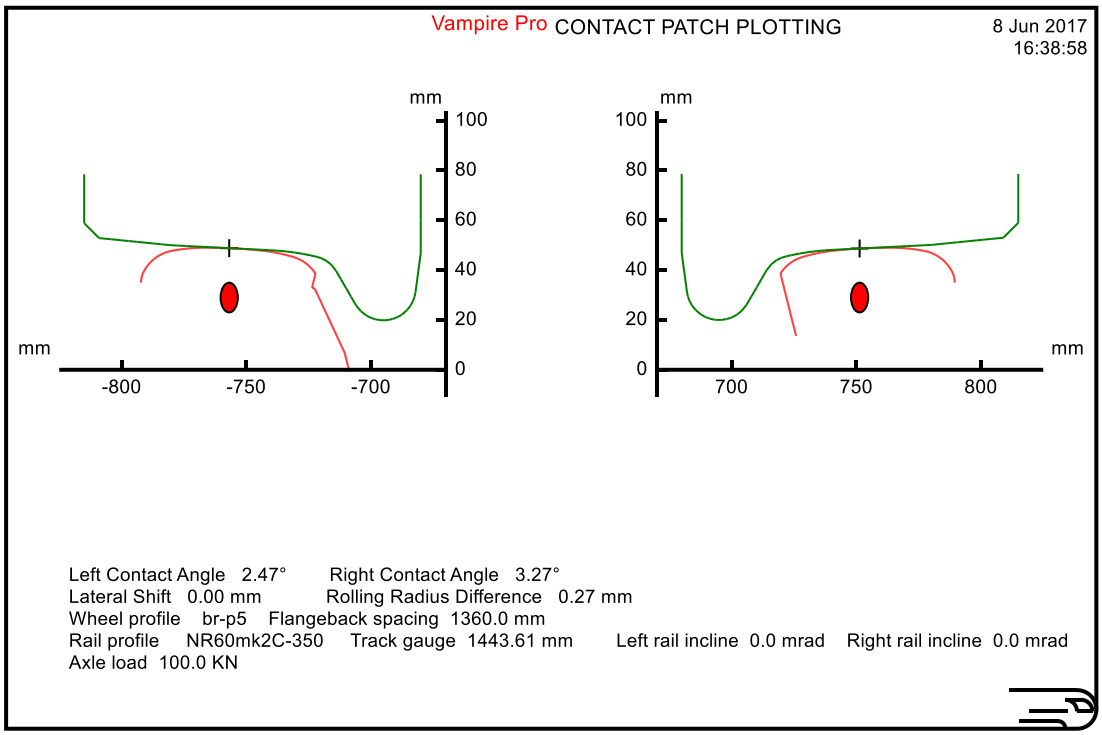

VAMPIRE Plot

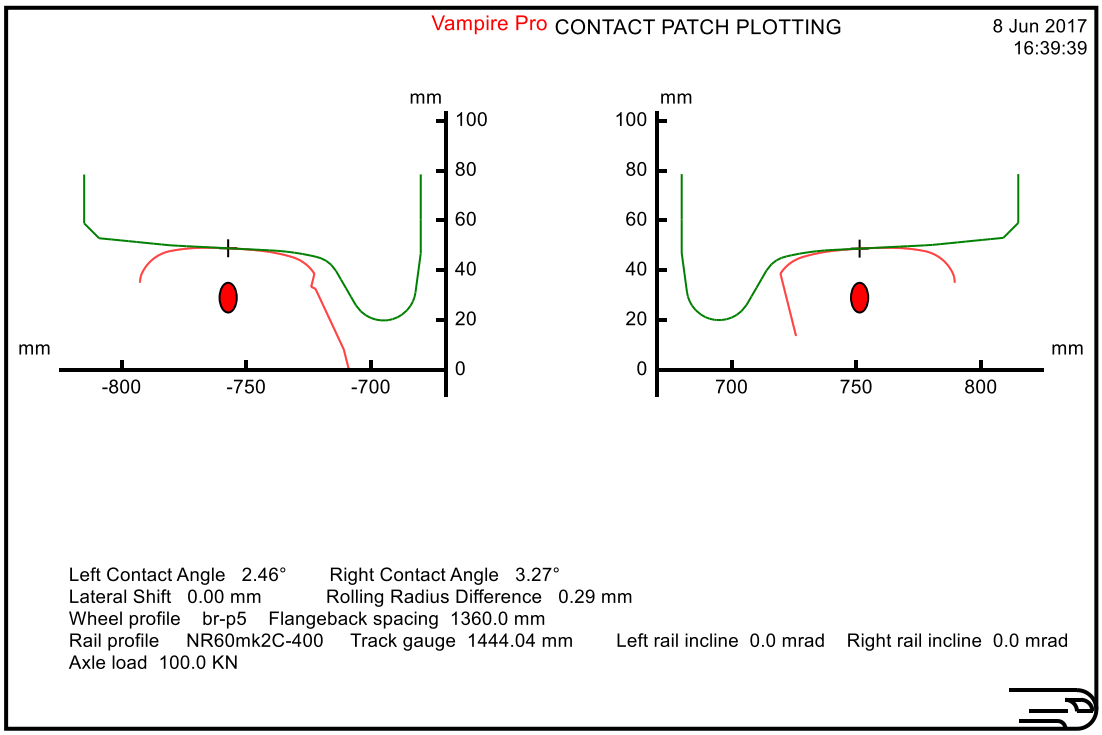

VAMPIRE Plot

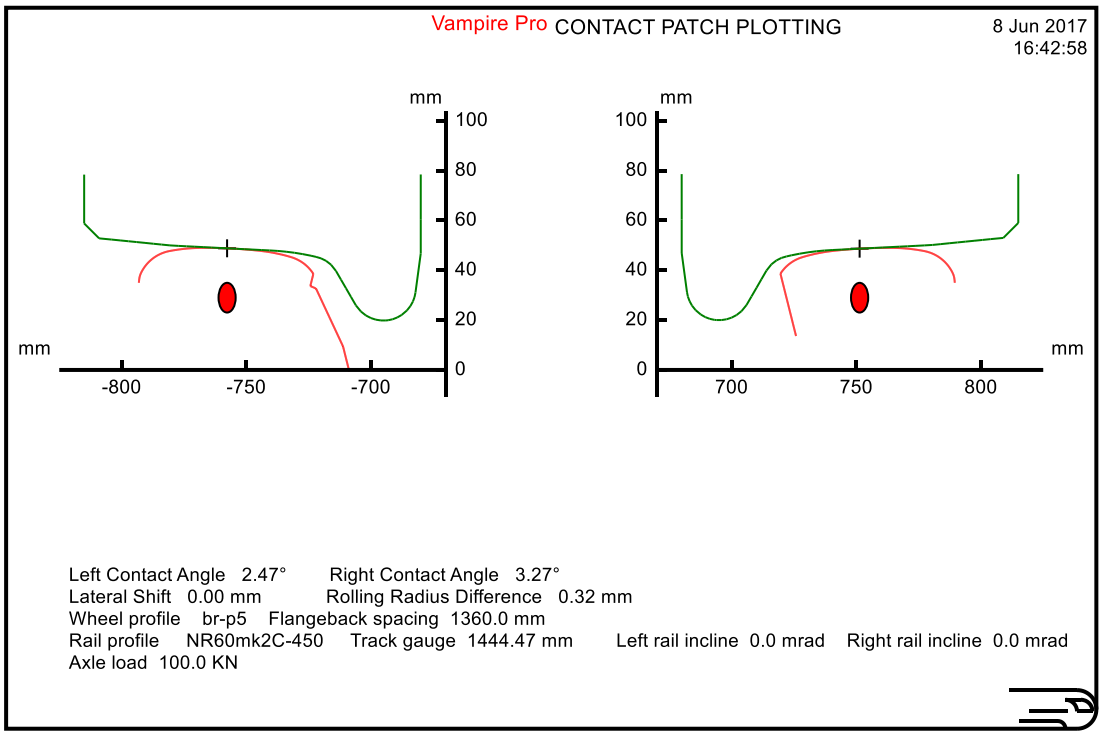

VAMPIRE Plot

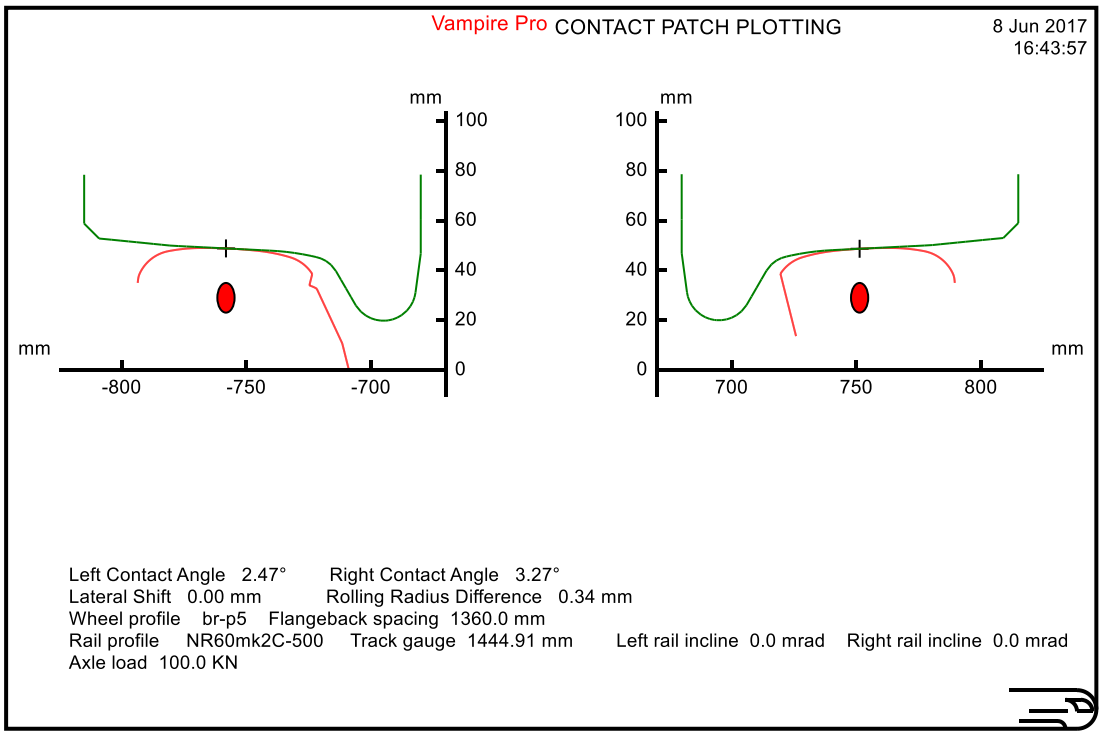

VAMPIRE Plot

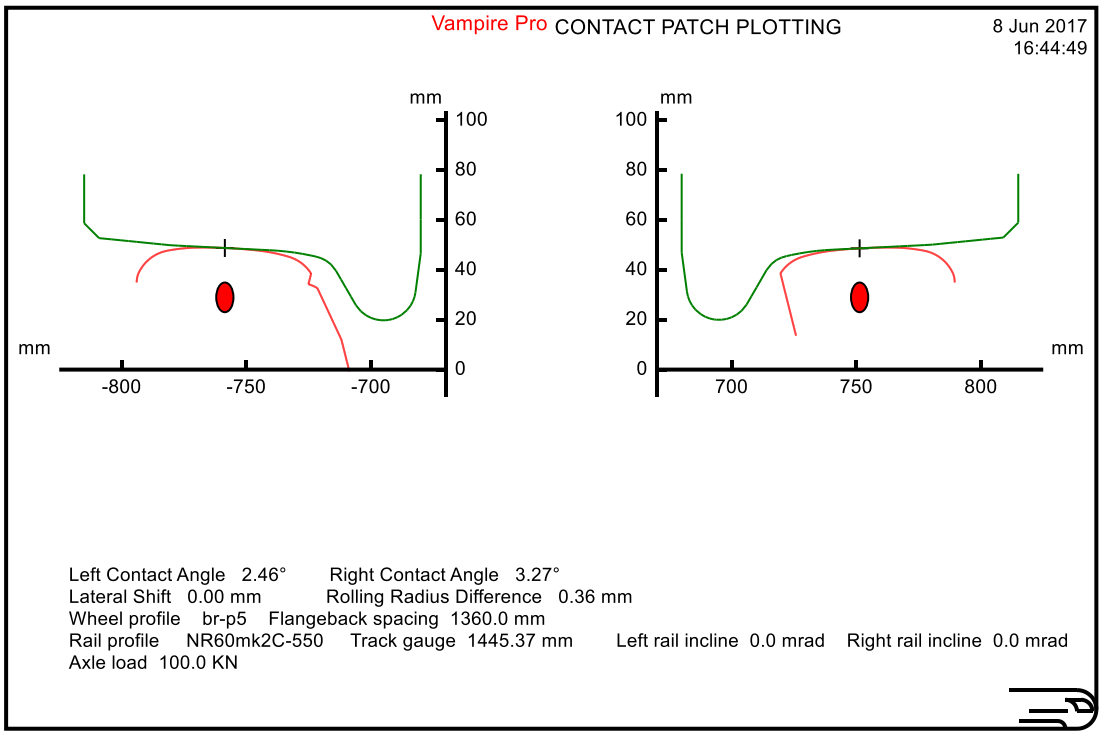

VAMPIRE Plot

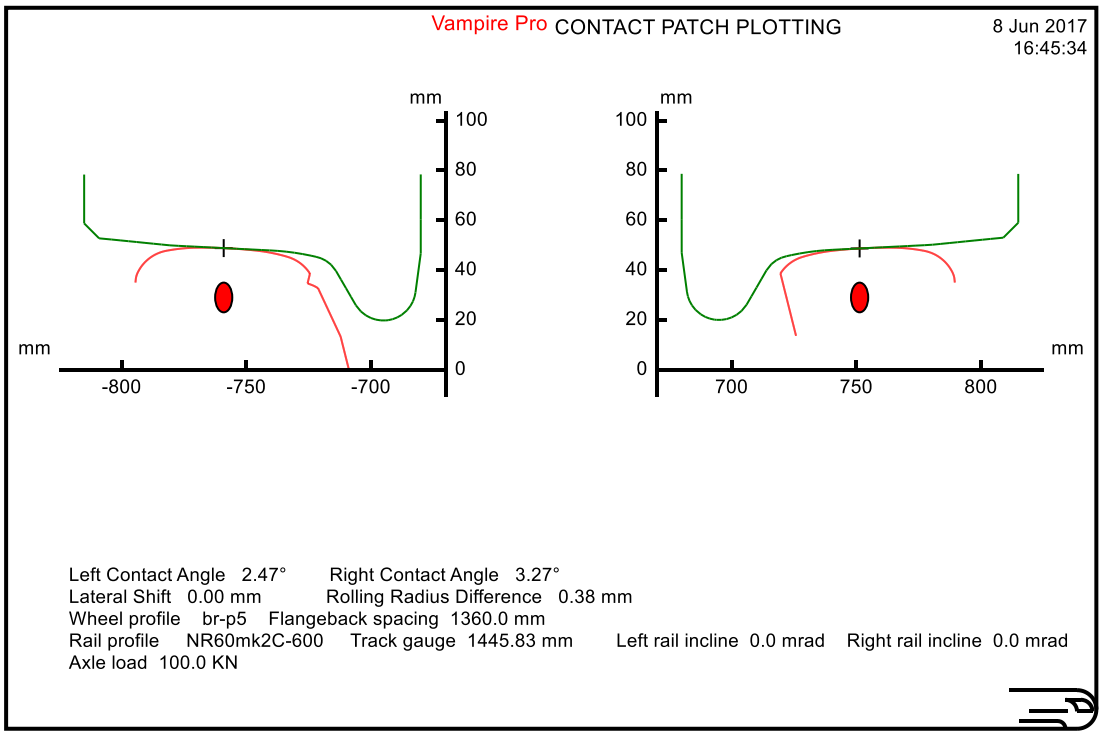

VAMPIRE Plot

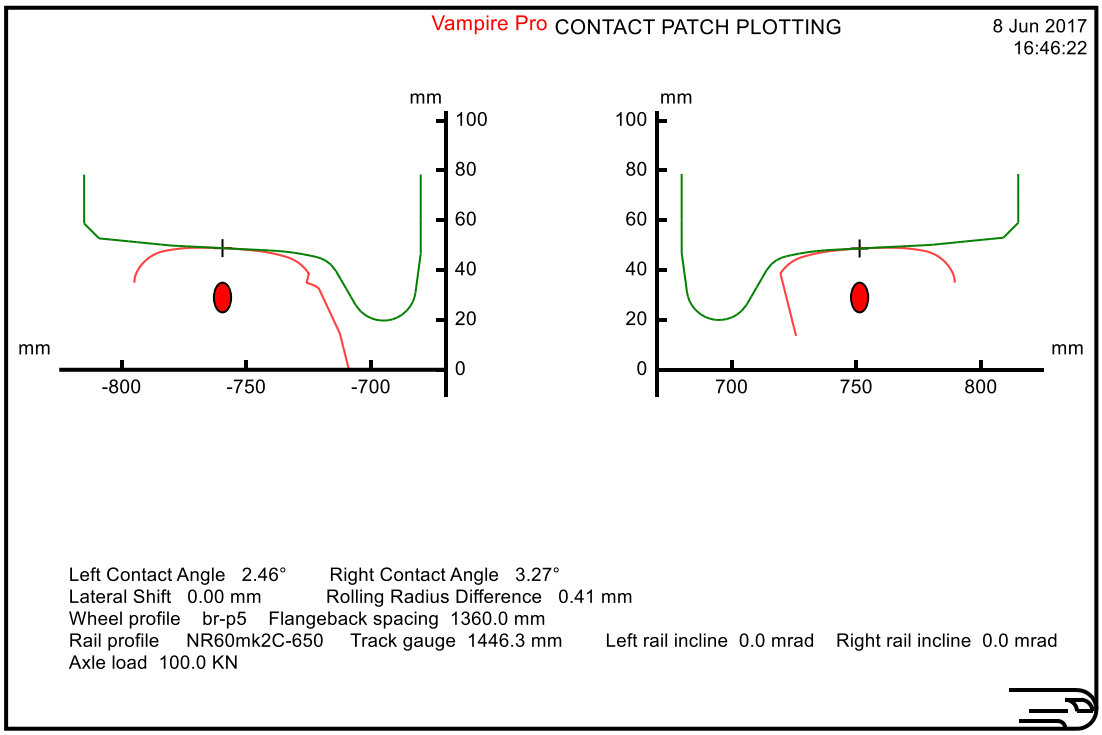

VAMPIRE Plot

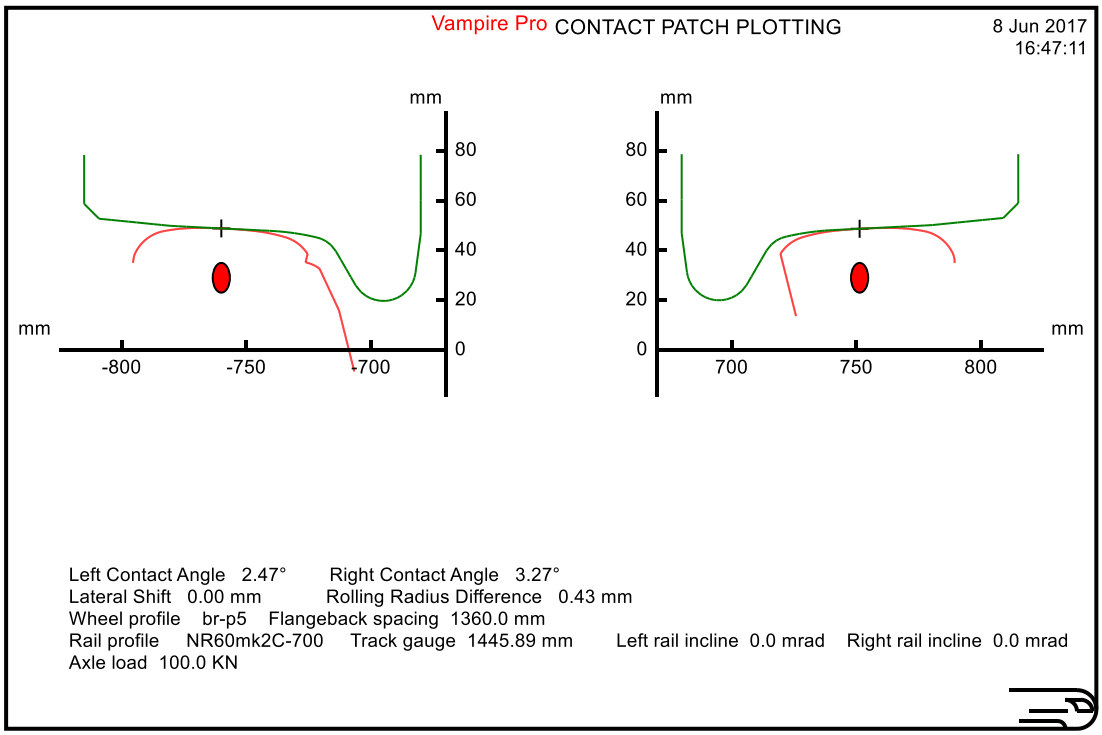

VAMPIRE Plot

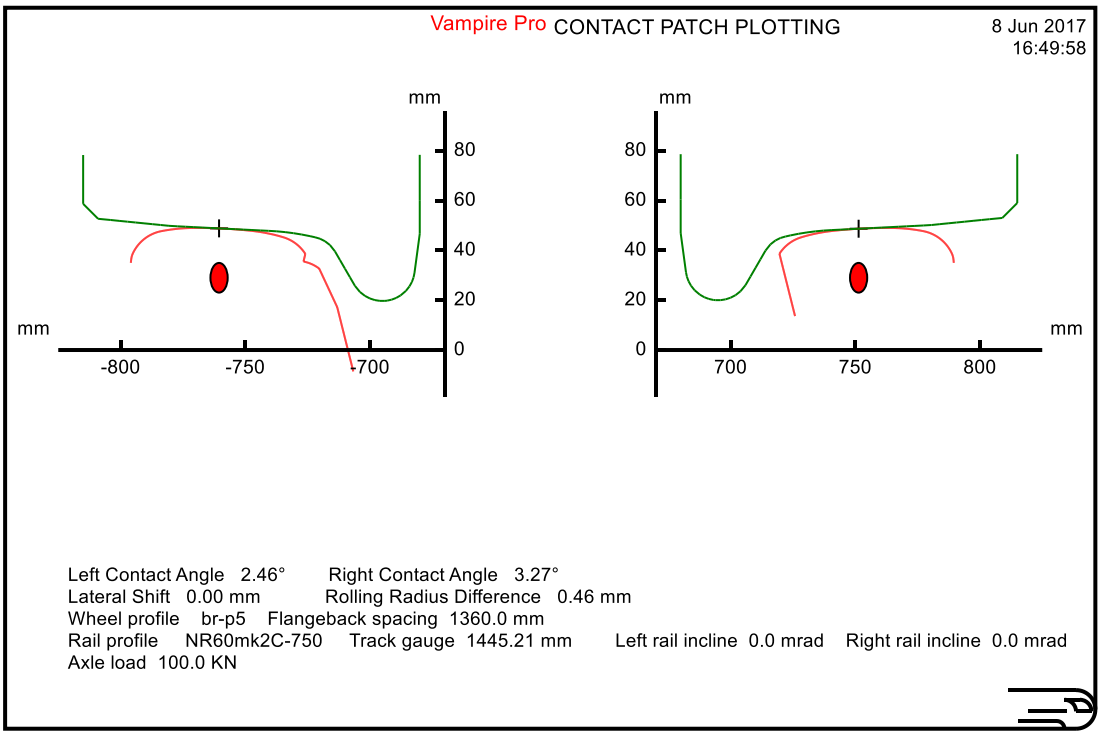

VAMPIRE Plot

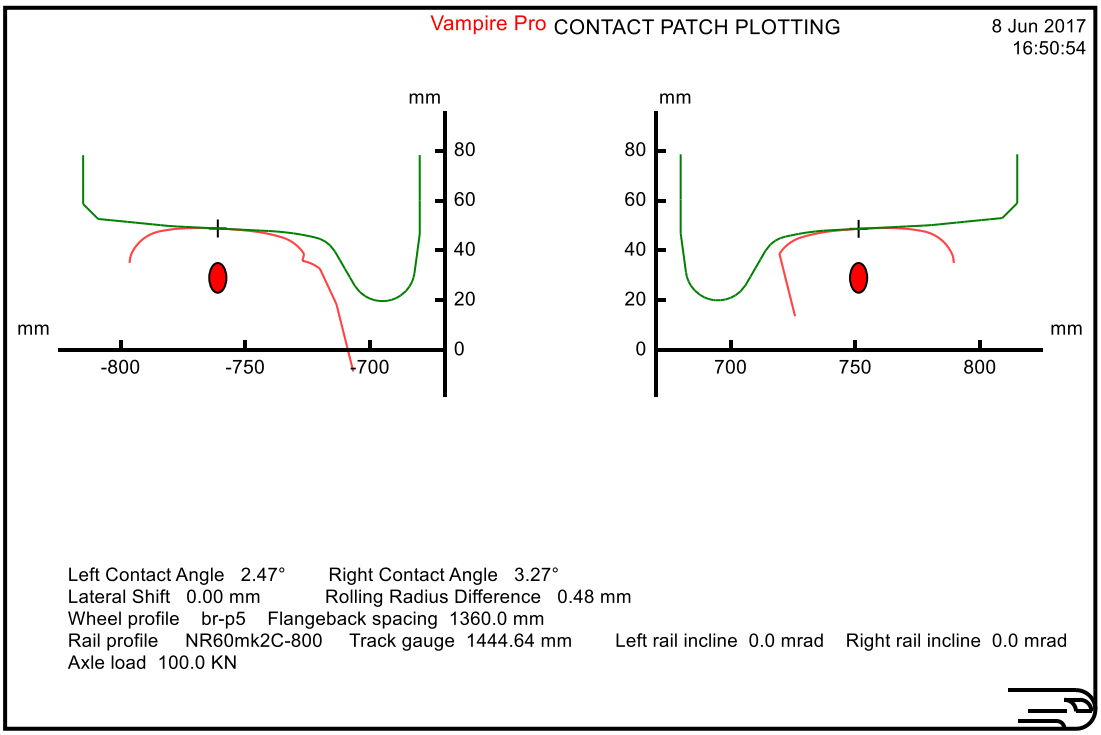

VAMPIRE Plot

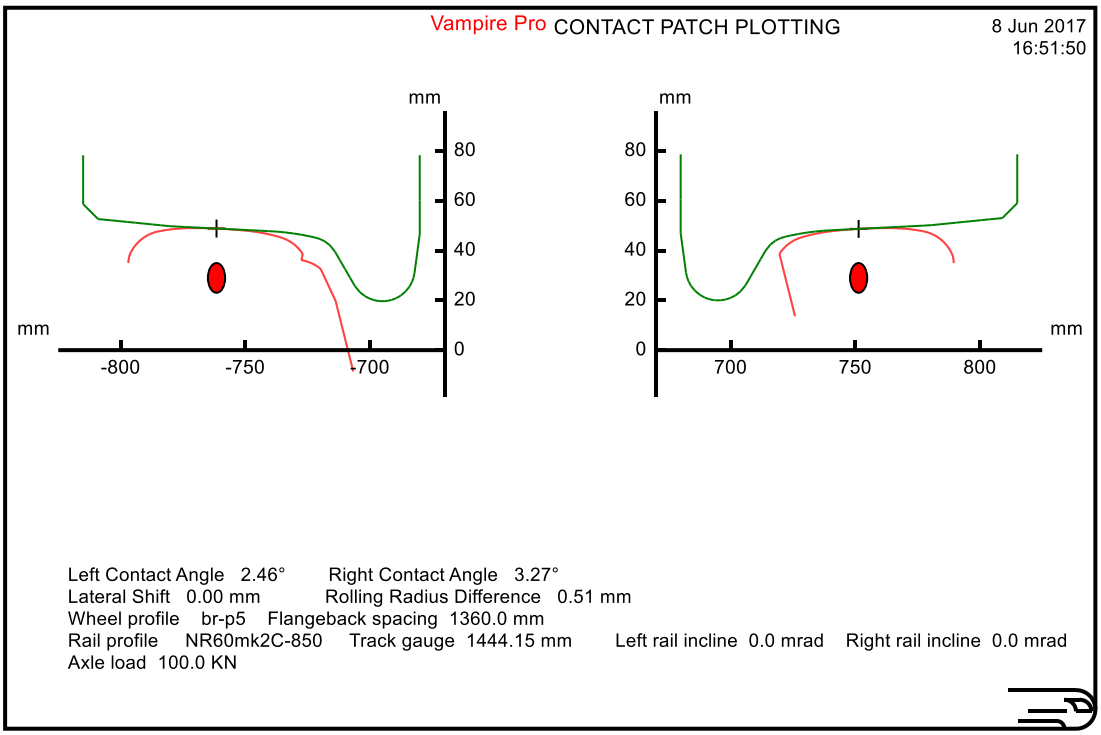

VAMPIRE Plot

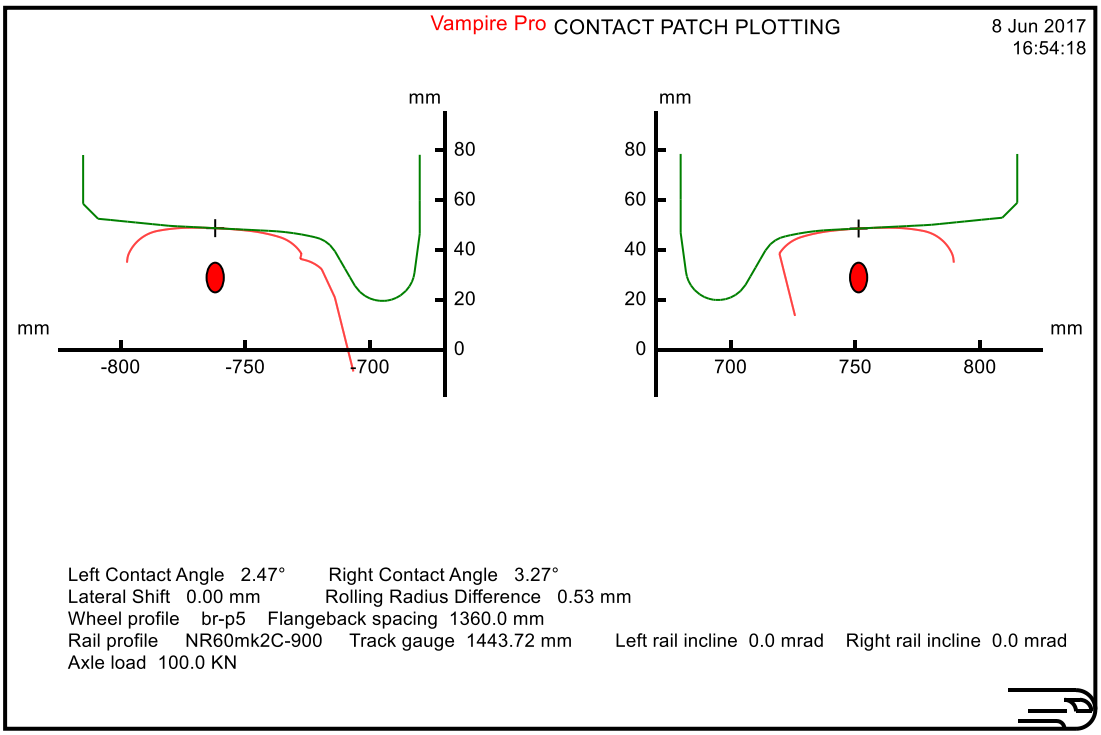

VAMPIRE Plot

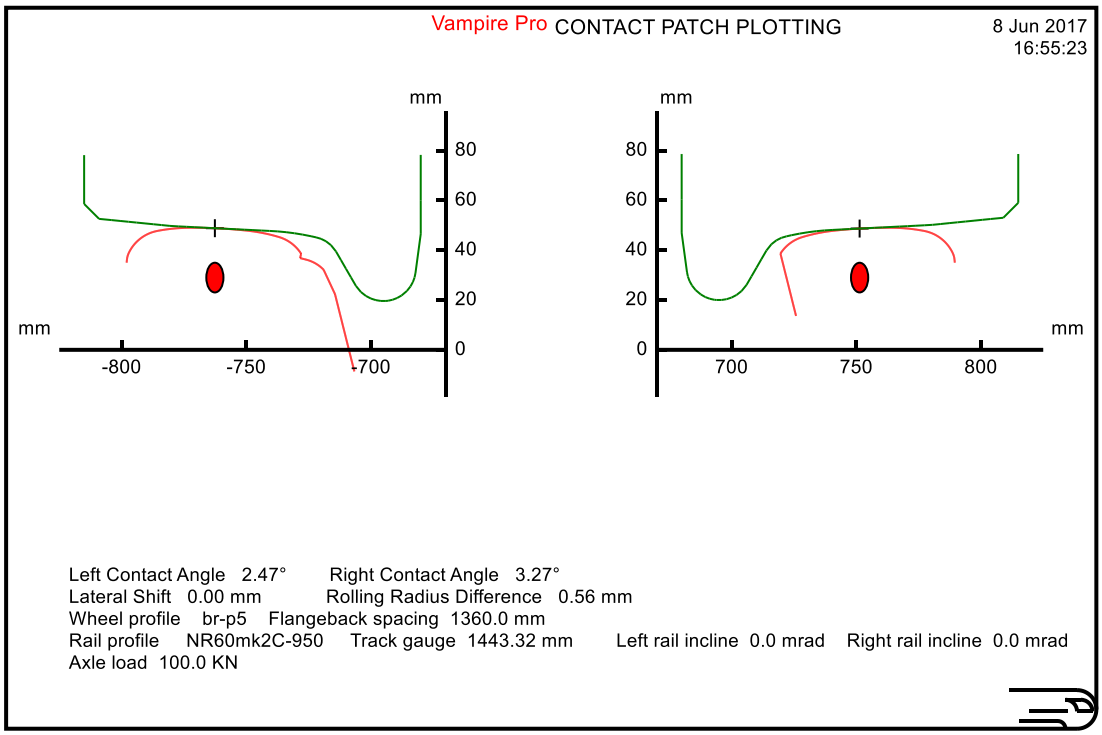

VAMPIRE Plot

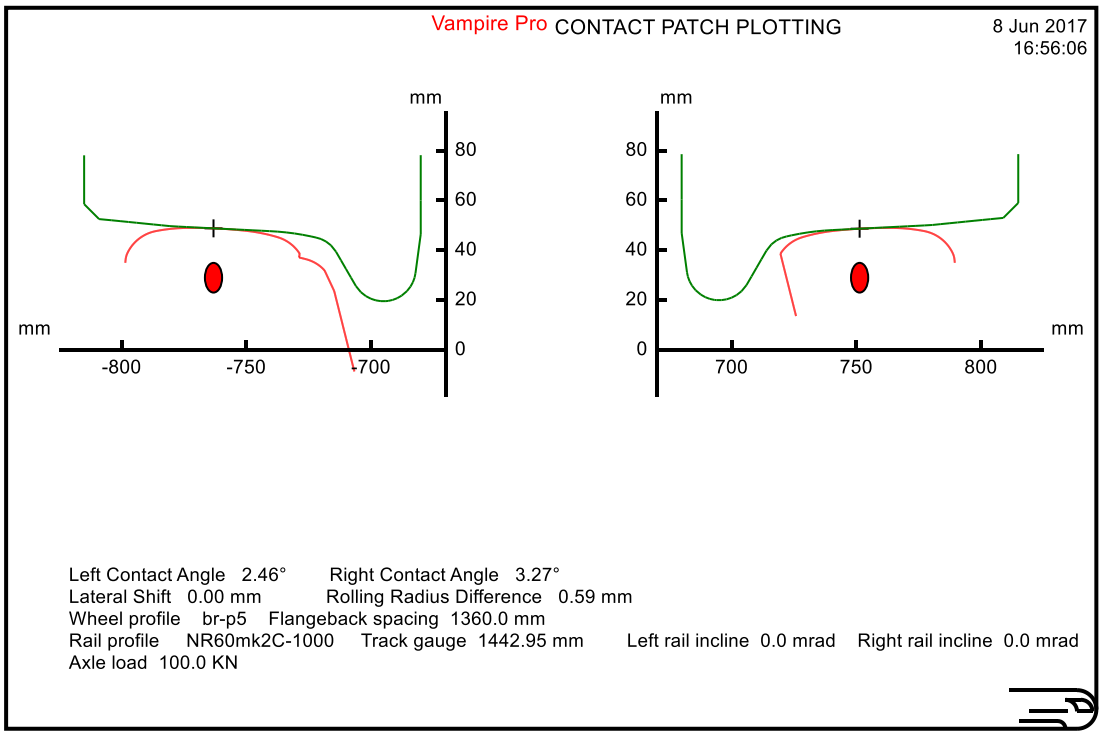

VAMPIRE Plot

P5

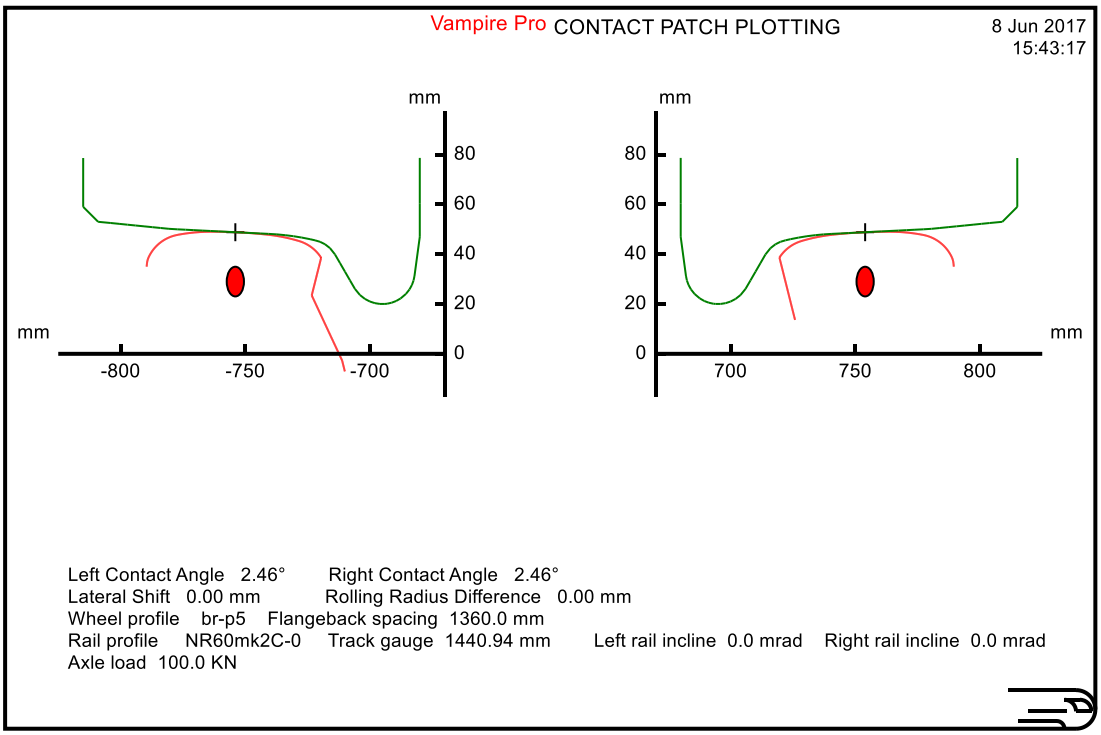

VAMPIRE Plot

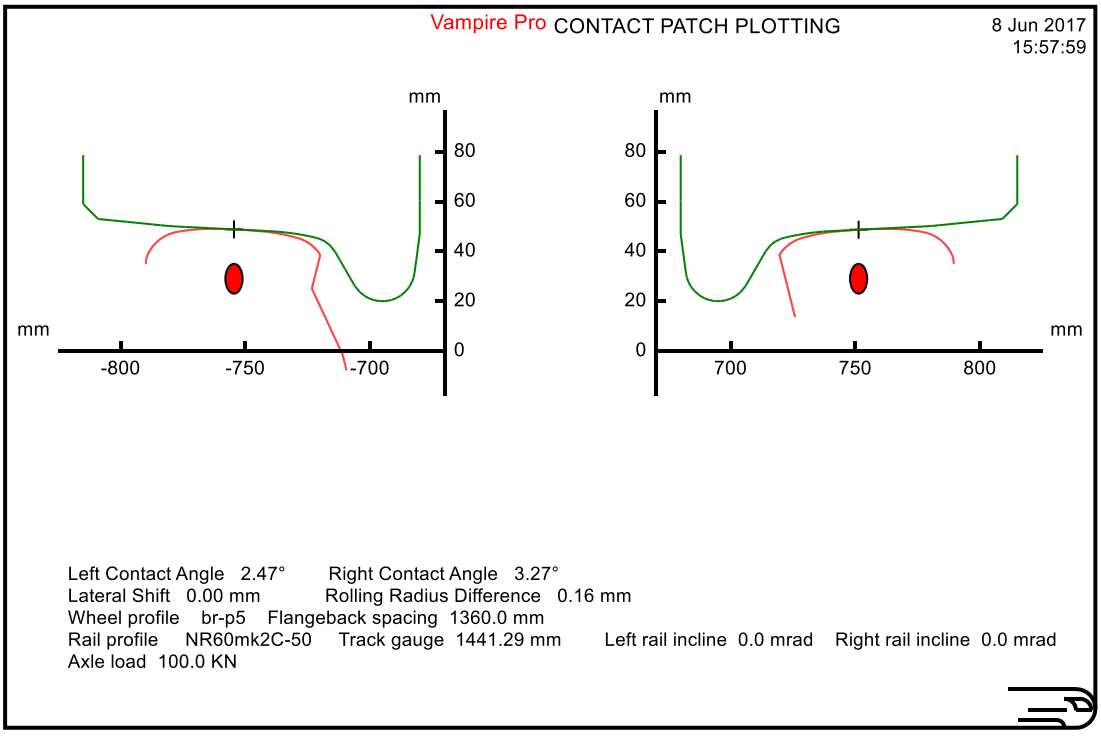

VAMPIRE Plot

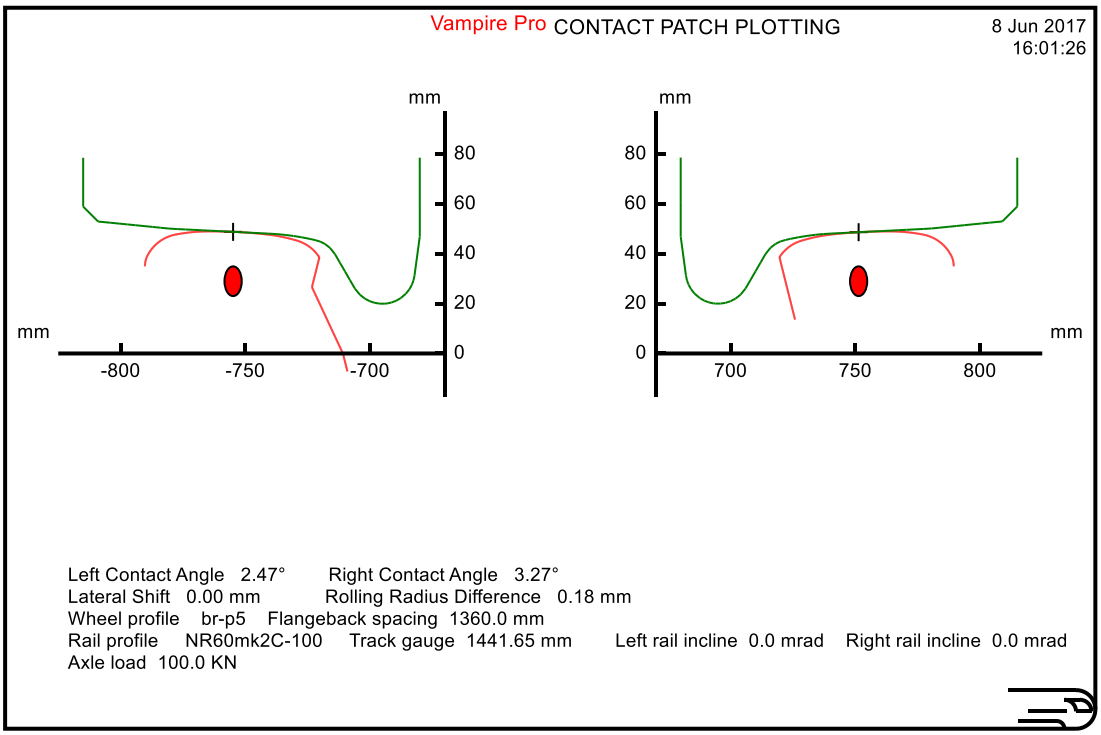

VAMPIRE Plot

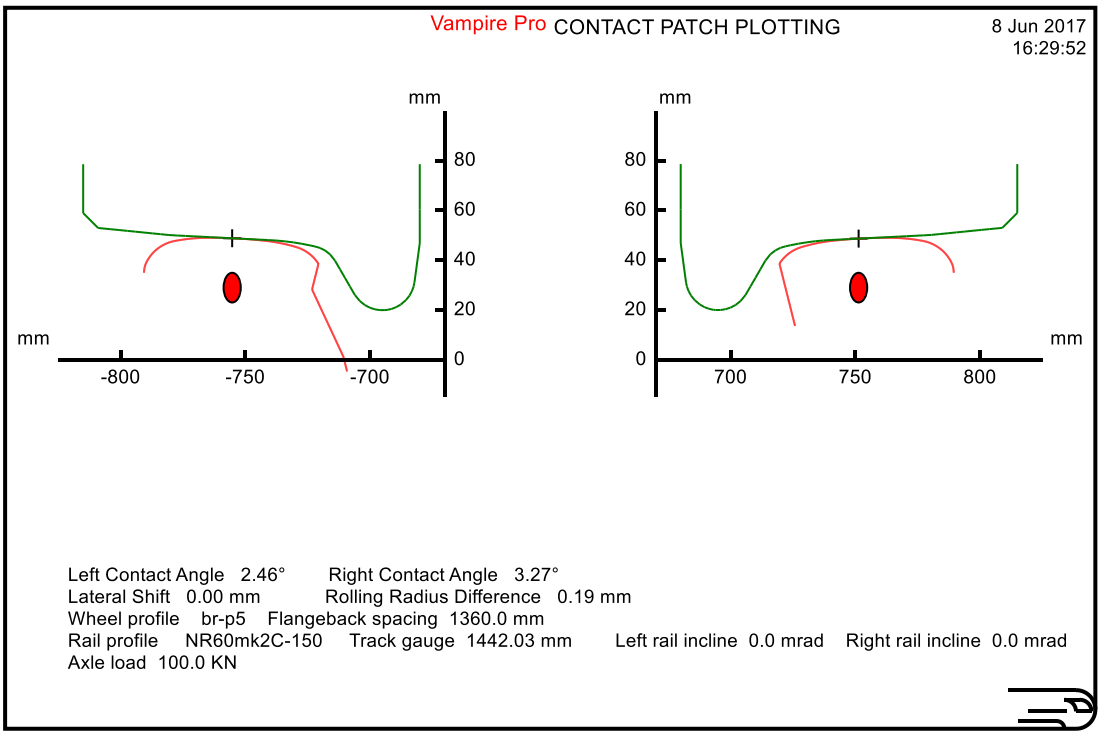

VAMPIRE Plot

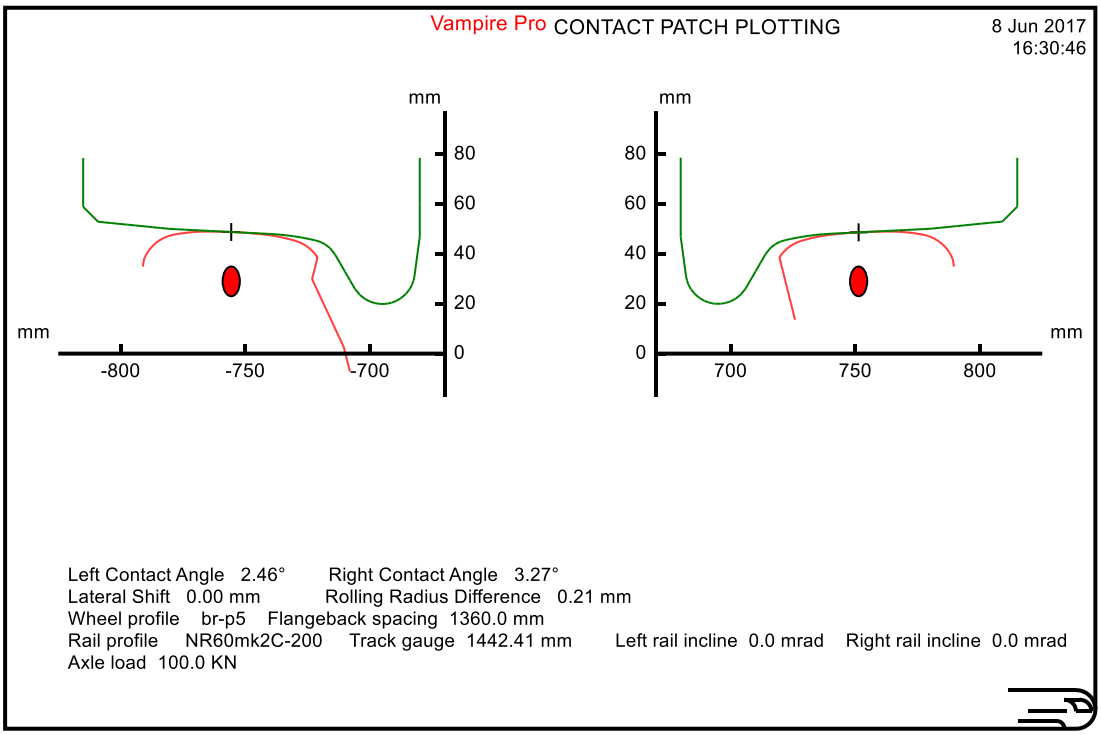

VAMPIRE Plot

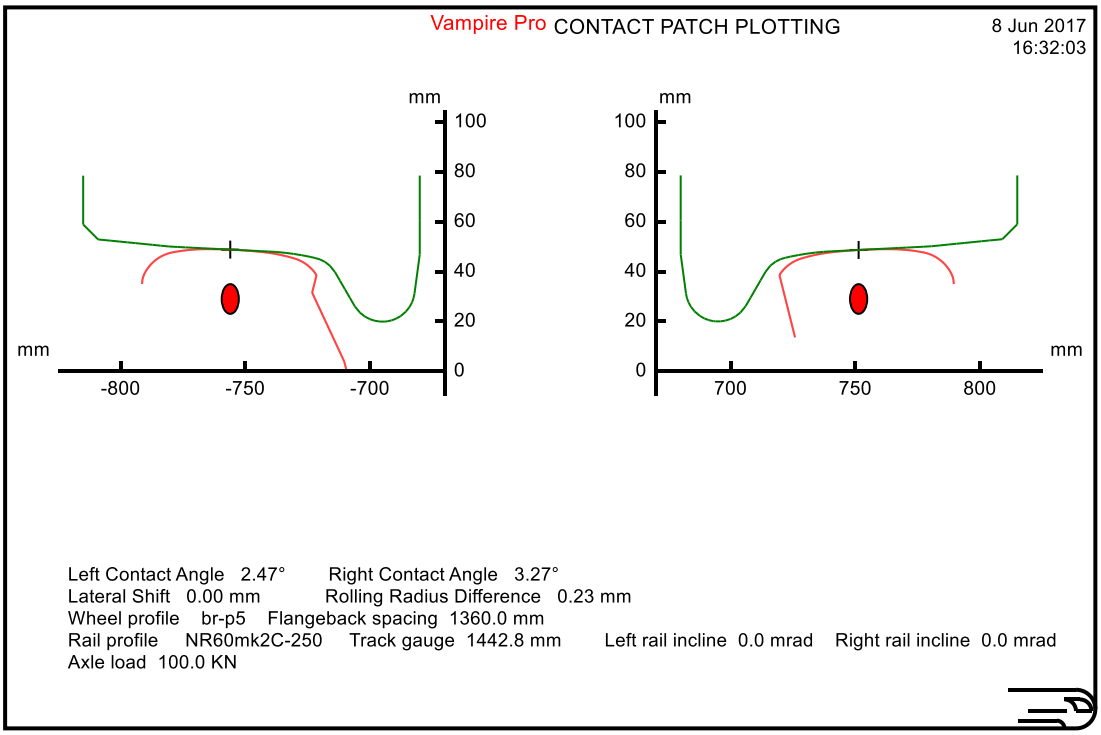

VAMPIRE Plot

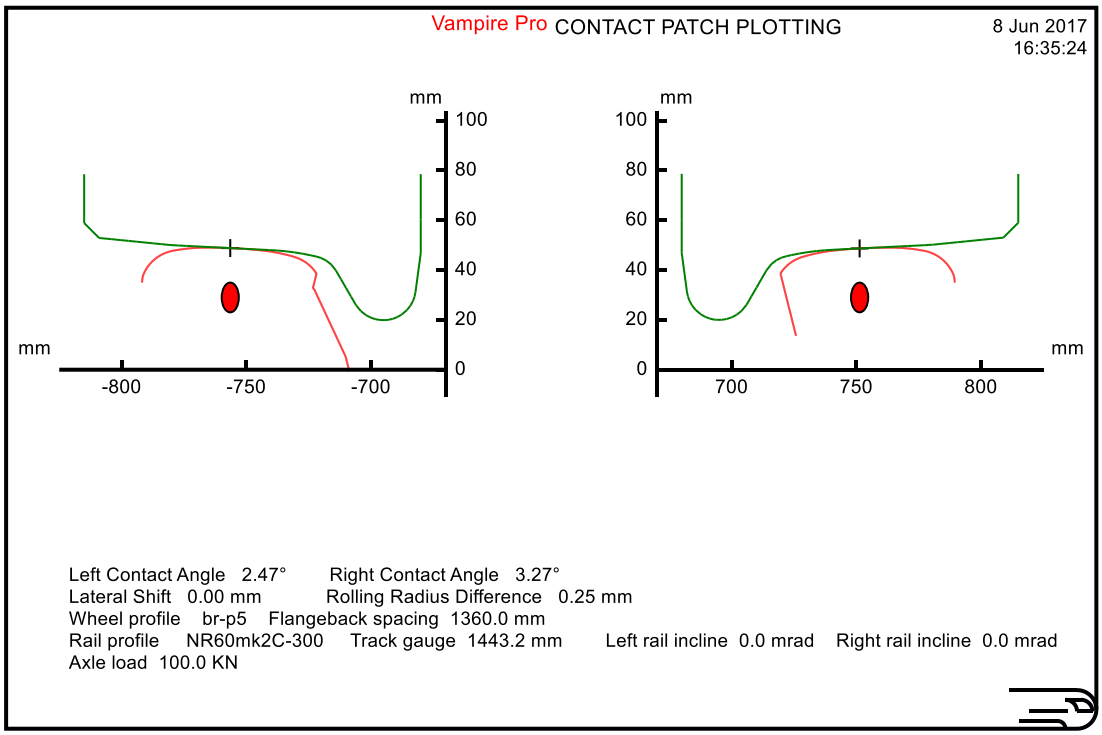

VAMPIRE Plot

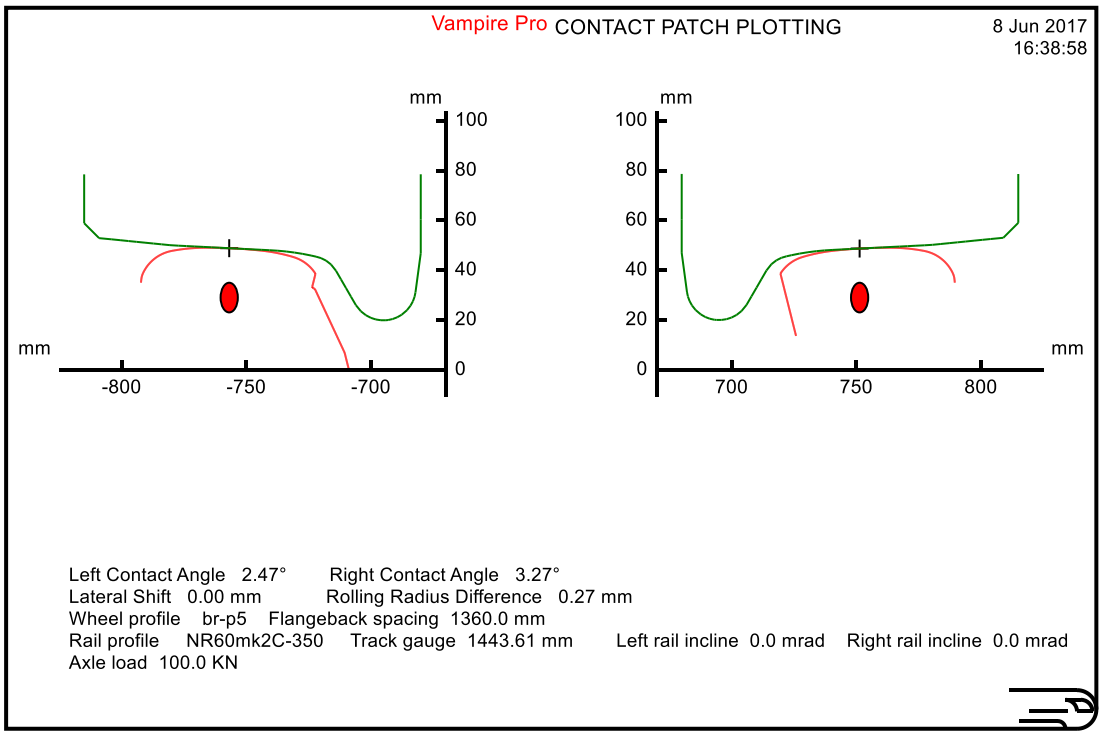

VAMPIRE Plot

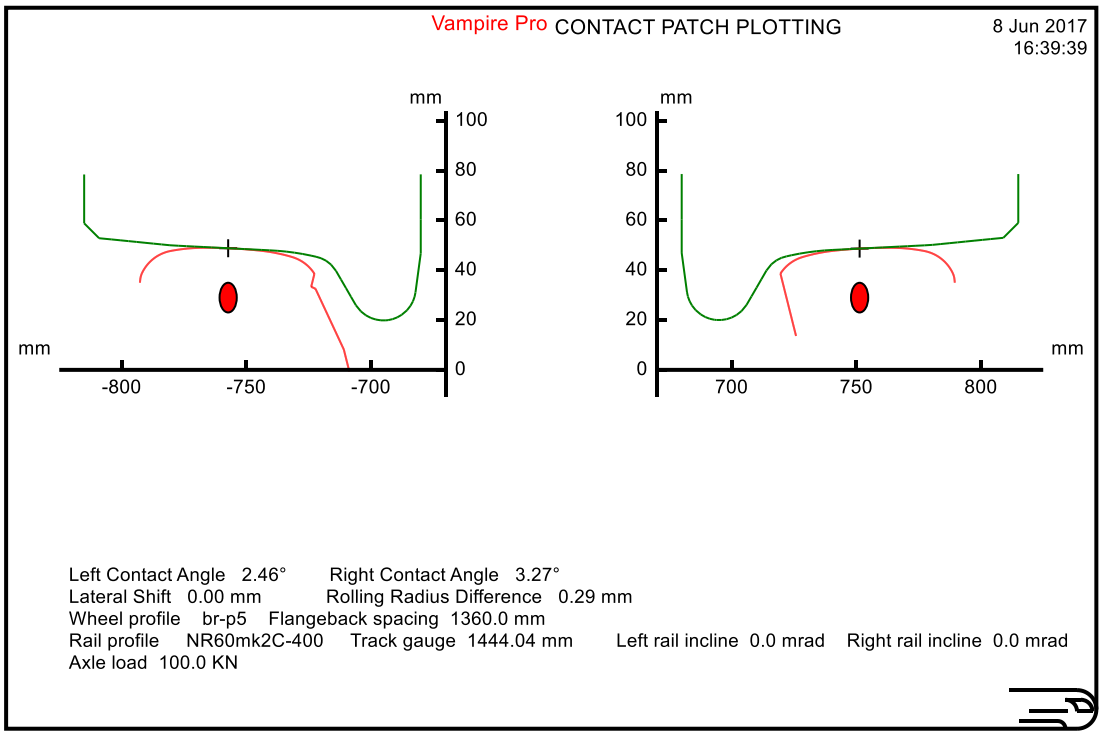

VAMPIRE Plot

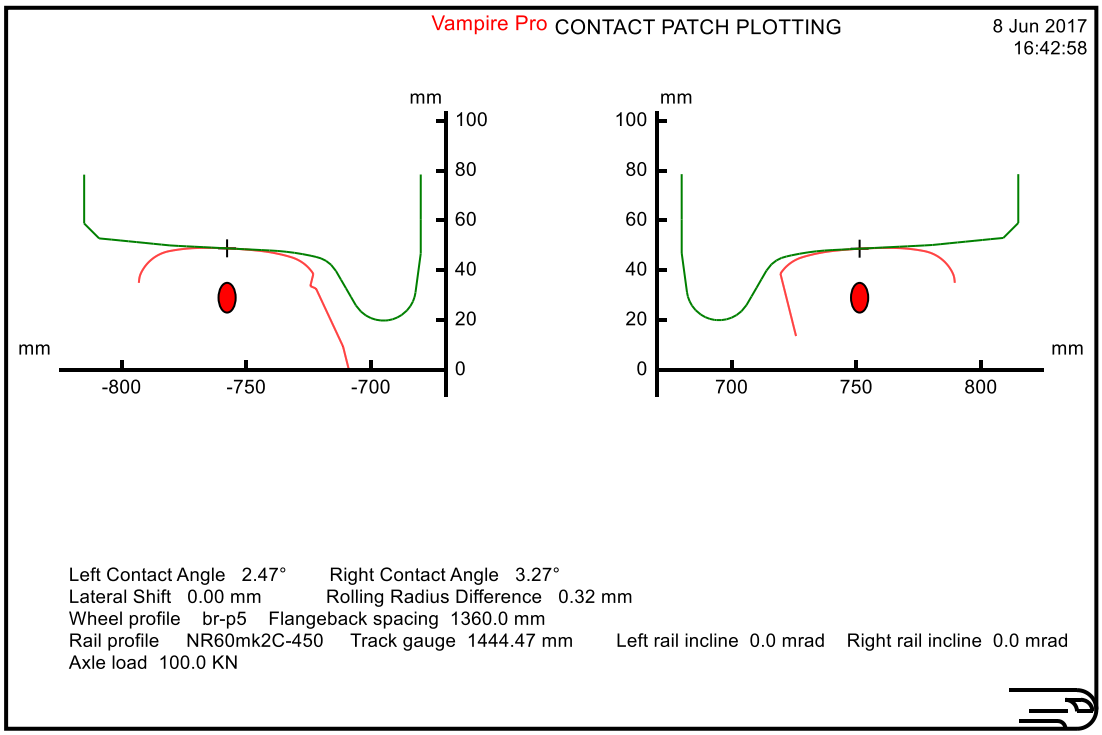

VAMPIRE Plot

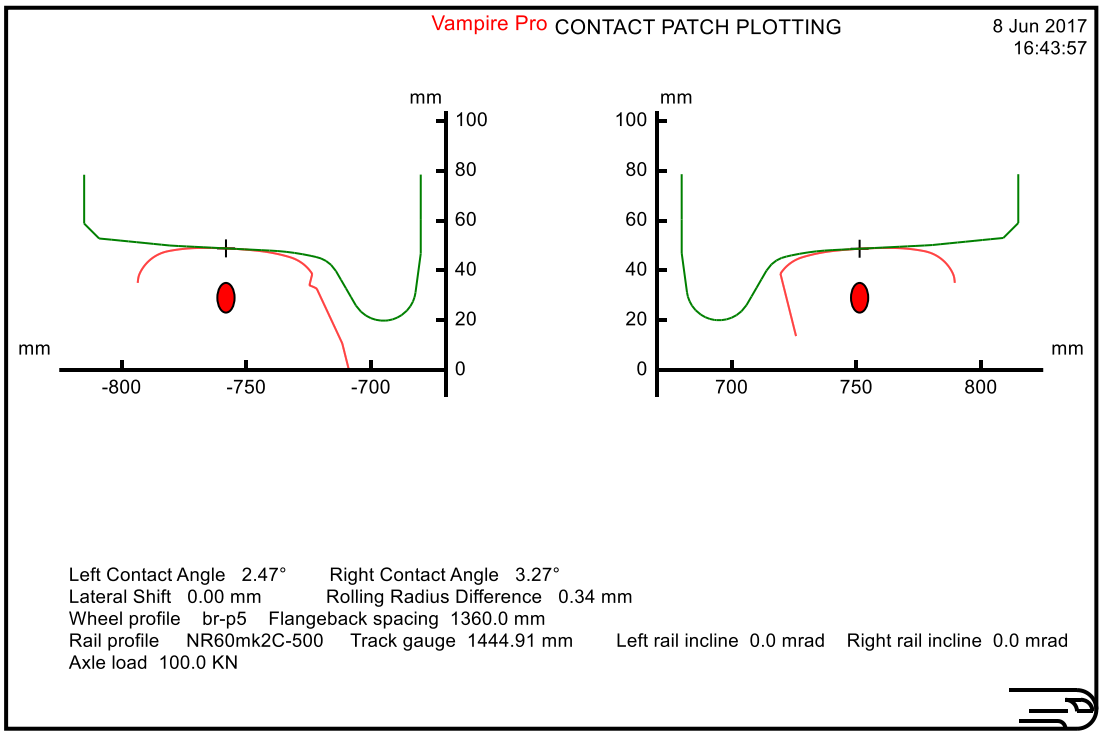

VAMPIRE Plot

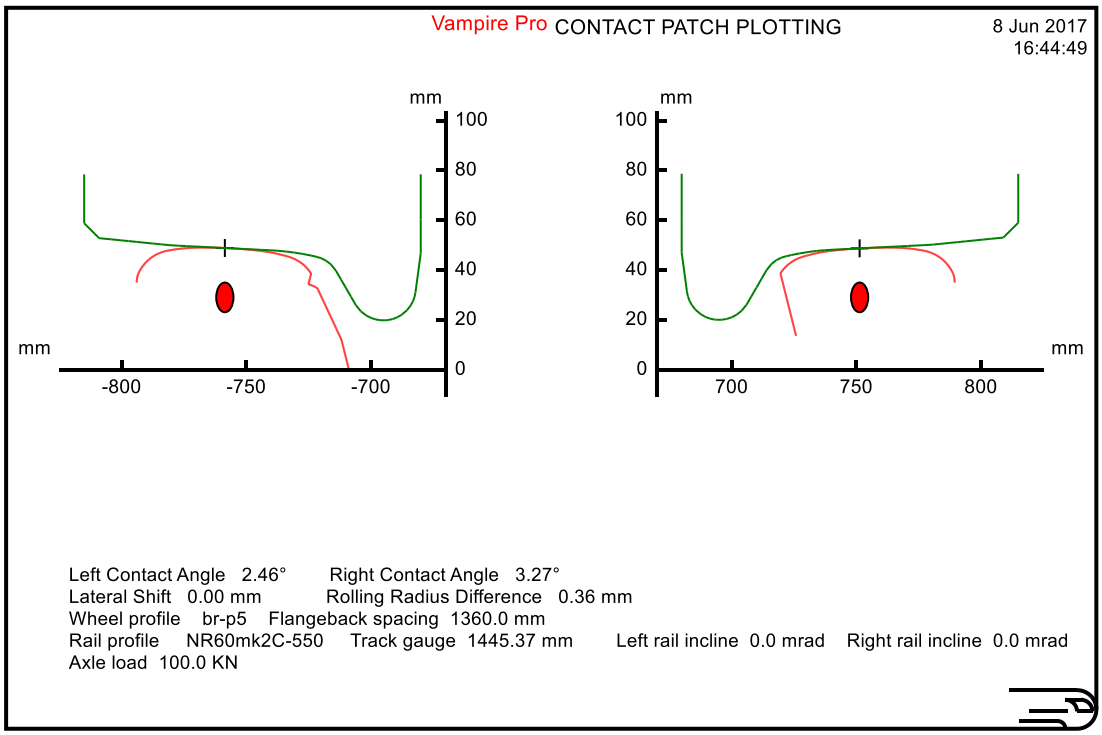

VAMPIRE Plot

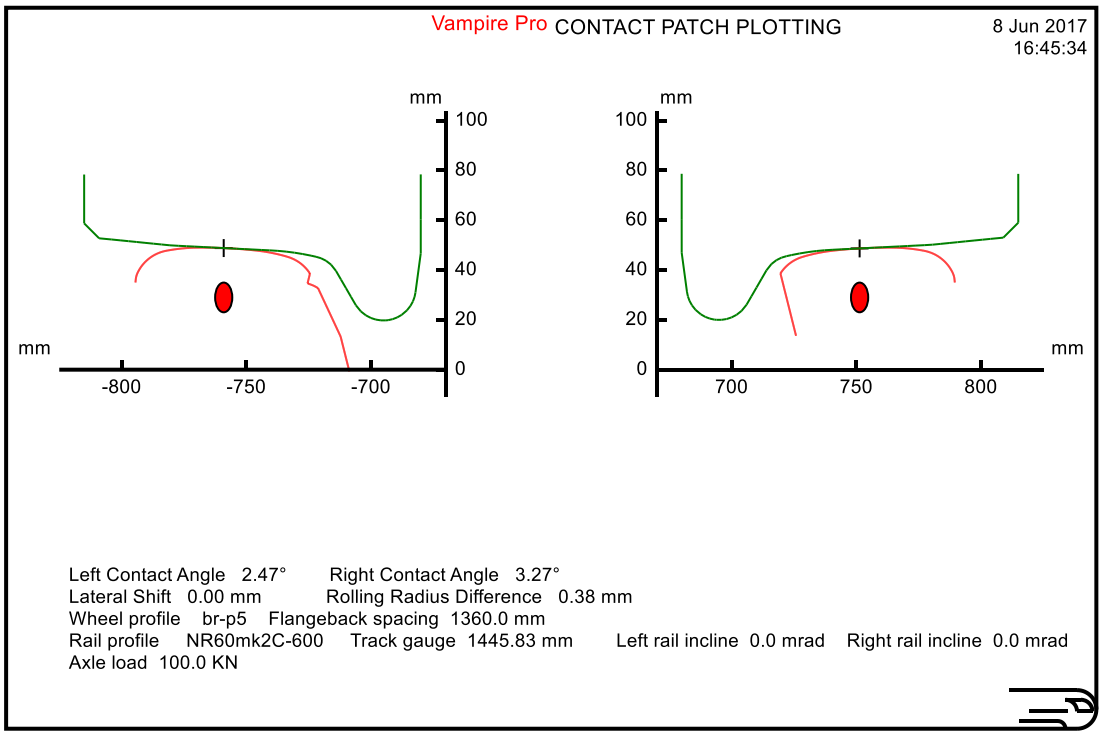

VAMPIRE Plot

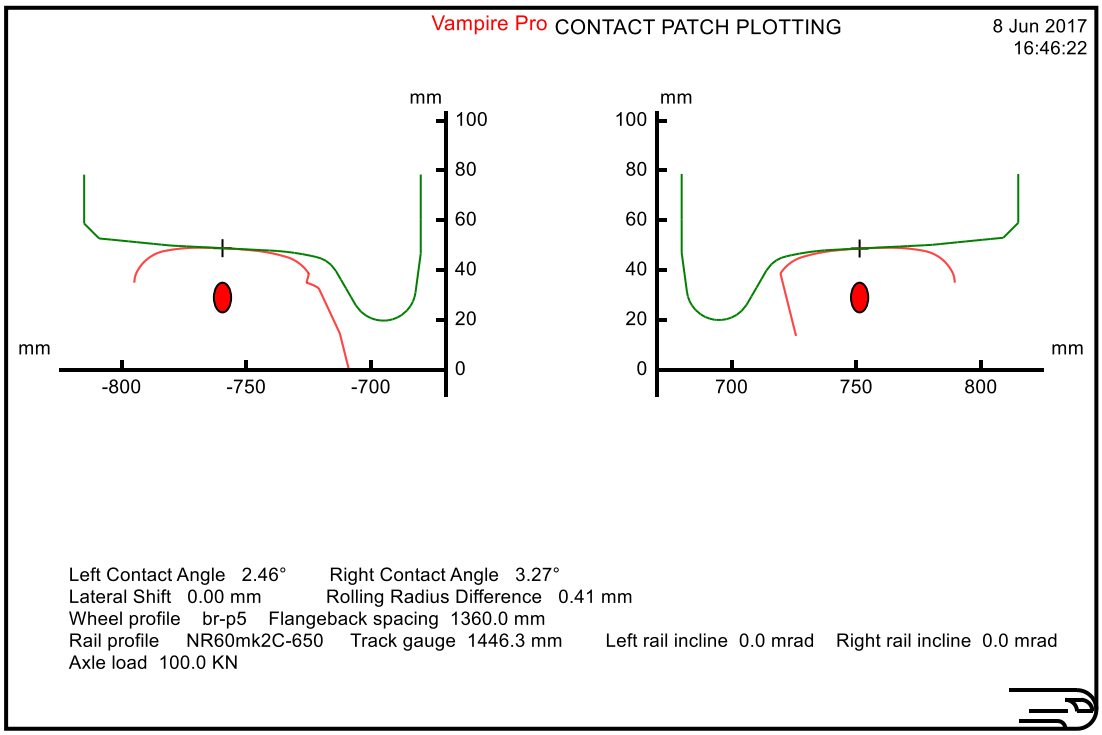

VAMPIRE Plot

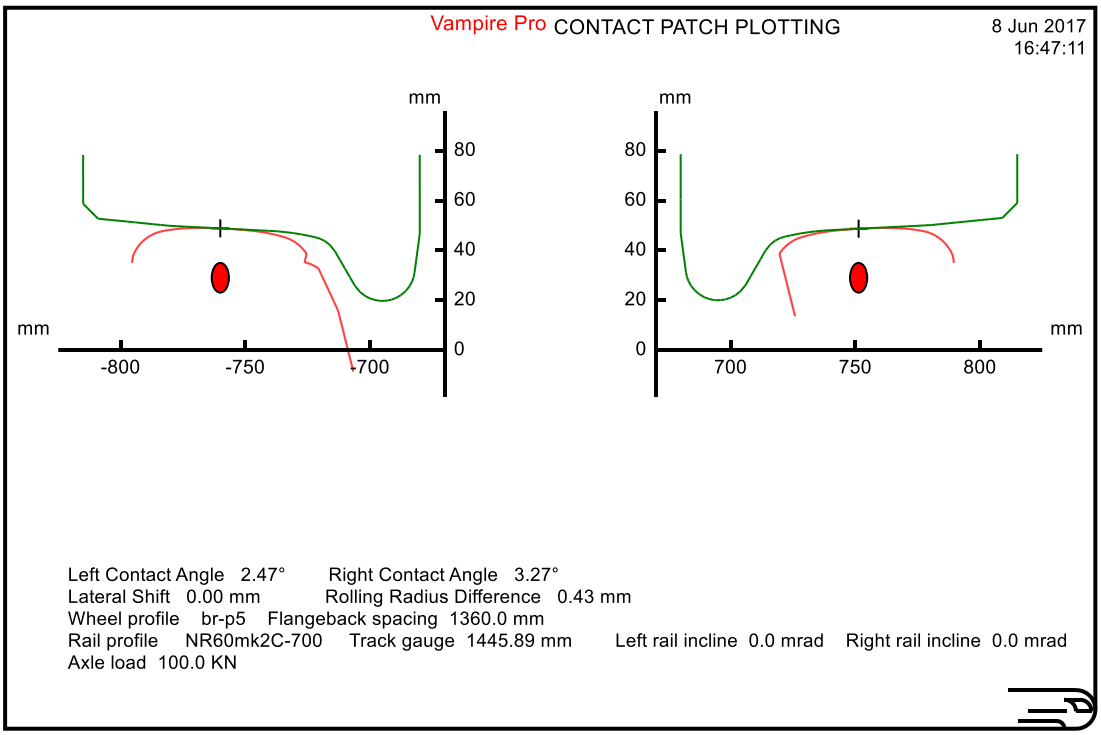

VAMPIRE Plot

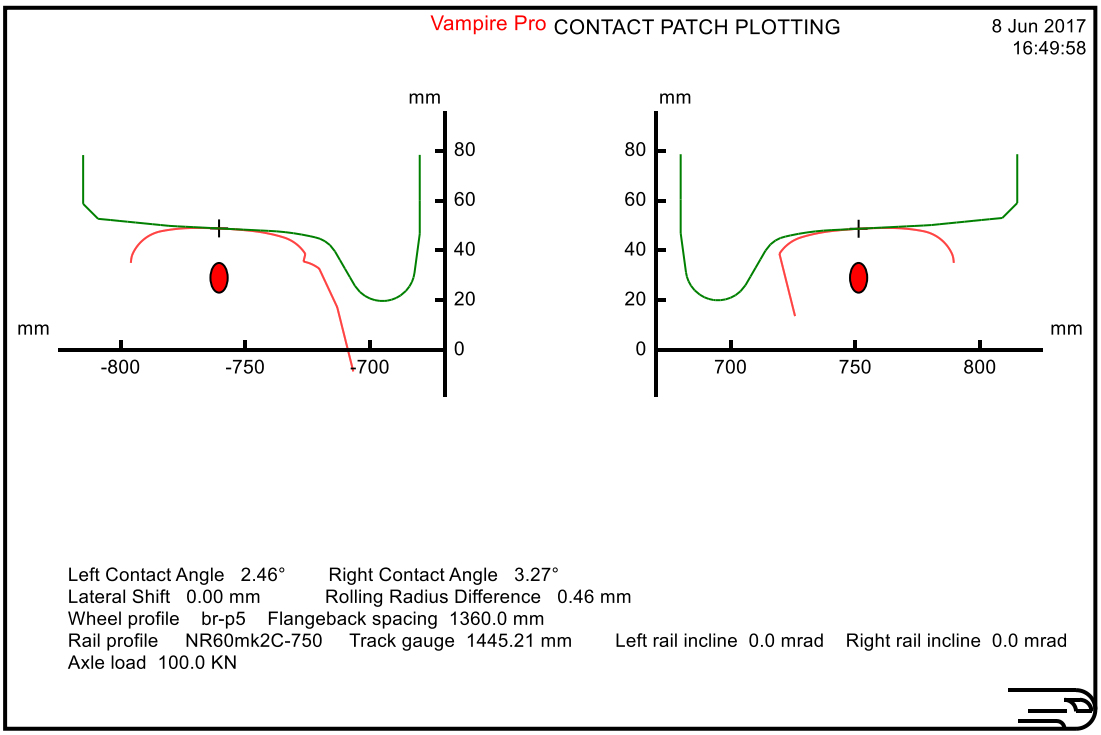

VAMPIRE Plot

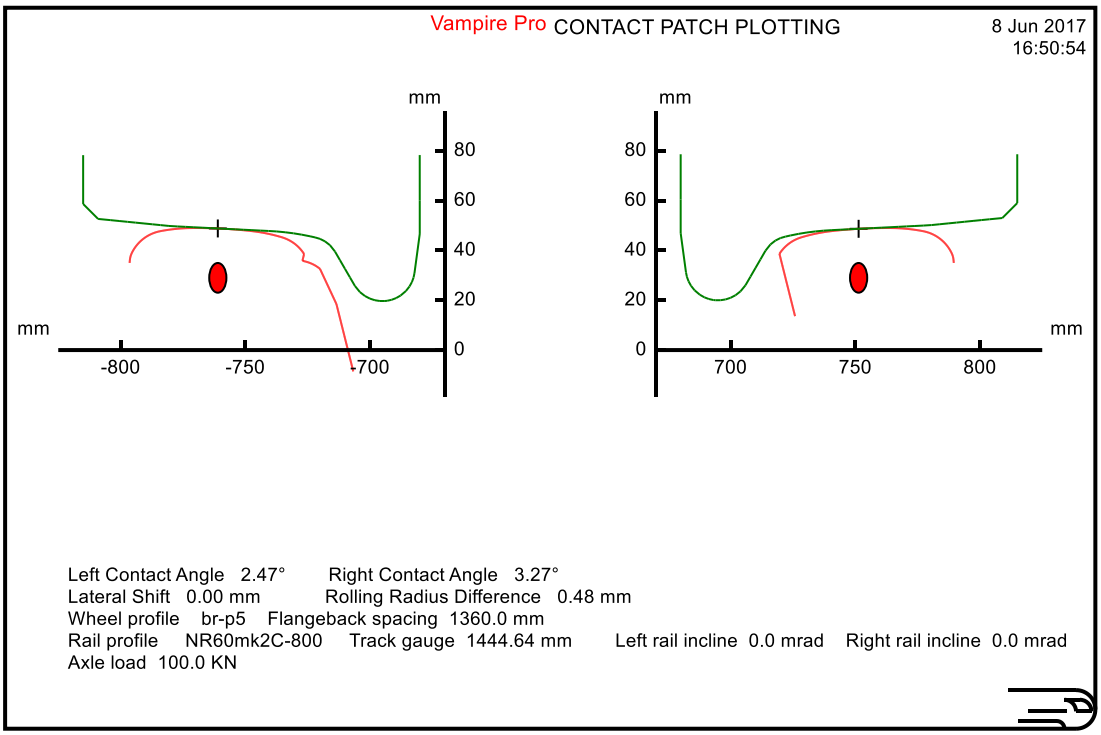

VAMPIRE Plot

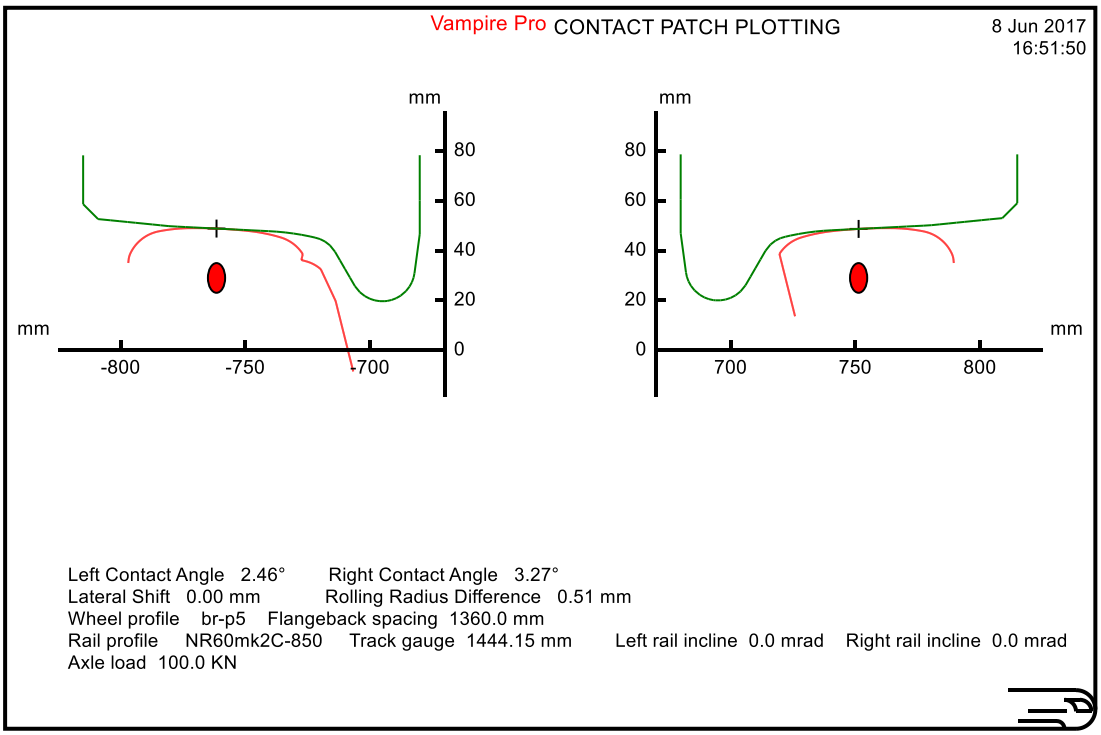

VAMPIRE Plot

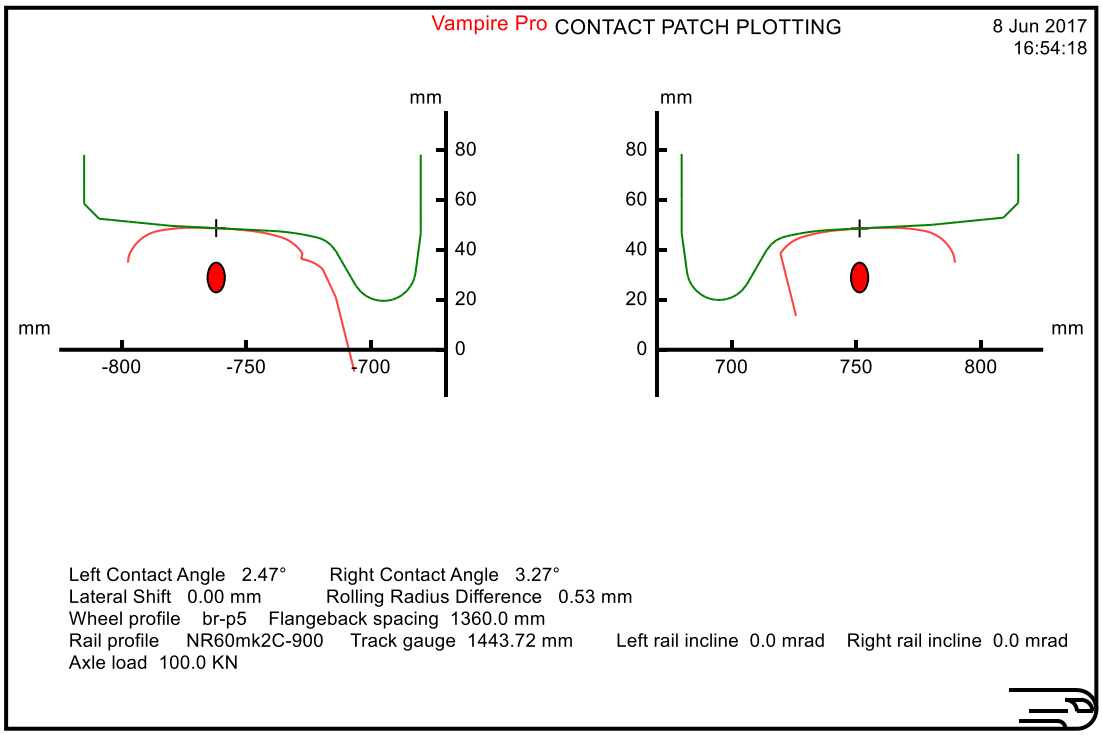

VAMPIRE Plot

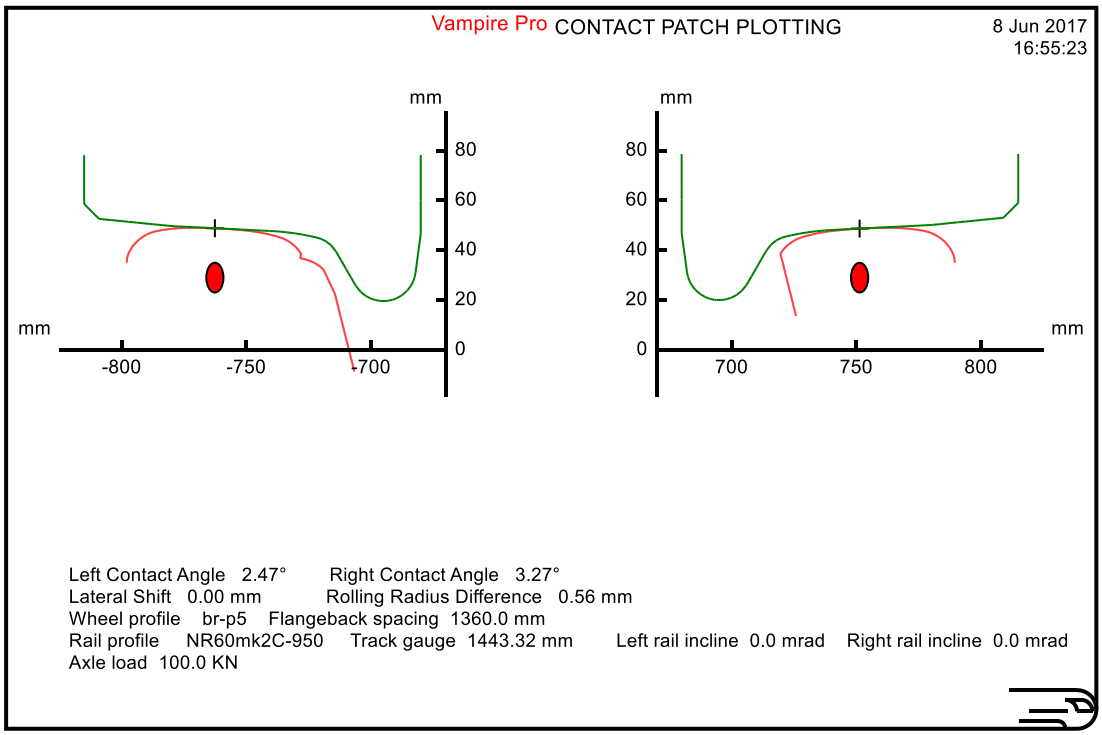

VAMPIRE Plot

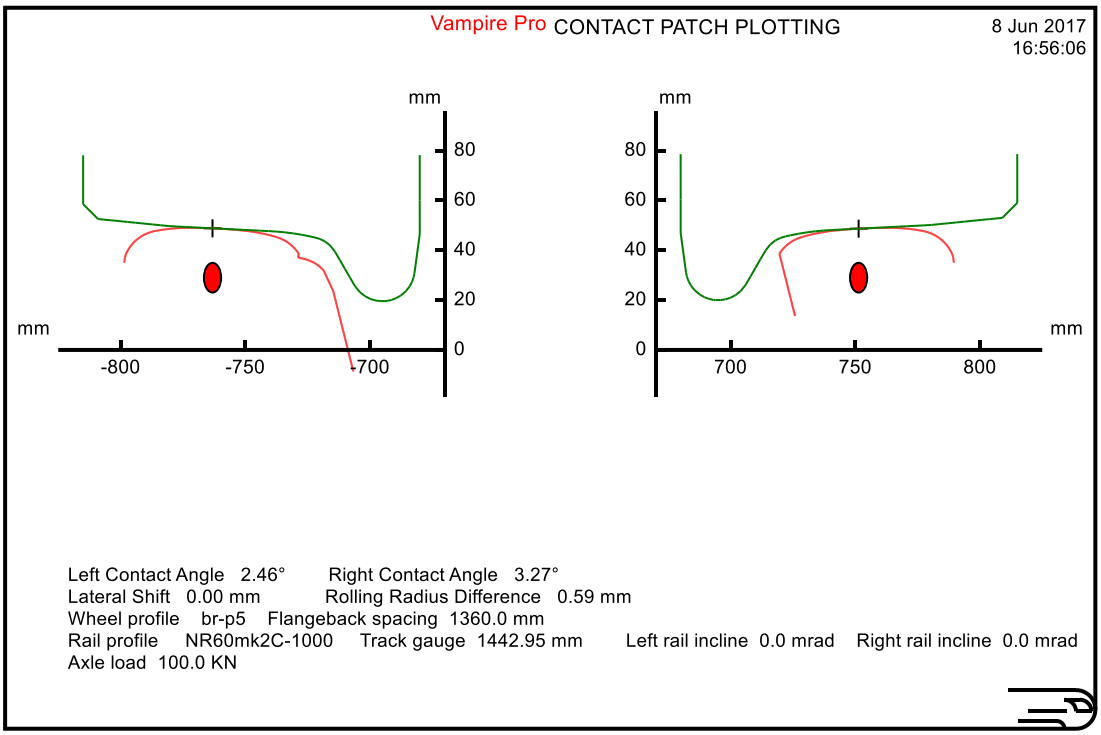

VAMPIRE Plot

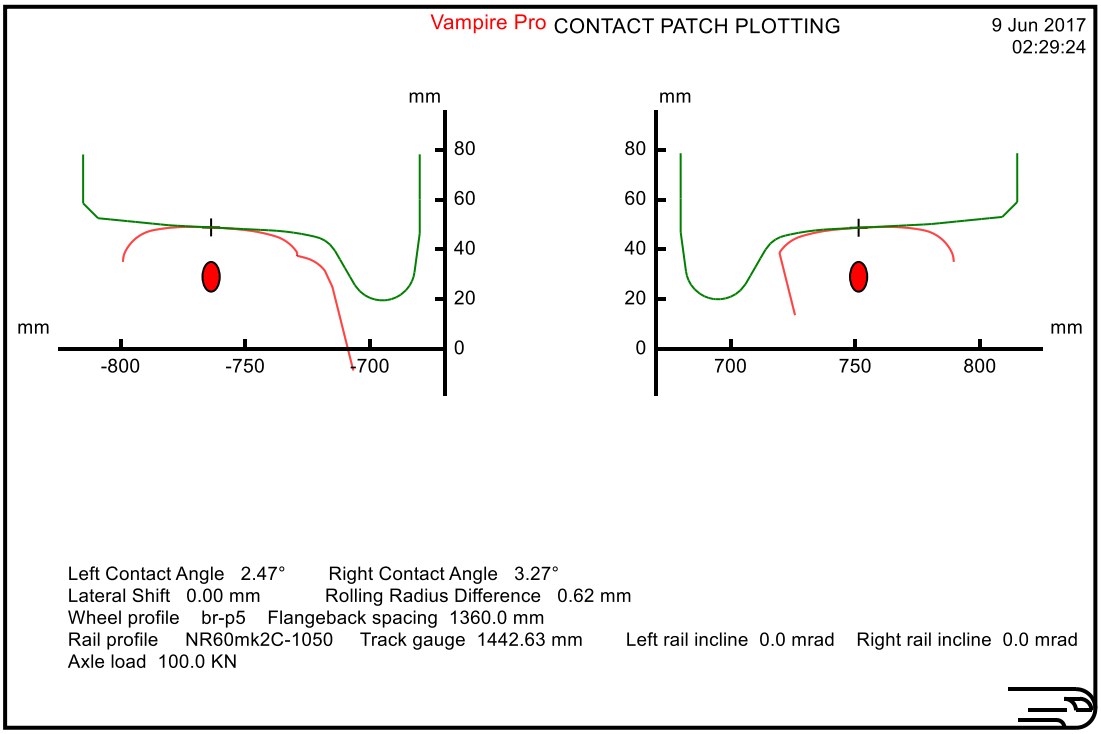

VAMPIRE Plot

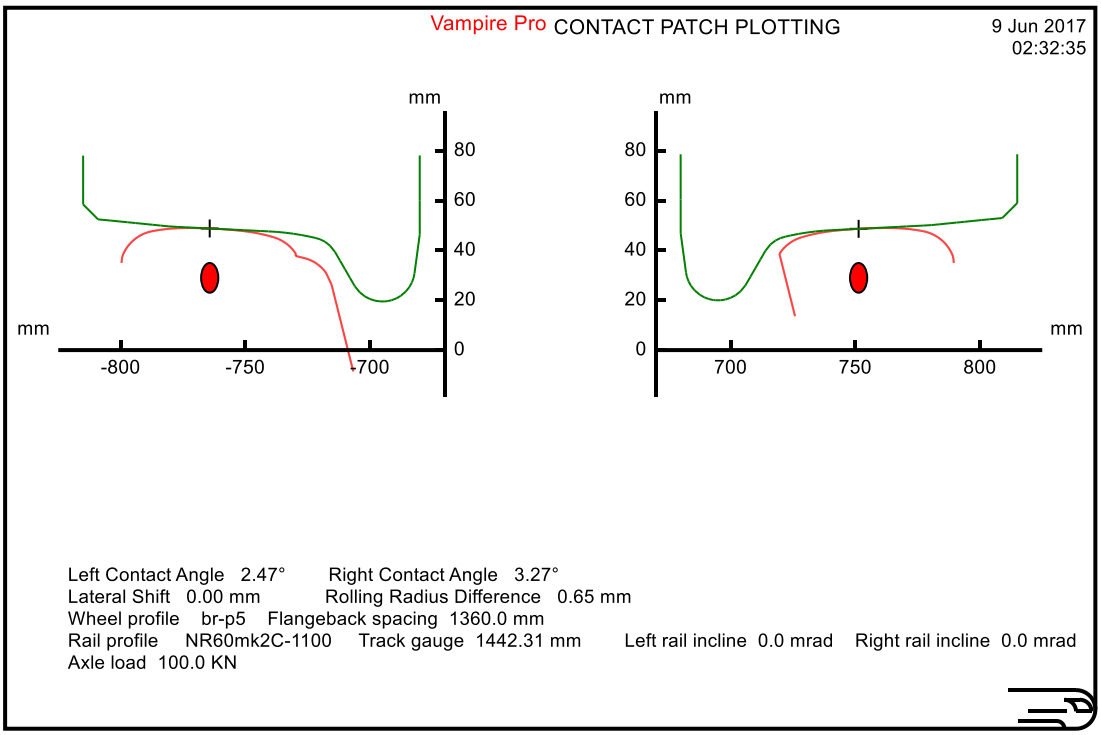

VAMPIRE Plot

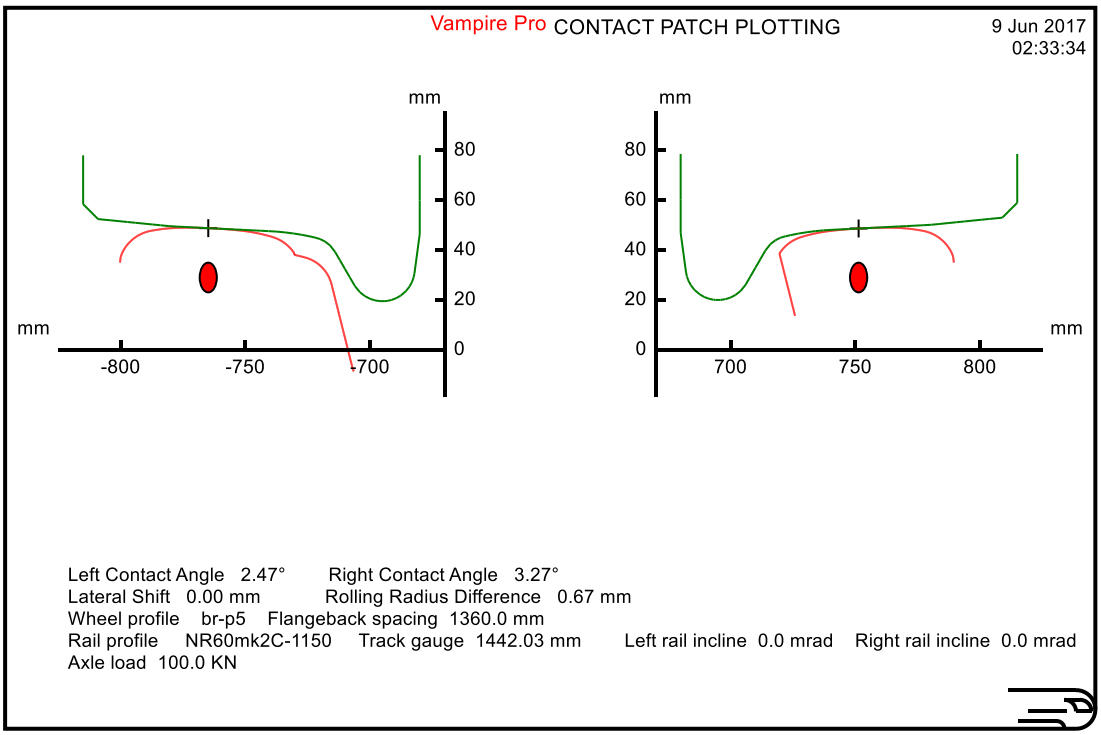

VAMPIRE Plot

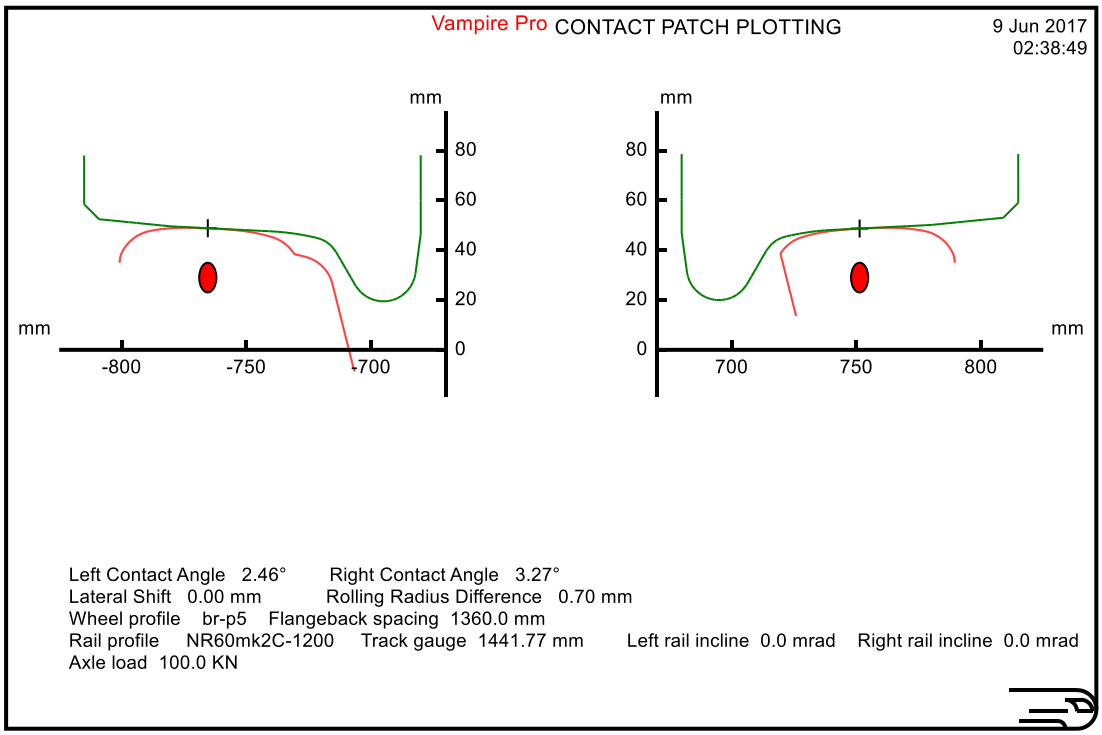

VAMPIRE Plot

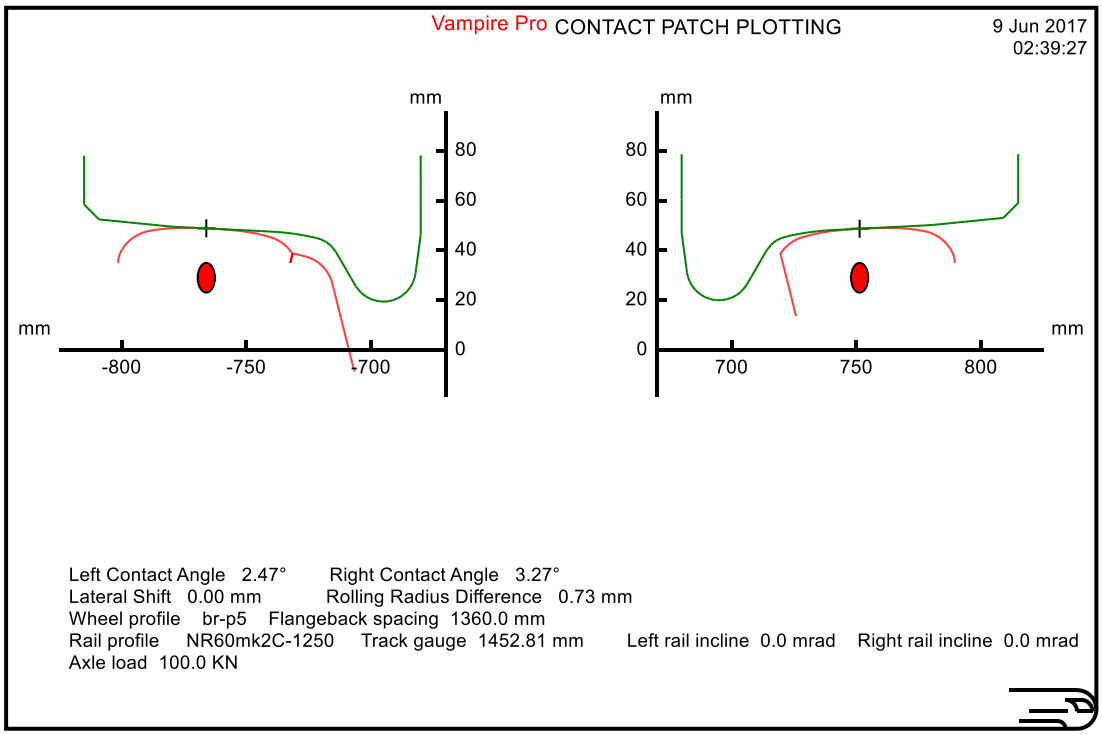

VAMPIRE Plot

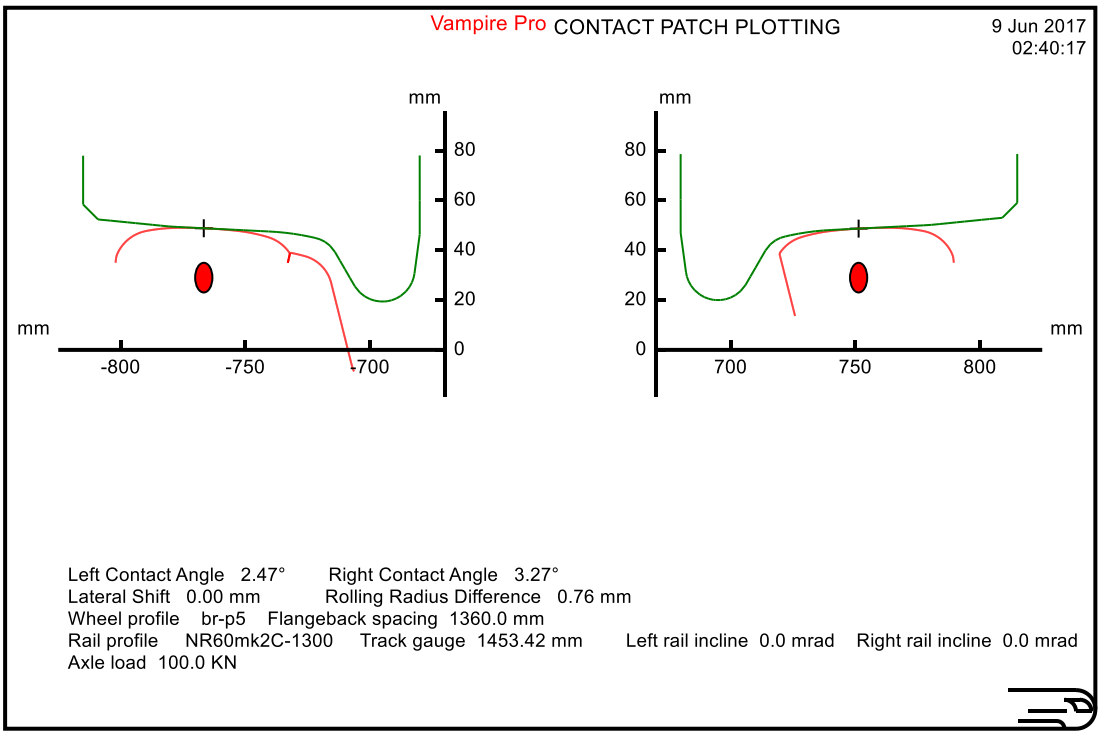

VAMPIRE Plot

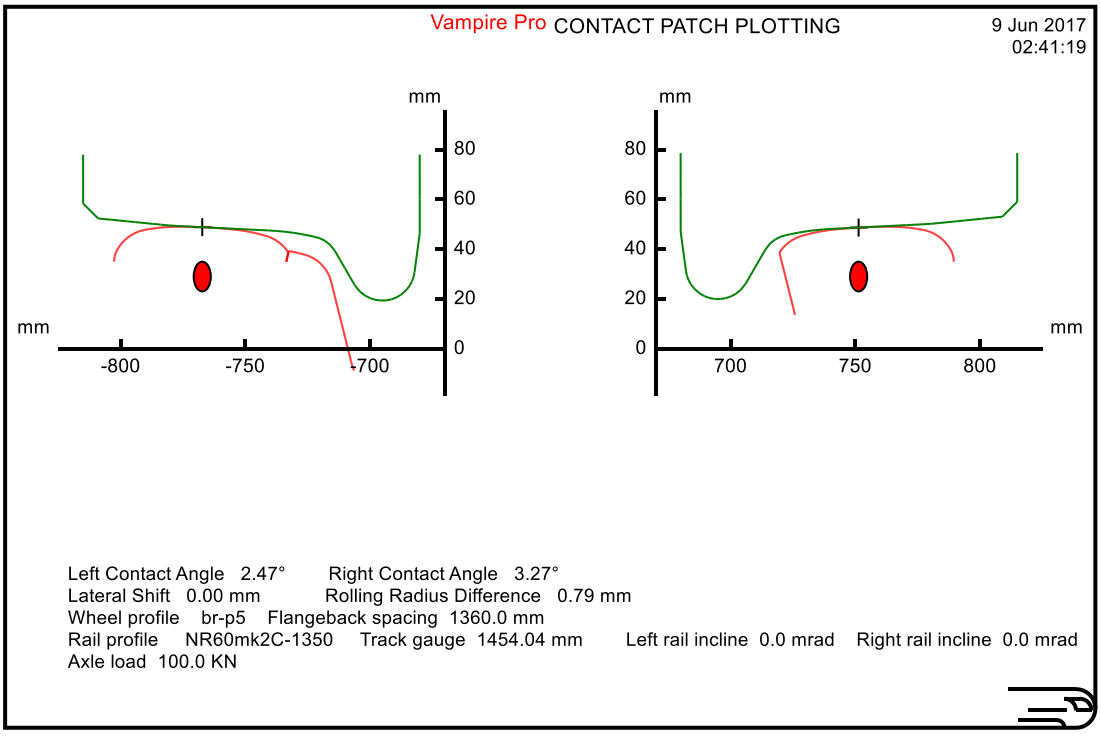

VAMPIRE Plot

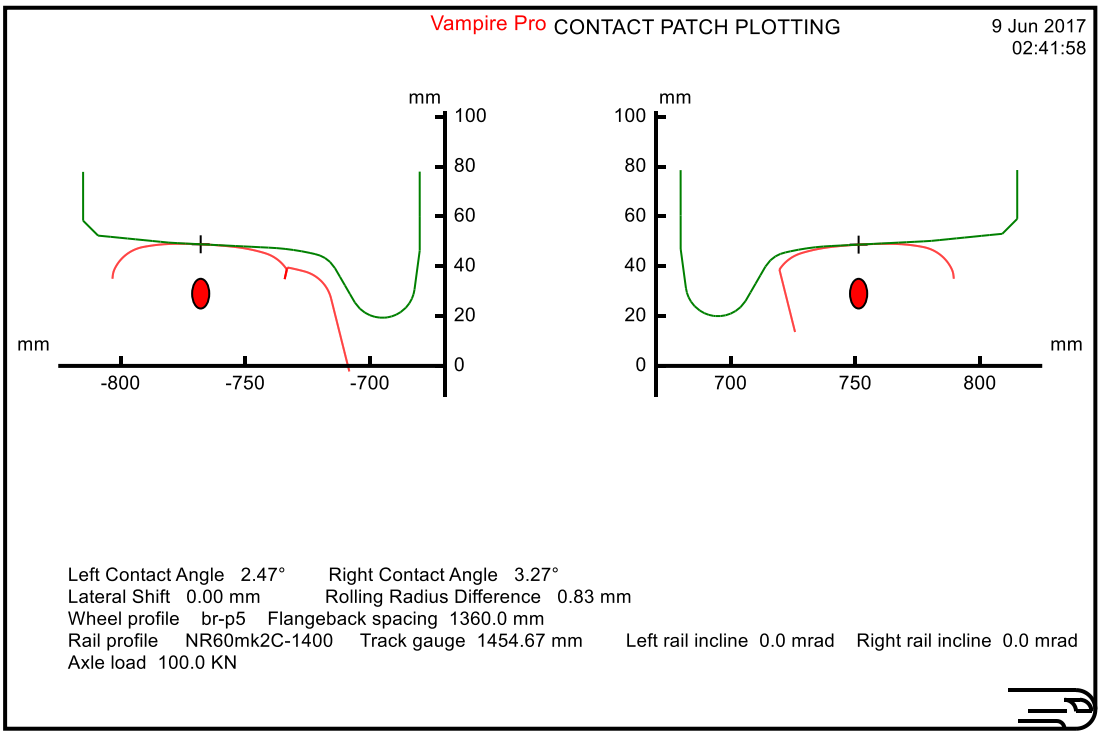

VAMPIRE Plot

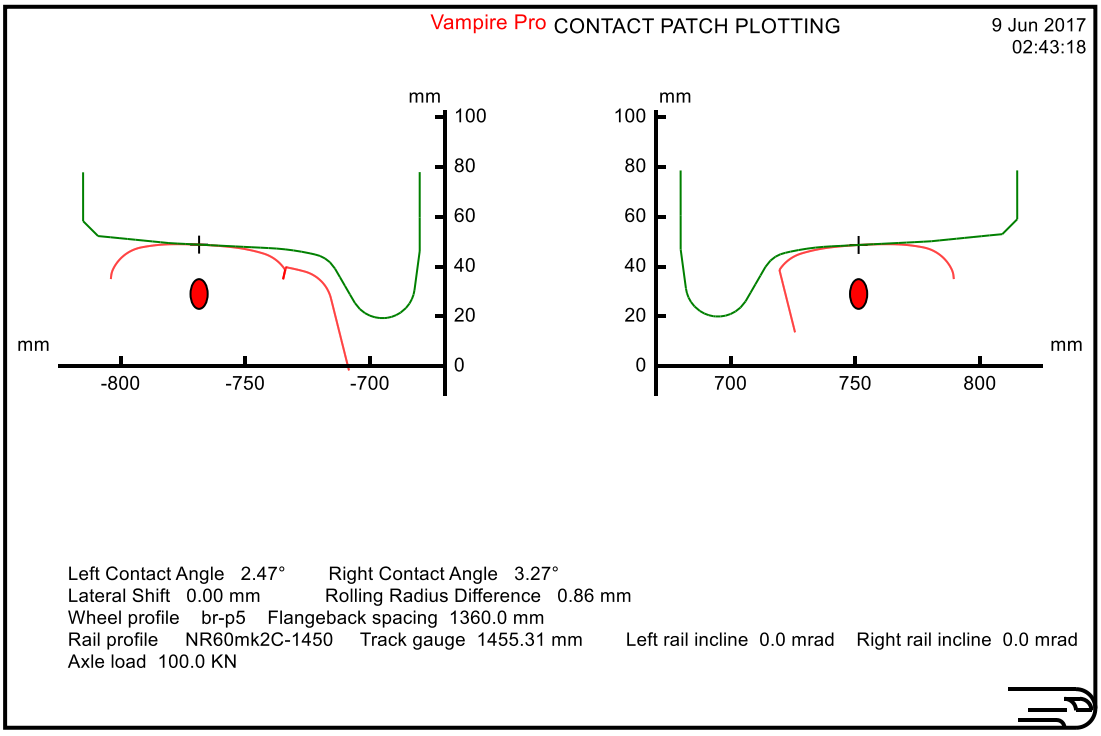

VAMPIRE Plot

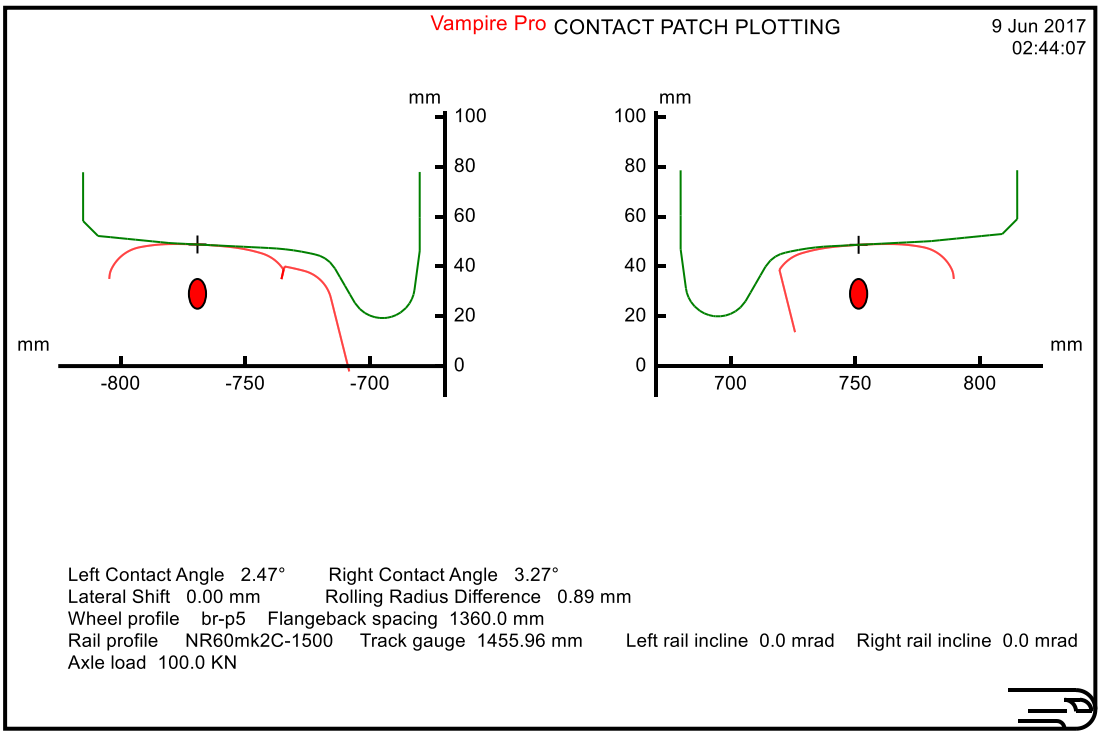

VAMPIRE Plot

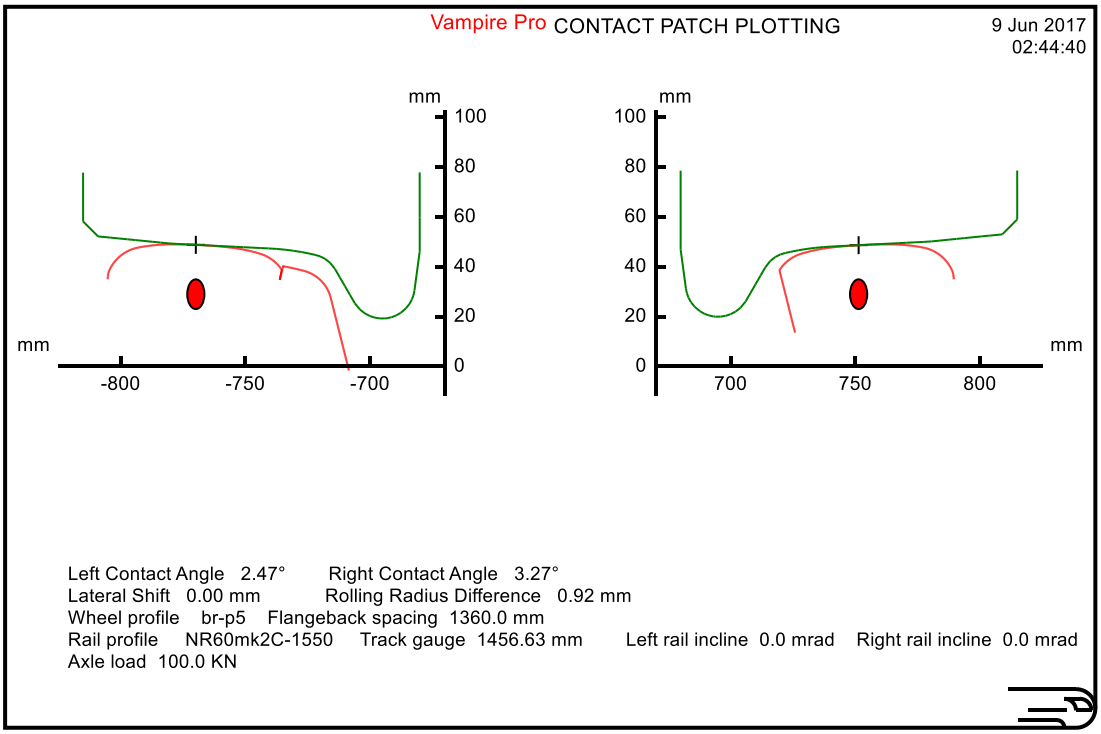

VAMPIRE Plot

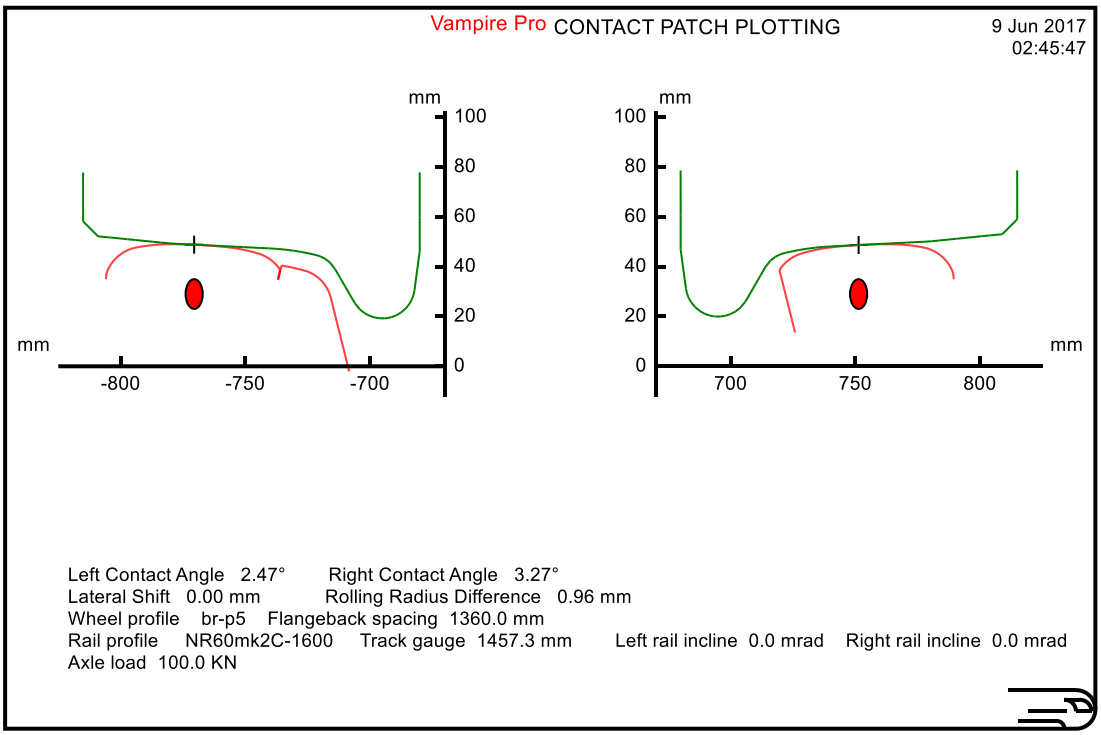

VAMPIRE Plot

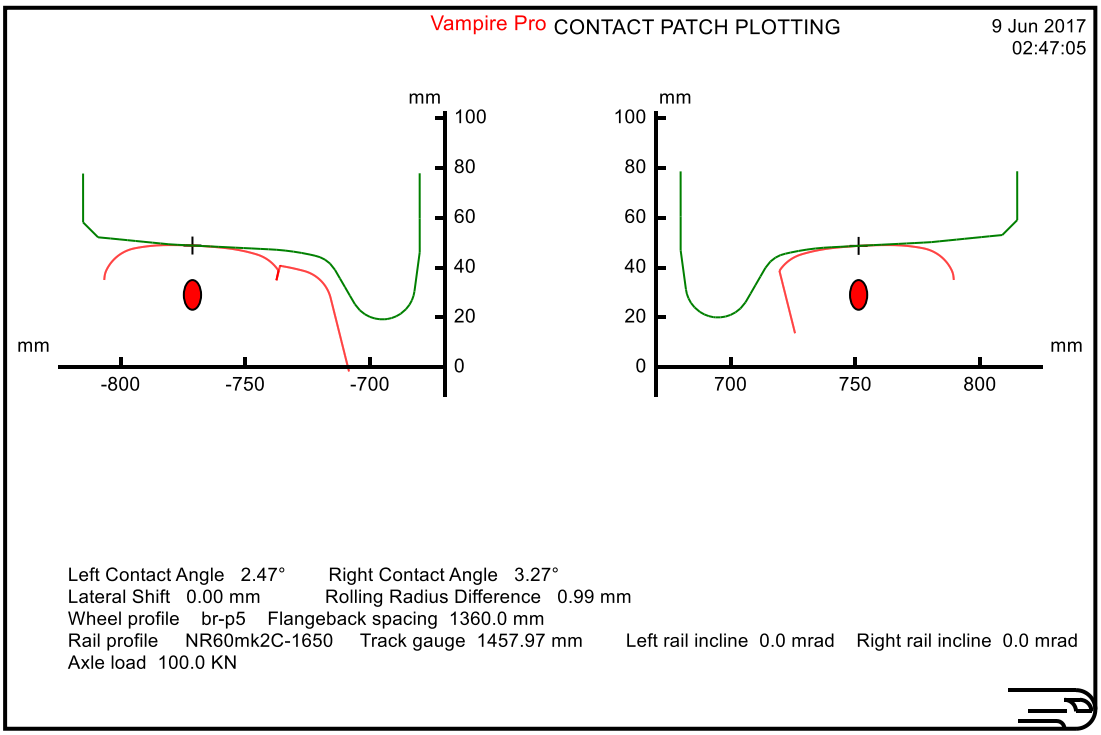

VAMPIRE Plot

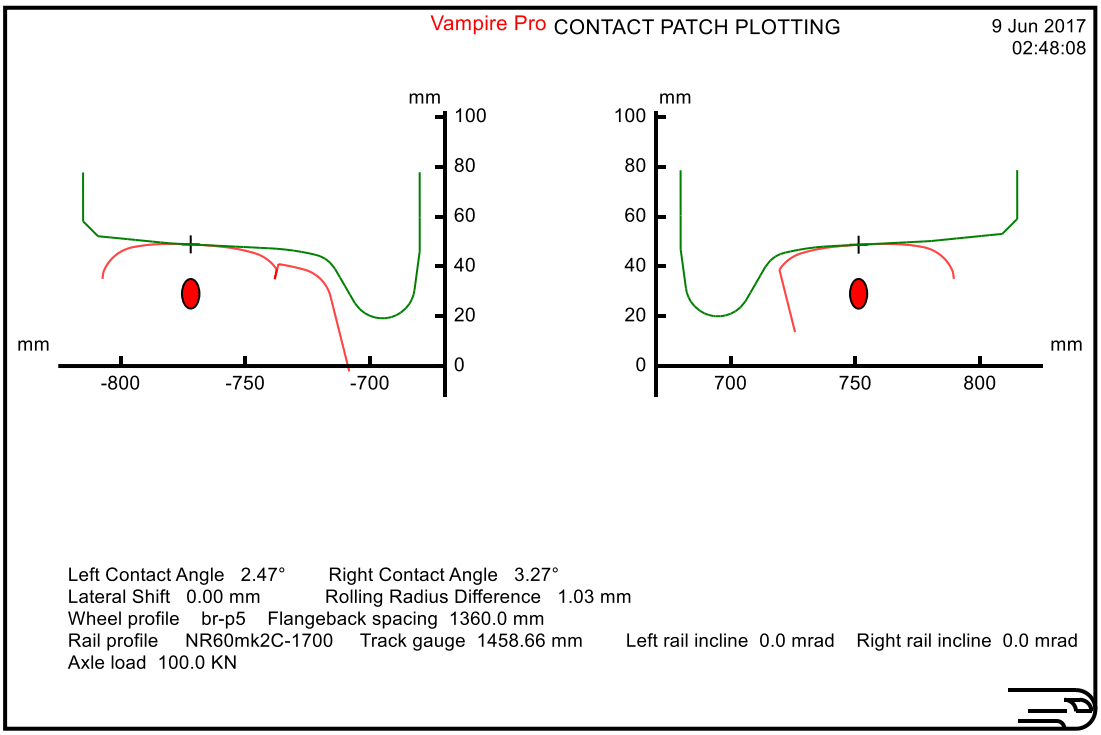

VAMPIRE Plot

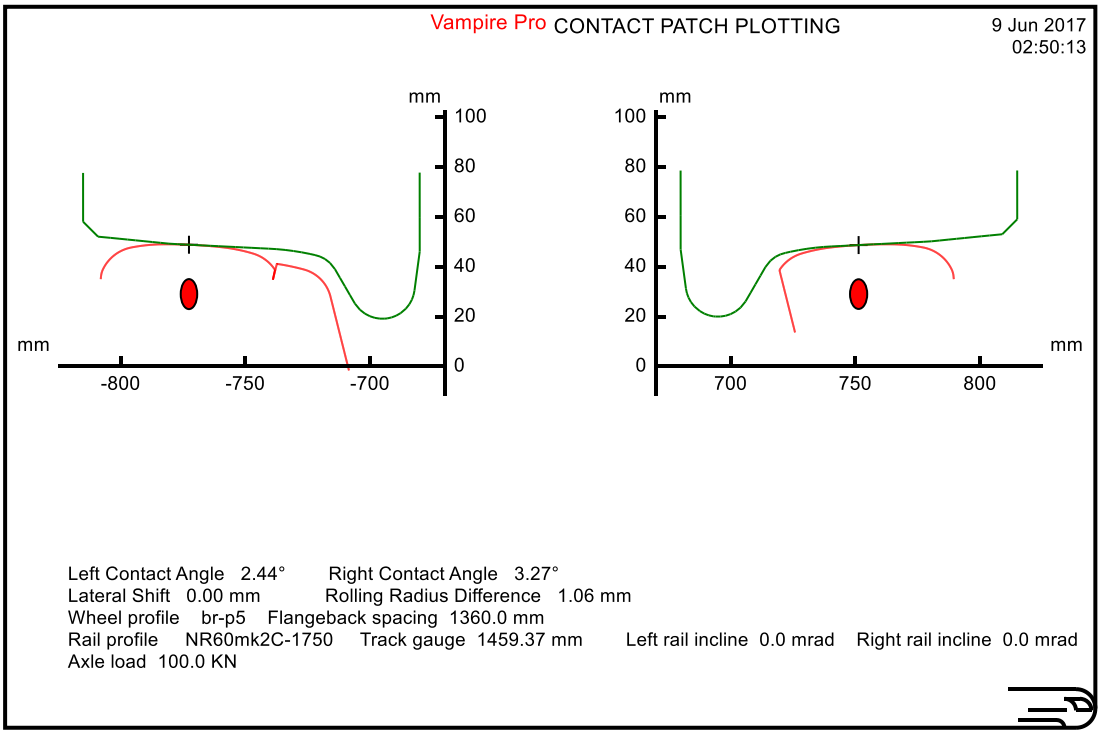

VAMPIRE Plot

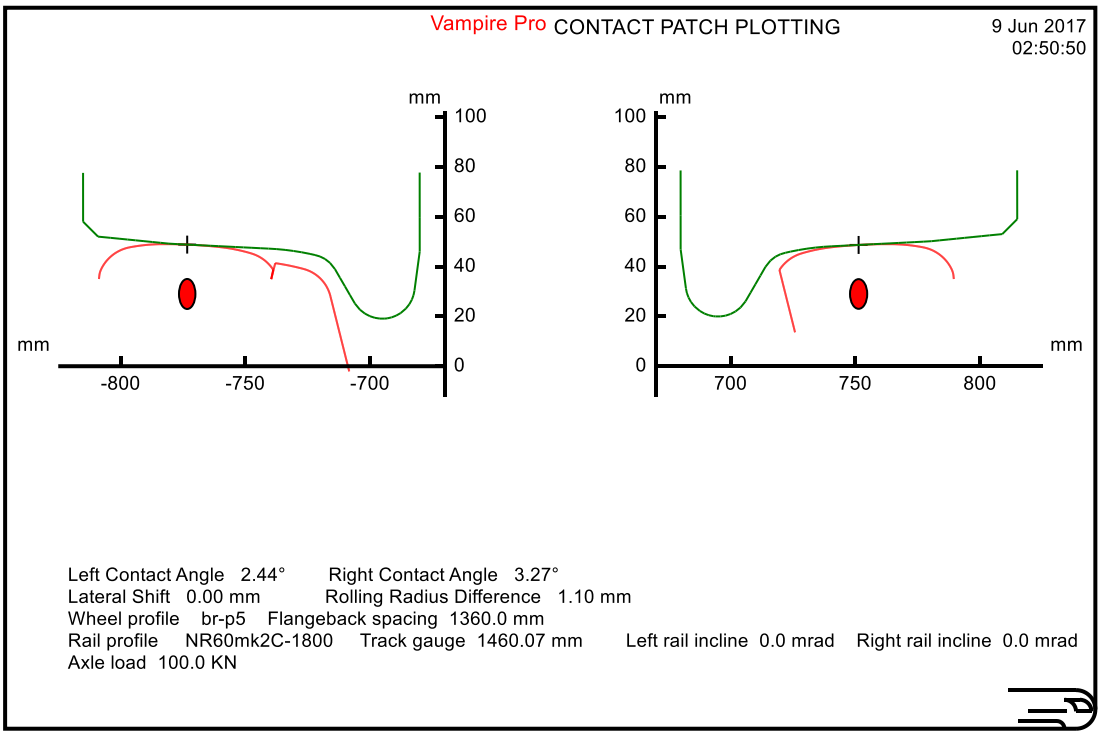

VAMPIRE Plot

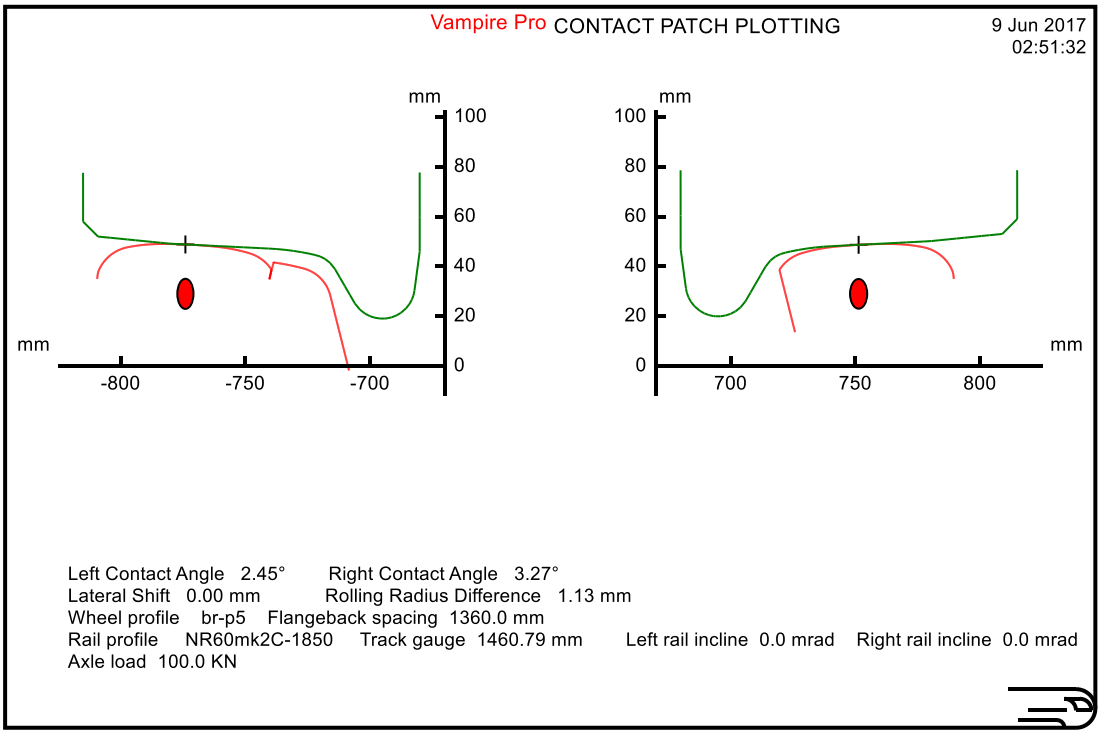

VAMPIRE Plot

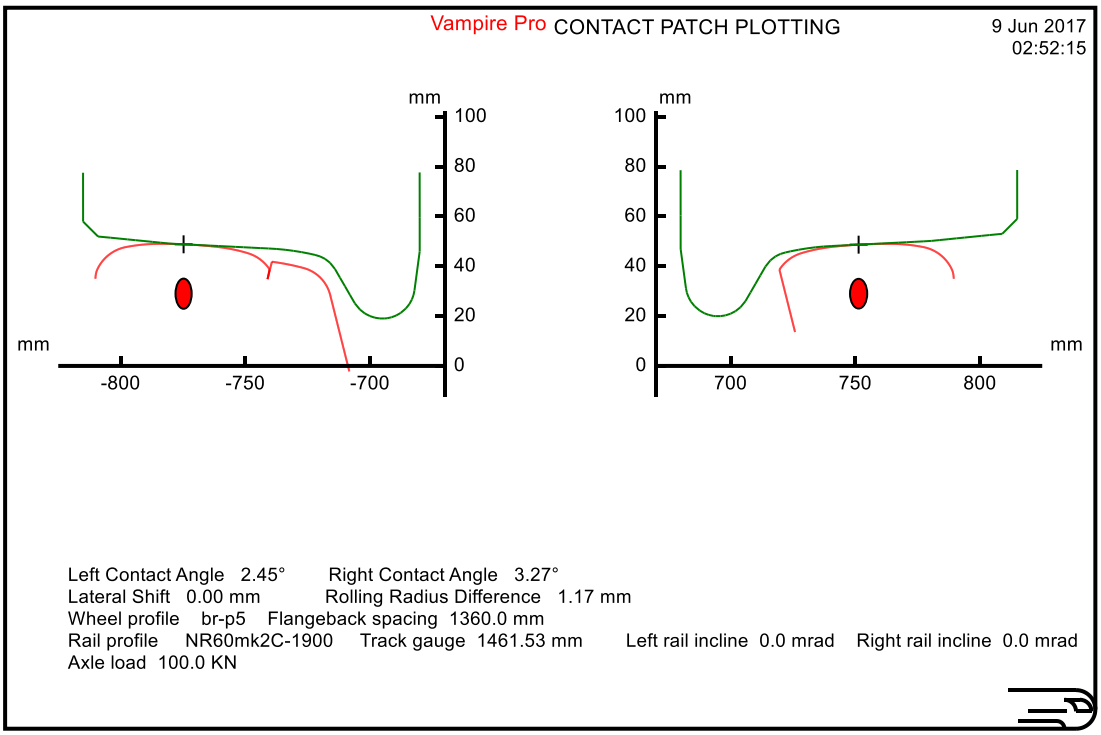

VAMPIRE Plot

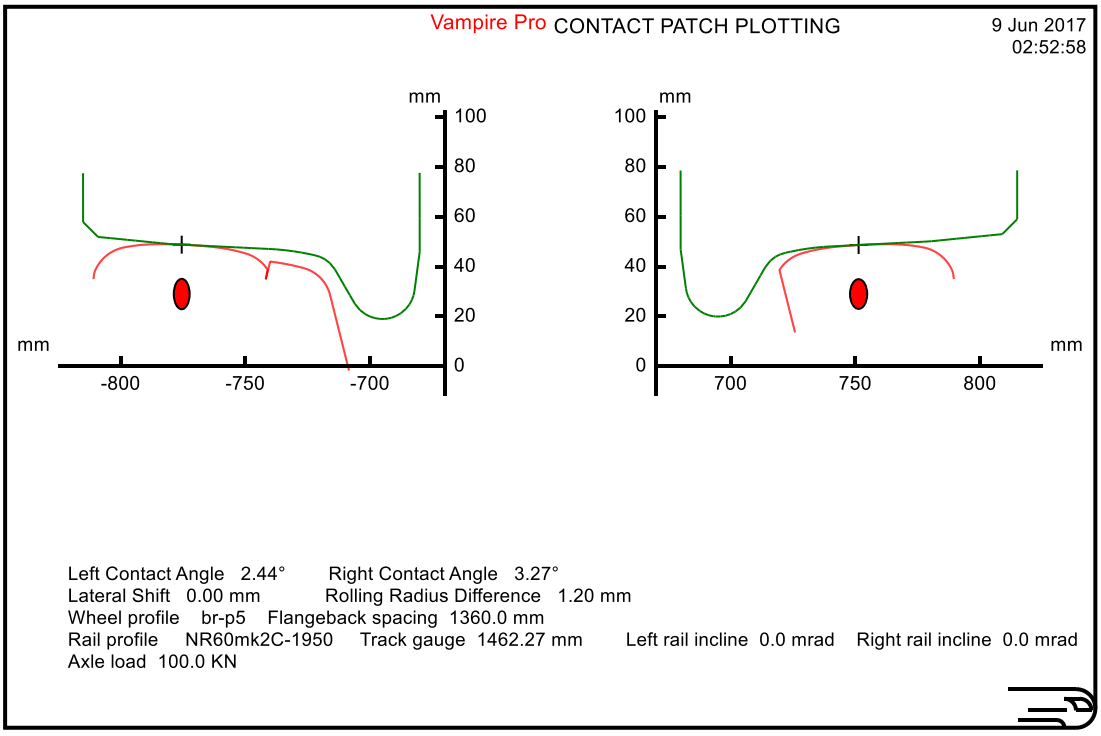

VAMPIRE Plot

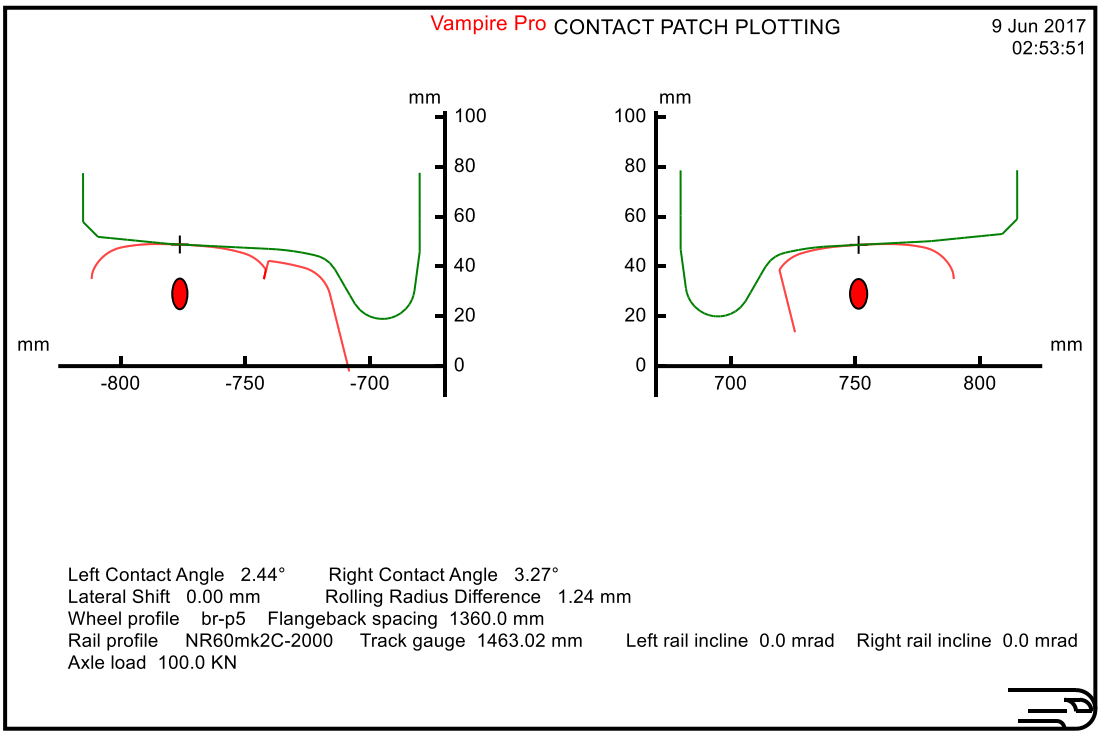

VAMPIRE Plot

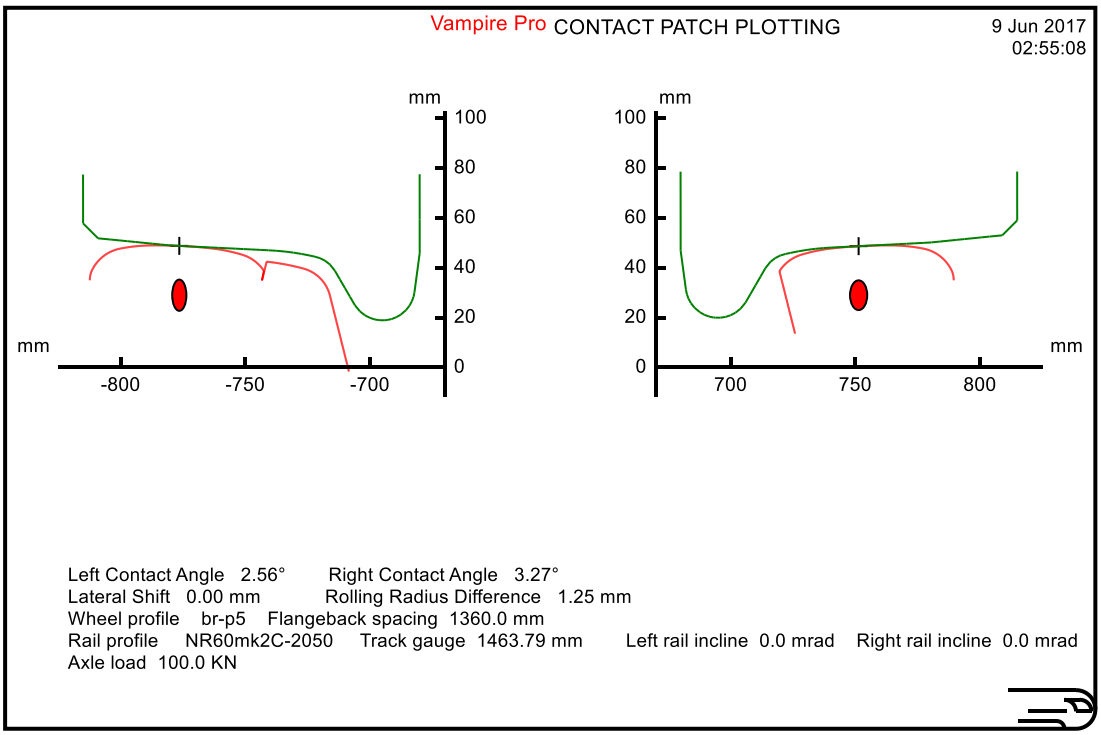

VAMPIRE Plot

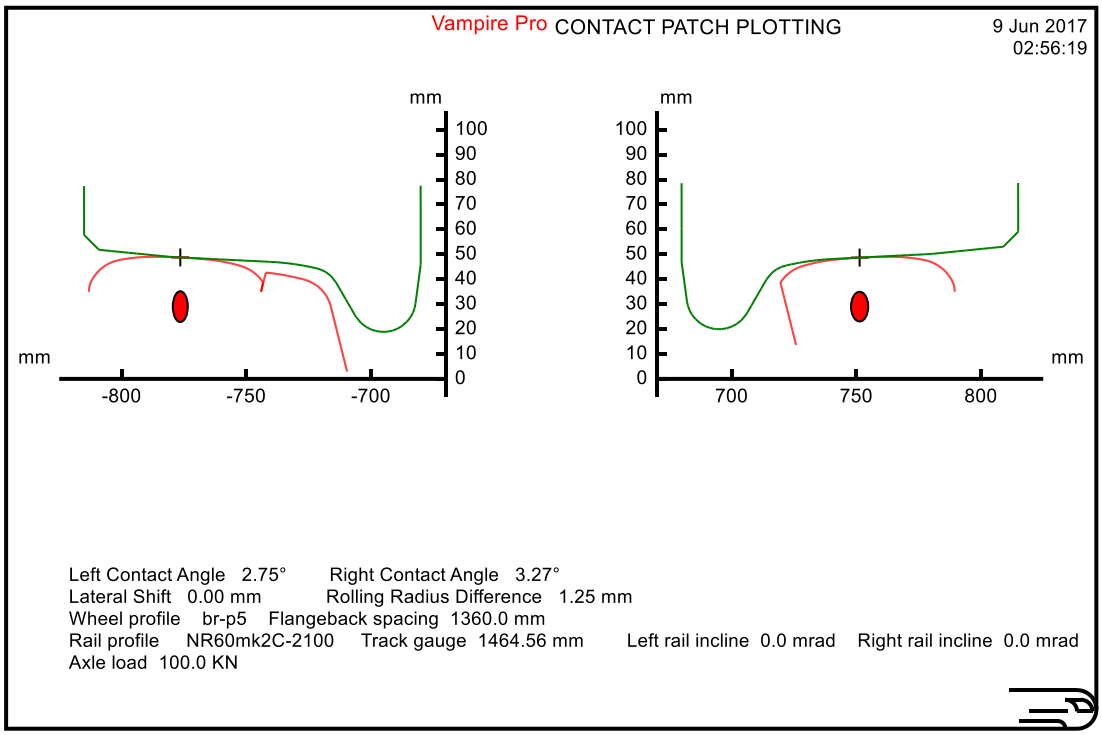

VAMPIRE Plot

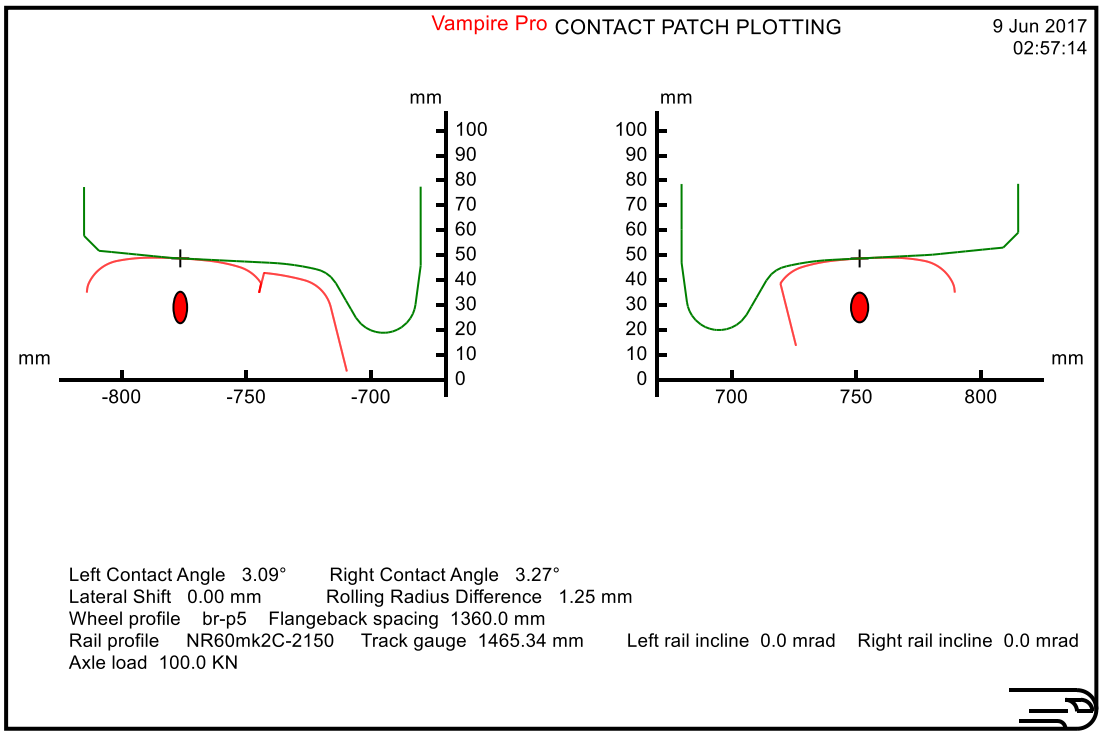

VAMPIRE Plot

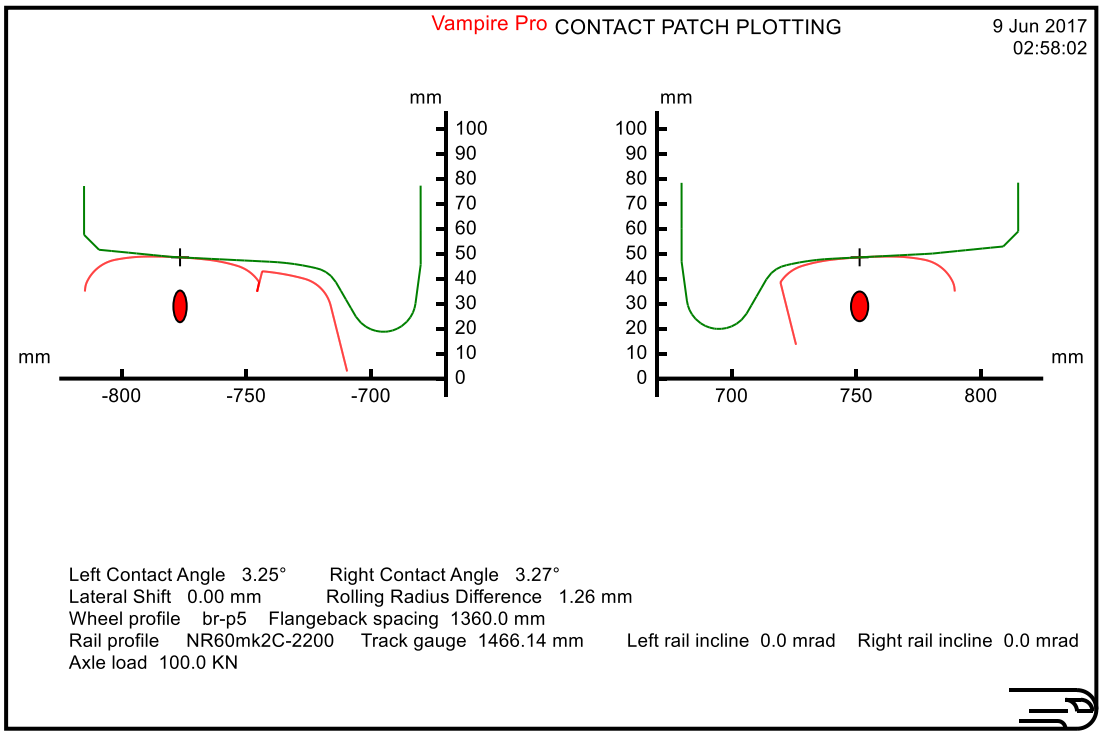

VAMPIRE Plot

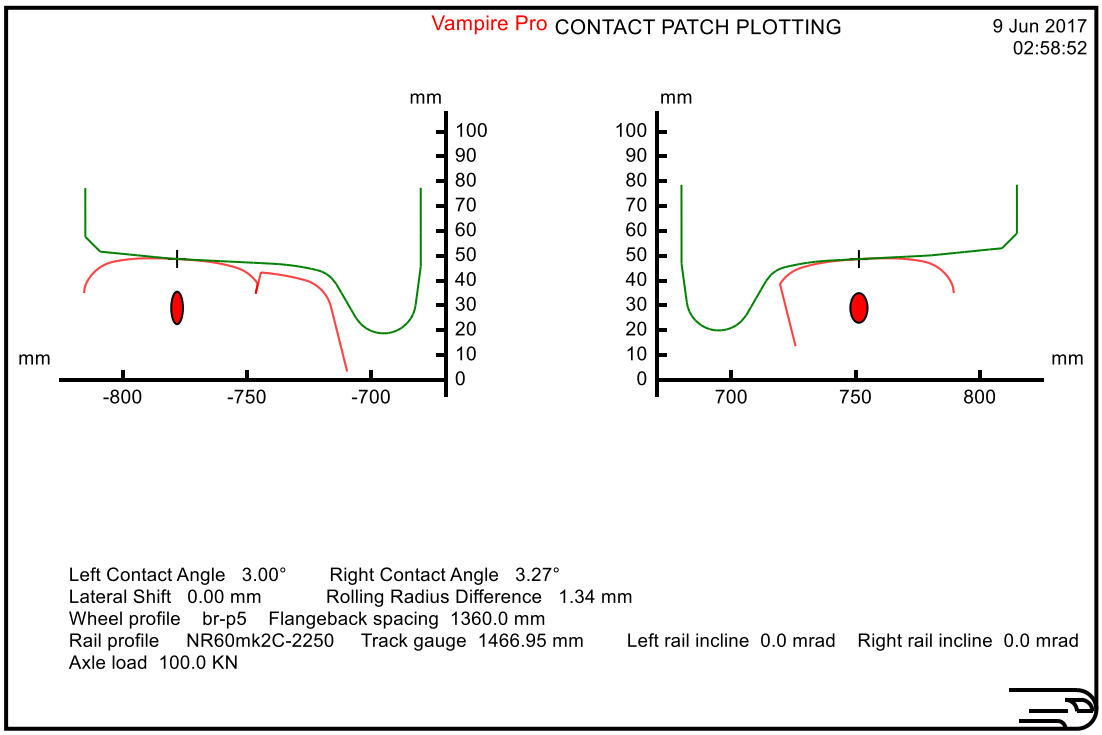

VAMPIRE Plot

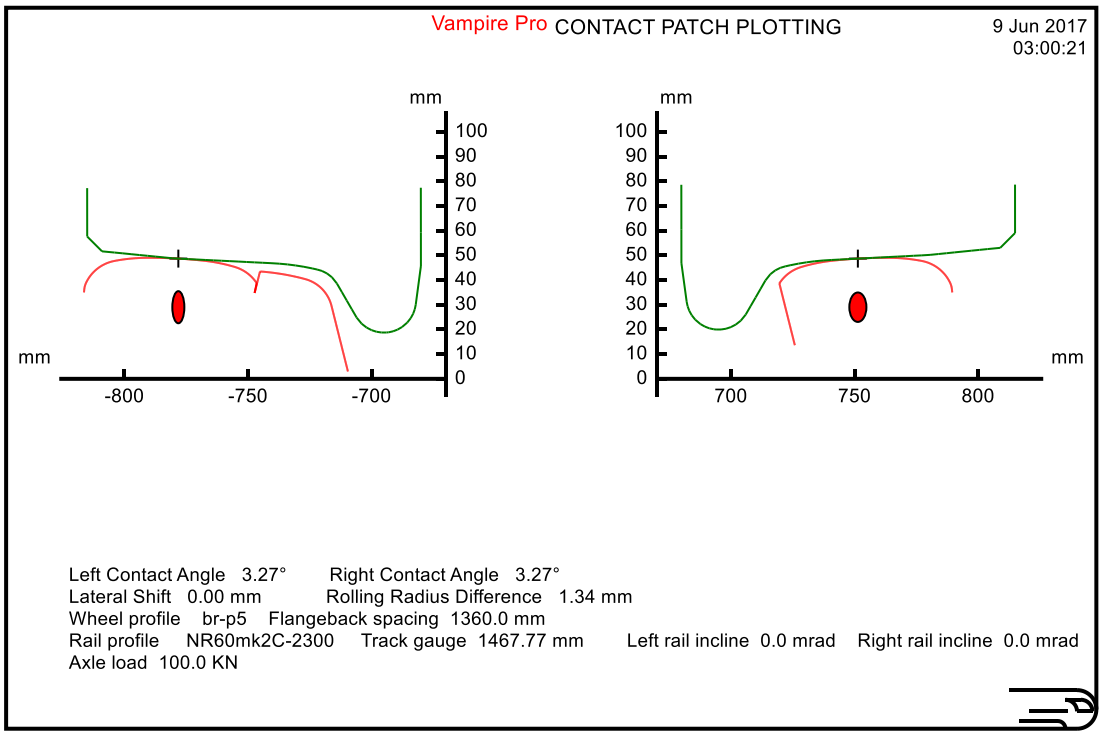

VAMPIRE Plot

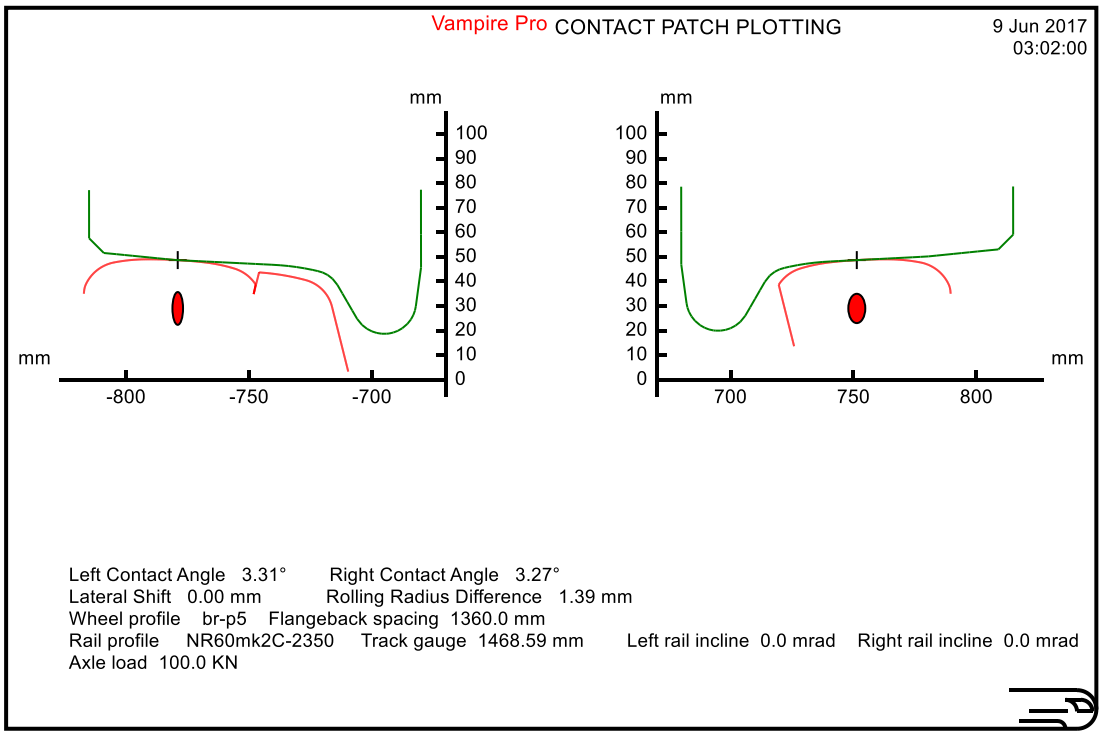

VAMPIRE Plot

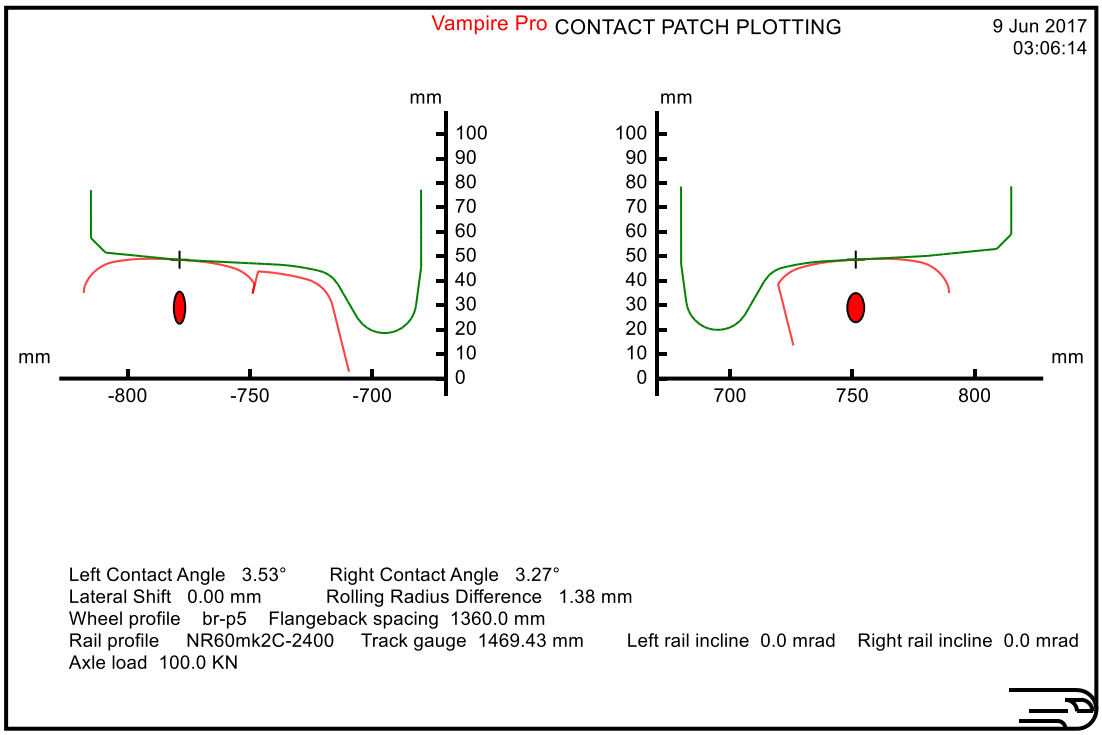

VAMPIRE Plot

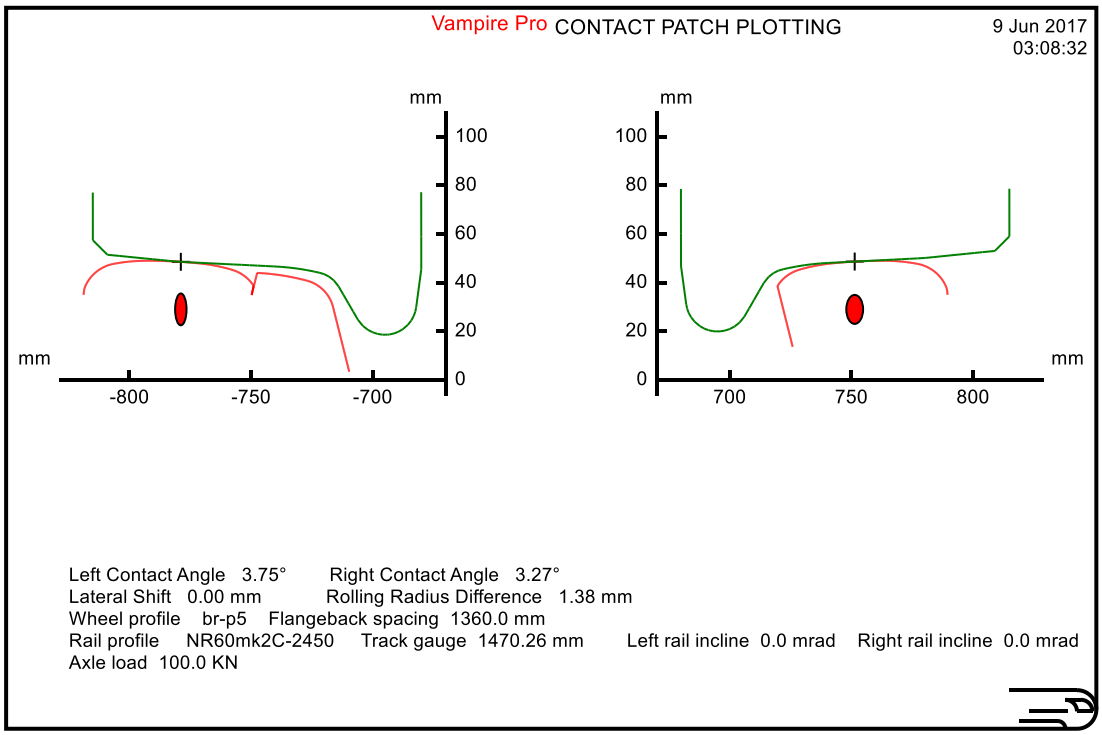

VAMPIRE Plot

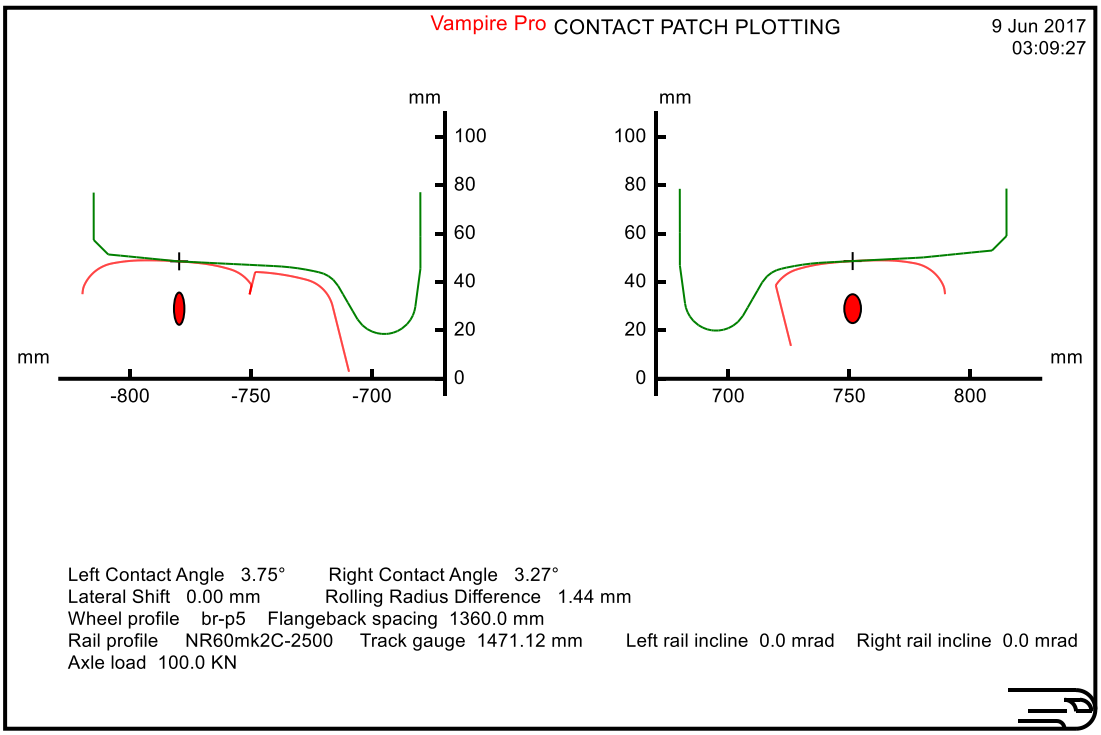

VAMPIRE Plot

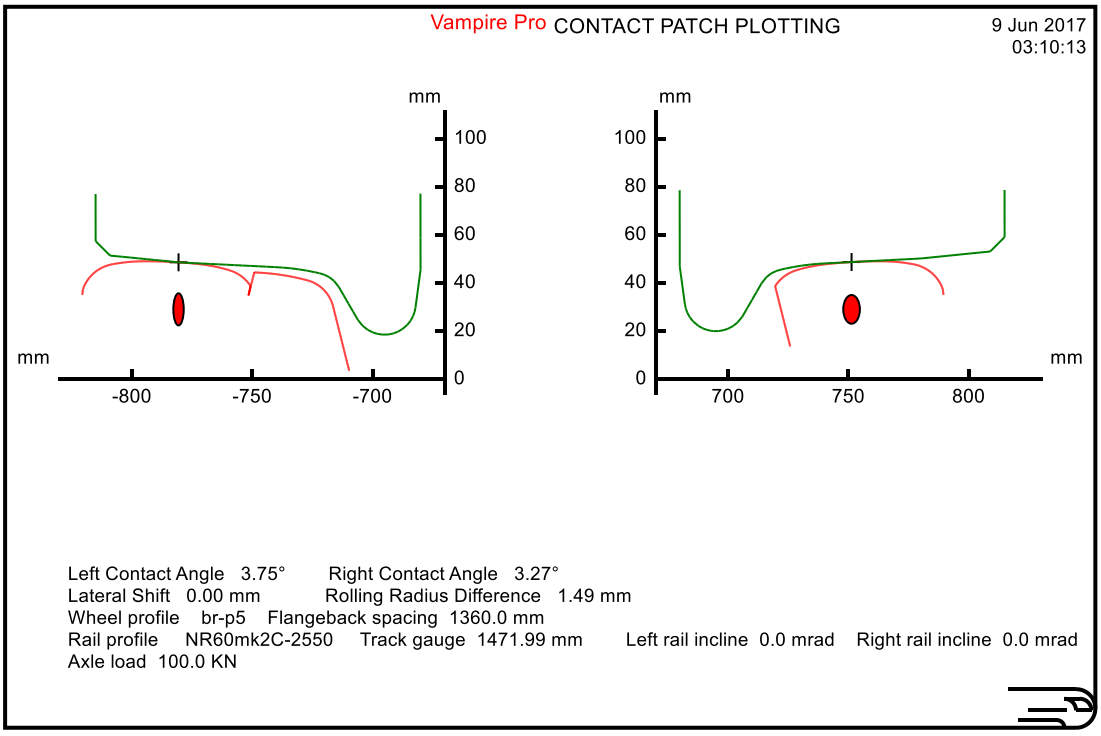

VAMPIRE Plot

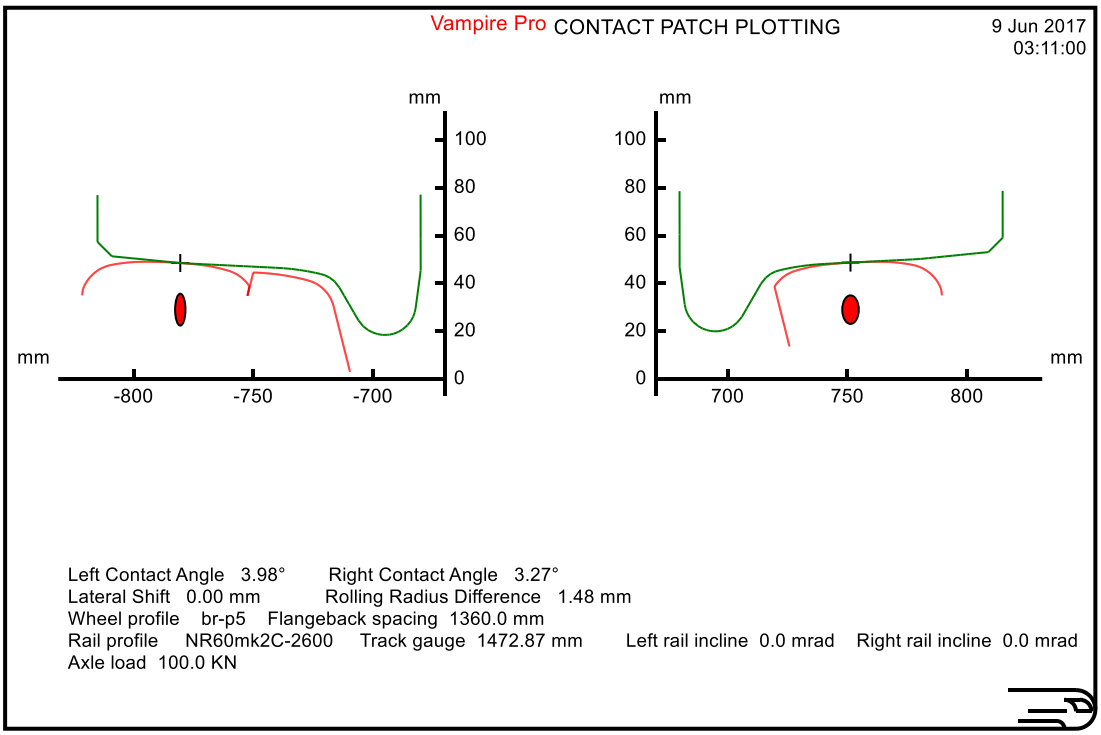

VAMPIRE Plot

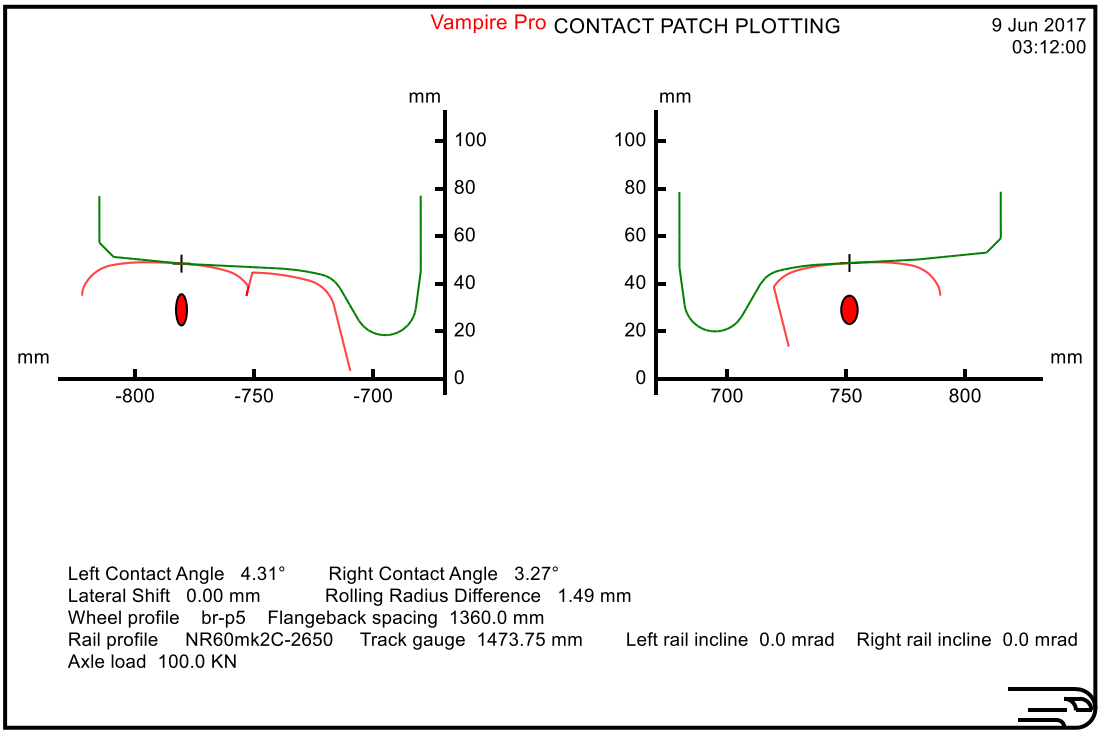

VAMPIRE Plot

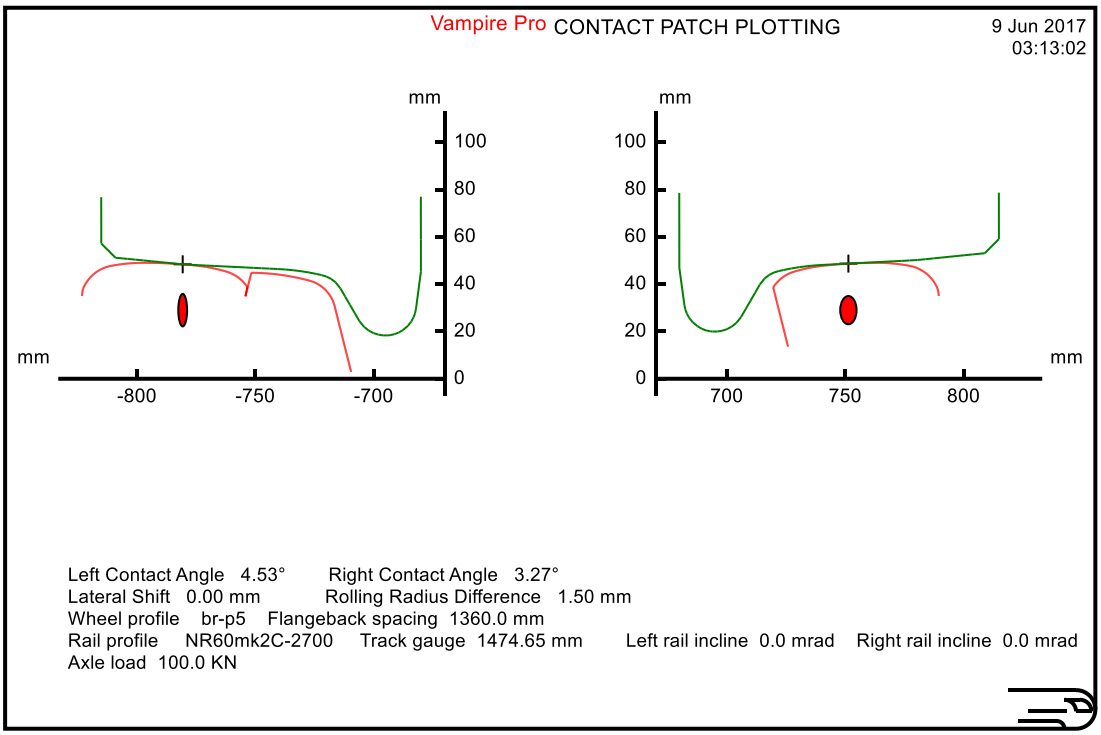

VAMPIRE Plot

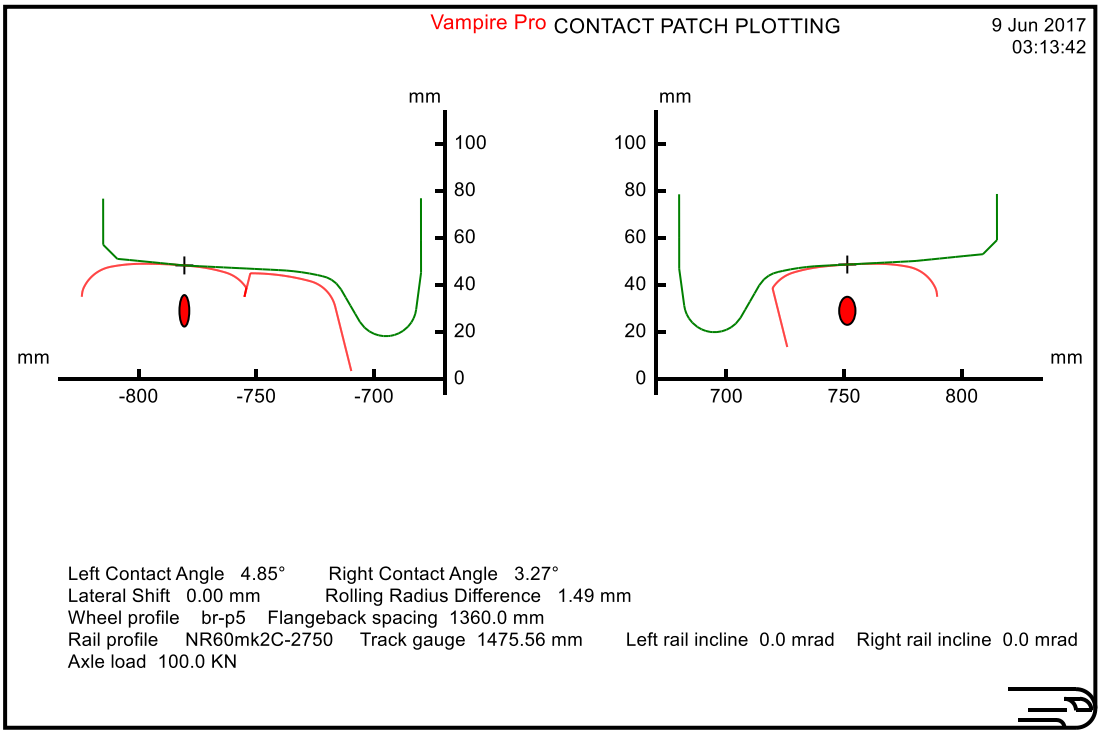

VAMPIRE Plot

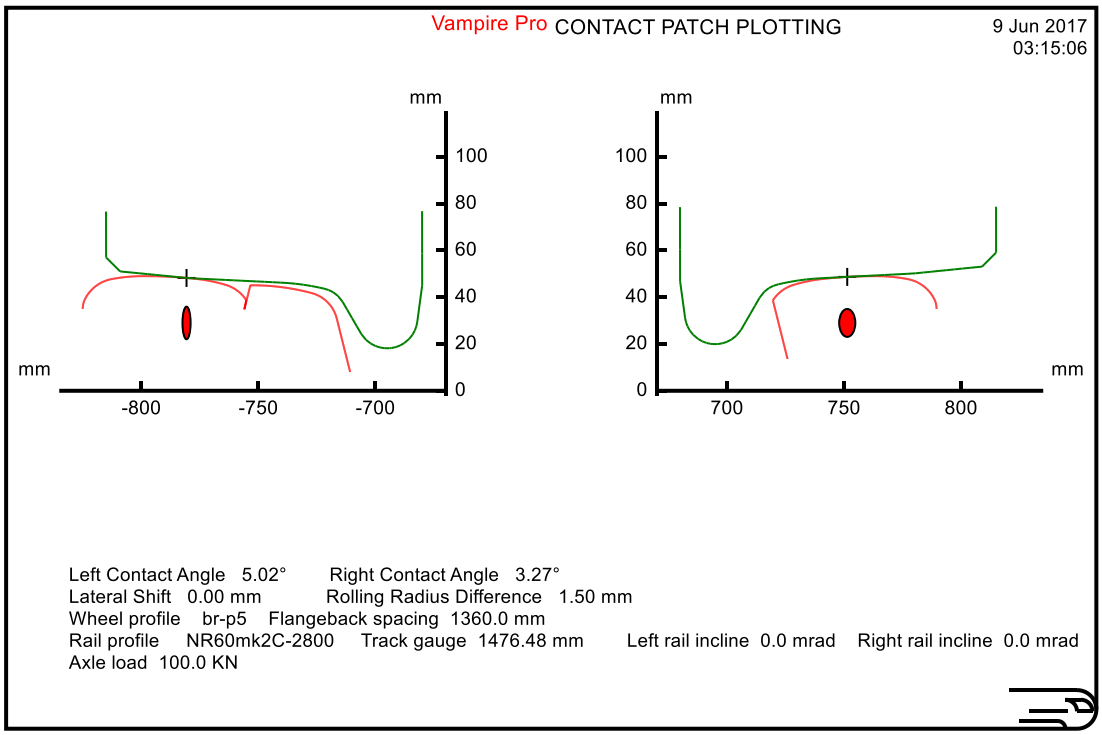

VAMPIRE Plot

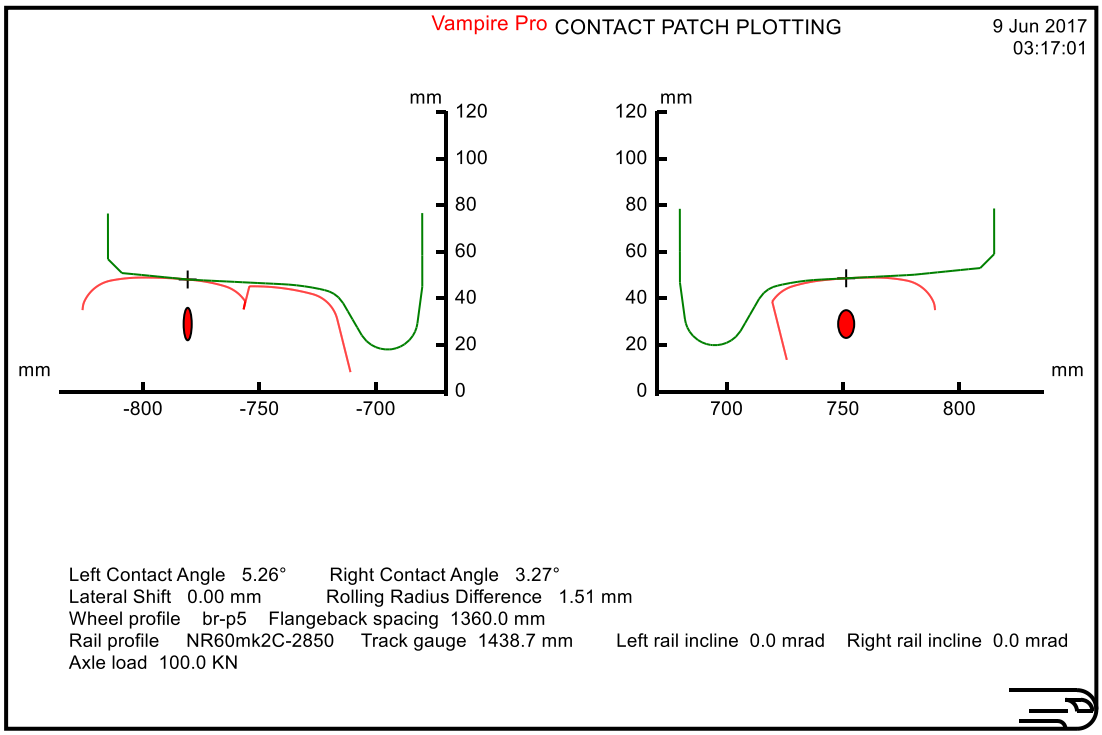

VAMPIRE Plot

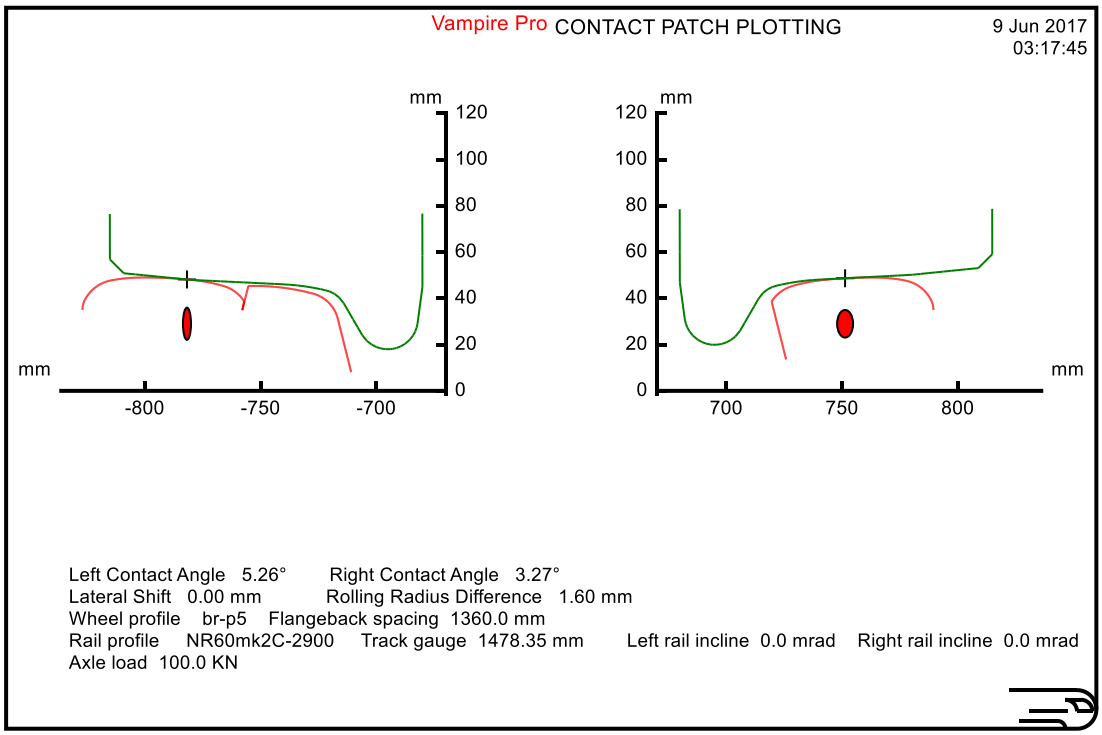

VAMPIRE Plot

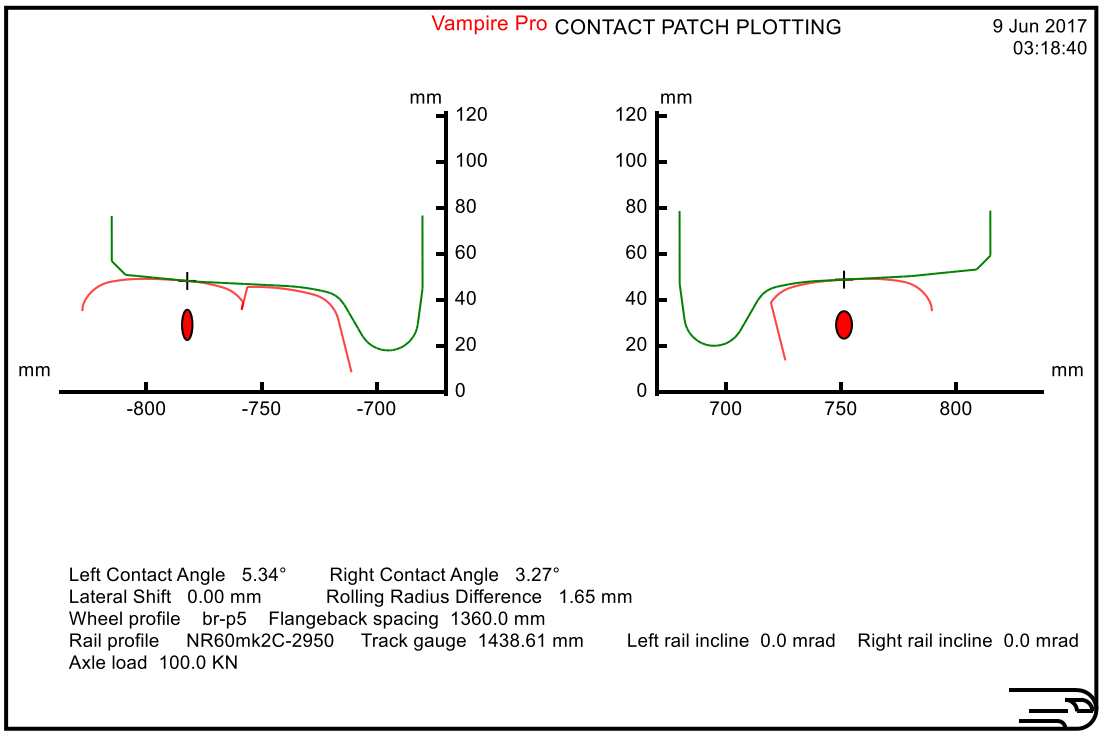

VAMPIRE Plot

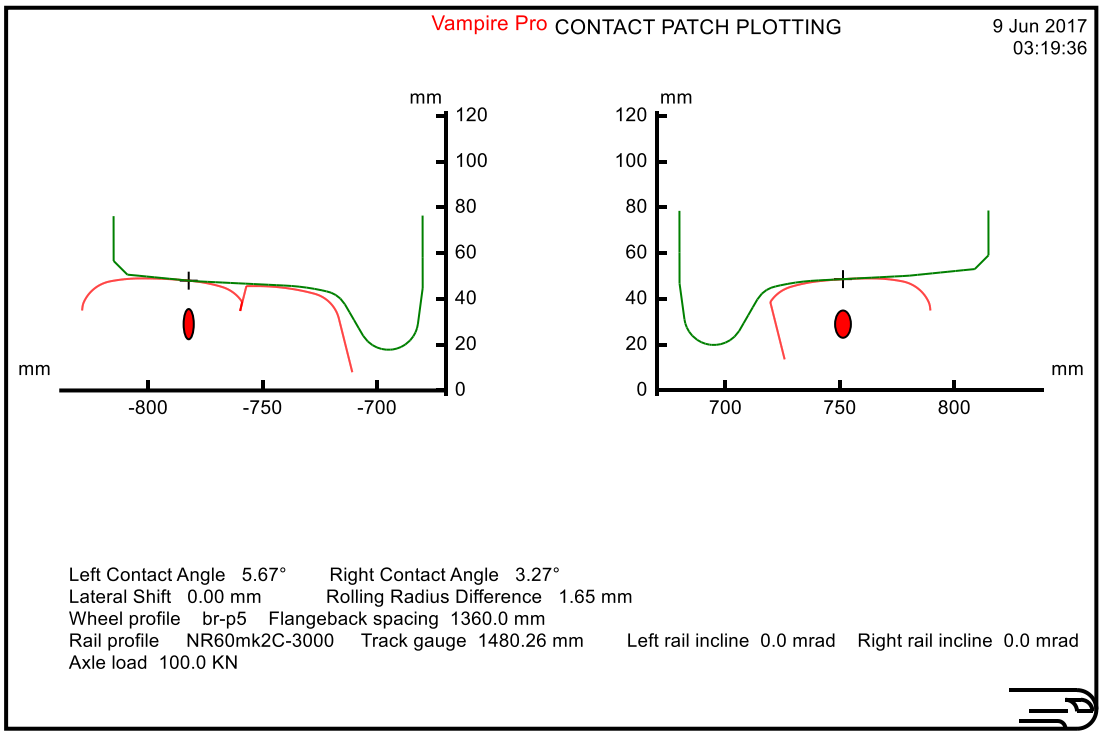

VAMPIRE Plot

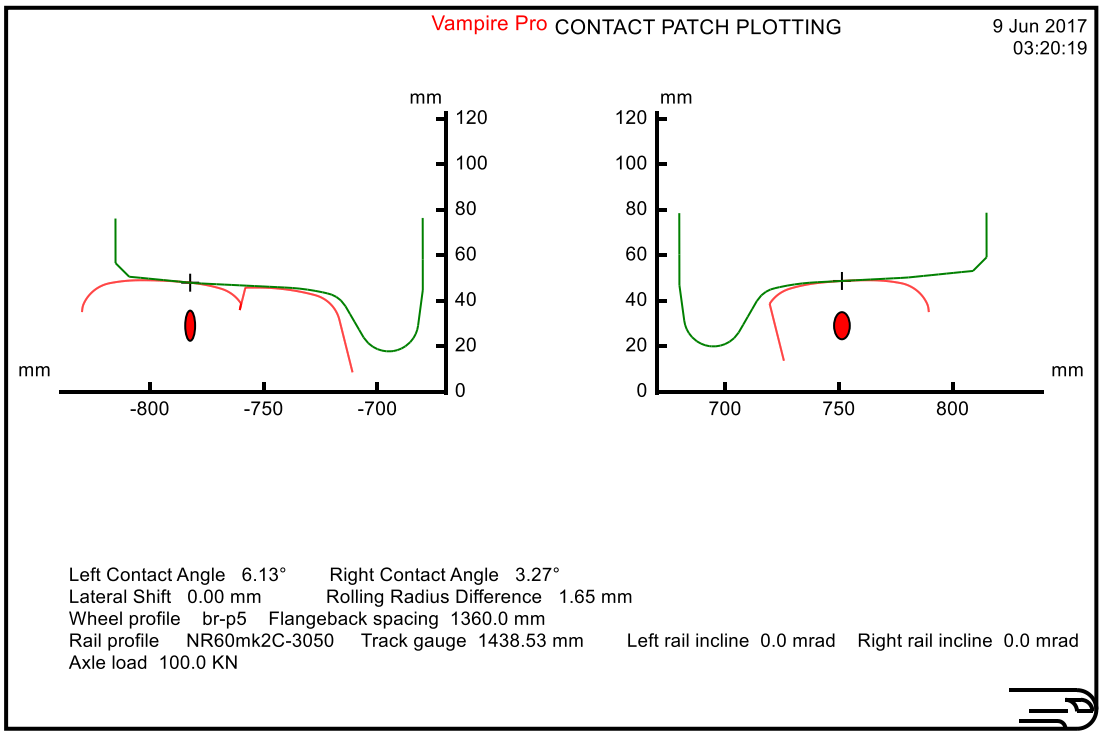

VAMPIRE Plot

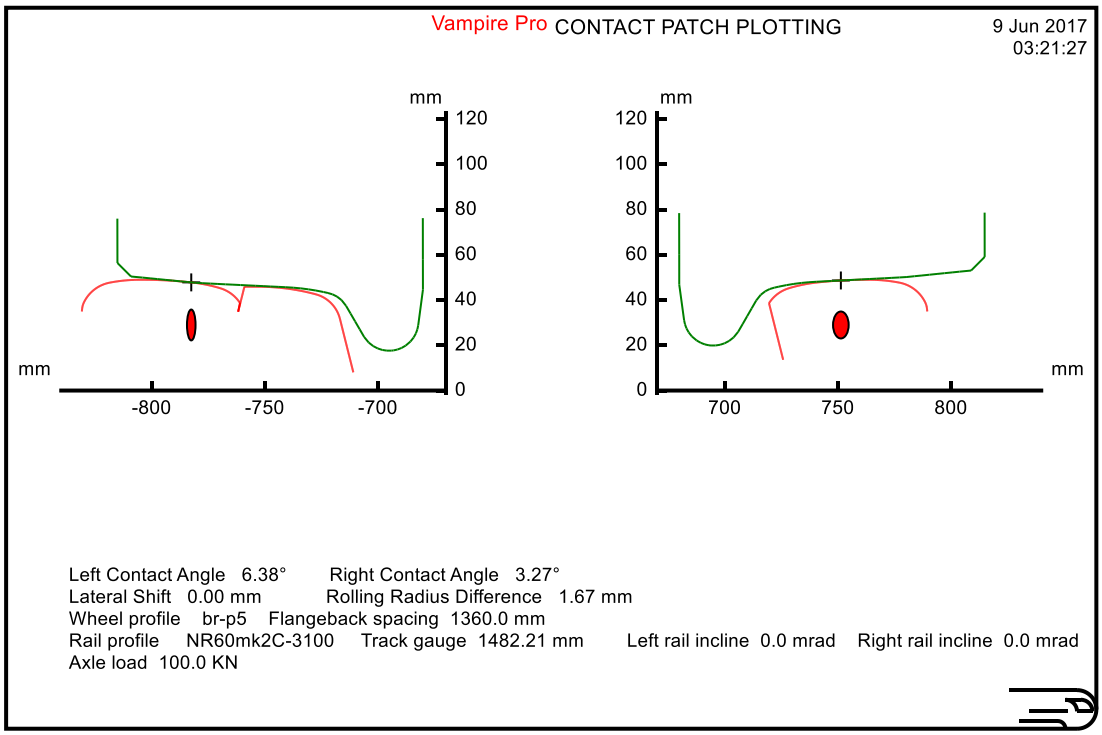

VAMPIRE Plot

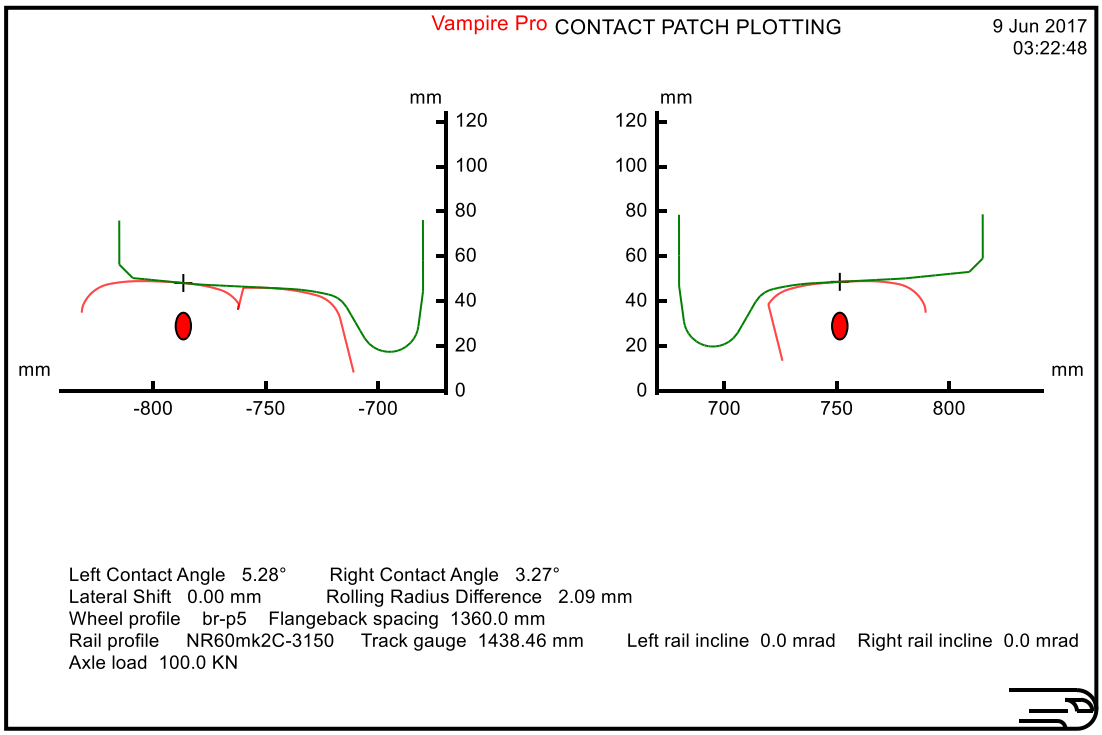

VAMPIRE Plot

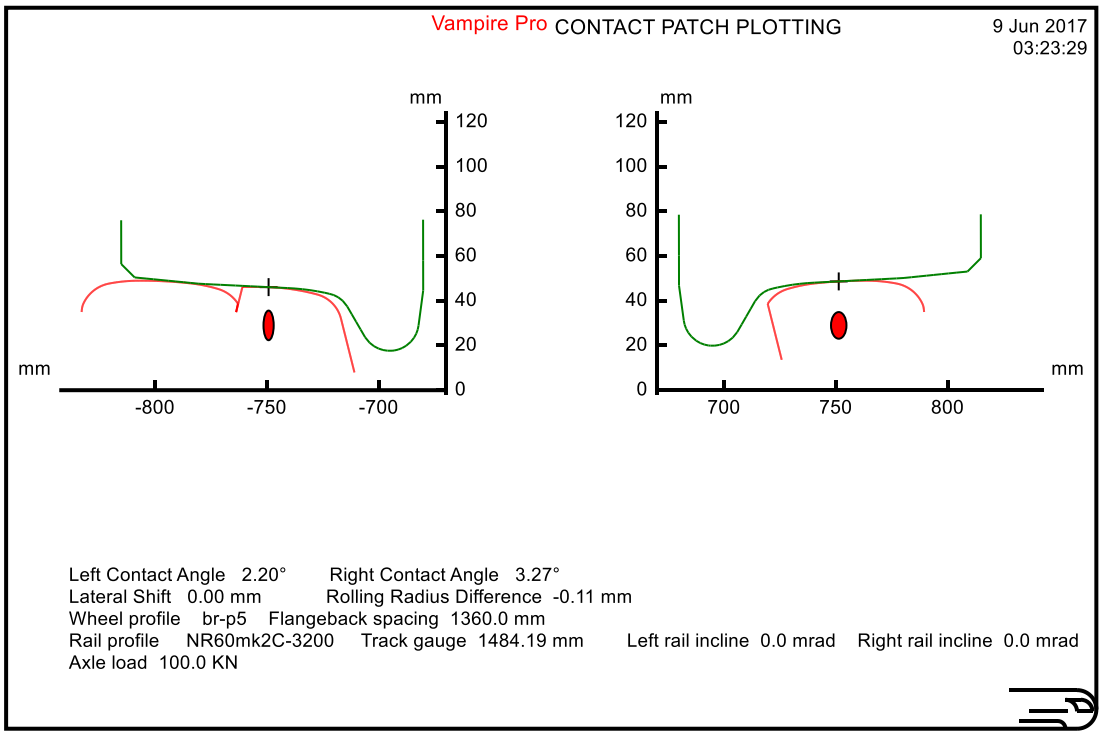

VAMPIRE Plot

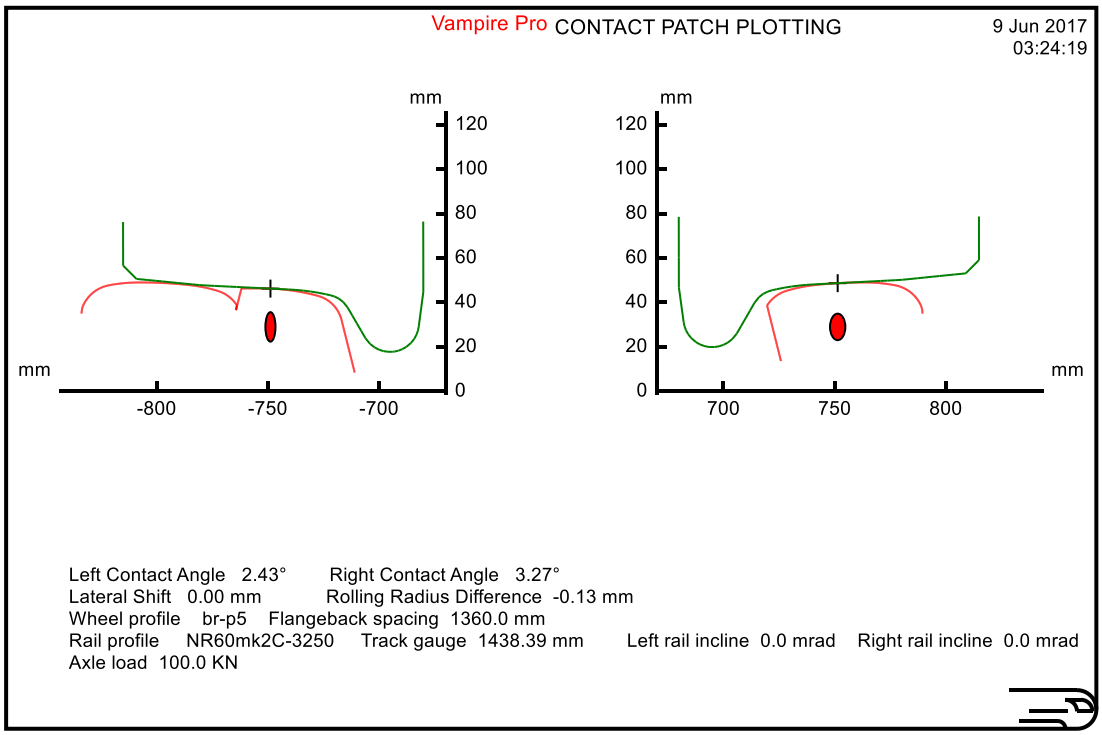

VAMPIRE Plot

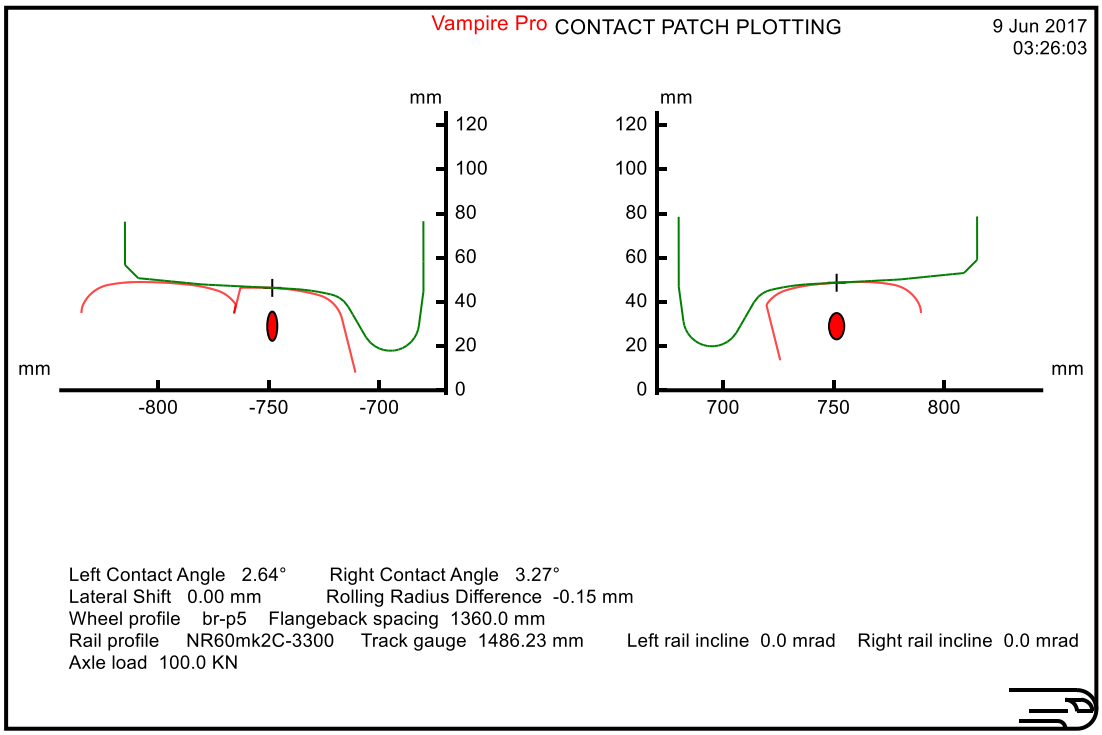

VAMPIRE Plot

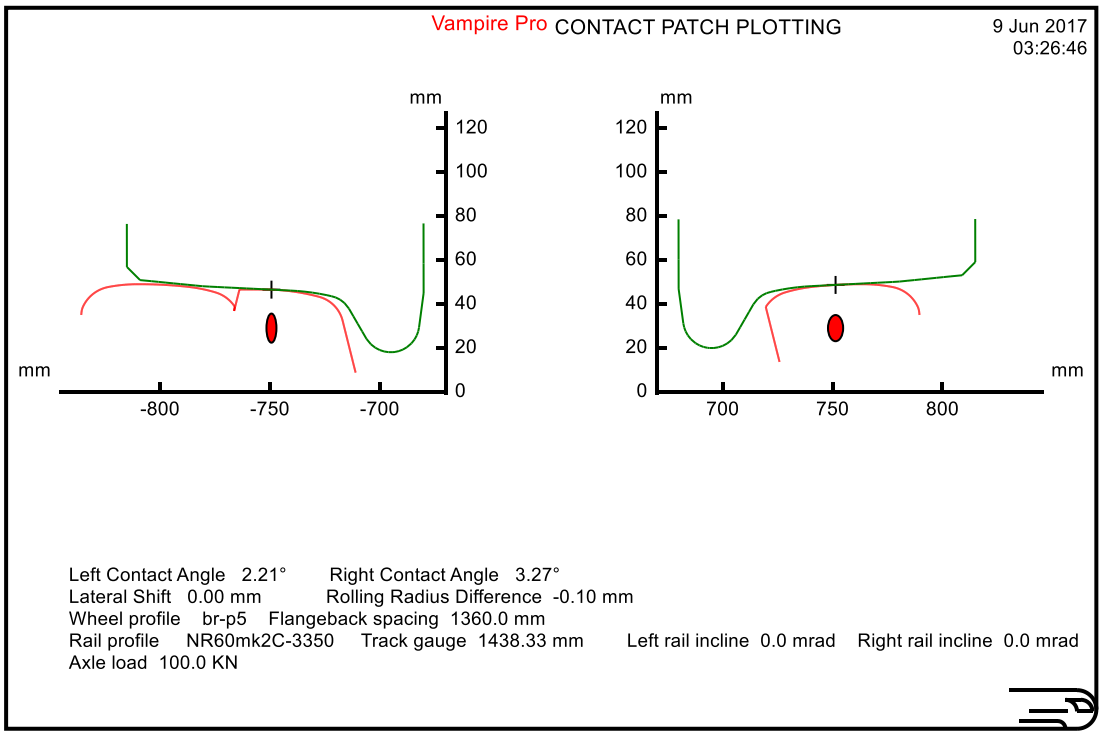

VAMPIRE Plot

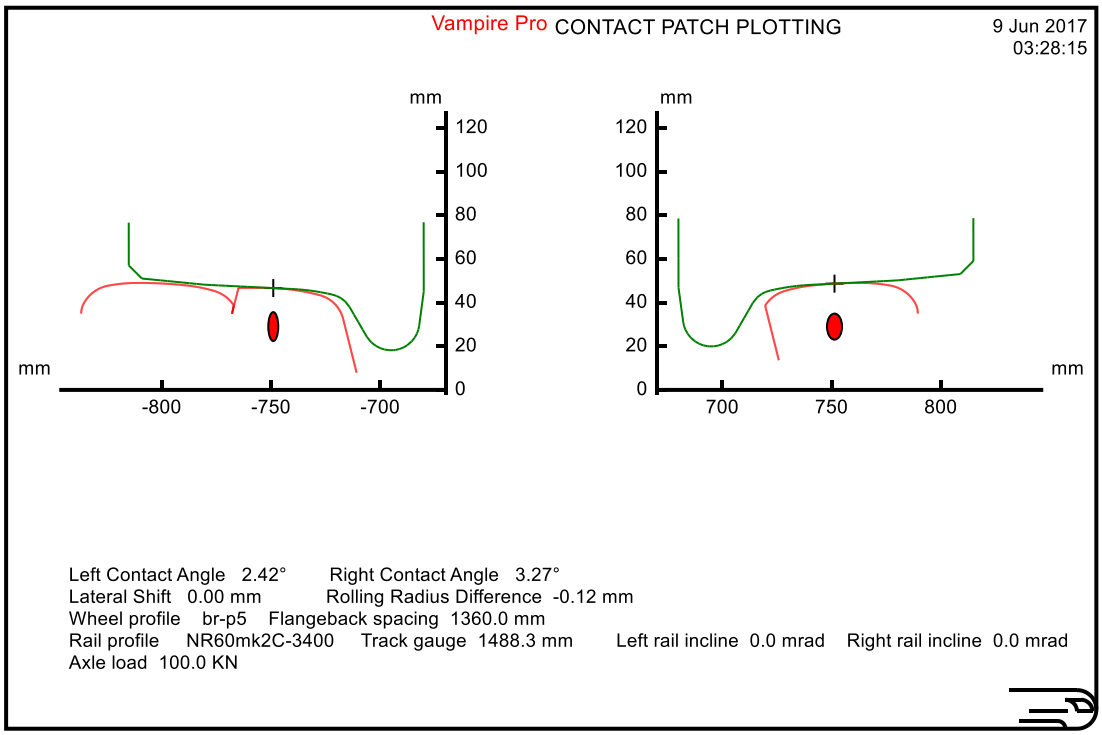

VAMPIRE Plot

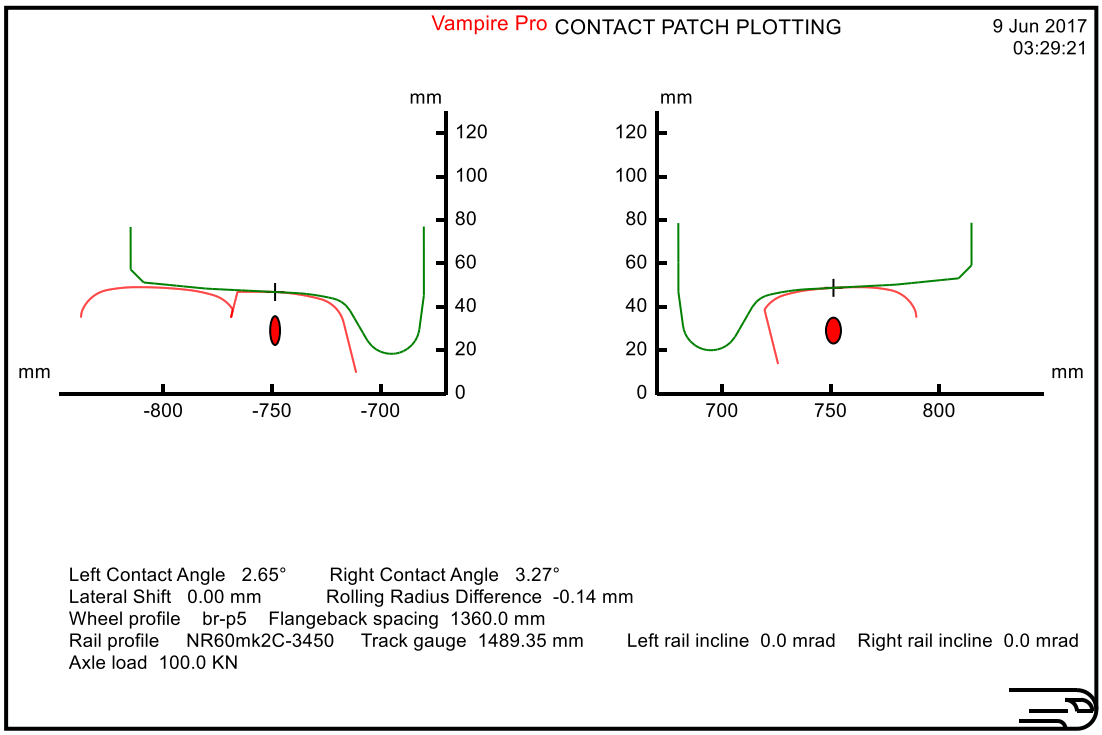

VAMPIRE Plot

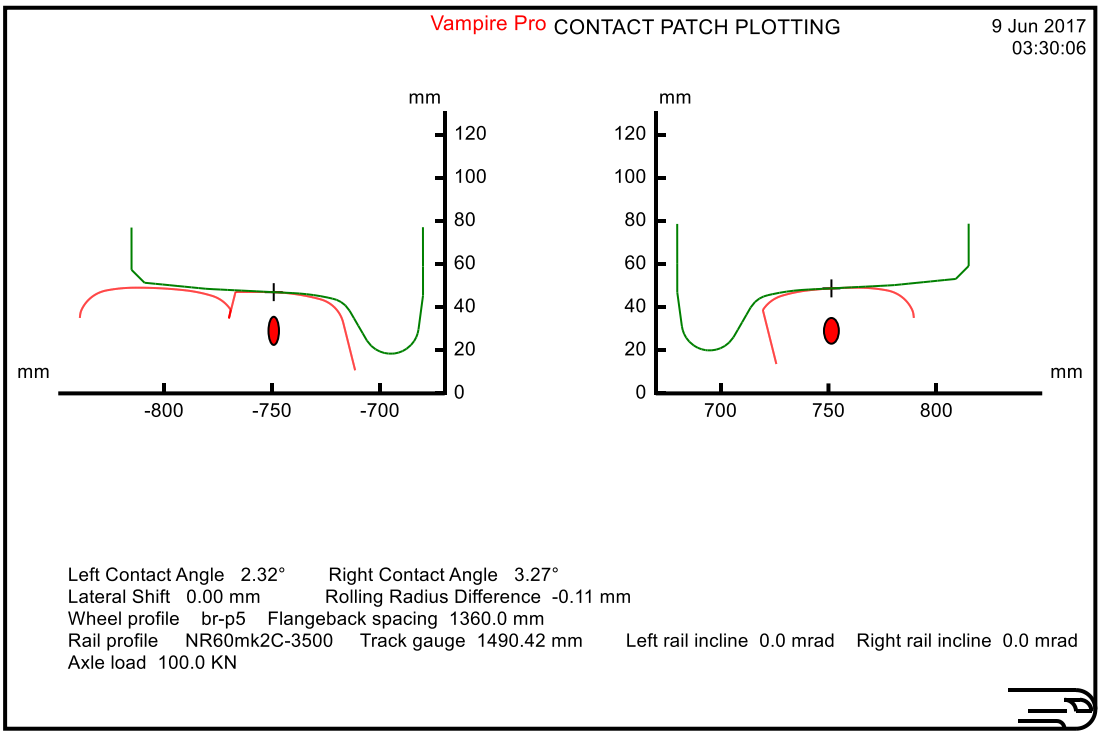

VAMPIRE Plot

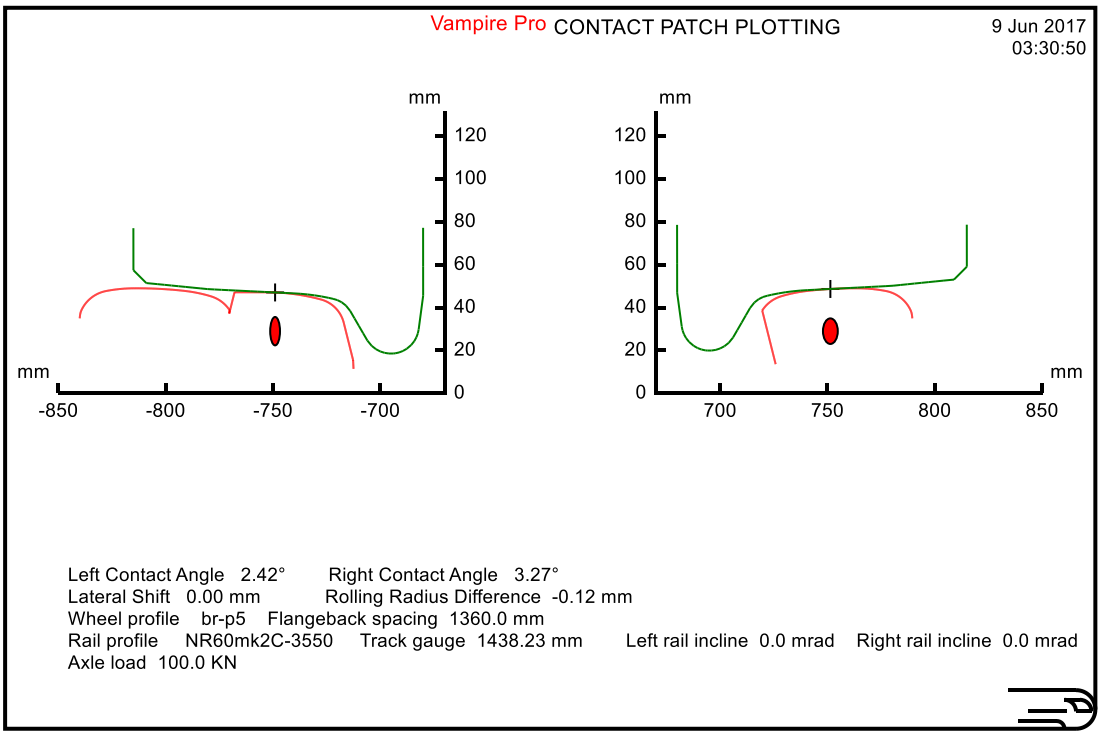

VAMPIRE Plot

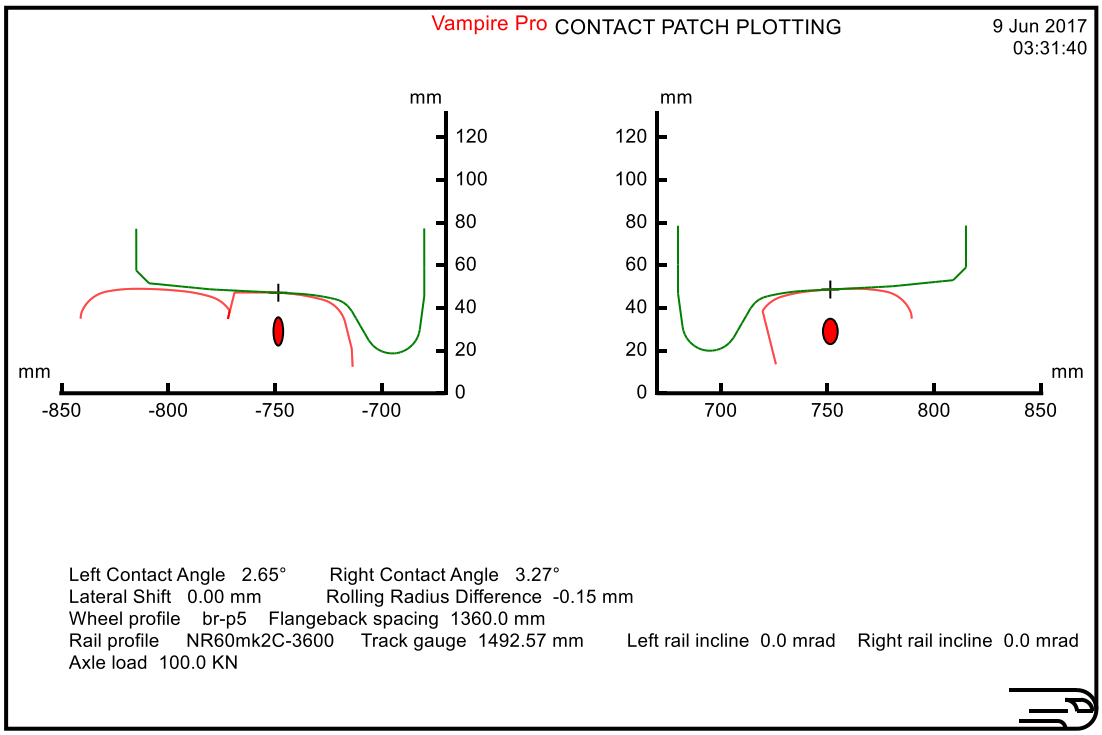

VAMPIRE Plot

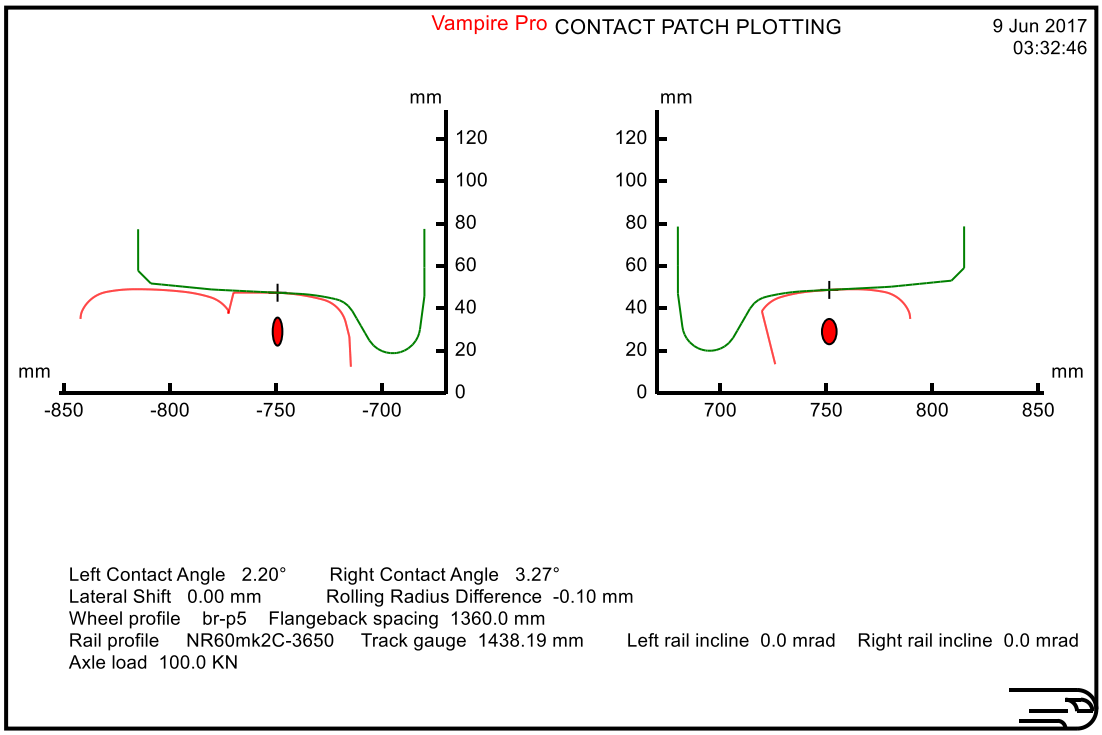

VAMPIRE Plot

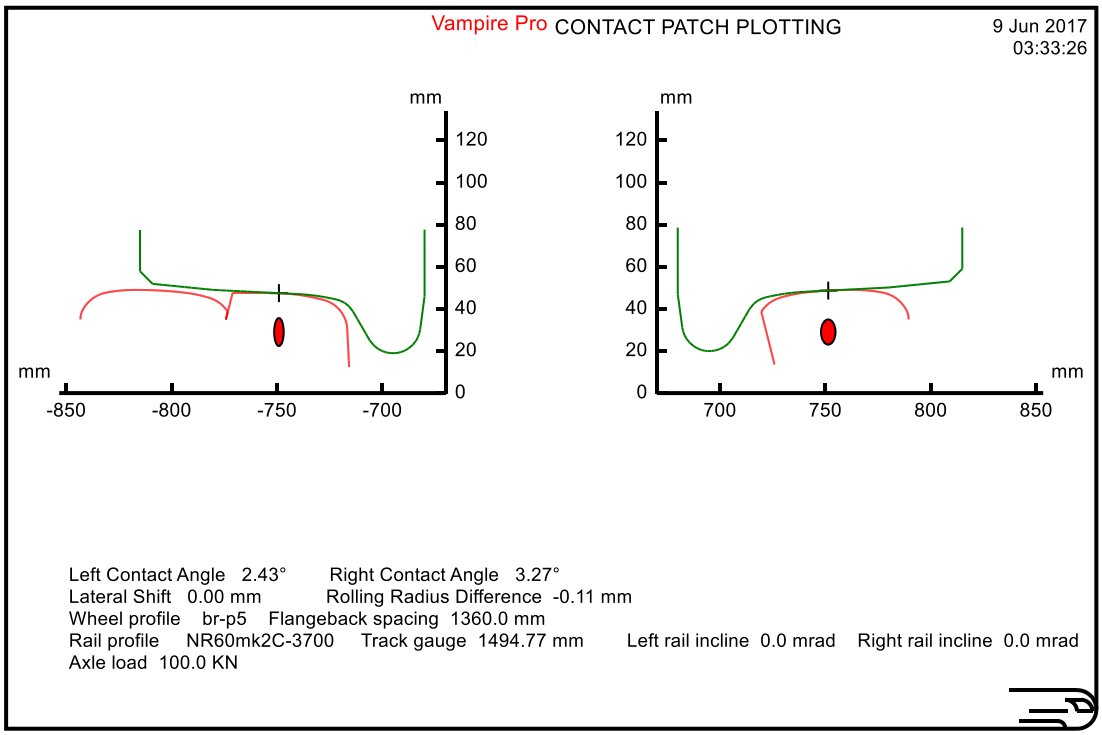

VAMPIRE Plot

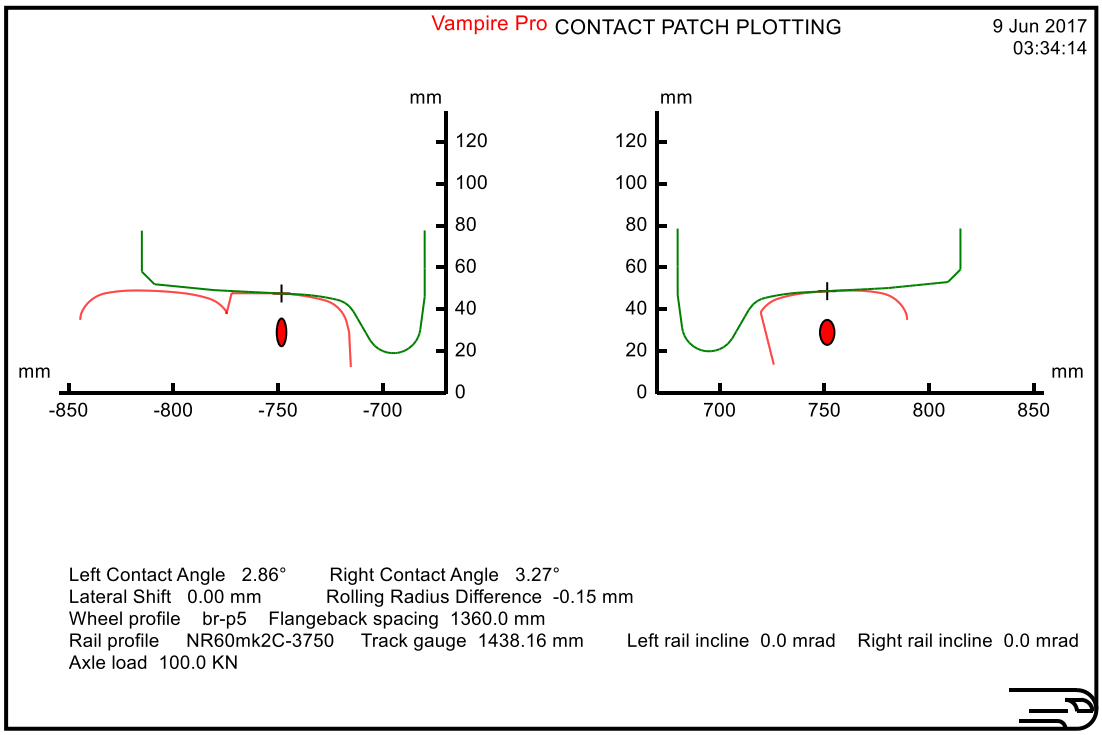

VAMPIRE Plot

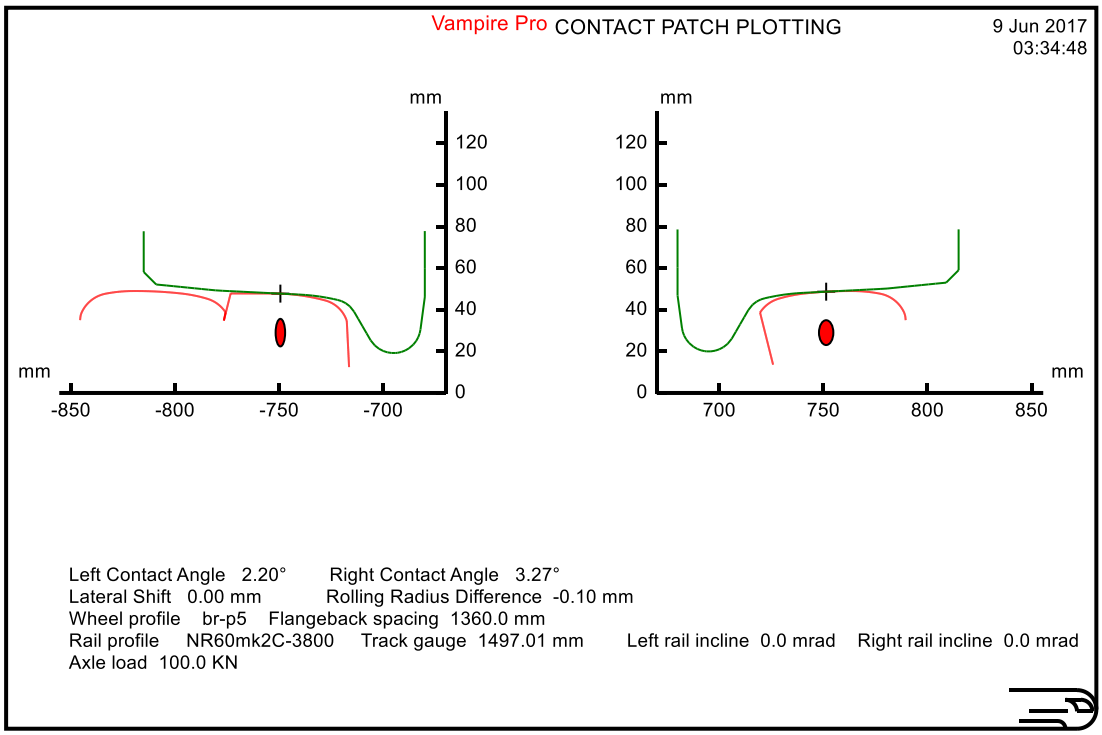

VAMPIRE Plot

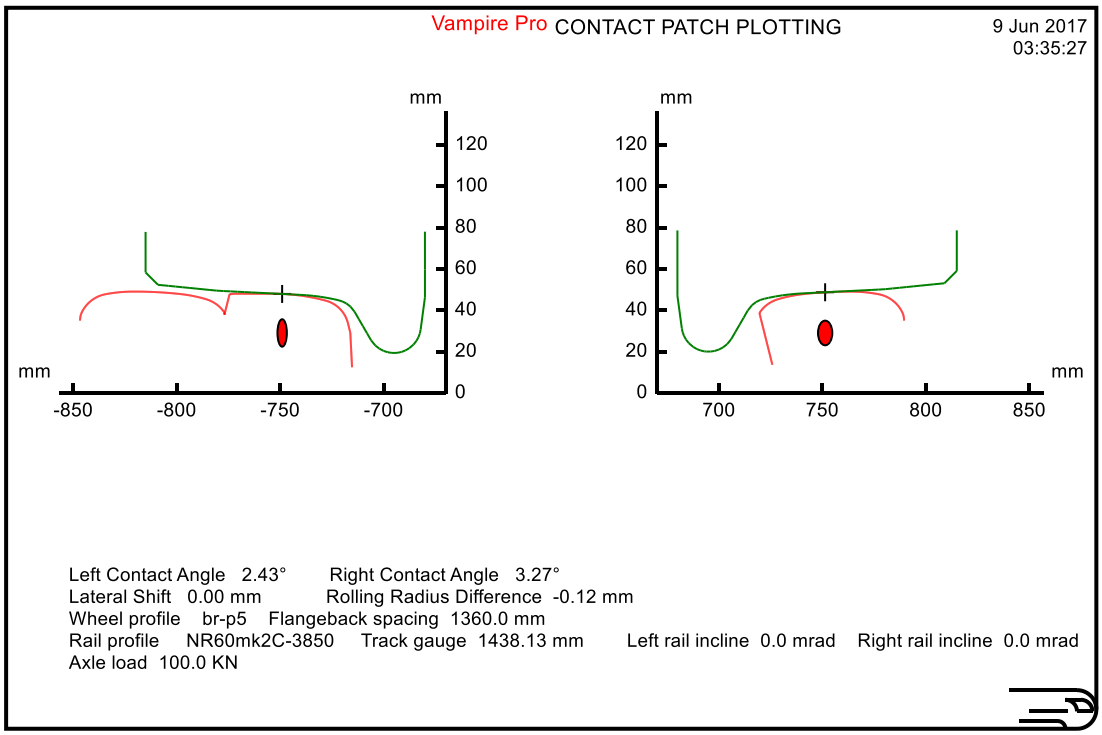

VAMPIRE Plot

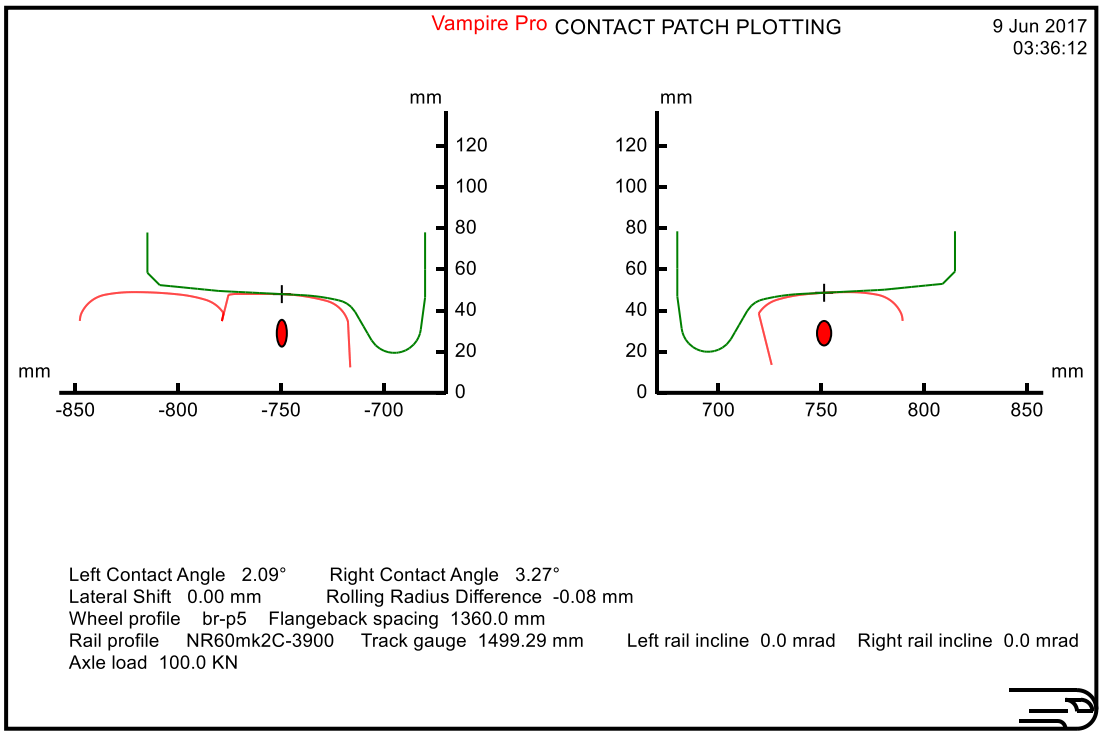

VAMPIRE Plot

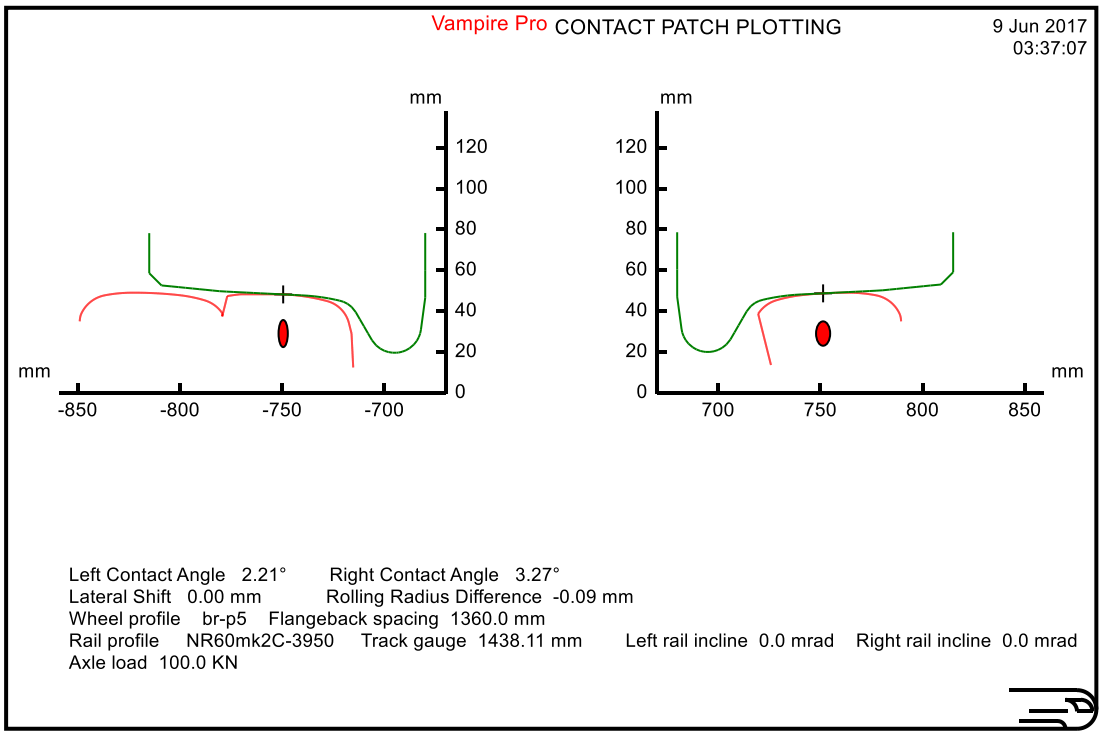

VAMPIRE Plot

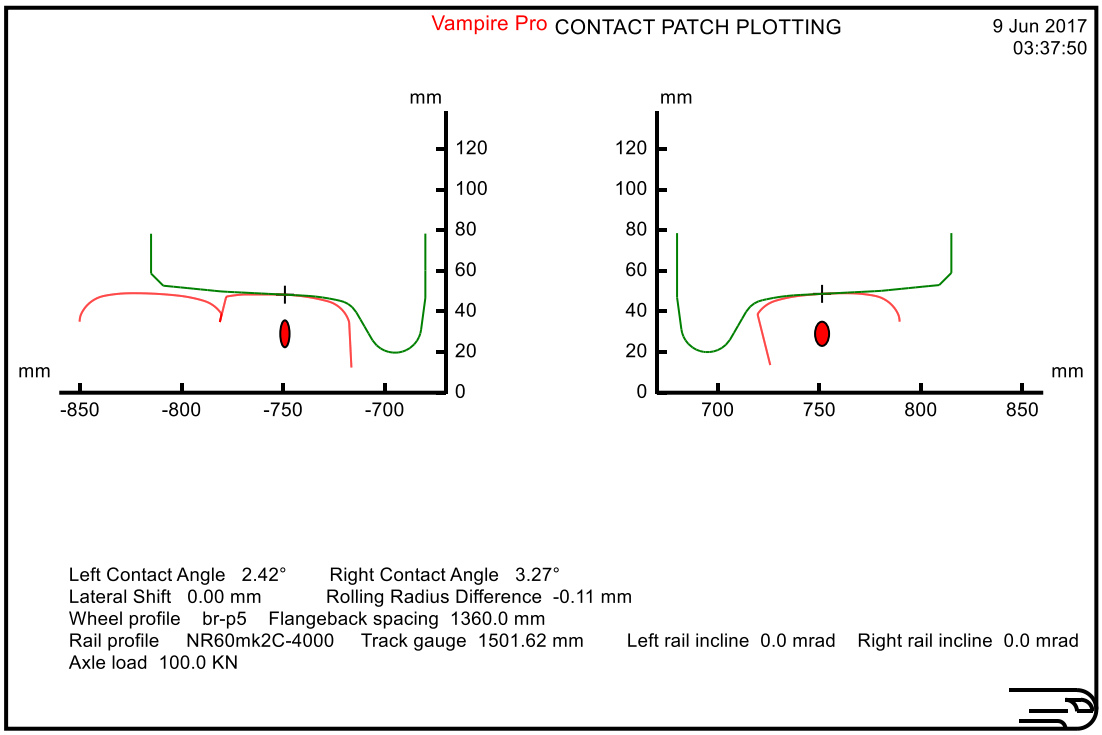

VAMPIRE Plot

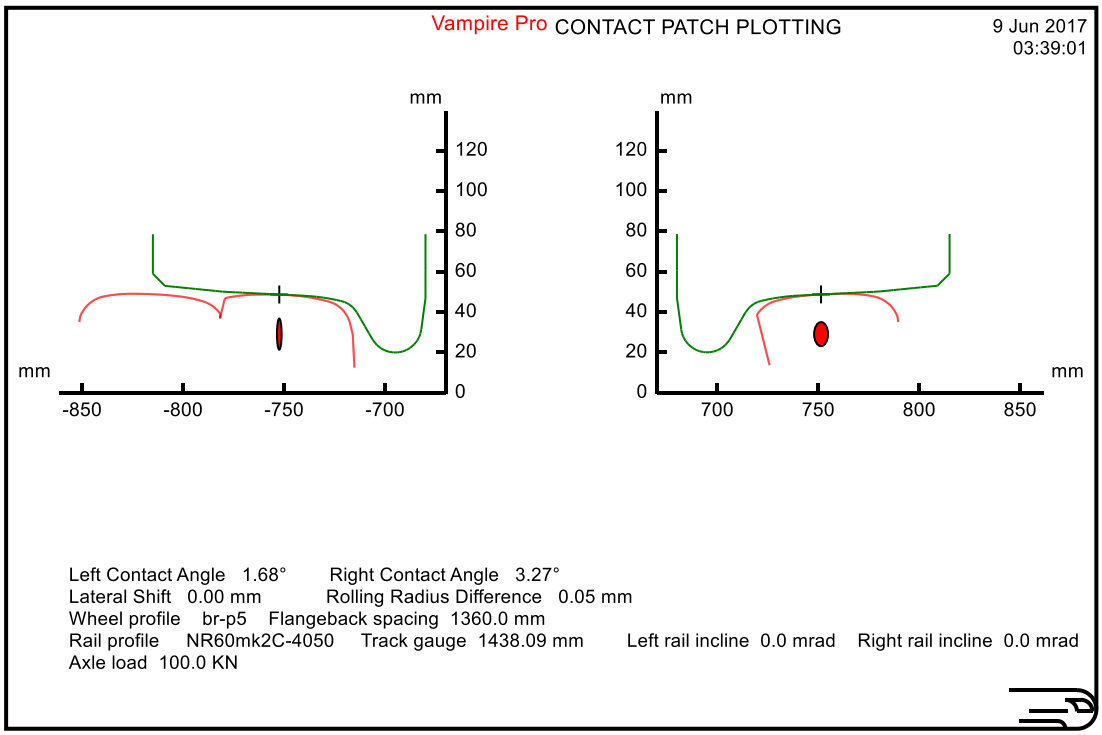

VAMPIRE Plot

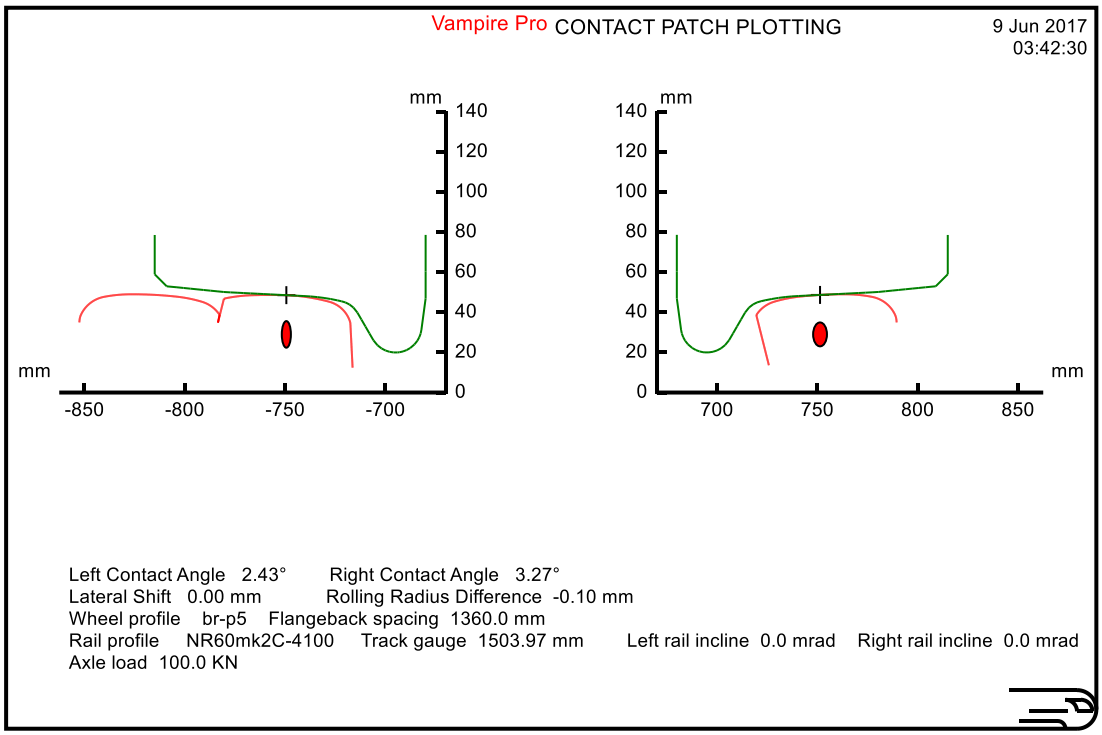

VAMPIRE Plot

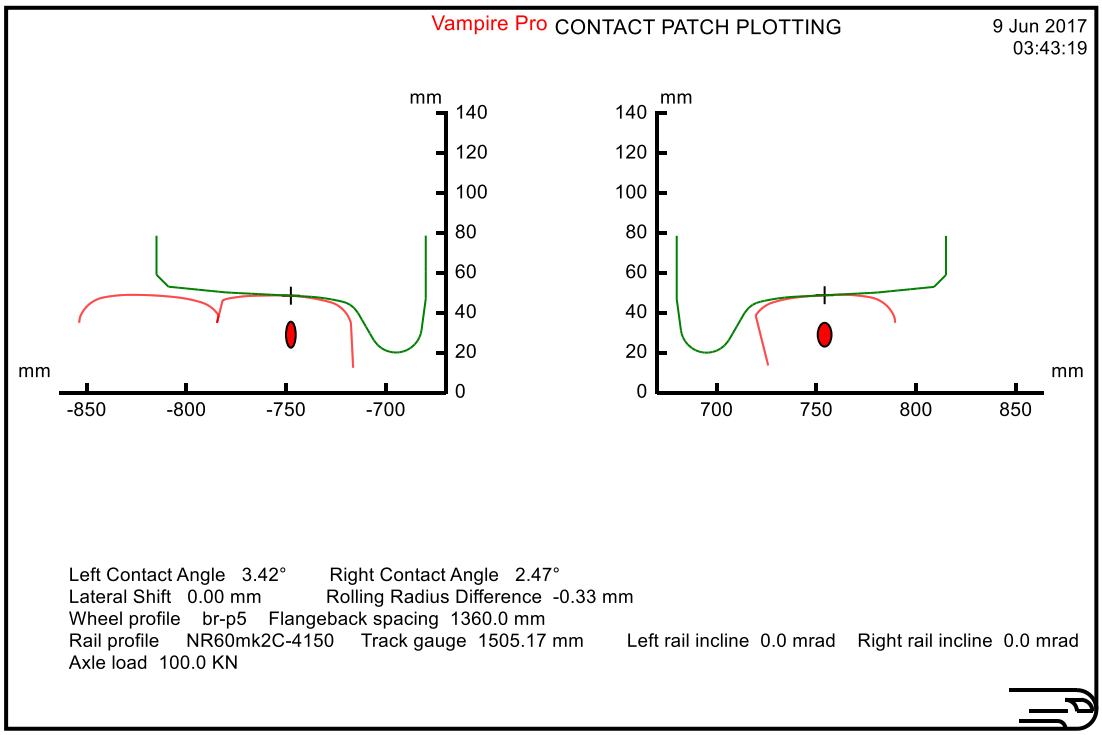

VAMPIRE Plot

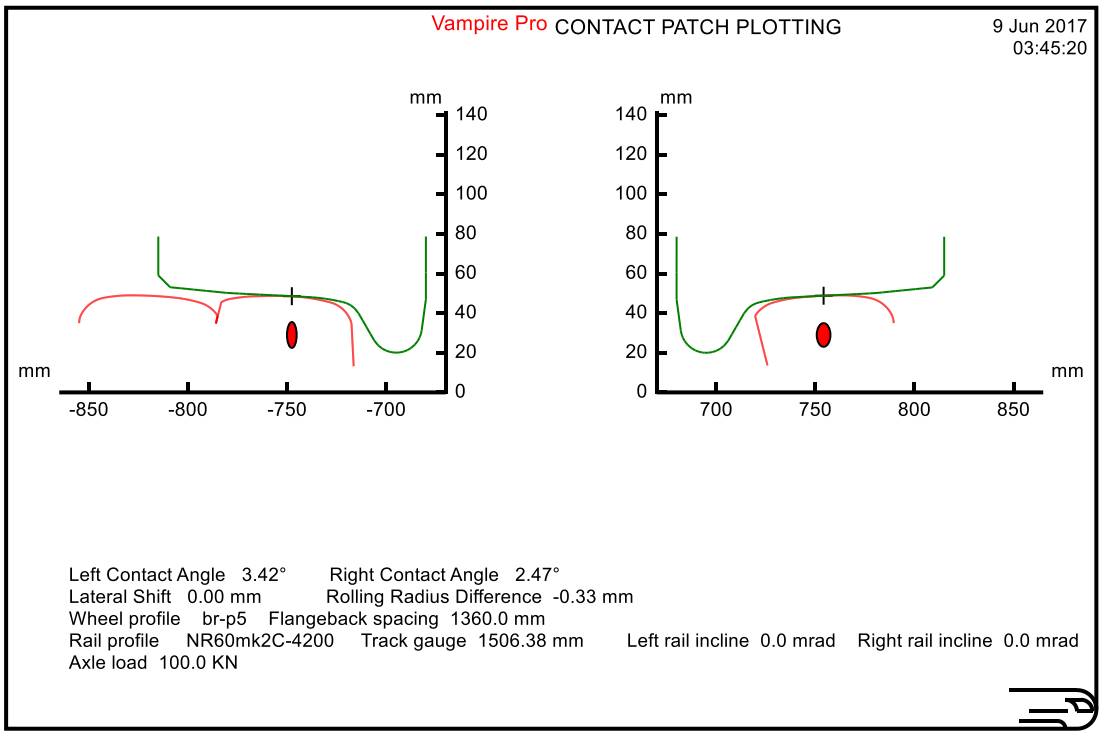

VAMPIRE Plot

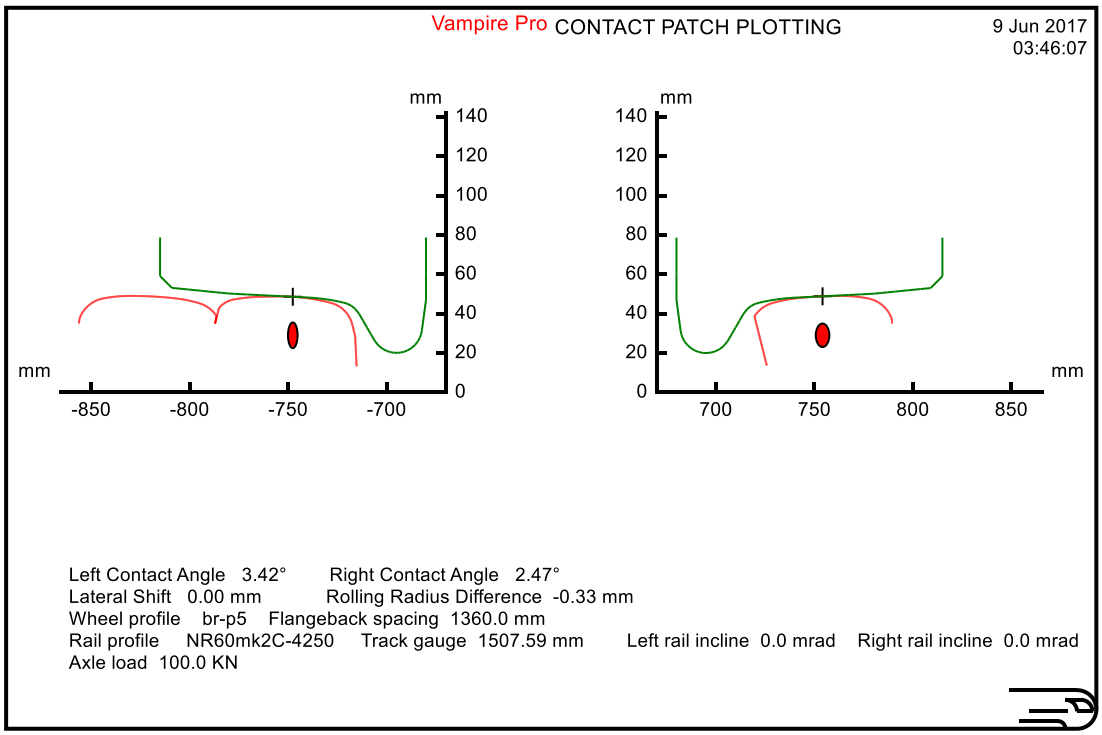

VAMPIRE Plot

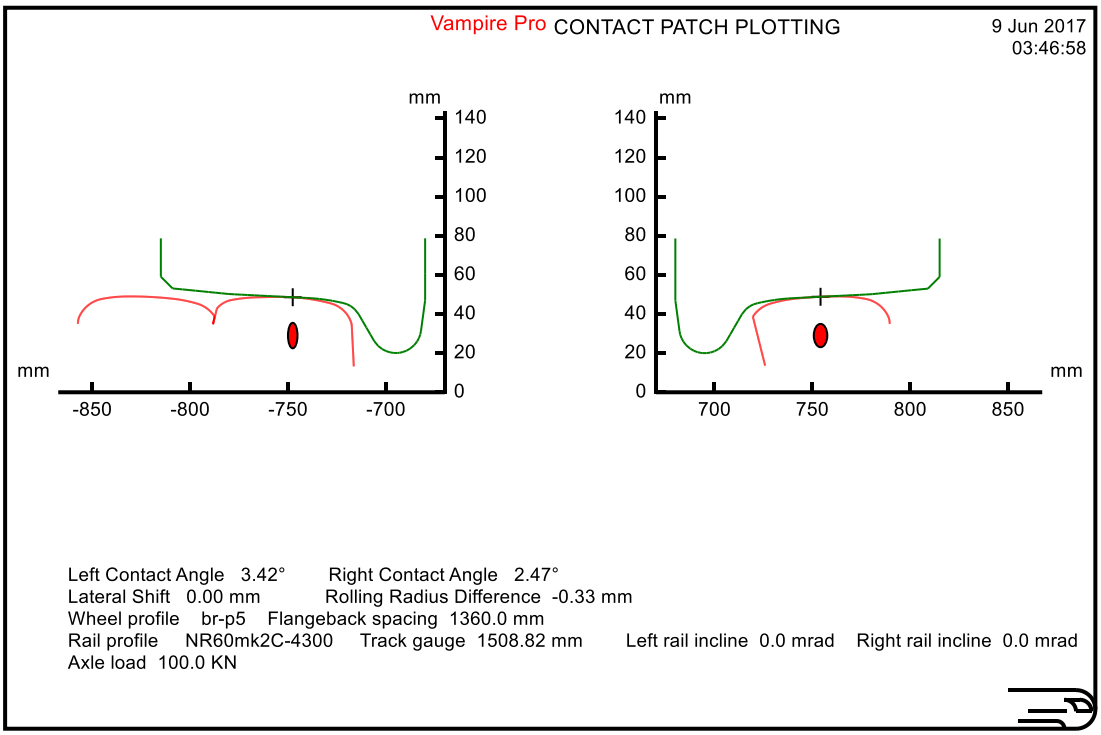

VAMPIRE Plot

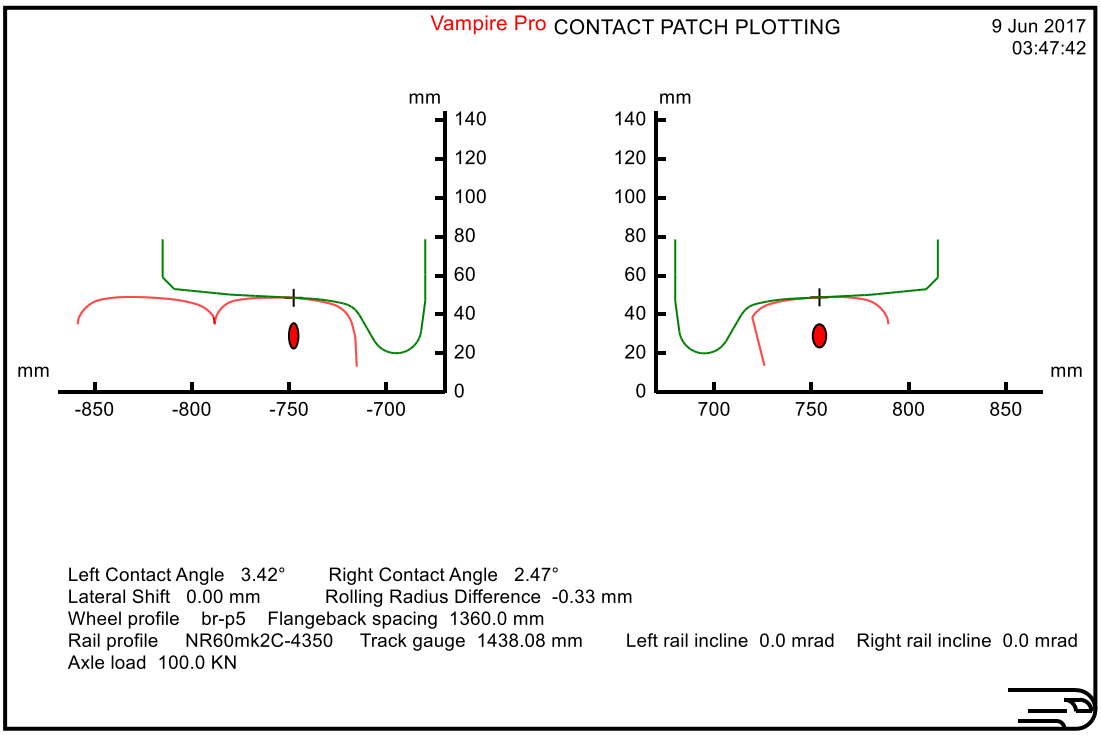

VAMPIRE Plot

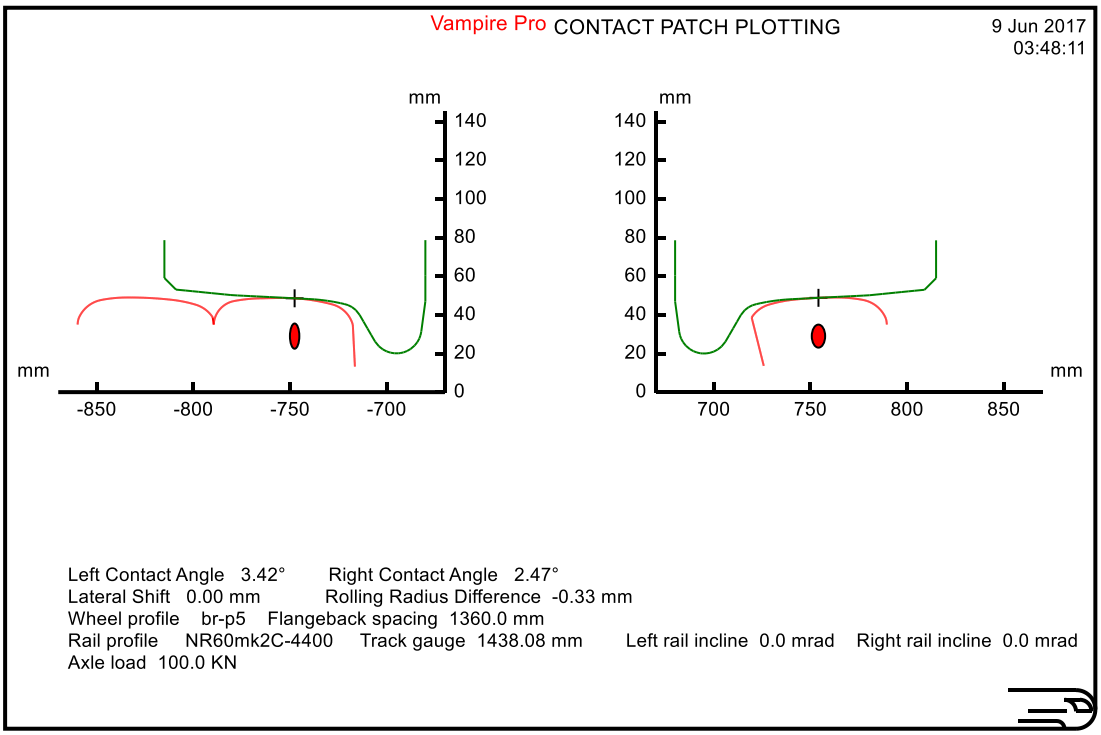

VAMPIRE Plot